

# **Validation of FWD Testing Results at the Virginia Smart Road: Theoretically and by Instrument Responses**

Alexander Kwasi Appea

Dissertation submitted to the Faculty of the Virginia Polytechnic Institute and State University in  
partial fulfillment of the requirements for the degree of

Doctor of Philosophy  
in  
Civil Engineering

Imad L. Al-Qadi, Chair  
Gerardo W. Flintsch  
Thomas L. Brandon  
John C. Duke Jr.  
John Collura

January 24, 2003  
Blacksburg, Virginia

Keywords: Falling weight deflectometer, pavements, instrumentation, hot-mix asphalt,  
backcalculation

Copyright 2003, Alexander K. Appea

# **Validation of FWD Testing Results at the Virginia Smart Road: Theoretically and by Instrument Responses**

Alexander Kwasi Appea

## **(ABSTRACT)**

Falling weight deflectometer (FWD) is currently used by most highway agencies to determine the structural condition of the highway network. Utilizing the deflections measured by the FWD, the resilient moduli of layers in the flexible pavement is determined using backcalculation software packages. The moduli can be input into semi-empirical mechanistic equations to estimate the remaining life of the pavement system and aid in informing pavement engineers about timing of maintenance and rehabilitation needs. There have been concerns among practitioners and the research community about the adequacy of the resilient moduli determined by the backcalculation software. Some of the backcalculation models have been simplified and field verification may be needed. Field-measured stresses and strains may be used to quantify the reliability of the backcalculated moduli. The Virginia Smart Road, which has 12 different flexible pavement designs and was built and instrumented with pressure cells, strain gages, thermocouples, frost probes and moisture sensors. To validate the backcalculated moduli theoretically and through instrument response, this research was conducted with following objectives: 1) to determine the resilient moduli of the unbound granular materials on the Virginia Smart Road using small and large plates of the FWD; 2) to investigate the extent of spatial and temporal variability of the FWD deflections among pavement sections; 3) to develop a temperature correction model for the backcalculated HMA resilient moduli; 4) to define an appropriate backcalculation approach and compare the four widely used software approaches; and 5) to correlate backcalculated and laboratory measured moduli. In addition, the FWD measurements were used to establish a comparison between in-situ measured and computed stresses and strains in the pavement. The analytical approaches used are linear elastic, viscoelastic, and viscoelastic combined with nonlinearity. Results show that estimation of unbound granular materials moduli using surface deflections is more reliable when 457-mm-diameter loading plate is used. Analysis of deflections from different sensors showed evidence of spatial and temporal variability. The lowest coefficient of variation of deflections (7%) within sections occurred at low temperatures (2 to 6 °C), while the highest coefficient of variation (42%) occurred at temperatures between 35 to 40 °C. This resulted in the development of a deflection temperature correction model. The model was validated at different temperature ranges. A backcalculation procedure was defined to achieve good root mean square error

using four selected software packages. This resulted in the selection of the most reliable software to perform moduli backcalculation. A correlation was established between the nonlinear models produced by backcalculation and laboratory testing of the granular 21-B material. However, for the HMA materials, difference in loading period between laboratory testing and FWD loading pulse could affect the results. The study found that when utilizing the backcalculated moduli, computed strains using viscoelastic modeling were comparable to in-situ measured values. Similarly, calculated stresses compared well with the field-measured stresses; especially at high temperatures. Mix properties, temperature of testing and loading were found to have an effect on the agreement between the measured and computed strains in the wearing surface. The study also recommended further validation of FWD measurements using embedded instruments to calibrate analytical models and further analysis of deflection data so that optimum number of testing points can be determined to limit amount of testing performed for determination of deflection variability.

## **ACKNOWLEDGEMENTS**

I would like to express my utmost gratitude to Dr Imad L. Al-Qadi for his guidance, time and support during this research. I also would like to thank Dr Gerardo Flintsch for some of his untiring efforts in making useful suggestions as the research work progressed. Special thanks to the committee members, Dr John Duke Jr, Dr Thomas Brandon, and Dr John Collura for time and effort and agreeing to be members of my PhD committee.

Thanks to all the guys in the Roadway Infrastructure Group (RIG) with whom I developed a working bond during the course of the project, especially Dr Amara Loulizi, Samer Lahouar (you would have a special place in my heart), Mostafa Elseifi (my coffee mate), Edgar Izeppi.

Sincere gratitude goes towards my father, Austin Peter Appea and brother Kwame and only sister Louisa for their love and encouragement, Professor Clifford and Phyllis Randall not forgetting Professor Wiredu of University of South Florida for his continual encouragement.

Finally I thank my special friend Yvonne for always wanting to talk with me even when I was tired while doing a lot of the writing.

## TABLE OF CONTENTS

CHAPTER ONE INTRODUCTION .....	1
1.1 INTRODUCTION .....	1
1.2 BACKGROUND .....	2
1.2.1 In-situ Nondestructive Testing .....	3
1.2.2 Backcalculation Techniques .....	4
1.3 PROBLEM STATEMENT .....	11
1.4 OBJECTIVES .....	12
1.5 SCOPE OF WORK .....	13
REFERENCES .....	13
CHAPTER TWO LITERATURE REVIEW .....	19
2.1 INTRODUCTION .....	19
2.2 BACKCALCULATION PROCEDURES: FORWARD COMPUTATIONAL MODELS AND ERROR MINIMIZATION .....	22
2.3 FACTORS AFFECTING BACKCALCULATED MODULI .....	38
2.3.1 Inertial Forces .....	39
2.3.2 Spatial Variations .....	39
2.3.3 Effect of Thickness Variation .....	40
2.3.4 Effects of Pavement Discontinuities .....	41
2.4 CALIBRATION OF THE FALLING WEIGHT DEFLECTOMETER .....	41
2.5 VERIFICATION OF FIELD BACKCALCULATION WITH LABORATORY VALUES .....	42
2.6 TEMPERATURE CORRECTIONS OF FWD TESTING .....	43
2.7 CASE STUDIES OF FIELD INSTRUMENTATION TO VERIFY FWD RESULTS .....	45
REFERENCES .....	51
CHAPTER THREE ESTIMATION OF MODULI OF UNBOUND MATERIAL USING FALLING WEIGHT DEFLECTOMETER DEFLECTIONS MEASURED WITH SMALL AND LARGE PLATES .....	57
Abstract .....	57
3.1 INTRODUCTION .....	58
3.2 SUBGRADE MODULI DETERMINATION .....	60
3.2.1 Maximum Deflection ( $D_0$ ) Analysis .....	60
3.2.2 Surface Modulus Using All Deflections ( $D_i$ ) And A Point Load .....	64
3.2.3 Two-Layer System Analysis Of Subgrade .....	69
3.2.4 Nonlinear Analysis .....	72

3.2.5 Ullidtz Method For Estimating The Depth To Bedrock	79
3.2.6 Summary of The Subgrade Analysis	82
3.3 Granular Subbase (21-B) Analysis	85
3.3.1 Two-Layer Linear Elastic System	86
3.3.2 Single-Layer System	87
3.4 SUMMARY AND CONCLUSIONS	88
REFERENCES	90
CHAPTER FOUR FWD SPATIAL AND TEMPORAL VARIABILITY WITHIN AND BETWEEN PAVEMENT SECTIONS	91
Abstract	91
4.1 BACKGROUND	92
4.2 SITE TESTING	93
4.3 SEASONAL VARIATION	94
4.4 VARIABILITY WITHIN-SECTION	100
4.5 VARIABILITY DUE TO TEMPERATURE	106
4.6 STATISTICAL ANALYSIS	114
4.7 FINDINGS AND CONCLUSIONS	115
REFERENCES	117
CHAPTER FIVE MODULI BACKCALCULATION OF THE VIRGINIA SMART ROAD PAVEMENT SECTIONS	119
Abstract	119
5.1 INTRODUCTION	121
5.2 BACKCALCULATION SCHEMES AND PROGRAMS	122
5.2.1 PEDMOD	124
5.2.2 EVERCALC	125
5.2.3 ELMOD	127
5.2.4 MICHBACK	128
5.2.5 Temperature Correction in Backcalculation Software	130
5.3 EVALUATION OF SOFTWARE UTILIZING DATA OBTAINED AT THE VIRGINIA SMART ROAD	132
5.4 DEVELOPMENT OF A BACKCALCULATION PROCEDURE	137
5.5 BACKCALCULATION RESULTS	138
5.5.1 Subbase Moduli	139
5.5.2 Cement-Treated Base Moduli	139

5.5.3 Combined HMA Base and Wearing Surface Moduli .....	139
5.6 DISCUSSION.....	144
5.7 FINDINGS AND CONCLUSIONS.....	150
REFERENCES .....	151
CHAPTER SIX RELATIONSHIP BETWEEN BACKCALCULATED AND LABORATORY	
MEASURED RESILIENT MODULI OF SUBBASE MATERIAL AND HOT- MIX	
ASPHALT.....	154
Abstract .....	154
6.1 INTRODUCTION .....	155
6.2 SPECIMEN PREPARATION AND LABORATORY TESTING OF 21-B .....	155
6.2.1 Test procedure.....	156
6.2.2 Resilient Modulus Model.....	158
6.2.3 Comparison between Field and Laboratory Resilient Modulus Results .....	159
6.3 FIELD RESILIENT MODULI RELATIONSHIP.....	162
6.4 COMPARISON BETWEEN LABORATORY AND FIELD RESILIENT MODULUS OF HMA.....	172
6.5 SUMMARY AND CONCLUSIONS.....	177
REFERENCES .....	178
CHAPTER SEVEN USING FWD LOADING TO ESTABLISH A COMPARISON BETWEEN IN-SITU	
MEASURED AND COMPUTED STESSES AND STRAINS.....	
Abstract .....	181
7.1 INTRODUCTION .....	182
7.2 FIELD TESTING .....	184
7.3 INSTRUMENT DESCRIPTION.....	186
7.4 BACKCALCULATION APPROACHES .....	187
7.5 PAVEMENT MODELING.....	191
7.6 INSTRUMENT RESPONSE AND DATA ANALYSES .....	193
7.6.1 Analysis Of The Pressure Response Data .....	195
7.6.2 Strain Gage Analysis .....	205
7.6.3 Mechanistic Empirical Modeling.....	210
7.7 SUMMARY AND CONCLUSIONS.....	213
REFERENCES .....	214
CHAPTER EIGHT SUMMARY, FINDINGS, CONCLUSIONS, AND RECOMMENDATIONS.....	
8.1 FINDINGS.....	217
8.2 CONCLUSIONS.....	218

8.3 RECOMMENDATIONS.....	219
APPENDIX A SAS OUTPUT .....	220
APPENDIX B RESULTS OF MODULI BACKCALCULATION.....	254
APPENDIX C RESULTS OF BACKCALCULATION SOFTWARE FOR PRESSURE CELLS.....	263
VITAE .....	279

## LIST OF TABLES

<b>Table 2.1</b>	Examples of Backcalculation Software and associated features .....	21
<b>Table 2.2</b>	Backcalculated Moduli .....	28
<b>Table 3.1</b>	Layer Structure of the Experimental Pavement Sections .....	58
<b>Table 3.2</b>	Moduli Computed Utilizing the Large (457 mm) Plate (MPa) .....	62
<b>Table 3.3</b>	Moduli Computed Utilizing the Small (300 mm) Plate (MPa) .....	63
<b>Table 3.4</b>	Subgrade Moduli Using All Sensors for the Large Plate (MPa) .....	66
<b>Table 3.5</b>	Subgrade Moduli Using All Sensors for the Small Plate (MPa) .....	67
<b>Table 3.6</b>	Subgrade Modulus Based on ELSYM5 Analysis (40 kN) .....	72
<b>Table 3.7</b>	Summary of Subgrade Moduli Computed Using Different Methods .....	83
<b>Table 3.8</b>	Summary of Percentage Differences between Large Plate and Small Plate .....	84
<b>Table 3.9</b>	21-B Moduli Considering a Two-Layer System (MPa) .....	87
<b>Table 3.10</b>	Combined Subbase-Subgrade Moduli (MPa) .....	88
<b>Table 4.1</b>	Summary of Deflection Data for Instrumented and NonInstrumented lanes .....	105
<b>Table 4.2</b>	Model Equations and R-square for Deflections vs. Temperature for all Sections .....	110
<b>Table 5.1</b>	Main Advantages and Disadvantages of the Software Packages Evaluated .....	133
<b>Table 5.2</b>	Summary of Subgrade Moduli Computed Using Different Methods (MPa) .....	134
<b>Table 5.3</b>	Backcalculated Moduli for Selected Sections Using Different Software Packages in November 2000 and April 2001 .....	135
<b>Table 5.4</b>	Strength Development of 21-A Layer with Time .....	140
<b>Table 5.5</b>	Adjustment Factors Used for the 21-A Moduli .....	140
<b>Table 5.6</b>	Range for Pavement Materials .....	146
<b>Table 5.7</b>	Root Mean Square Error results for Section A, B, C, D and H for the Backcalculation Software .....	147
<b>Table 6.1</b>	Properties of 21-B Specimens .....	157
<b>Table 6.2</b>	Average 21-B Moduli Based on the K- $\theta$ Lab Model (MPa) .....	161
<b>Table 6.3</b>	Modulus Relationship for the Sections with 176 mm Base Using All Sensors ( $D_0$ – $D_6$ ) .....	166
<b>Table 6.4</b>	Modulus Relationship for the Sections with 75 mm Base Using All Sensors ( $D_0$ – $D_6$ ) .....	167
<b>Table 6.5</b>	Modulus Relationship for the Sections with 150 mm Base Using All Sensors ( $D_0$ – $D_6$ ) .....	167
<b>Table 6.6</b>	Modulus Relationship for the Sections with 176 mm Base Using Sensors $D_0$ through $D_6$ .....	168
<b>Table 6.7</b>	Modulus Relationship for the Sections with 75 mm Base Using Sensors $D_0$ through $D_6$ .....	168

<b>Table 6.8</b> Modulus Relationship for the Sections with 150 mm Base Using Sensors D <sub>0</sub> through D <sub>6</sub> .....	169
<b>Table 6.9</b> Mix Properties for HMA Wearing Surface for Sections A through H.....	173
<b>Table 6.10</b> Mix Properties for HMA Wearing Surface and BM 25.0 Layer for Sections A through H .. .....	173
<b>Table 6.11</b> Laboratory Measured HMA Resilient Modulus (MPa) of Field Cores .....	174
<b>Table 6.12</b> Ratio between Backcalculated Resilient Moduli and Laboratory Measured Moduli ...	175
<b>Table 7.1</b> Computed and Field-Measured Stresses (November 2000). .....	199
<b>Table 7.2</b> Computed and Field-Measured Stresses (April 2001) .....	200
<b>Table 7.3</b> Percentage Differences for November and April for 40 kN Loading.....	204
<b>Table 7.4</b> Percentage Differences for November and April for 49 kN Loading.....	204
<b>Table 7.5</b> Percentage Differences for February and August for 40 kN Loading .....	204
<b>Table 7.6</b> Percentage Differences for February and August for 49 kN Loading .....	205
<b>Table 7.7</b> Calculated and Field Measured Strains.....	207
<b>Table 7.8</b> Percentage Differences between Measured and Computed Strains.....	208

## LIST OF FIGURES

<b>Figure 1.1</b>	Common Features of All Backcalculation Analyses Approaches .....	5
<b>Figure 2.1</b>	Typical Backcalculation Procedure .....	22
<b>Figure 2.2</b>	Stress on semi-infinite plane .....	24
<b>Figure 3.1</b>	Falling Weight Deflectometer (FWD) Unit .....	60
<b>Figure 3.2</b>	In situ Subgrade Moduli Using $D_0$ .....	63
<b>Figure 3.3</b>	Subgrade Moduli Versus Applied Pressure .....	64
<b>Figure 3.4</b>	Surface Moduli Using Synthetic Deflections Basins .....	65
<b>Figure 3.5</b>	Subgrade Moduli Using All Loads .....	66
<b>Figure 3.6</b>	Computed Surface Moduli Using Deflections Measured Utilizing the Large Plate on Top of the Subgrade .....	68
<b>Figure 3.7</b>	Computed Surface Moduli Using Deflection Measured Utilizing the Small Plate on Top of the Subgrade .....	68
<b>Figure 3.8</b>	Synthetic Normalized Deflection Basins for the Large Plate on Top of the Subgrade ..	70
<b>Figure 3.9</b>	Synthetic and Measured Normalized Basins for the Large Plate on Top of the Subgrade (Section E) .....	71
<b>Figure 3.10</b>	Measured and Computed Deflections for Sections A and B from Small .....	74
<b>Figure 3.11</b>	Measured and Computed Deflections for Sections C and D from Small Plate .....	74
<b>Figure 3.12</b>	Measured and Computed Deflections for Sections E and F from Small Plate .....	75
<b>Figure 3.13</b>	Measured and Computed Deflections for Sections J from Small Plate .....	75
<b>Figure 3.14</b>	Measured and Computed Deflections for Sections K from Small Plate .....	76
<b>Figure 3.15</b>	Measured and Computed Deflections for Sections A and B from Large Plate .....	76
<b>Figure 3.16</b>	Measured and Computed Deflections for Sections C and D from Large Plate .....	77
<b>Figure 3.17</b>	Measured and Computed Deflections for Sections E and F from Large Plate .....	77
<b>Figure 3.18</b>	Measured and Computed Deflections for Sections J from Large Plate .....	78
<b>Figure 3.19</b>	Measured and Computed Deflections for Sections K from Large Plate .....	78
<b>Figure 3.20</b>	Depth to Bedrock Estimation for the Synthetic Basins (Large Plate) .....	79
<b>Figure 3.21</b>	Comparison between Assumed and Estimated Depth to Rigid Foundation Using Synthetic Basins (Large Plate) .....	80
<b>Figure 3.22</b>	Depth of Stiff Layer Estimation for Section A .....	80
<b>Figure 3.23</b>	Depth of Stiff Layer Estimation for Section J using Deflection from Subgrade and Wearing Surface respectively .....	81
<b>Figure 3.24</b>	Average Subgrade Moduli Determined Using Different Analyses Summarized in Table 3.7 .....	85

<b>Figure 4.1</b>	Pavement Design for the Virginia Smart Road .....	94
<b>Figure 4.2</b>	Deflection Bowls for Sections A through D in August 2000 .....	95
<b>Figure 4.3</b>	Deflection Bowls for Sections A through D in January 2001 .....	96
<b>Figure 4.4</b>	Deflection Bowls for Sections A through D in February 2001 .....	96
<b>Figure 4.5</b>	Deflection Bowls for Sections A through D in April 2001 .....	97
<b>Figure 4.6</b>	Deflection Bowls for Sections E through H through in August 2000 .....	97
<b>Figure 4.7</b>	Deflection Bowls for Sections E through H through in January 2001 .....	98
<b>Figure 4.8</b>	Deflection Bowls for Sections E through H through in February 2001 .....	98
<b>Figure 4.9</b>	Deflection Bowls for Section E through L in April 2001 .....	99
<b>Figure 4.10</b>	Deflections on the Instrumented Lane in April and May 2000 .....	99
<b>Figure 4.11</b>	Variability of Center Deflections Measured in May 2000 .....	100
<b>Figure 4.12</b>	Variability of Center Deflections Measured in August 2000 .....	101
<b>Figure 4.13</b>	Deflection Bowls for Sections E through H through in August 2000 .....	101
<b>Figure 4.14</b>	Deflection Bowls for Sections E through H through in January 2001 .....	102
<b>Figure 4.15</b>	Deflection Bowls for Sections E through H through in August 2000 .....	102
<b>Figure 4.16</b>	Variability of Center Deflection Measured in July 2001 .....	103
<b>Figure 4.17</b>	Variability of Center Deflection Measured in August 2001 .....	103
<b>Figure 4.18</b>	Variability of Deflection Measured by Sensor 8 in May 2000 .....	104
<b>Figure 4.19</b>	Variability of Deflection Measured by Sensor 8 in April 2000 .....	104
<b>Figure 4.20</b>	Temperature Correction Relations for Sections A through D .....	108
<b>Figure 4.21</b>	Temperature Correction Relations for Sections E through H .....	108
<b>Figure 4.22</b>	Temperature Correction Relations for Sections I through L .....	109
<b>Figure 4.23</b>	Average Section Deflections (after Temperature Correction) for 2000-2001 .....	109
<b>Figure 4.24</b>	Comparison of Deflection-Correction Models for Center Deflections Under FWD Load .....	111
<b>Figure 4.25</b>	Temperature Correction Factor for the Maximum Deflection .....	112
<b>Figure 4.26</b>	Deflection Reduction (%) from 35 to 5 °C .....	113
<b>Figure 4.27</b>	Deflection Reduction (%) from 25 to 15 °C .....	113
<b>Figure 5.1</b>	Pavement Design for the Virginia Smart Road .....	124
<b>Figure 5.2</b>	Computed Surface Moduli Using Deflections Measured with the Large Plate on Top of the Subgrade .....	136
<b>Figure 5.3</b>	Depth to Stiff Layer Estimation for Section G .....	137
<b>Figure 5.4</b>	Resilient Moduli of BM-25.0 Layer at Different Testing Periods from FWD .....	141
<b>Figure 5.5</b>	Backcalculated Resilient Moduli of BM-25.0 Layer Versus Temperature .....	142

<b>Figure 5.6</b> HMA Resilient Moduli for Sections A through D .....	143
<b>Figure 5.7</b> HMA Resilient Moduli for Sections E through H .....	143
<b>Figure 5.8</b> HMA Resilient Moduli for Sections I through L .....	144
<b>Figure 5.9</b> Resilient Moduli of the HMA for Sections A through H in January 2001 from Backcalculation Software .....	148
<b>Figure 5.10</b> Resilient Moduli of the HMA for Sections A through H in April 2001 from Backcalculation Software .....	149
<b>Figure 5.11</b> Resilient Moduli of the HMA for Sections A through H in October 2001 from Backcalculation Software .....	149
<b>Figure 6.1</b> Laboratory Measured Resilient Modulus for 21-B .....	160
<b>Figure 6.2</b> Theoretical Resilient Modulus Distribution .....	161
<b>Figure 6.3</b> Measured and Calculated Deflections for 21-B (Section A) .....	162
<b>Figure 6.4</b> Measured and Calculated Deflections for 21-B (Section B) .....	163
<b>Figure 6.5</b> Measured and Calculated Deflections for 21-B (Section C) .....	163
<b>Figure 6.6</b> Measured and Calculated Deflections for 21-B (Section E) .....	164
<b>Figure 6.7</b> Measured and Calculated Deflections for 21-B (Section H) .....	164
<b>Figure 6.8</b> Measured and Calculated Deflections for 21-B (Section K) .....	165
<b>Figure 6.9</b> Measured and Calculated Deflections for 21-B (Section L) .....	165
<b>Figure 6.10</b> Measured and Calculated Deflections for 21-B (Section J) .....	166
<b>Figure 6.11</b> Comparison between Laboratory Tested 21-B and Backcalculated Moduli for All Test Sections .....	170
<b>Figure 6.12</b> Backcalculated Moduli Using EVERCAL as a Function of the Bulk Stress in the Center of the Layer .....	170
<b>Figure 6.13</b> Laboratory - Backcalculated (using EVERCAL) Moduli Comparison .....	171
<b>Figure 6.14</b> Laboratory Resilient and Backcalculated Moduli at 5 °C .....	175
<b>Figure 6.15</b> Laboratory Resilient and Backcalculated Moduli at 25 °C .....	176
<b>Figure 6.16</b> Laboratory Resilient and Backcalculated Moduli at 40 °C .....	176
<b>Figure 6.17</b> Variation of Temperature with Depth in the Wearing Surface and BM-25.0 Layer for One of the Sections .....	177
<b>Figure 7.1</b> Flexible Pavement Design of the Virginia Smart Road .....	185
<b>Figure 7.2</b> Pressure Cell .....	187
<b>Figure 7.3</b> H-type strain gage .....	187
<b>Figure 7.4</b> Temperature Correction Model .....	190

<b>Figure 7.5</b> Backcalculated Moduli Using EVERCALC as a Function of the Bulk Stress in the Center of the Layer..	193
<b>Figure 7.6</b> Compressive Stress Response of Pressure Cell AP2-1 from FWD Loading Testing..	194
<b>Figure 7.7</b> Tensile Strain Response of Strain Gauge DSH1-2L during FWD Testing. ....	194
<b>Figure 7.8</b> Stress Reponses Collected in January 2001 for Instrument AP2-1. ....	196
<b>Figure 7.9</b> Stress Reponses Collected in January 2001 for Instrument BP5-3. ....	196
<b>Figure 7.10</b> Stress Reponses Collected in January 2001 for Instrument DP1-2. ....	197
<b>Figure 7.11</b> Stress Reponses Collected in January 2001 for Instrument AP7-2. ....	197
<b>Figure 7.12</b> Stress Reponses Collected in January 2001 for Instrument DP4-1. ....	198
<b>Figure 7.13</b> Measured and Computed Stresses for 40 kN Loading in February 2001 and August 2001. ....	202
<b>Figure 7.14</b> Measured and Computed Stresses for 40 kN Loading in February 2001 and August 2001 .....	203
<b>Figure 7.15</b> Creep Master Curve for Section B .....	206
<b>Figure 7.16</b> Measured (DSH1-2L) and Calculated Strains at Temperatures 30°C and 45°C .....	209
<b>Figure 7.17</b> Number of Cycles to Failure for 31 kN Load at Different Temperatures .....	211
<b>Figure 7.18</b> Number of Cycle to Failure for 40 kN Load at Different Temperatures .....	212
<b>Figure 7.19</b> Number of Loading Cycles as a Function of Resilient Moduli for the Types of Analysis .....	212

## CHAPTER ONE

### 1.1 INTRODUCTION

With the aging of the nation's infrastructure, the need for reconstruction and rehabilitation of most of the highway network in the United States has become increasingly important. The remaining life of pavement systems showing signs of structural deficiency that requires strengthening needs evaluation as part of the redesign and rehabilitation process, because it is known that considerable savings in the rehabilitation cost can be made by accurately predicting the structural capacity of the existing pavement system. Therefore it is important to be able to determine the structural condition of a given pavement with a reliable form of measurement or instrumentation.

Pavements may be designed empirically, mechanistic-empirically and mechanistically. Full and defensible implementation of mechanistic pavement design methodologies still requires validation of "theoretical" materials models versus true performance within a pavement, and comparison of real pavement performance with design method predictions. Furthermore, current models essentially rely on incremental-static loading analyses, whereas pavements undergo continuous-dynamic vehicular and environmental loadings.

Pavements deteriorate under the combined action of loading and environmental affects, with the rate of disintegration or permanent deformation being related to the critical stresses and strains in the pavement layers. To predict pavement performance for design or rehabilitation purposes, the critical stresses and strains must be known. These stresses and strains are related to the structural capacity of a pavement system. Flexible pavement distresses are said to be related to (a) the tensile strain at the bottom of hot-mix asphalt (HMA) layer and (b) vertical compressive strain on the top of the subgrade (Yoder and Witczak, 1975).

In the mechanistic-empirical method, theoretical models are used to analyze stress, strain and deformation responses for given loadings in a pavement structure, whereas performance models for predicting roughness, rutting, and cracking based on these responses are empirical. Pavements are modeled as a multilayered elastic or viscoelastic structural systems. Viscoelastic behavior implies that the pavement exhibits elastic behavior at high rates of loading and becomes viscous at low rates of loading. The emergence of the semi-empirical design procedures that are found in the AASHTO

Guide for Design of Pavement Structures (1986) has also created the need for methods to evaluate the elastic moduli of paving materials. In addition, the emphasis on pavement rehabilitation and maintenance activities has increased the need for in-situ evaluation. One of the widely used evaluation technique is falling weight deflectometer (FWD).

## 1.2 BACKGROUND

Stresses and strains can be determined by directly measuring them in the pavement, which is less prevalent, or by the indirect prediction of mechanistic analysis. The estimation of stresses and strains using mechanistic analysis requires a knowledge of the material's mechanical characteristics, such as elastic modulus and Poisson's ratio of each layer. Material moduli are normally obtained by laboratory testing, which is destructive or by nondestructive testing (NDT).

Laboratory testing of field obtained material samples (intact core or a recompacted specimen) can be used to approximate the in-situ response. For granular materials, the resilient moduli,  $M_r$ , is defined by an applied cyclic deviator stress ( $\sigma_1$ , vertical stress minus  $\sigma_3$ , horizontal stress) divided by the recoverable axial strain. The resilient modulus from a confined or unconfined and axially cyclic loaded cylindrical material specimen is defined as follows:

$$M_r = \sigma_d / \varepsilon_r \quad (1.1)$$

where,

$\sigma_d$  = applied deviator ( $\sigma_1 - \sigma_3$ ) stress; and

$\varepsilon_r$  = recoverable (resilient) axial strain.

For HMA the resilient modulus can be obtained using Hooke's Law:

$$E = \frac{1}{\varepsilon_{cTRx}} * \left( \sigma_{x_{corr}} - (\nu) * \sigma_{Y_{corr}} \right) \quad (1.2)$$

where,

$\sigma_{x_{corr}}$  = corrected horizontal point stress occurring at the center of the specimen's face; and

$\sigma_{Y_{\text{corr}}}$  = corrected vertical point stress occurring at the center of the specimen's face;

$\varepsilon_{cTR_x}$  = horizontal point strain at the center of the specimen's face.

Laboratory determination of moduli can, however, be extremely difficult due to the problems involved in reproducing the in-situ conditions of materials and obtaining the proper loading conditions. Therefore, nondestructive in-situ testing is preferable.

### 1.2.1 In-situ Nondestructive Testing

With the trend towards mechanistic pavement analysis and design, which are based on fundamental engineering principles, the use of deflection data has become more important.

Nondestructive testing uses deflection basin data generated from a typical loading device to quantify the response of a pavement structure to known load drops. These devices may be grouped into three categories: static deflection measurements, steady-state vibration, and impulse. One of the most common tools to measure nondestructive surface deflection is the falling weight deflectometer (FWD), which is an impulse deflection device (Frazier, 1991). The FWD has gained widespread acceptance, because it is believed to provide realistic deflection basin parameters that can be used as an input into a mechanistic pavement model. This may allow a quick and adequate determination of the structural condition of a given pavement (Ali and Khosla, 1985). It may also provide estimates of material properties for levels and frequencies of load similar to those exerted by truck wheels. Although other devices include the steady state vibration device (Dynalect and Road Rater), spectral analysis of surface waves, and laser measurements of deflections under moving loads are used (Lytton, 1989), more details are presented on FWD, because it is used in this study.

In the FWD testing, a weight is lifted to a given height above the pavement and dropped onto a spring buffer system. The spring-buffer system transfers the load to the pavement over approximately 30  $\mu\text{sec}$ . The load applied to the pavement and the vertical motions at various radial distances from the center of the load are measured by using velocity transducers. The load is adjusted by varying the drop height and weight. The width of the load pulse is controlled by buffer characteristics to simulate a moving wheel load and load ranges available from 5 kN to 245 kN. The deflections at the radial distances are calculated from outputs of the velocity transducers.

### 1.2.2 Backcalculation Techniques

Analysis of the deflection basin involves measurement of deflection at various distances from the load and selection of layer moduli such that the theoretical deflection basin matches the measured deflection values. Developments in analytical techniques, coupled with improved deflection measurement capabilities, have resulted in several backcalculation techniques widely used in pavement evaluation. During the past two decades, research in the area of backcalculation of multilayered pavement properties has grown dramatically (Graves and Drnevich, 1991). The moduli calculated under NDT are for a specific loading condition and for the environmental conditions at the time of testing. Structural evaluation of pavement deflection response using nondestructive testing data has been growing since the introduction of the static Benkelman beam in the early 1950's and progressing through various vibratory loading devices (Uzan *et al.* 1989).

Backcalculation process consists of various analytical techniques that include iteration, database searching, closed-form solutions, and simultaneous equations, using nonlinear regression equations developed from layered elastic analysis output data (May and Von Quintas, 1994). The iterative analysis procedure adjusts layer moduli, compares computed and measured deflections, and repeats the process until the theoretical and measured deflections reach an acceptable match. The database searching approach involves searching through a database of precalculated deflection basins calculated or computed from a factorial of known layer moduli and thicknesses until a basin that closely matches the measured deflection basin is found. The moduli derived from backcalculation are considered representative of the pavement response to load and can be used to calculate stresses and strains in the pavement structure. A schematic of the backcalculation procedure is shown in Figure 1.1. The backcalculated analysis had a significant effect on the magnitudes of the layer moduli.

Layered elastic theory has been used extensively for the backcalculation process, because flexible pavement analyses have been mainly based on elastic theory. However, there are quasi-static methods such as WESLEA, Boussinesq-Odemark transformed section methods, nonlinear elastic viscoelastic, and finite element methods. Generally, it is expected that the selection of a method for analyzing NDT data to determine layer moduli should be compatible with the analysis procedure that will eventually be used for designing the flexible pavement rehabilitation. The moduli obtained through backcalculation are used in a mathematical model to calculate stresses

and strains. The stresses and strains can then be used in distress models to evaluate damage accumulation under traffic and predict pavement failure. They can also be used to evaluate corrective measures, such as overlay thickness.

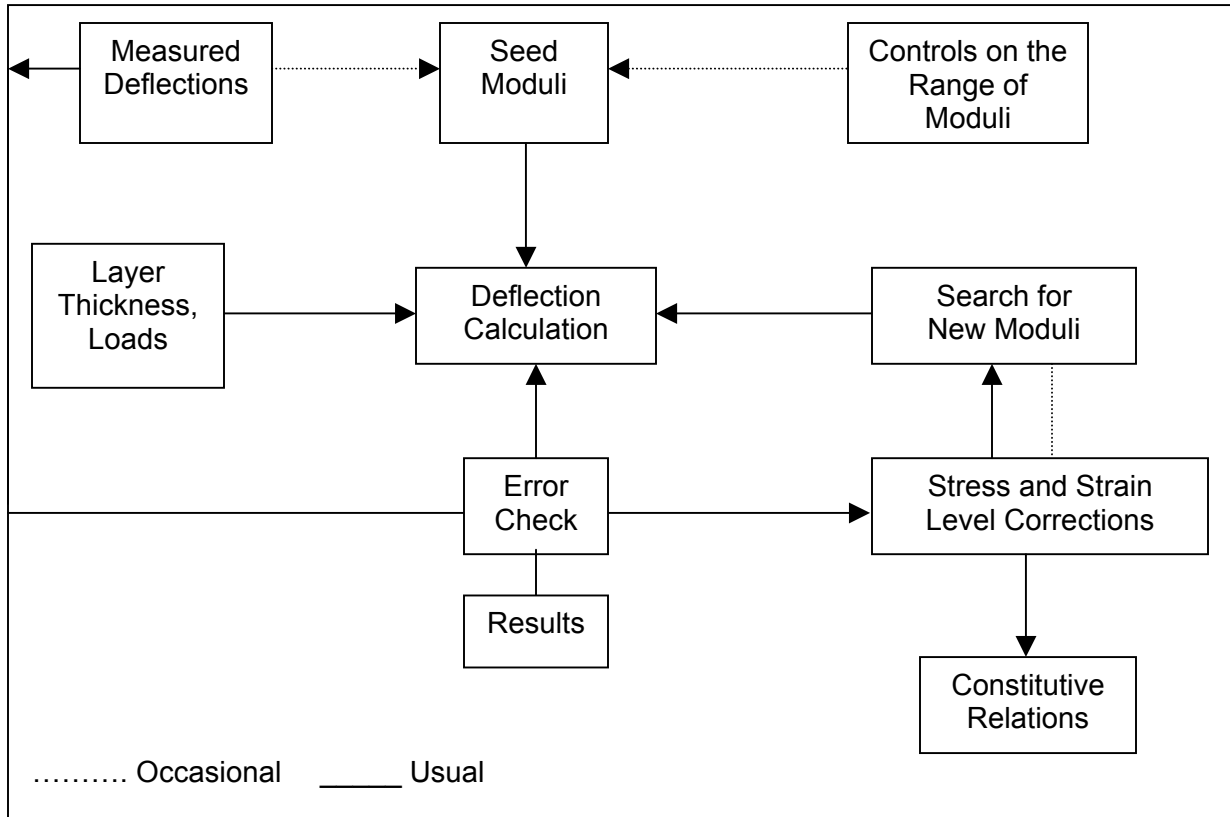


**Figure 1.1** Common Features of All Backcalculation Analyses Approaches.

The following are two typical models (Asphalt Institute and Shell equations, respectively) that show the relationship between the number of loading cycles to the fatigue failure of flexible pavement as a function of the hot-mix asphalt HMA modulus and tensile strain at the bottom of HMA:

$$N_f = 0.0685(\varepsilon_t)^{-5.671} (E_1)^{-2.363} \quad (1.3)$$

$$N_f = 0.0796(\varepsilon_t)^{-3.291} (E_1)^{-0.854} \quad (1.4)$$

where,

$\varepsilon_t$  = tensile strain at the bottom of the HMA;

$E_1$  = resilient modulus of the HMA layer; and

$N_f$  = the allowable number of load repetitions causing fatigue cracking.

The first backcalculation method is a closed form solution for two layers developed by Scrivner (1973), who based it on Burmister's equations:

$$\frac{4\pi wr}{3p} E_1 = 1 + \int_0^{10r/h} (\nu - 1) J_0(x) dx \quad (1.5)$$

where,

$w$  = surface deflection at a radial distance,  $r$ , from the applied load,  $p$ ;

$E_1$  = elastic modulus of the surface layer;

$h$  = thickness of the surface layer;

$J_0(x)$  = the Bessel function of the 0<sup>th</sup> order;

$x = mr/h$ , where  $m$  is a continuous variable of integration;

$\nu = (1 + 4Ne^{-2m} - N^2e^{-4m}) / [1 - 2N(1+2m)e^{-2m} + N^2e^{-4m}]$ ; and

$$N = \frac{E_1 - E_2}{E_1 + E_2}.$$

The ratio  $w_1r_1/w_2r_2$  was useful in analyzing Dynaflect deflection basins and a graph was developed illustrating the full range of values of the solutions. These solutions showed that two different modulus ratios may result in the same deflection ratio. It was, therefore, up to the pavement analyst to select a more reasonable value of the modulus ratio. Other empirical solutions developed to solve backcalculation also produced more than one solution.

When evaluating most backcalculation procedures, the following assumptions are usually made:

- The load is static;
- The materials are continuous and homogeneous; and
- A linear elastic relationship exists between strain and stress of the pavement materials, i.e. Hooke's Law applies.

Mathematically, the deflection may be calculated as follows:

$$w_i^c = f_i(E_k, \nu_k, h_k, r_i, O) \quad (1.6)$$

where,

$E_k, \nu_k$  = modulus of elasticity and Poisson's ratio of Layer  $k$  ( $k=1$  to  $n$  layers)

$h_k$  = thickness of layer  $k$ ;

$r_i$  = radial distance; and

$O$  = other variables, such as pressure, contact radius area, and interface conditions.

In the case of linear elasticity,

$$w_i^c = \frac{pa}{E_{sg}} f_i \left( \frac{E_1}{E_{sg}}, \dots, \frac{E_k}{E_{sg}}, \dots, \frac{E_n}{E_{sg}} \right) \quad (1.7)$$

where,

$p$  = pressure;

$a$  = radius of contact area; and

$E_{sg}$  = subgrade modulus of elasticity.

Many layered elastic solutions have been developed and are currently used by many of the highway agencies, researchers, and contractors. Besides the assumptions inherent to layered elastic theory, most of these solutions assume the following:

- The dynamic loadings can be modeled by the pseudo static load uniformly distributed over a circular area;
- The thickness and the number of layers comprising the pavement system are known; and
- The Poisson's ratio can be estimated.

All the self-iterative procedure solutions make use of computerized elastic layered solutions to backcalculate the layer moduli. However, all these assumptions are simplifications of a complex reality. Tam and Brown (1989) examined some of these simplifications and concluded that inertial effects were insignificant and a static model could be used. However, this conclusion differs from that obtained by other researchers as discussed below.

Deflection basins from dynamic loading differ in several respects from the deflection basins from static loading. A practice has developed over the years in which the data is analyzed using only the peak load and displacements together with an elastostatic model for estimating the pavement and subgrade moduli (Lytton 1989). Previous studies indicate that static analysis of the FWD data may, in general, lead to inaccurate estimates of pavement moduli (Mamlouk *et al.* 1994; Sebaaly *et al.* 1985, Shao *et al.* 1985). Roesset and Shao (1985) and Chang *et al.* (1992) have indicated that significant errors in predicted moduli may develop when inertial effects (due to the dynamic loading) are neglected. A rigorous elastodynamic analysis of the FWD

indicates that the inertia of the pavement plays a significant role in the displacement of the pavement (Stolle and Sedran, 1995). Foinquinos *et al.* (1995) suggest that dynamic deflection basins due to the FWD load can be substantially different from those obtained under static conditions. Their study also shows that when complete time histories of FWD deflections are stored, they can provide substantial insight into the properties of the pavement system. In addition, the dynamic effects of the load drops from the FWD should not be ignored in the deflection analysis.

Numerical analyses showed that the stress distribution under the FWD plate is reasonably uniform for rigid pavements, but is influenced by the plate-pavement interaction for flexible pavements (Boddapati and Nazarian, 1995). Uzan *et al.* (1990) have found that the deviation of assumption of uniform stress distribution could cause significant error of the deflection obtained from the sensors. The Royal Dutch/Shell Laboratory in Amsterdam began studying pavement dynamics using a road vibration machine in 1953 (Nijboer *et al.* 1953). They used both dynamic deflections and wave propagation to determine the stiffness of different pavement layers. Structural properties of a pavement were derived from the surface deflection by Classen *et al.* (1976), who also presented a deflection bowl under a test load. In 1977, Vaswani (1977) used the deflection shape and size of the deflected basin to evaluate the modulus of two layers. In 1980, Bush and Alexander (1985) investigated the use of layered theory in deflection basin measurements as part of pavement evaluation. Certain engineering properties of pavement materials were interpreted from FWD data by Magnuson *et al.* (1991) using dynamic analysis. Sebaaly and Holikatti (1994) have indicated that almost all the FWD field data had instantaneous deflection basins that greatly differed from the deflection basins generated by the peak response.

In addition to the linear and nonlinear responses, most pavement materials exhibit plastic, viscous, viscoelastic and/or viscoplastic responses under load (Rada *et al.* 1989). While there are still some problems that have not been fully resolved, especially in the interpretation of the measured data, a distinct nonlinear phenomenon (load dependence) has been noticed in the FWD measurements on pavements. Chang *et al.* (1992) have studied the occurrence of nonlinear behavior of pavement materials when using FWD testing and found that the nonlinear effects on the measured deflections are directly related to the magnitude of the load, the type of pavement, the stiffness of the subgrade, and the thickness of the pavement surface. They conclude that material nonlinearities are quite localized and are important for FWD tests on

flexible pavements where the subgrade is relatively soft and/or when the pavement is thin.

Dynamic modeling of the load response system may vary in complexity according to the structure analyzed (finite or infinite beam/plate, elastic or damped-elastic winkler foundation, or damped-elastic layers) and the loading (stationary, moving, constant, harmonic, or random). The solutions can vary from closed-form expressions using Fourier and Laplace transforms to numerical algorithms using direct time-integration methods, numerical convolution, and the method of complex response. On a field response and dynamic modeling of HMA sections under moving trucks, Chatti *et al.* (1995) have found that static analysis using backcalculated layer moduli appears to be sufficient in analyzing FWD field tests; however, static backcalculation using FWD (dynamic) deflections will lead to stiffened elastic properties.

All these findings make it clear that the layered elastic solutions are really an approximation of actual in-situ conditions. However, they provide the best compromise between practicality and exact theoretical solution at the present time. Analysis of data from some testing facilities, such as the WesTrack have repeatedly demonstrated that a solution based solely on the best possible match between the theoretical and measured deflection basins does not necessarily produce accurate or meaningful results (Seeds *et al.* 1999). Therefore, analysis of deflection data requires considerable engineering judgment for selecting the seed moduli and reasonable ranges of moduli in order to arrive at an acceptable set of moduli.

Also, for a fair assessment of the structural condition of pavement, the backcalculated moduli of HMA must also be corrected to a standard set of environmental conditions, especially temperature. Temperature correction may be investigated and validated in a more fundamental manner using mechanics and rheological data for asphalt binders and HMA, thus providing a theoretical basis for formulating accurate temperature-correction procedures.

In view of the variability of results due to some of the assumptions used in the analytical models, the validity of the models needs to be verified. This can be accomplished through direct measurement of stresses and strains. In one such attempt, Ullidtz (1996) installed three gages in a well compacted layer of sand, whose surface was loaded using an FWD with an average contact stress of 300 kPa. The measured and theoretical stresses were found to be in good agreement. The theoretical stress

was determined using Boussinesq's equation assuming the stress under the FWD loading plate followed a parabolic distribution:

$$\sigma_o(r) = 2 \sigma_0 \frac{a^2 - r^2}{a^2} \quad (1.8)$$

where,

$\sigma_0$  = mean stress level ( $\cong$  300 kPa) under the loading plate;

$\sigma_o(r)$  = mean stress at distance  $r$  from the center of the plate; and

$a$  = radius of the plate (150 mm).

For a rigid plate on a granular material, the stress distribution is approximated by a parabolic shape, since stresses close to zero are found at the edge of the plate. The theory of elasticity has established that the contact stress distribution under a perfectly rigid foundation increases from the center to the edge. The contact stress under a circular area, for values below the yield stress, is given by the following equation (Timoshenko and Woinowsky-Kreiger, 1959):

$$\sigma = \sigma_0 \frac{1}{\sqrt{1 - \left(\frac{r}{a}\right)^2}} \quad (1.9)$$

where,

$\sigma_0$  = average stress;

$C$  = constant;

$r$  = radial distance; and

$a$  = radius of the circular area.

A uniform stress distribution resulted in large difference between the measured and the calculated values at the centerline of the FWD. The measured stress was about twice that predicted from the theory of elasticity (Ullitz and Askegaard, 1996). Some of the factors that could have influenced the results are that the sand material was not an infinite half-space, but limited by different material, both at the sides and at the bottom, and also sand was not a linear elastic material. The use of a probabilistic stress distribution under the loading plate, as suggested by Harr (1977), resulted in the following equation that describes the point load:

$$\sigma_z = \frac{P}{2\pi\nu z^2} \exp\left(\frac{-r^2}{2\nu z^2}\right) \quad (1.10)$$

where,

P = point load;

z = depth;

r = horizontal distance; and

$\nu$  = coefficient of lateral stress (0.16 was used).

There was a good agreement between predicted vertical stresses and measured stresses. However, measurements of stresses and strains were recommended for different loading combinations and materials. Attempts were made to verifying backcalculation procedures through instrumentation of pavements sections with multidepth deflectometers (MDD) with some success with analysis based only on linear elasticity (Scullion *et al.*,1989). Multidepth deflectometers are used to measure depth deflection profiles of pavements. Effective elastic moduli of multilayered pavement structures can be backcalculated from these measurements.

It is recognized that a few problems inherent in the backcalculation approaches exist. Hence, verification of modulus backcalculation procedures remain a crucial concern particularly with the development of the new AASHTO design procedures that advocate NDT evaluations to determine current structural capacity for pavement rehabilitation designs.

### 1.3 PROBLEM STATEMENT

Analytical studies performed in the past two decades have highlighted the problems and errors associated with the currently used backcalculation methods. The difference between the calculated stresses and strains and the actual values in the pavement materials is highly dependent upon how well the mathematical model of the pavement structure represents the actual characteristics of the materials and the structured system. Pavement materials tend to be non-continuous (particulate), non-homogenous, anisotropic, viscous, plastic, viscoelastic as well as highly variable in space and time (Ullidtz *et al.* 1989). In the pavement industry, there are several backcalculation available procedures that can be applied to two, three or four layer pavement systems with or without the presence of a rigid bedrock layer. Most of these procedures use

linear elastic layered models, but while such models are simple and useful, they do have limitations. Similar theories are used in backcalculation analyses, where differences in the results are usually stem from using different software. The continuing development of similar backcalculation software only exacerbates this problem especially because newly developed software packages rather have little to differentiate them from the existing ones. Also, since pavement surface deflection measurements include irregularities resulting from pavement distress, variation in layer thickness, nonlinear material response, presence of bedrock, and/or moisture and temperature effects, there is a need to verify stresses and strains calculated using moduli from backcalculation that takes into account actual pavement properties and environmental factors such as temperature.

#### **1.4 OBJECTIVES**

In order to demonstrate the various ways of verifying instrument responses by means of backcalculation procedures; the main goal of this research was to calculate stresses and strains and compare them to measured values in the pavement. Falling weight deflectometer measurements were used to compare between in-situ measured and computed stresses and strains in pavement; linear and nonlinear elastic models were used to calculate stresses and strains at instrument locations; and viscoelastic analysis was used to calculate strains. During the steps taken to achieve the main goal of this study, the following objectives were investigated.

- Estimation of unbound material moduli utilizing FWD deflections measured using small and large loading plates.
- Investigation of the extent of spatial variability of deflections from FWD within and between different pavement sections.
- Develop a procedure for backcalculation of layer moduli from the Virginia Smart Road deflection data
- Development of a temperature-correction model to correct the backcalculated HMA resilient moduli.
- Comparison of various software approaches.
- Correlation between backcalculated and laboratory measured moduli of pavement materials.

## 1.5 SCOPE OF WORK

The dissertation is divided into eight chapters. Chapter one is an introduction. Chapter two presents the literature review. Chapter three presents the estimation of moduli of unbound material utilizing small and large loading plates. Chapter four discusses the spatial variability of FWD deflections within and between different pavement sections. The comparison of various software approaches and backcalculation moduli of the Virginia Smart Road pavement sections are presented in Chapter five. Chapter six presents the relationship between backcalculated and laboratory measured resilient moduli of subbase and HMA materials. Chapter seven presents the use of FWD to calibrate and validate FWD analysis approaches through comparison between in-situ measured and computed stresses and strains in the pavement. Summary, findings and conclusions are presented in chapter eight.

## REFERENCES

AASHTO (1986). American Association of State Highway and Transportation Official. "Guide for Design of Pavement Structures." Washington, D.C.

AASHTO (1993). American Association of State Highway and Transportation Official. "Guide for Design of Pavement Structures." Washington, D.C.

Ali, N. A., and Khosla, N. P. (1987). "Determination of Layer Moduli Using a Falling Weight Deflectometer." *Transportation Research Record 1117*, National Research Council, Washington, D.C., pp. 1-10.

Bush III, A.J. and Alexander, D.R. (1985). "Pavement Evaluation Using Deflection Basin Measurements and Layered Theory." *Transportation Research Record 1022*, National Research Council, Washington, D.C., pp. 16-22.

Chang, D. W., Kang, Y .V., Roesset, J .M., and Stokoe, K. H., II. (1992). "Effect of Depth of Bedrock on Deflection Basins Obtained with Dynaflect and Falling Weight Deflectometer Tests." *Transportation Research Record 1355*, National Research Council, Washington, D.C., pp. 8-16.

Chatti, K., Yun, K. K., Kim, H. B., and Utamsingh, R. (1995). "PACCAR Full-Scale Pavement Tests." Final Report Submitted to the California Dept of Transportation, Dept of Civil and Environmental Engineering, Michigan State University, East Lansing, MI.

Chatti, K., and Kyong, K. K. (1996). "SAPSI-M: Computer Program for Analyzing Asphalt Concrete Pavements under Moving Loads." *Transportation Research Record 1539*, National Research Council, Washington, D.C., pp. 88-93.

Cheng Ling Ong, Newcomb, D. E., and Siddharthan, R. (1991). "Comparison of Dynamic and Static Backcalculation Moduli for Three-Layer Pavements." *Transportation Research Record 1293*, National Research Council, Washington, D.C., pp. 86-93.

Chou, Y. J., and Lytton, R. L. (1991). "Accuracy and Consistency of Backcalculated Pavement Layer Moduli." *Transportation Research Record 1539*, National Research Council, Washington, D.C., pp. 72-85.

Classen, A. I .M., Valkering, C .P., Ditmarsch, R. (1976). "Pavement Evaluation with the Falling Weight Deflectometer." Proceedings of the Association of Asphalt Paving Technologists, Vol. 45, New Orleans, LA, pp. 23-35.

Frazier, P., Jr. (1991). "Estimation of Paving Materials Design Moduli from Falling Weight Deflectometer Measurements." *Transportation Research Record 1293*, National Research Council, Washington, D.C., pp. 42-51.

Foinquinos, R., Roesset, J. M., and Stokoe, K .H.,II (1995). "Response of Pavement Systems to Dynamic Loads Imposed by Nondestructive Tests." *Transportation Research Record 1504*, National Research Council, Washington, D.C., pp. 57-67.

Graves, R. C., and Drnevich, V. P. (1991). "Calculating Pavement Deflections with Velocity Transducers." *Transportation Research Record 1239*, National Research Council, Washington, D.C., pp. 12-23.

Harr, M. T. (1977). Mechanics of Particulate Media. McGraw-Hill, New York, NY.

Lytton, R. L., (1989). "Backcalculation of Pavement Layer Properties." *Nondestructive Testing of Pavements and Backcalculation of Moduli*, Von Quintas, H. L., Bush, A. J. III, and Baladi, G. Y., Eds., ASTM STP 1026, American Society for Testing and Materials, Philadelphia, PA, pp. 7-38

Magnuson, A. H., Lytton, R. L., and Briggs, R. C., (1991). "Comparison of Computer Predictions and Field Data for Dynamic Analysis of Falling Weight Deflectometer Data." *Transportation Research Record 1293*, National Research Council, Washington, D.C., pp. 61-71.

Mamlouk, M .S., and Davis, T. G. (1984). "Elasto-Dynamic Analysis of Pavement Deflections." *Journal of Transportation Engineering*, ASCE, Vol. 110, No. 6, pp. 536-550.

Nijboer, L. W. and Van der Poel, C. (1953). "A Study of Vibration Phenomena in Asphaltic Road Constructions." *Proceedings of the Association of Asphalt Paving Technologists*, Vol. 22, Houston, TX, pp. 197-231.

Scrivner, F. H., Michalak, C. H., and Moore, W. M. (1973). "Calculation of the Elastic Moduli of a Two-Layer Pavement System from Measured Surface Deflection." *Highway Research Record No. 431*, Highway Research Board, Washington, D.C., pp. 12-24.

Saraswatula, S. R. and Amirkhanian, S. N. (1992). "Pavement Management Systems – State of the Art, Pavement Management Implementation." ASTM STP 1121, Holtz, F. and Grambling, W. L., Eds., American Society of Testing and Materials, Philadelphia, PA, pp. 47-62.

Scullion, T., Briggs, R. C., and Lytton, R. L. (1989). "Using the Multidepth Deflectometer to Verify Modulus Backcalculation Procedures." *Nondestructive Testing of Pavements and Backcalculation of Moduli*, Von Quintas, H. L., Bush, A. J. III, and Baladi, G. Y.,

Eds., ASTM STP 1026, American Society for Testing and Materials, Philadelphia, PA, pp. 90-101.

Sebaaly, P. E., and Holikatti, S. (1994). "Phase Lag Effects on Analysis of FWD Data." *Nondestructive Testing of Pavements and Backcalculation of Moduli*, Von Quintas, H. L., Bush, A. J. III, and Baladi, G. Y., Eds., Vol. 2, ASTM STP 1198, American Society for Testing and Materials, Philadelphia, PA, pp 291-308.

Sebaaly, P., Davis, T. G., and Mamlouk, M. S. (1985). "Dynamics of Falling Weight Deflectometer." *Transportation Research Record 1022*, National Research Council, Washington, D.C., pp. 63-68.

Seeds, S., Alavi, S., Ott, W., Mikhail, M., and Mactutis, J. (1999). "Evaluation of Laboratory Determined and Nondestructive Test Based Resilient Modulus Values from WesTrack Experiment." *Nondestructive Testing of Pavements and Backcalculation of Moduli (Vol III) ASTM STP 1375*, Tayabji, S. D., and Lukanen, E. O., Eds., American Society for Testing and Materials, Philadelphia, PA, pp. 72-95.

Shao, K. Y., and Roeseet, J. M., (1985). "Dynamic Interpretation of Dynaflect and Falling Weight Deflectometer Tests." *Transportation Research Record 1022*, National Research Council, Washington, D.C., pp. 7-16.

Stolle, F. E. D., and Sedran, G. (1995). "Influence of Inertia on Falling Weight Deflectometer (FWD) Test Response." *Canadian-Geotechnical Journal*, Vol. 32, No. 6, pp. 1044-1048.

Timoshenko, S., and Woinowsky-Kreiger, S. (1959). Theory of Plates and Shells. McGraw-Hill, New York, NY.

Uddin, W., Meyer, A. H., Hudson, W. R., and Stokoe, K. H. II. (1985). "Project-Level Structural Evaluation for Pavements Based on Dynamic Deflections." *Transportation Research Record 1007*, National Research Council, Washington, D.C., pp. 37-45.

Ullidtz, P. and Ertman-Larsen, H. J (1989). "State of the Art? Stress, Strain and Deflection Measurements. State of the Art of Pavement Response Monitoring Systems for Roads and Airfields." Special Report 89-23, US Army Cold Regions Research and Engineering Laboratory Hanover, NH, pp. 148-161.

Ullidtz, P., Askegaard, V., and Sjolín, F. O. (1996). "Normal Stresses in a Granular Material under Falling Weight Deflectometer Loading." *Transportation Research Record* 1540, National Research Council, Washington, D.C., pp. 24-29.

Uzan, J., Lytton, R.L., and Germann, F. P. (1989). "General Procedure for Backcalculating Layer Moduli." *Nondestructive Testing of Pavements and Backcalculation of Moduli*, Von Quintas, H. L., Bush, A. J. III, and Baladi, G. Y., Eds., ASTM STP 1026, American Society for Testing and Materials, Philadelphia, PA, pp. 217-228.

Uzan, J., and Lytton, R. L. (1990). "Analysis of Pressure Distribution under Falling Weight Deflectometer Loading." *Journal of Transportation Engineering*, ASCE, Vol. 116, No. 2, pp. 12-30.

Van Cauwlaert, F. J., Alexander, D. R., White, T. D., and Barker, W. R. (1989), "Multilayer Elastic Program for Backcalculating Layer Moduli in Pavement Evaluation." *Nondestructive Testing of Pavements and Backcalculation of Moduli*, Von Quintas, H. L., Bush, A. J. III, and Baladi, G. Y., Eds., ASTM STP 1026, American Society for Testing and Materials, Philadelphia, PA, pp. 171-188.

Vaswani, N. K. (1977). "Determining Moduli of Materials from Deflections." *Journal of Transportation Engineering*, ASCE, Vol. 73, No. 12, pp. 125-141.

Yoder, E. J., and Witczak, M. W. (1975). Principles of Pavement Design, 2<sup>nd</sup> Edition, John Wiley & Sons, New York, NY.

Zafir, Z. (1993), "Moving Load Response of Layered Soil I: Formulation." *Journal of Engineering Mechanics*, Vol. 119, No. 99, pp. 2052-71.

## CHAPTER TWO

### LITERATURE REVIEW

#### 2.1 INTRODUCTION

The procedure of determining the Young's modulus of elasticity for pavement materials using measured surface deflections by working the elastic layer "backwards" is generally called backcalculation. Since the nature of road building has shifted in recent years toward preserving and rehabilitating existing roads, instead of building new ones, pavement rehabilitation projects involve the retention of most, if not all, of the layers in the existing pavement. It is therefore, important, as well as useful, to be able to test the pavement in place, nondestructively, and to process the data to determine the in situ layer moduli. This process involves backcalculation, a procedure that has gained popularity today because of important advances in the field of pavement engineering. Some of the advances listed by Irwin (2002) include the followings:

1. The realization that strong pavements have small deflections and weak pavements have large deflections, and pavement performance may therefore be related to deflection (concept developed over the period from 1935-1960).
2. The development of mechanistic theories that relate fundamental material properties to the stresses, strains, and deflections in a layered system (1940-1970).
3. The development of portable, accurate, and affordable instrumentation systems for measuring pavement deflections (1955-1980).

The advent of high speed digital computers has made it possible to accomplish the required computations in a reasonable amount of time. Also the development of equipment to provide pulse loading that would more closely approximate the timing and amplitude of a rolling wheel load began nearly simultaneously in the United States and in Europe. The use of a falling mass device to study seasonal changes in flexible pavements was reported by Isada (1966) and Bonitzer (1967) and Bohn *et al.* (1972) described the use of a falling weight deflectometer to evaluate pavement structural performance. In the United States, Isada (1966) reported on the use of a falling mass device to study seasonal changes in flexible pavements in the mid 1960's. Since there are now several methodologies and tools for backcalculation of layer moduli, it is important to review their history to establish a context for the verification of responses such as deflections, stresses and strains by means of performing backcalculation with

different types of software.

The last two decades have witnessed an explosion in the development of various types of equipment for nondestructive evaluation of pavement structure, including tools for backcalculation of layer moduli as well as methodologies. Lytton (1988) summarized the historical developments of nondestructive testing, backcalculation, theoretical considerations, and associated technologies. Examples of nondestructive evaluation applications include backcalculation of layer moduli and determination of the structural capacity of the pavement section, and the rate of deterioration of the pavement structure to identify the critical time for rehabilitation.

Nondestructive deflection measuring devices have been grouped into three categories: static deflection measurements, steady-state vibration, and impulse. Among the most used nondestructive surface deflection measuring equipment is the falling weight deflectometer (FWD), which is an impulse deflection device (Frazier, 1991). The FWD is believed to provide realistic deflection basin parameters that can be used as an input into a mechanistic pavement model to quickly and adequately determine the structural condition of a given pavement (Ali and Khosla, 1985). Deflection data collected from the FWD is used in performing a backcalculation procedure to determine the layer moduli of a pavement system.

Current backcalculation procedures involve the use of computer programs. Some of these are BISDEF, CHEVDEF, MODULUS, ELSDEF, ELMOD, EVERCALC, FPEDDI, ISSEM4, MODCOMP3, MODULUS, PADAL, WESDEF, and MICHBACK. Many of these software rely on the linear elastic layered theory for the basic structural model of the pavement system. Table 2.1 shows the main features of some of the backcalculation software. The primary criterion used for evaluating the accuracy of the results is based on the goodness of fit of computed deflections to measured deflections. Basically, these computer programs utilize forward calculation and a backcalculation scheme. Forward calculation methods are numerical, analytical or semi-empirical solutions to the response of pavement layers to an applied load. With these solutions, it is possible to backcalculate layer moduli by matching the predicted and the measured deflection basin by using a trial and error approach. Backcalculation schemes, developed as computer programs, perform these same operations, but in a more systematic manner. A typical scheme of a backcalculation program is shown in Figure 2.1. Uzan (1994) discussed some of the main backcalculation procedures and the essential differences between them and showed that some of these differences can lead

to different backcalculated moduli as a result of the differences in the forward computation models and different error minimization schemes.

**Table 2.1.** Examples of Backcalculation Software and Associated Features.

<b>Software</b>	<b>Pavement Type</b>	<b>Analysis Method</b>	<b>Moduli Calculation Method</b>	<b>Convergence Criteria</b>	<b>Forward Analysis Method and Program</b>	<b>Stresses and Strains*</b>
EVERCALC 5.0	Flexible	Static	Bowl Matching	Root Mean Square Error	Multilayered Linear Elastic, WESLEA	User defines positions
BOUSDEF	Flexible and Rigid	Static	Bowl Matching	Absolute Sum	Multilayered Linear Elastic, Boussinesq theory	Does not calculate
MODCOMP 5.0	Flexible and Rigid	Static	Bowl Matching	Root Mean Square Error	Multilayered Linear/Nonlinear Elastic, CHEVLAY2	forward calculation and user defines positions
PEDD	Flexible and Rigid	Static	Deterministic Equations and Bowl Matching	Minimum Absolute Difference	Multilayered Linear Elastic, ELSYM5	User defines positions
MICHBACK	Flexible	Static	Bowl Matching	Root Mean Square Error	Multilayered Linear Elastic, CHEVRON	Does not calculate
UMPED	Flexible and Rigid	Static	Deterministic Equations and Bowl Matching	Minimum Absolute Difference	Multilayered Linear Elastic, CHEVRON	User defines positions
ELMOD	Flexible and Rigid	Static	Bowl Matching	Root Mean Square Error	Odemark-Boussinesq (Method of Equivalent Thickness)	Fixed
MODULUS 5.0	Flexible and Rigid	Static	Bowl Matching	Root Mean Square Error	Multilayered Layer Elastic, WESLEA	No

\* Fixed or User Defines Positions

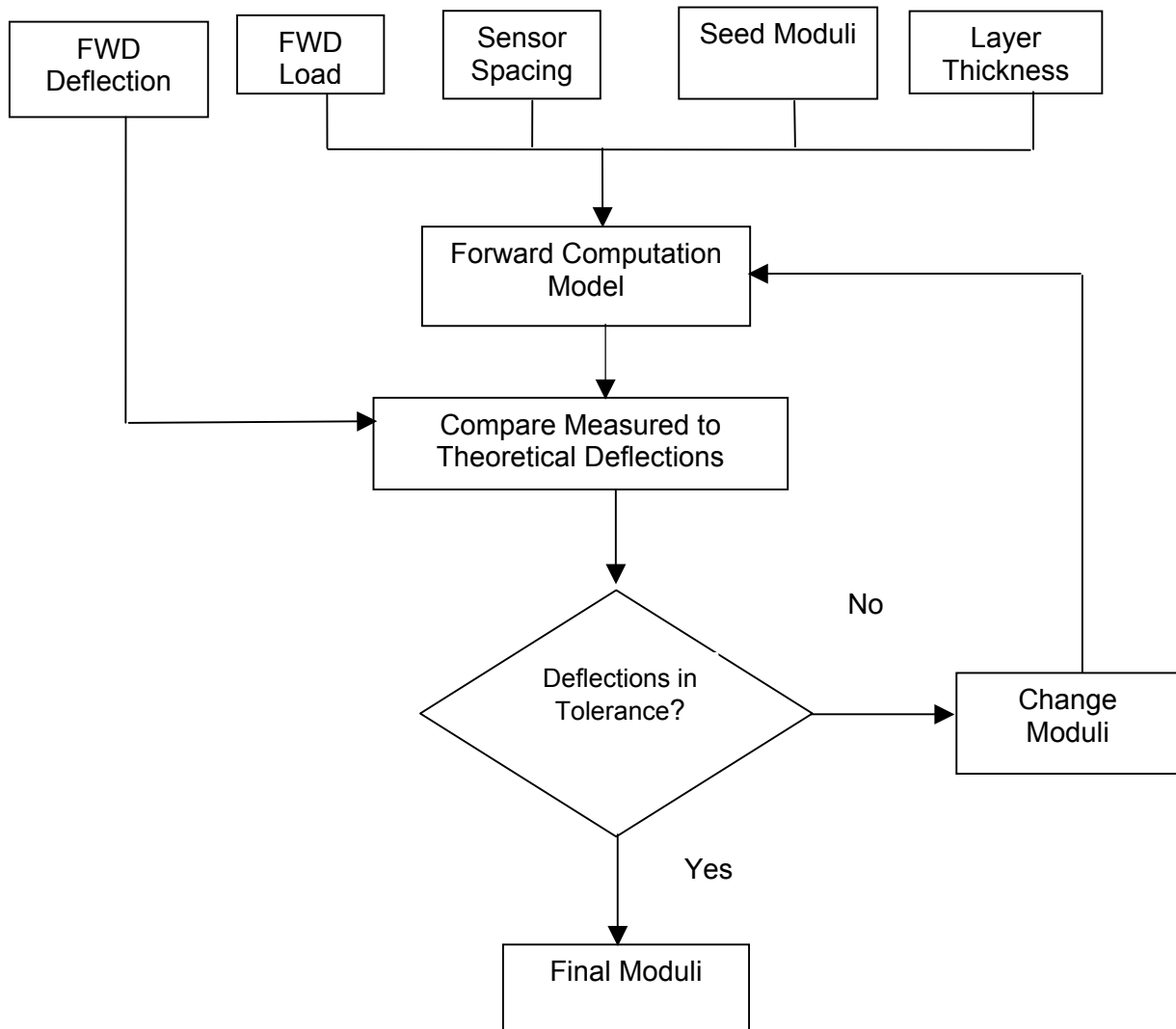


**Figure 2.1** Typical Backcalculation Procedure.

## **2.2 BACKCALCULATION PROCEDURES: FORWARD COMPUTATIONAL MODELS AND ERROR MINIMIZATION**

Theory of elasticity is by far the most widespread method used to determine pavement responses, i.e. critical stresses, strains or deflections in pavement layers caused by wheel loads in combination with environmental effects. Equations for calculating stresses, strains and displacements in a homogenous, isotropic and linear elastic semi-infinite space with modulus  $E$  and Poisson's ratio  $\nu$ , loaded by a point load, were

developed by Boussinesq (1885). Van Cauwelaert (1989) also presented the calculation of stresses and strains in a continuum using plane stress case. For linear elastic materials, the following three assumptions hold:

- Equilibrium
- Compatibility
- Hooke's law.

For plane stress condition, assumptions of equilibrium lead to

$$\frac{\delta\sigma_x}{\delta x} + \frac{\delta\tau_{xy}}{\delta y} = 0 \quad (2.1)$$

$$\frac{\delta\tau_{xy}}{\delta x} + \frac{\delta\sigma_y}{\delta y} = 0 \quad (2.2)$$

$$\tau_{xy} = \tau_{yx} \quad (2.3)$$

For compatibility conditions, assumptions leads to the following:

$$\frac{\delta^2\varphi_{xy}}{\delta x\delta y} = \frac{\delta^2\varepsilon_x}{\delta y^2} + \frac{\delta^2\varepsilon_y}{\delta x^2} \quad (2.4)$$

where  $\varphi$  is the shear (angular) strain.

Hooke's law for plane stress may also be written as follows:

$$\varepsilon_x = \frac{1}{E} [\sigma_x - \nu\sigma_y] \quad (2.5)$$

$$\varepsilon_y = \frac{1}{E} [\sigma_y - \nu\sigma_x] \quad (2.6)$$

$$\varphi_{xy} = \frac{2(1+\nu)}{E} \tau_{xy} \quad (2.7)$$

In solving equations 2.1 to 2.7, a stress function  $\phi$  is introduced to satisfy the following

equation:

$$\frac{\delta^4 \phi}{\delta x^4} + 2 \frac{\delta^4 \phi}{\delta x^2 \delta y^2} + \frac{\delta^4 \phi}{\delta y^4} = \left( \frac{\delta^2}{\delta x^2} + \frac{\delta^2}{\delta y^2} \right) \left( \frac{\delta^2 \phi}{\delta x^2} + \frac{\delta^2 \phi}{\delta y^2} \right) = \nabla^2 \nabla^2 \phi = 0 \quad (2.8)$$

The solution of the above equation is determined by the boundary conditions in linear elastic theory by separating the variables:

$$\phi(x, y) = \phi_1(x) \phi_2(y) \quad (2.9)$$

For a semi-infinite plane loaded by a uniformly distributed stress,  $p$ , over a width  $2a$  shown in Figure 2.2, the appropriate function for  $\phi_1(x)$  is

$$\phi_1(x) = \cos(mx) \quad (2.10)$$

where  $m =$  the integer 1, 2, 3.....

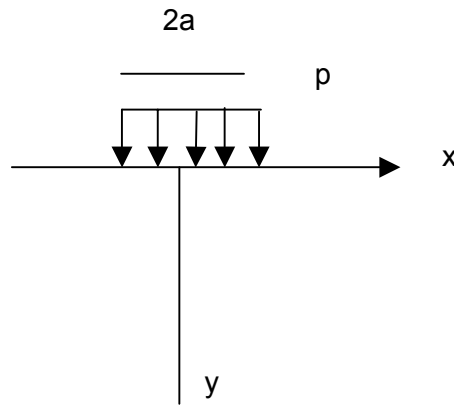


**Figure 2.2** Stress on semi-infinite plane.

The boundary condition for stresses at the surfaces are

$$\left. \begin{array}{l} \sigma_y = p \text{ for } -a < x < a \\ \sigma_y = 0 \text{ for } |x| > a \\ \tau_{xy} = 0 \end{array} \right\} \quad (2.11)$$

The final form of the stress function is

$$\phi = -\frac{2p}{\pi} \int_0^{\infty} \frac{\cos(mx) \sin(ma)}{m} (1+my)e^{-my} dm \quad (2.12)$$

The stresses at any point of the semi-infinite plane can now be calculated. Knowing the stresses, the strains can be found from equations 2.4 through 2.6. Since flexible pavements are layered systems with better materials that cannot be represented by a homogenous mass, the layered theory developed by Burmister (1943) must be used. With the advent of computers, this theory can be applied to a multilayer system of any number of layers (Huang, 1967, 1968a).

One of the current limitations in almost all linear elastostatic software used for backcalculation is that a uniform pressure is assumed for the applied load. This assumption, however, is flawed because the pressure distribution under the FWD is also affected by the profile of the pavement being tested. The other aspect of FWD testing that is typically ignored is the dynamic nature of the load. The dynamic effects are related to the pulse width as well as the variation in the stiffness of the subgrade. The presence of bedrock or stiff layers at a finite depth may result in amplification of the response. Several studies showing that when a rigid layer exists at some finite depth in the subgrade, the dynamic effect cannot be ignored (Davies and Mamlouk 1985; Chang *et al.* 1991) highlighted this limitation. Also, the duration of a FWD impulse is an important parameter that must be considered.

To develop layered theory, Burmister (1943) investigated the load and obtained exact solutions for the boundary stresses on the center line of a circular, uniformly distributed load acting on the surface of a three-layer half space. Computed codes with closed-form solutions for multilayered systems were also developed from the layered theory, and these are known as the forward computational models in many of the backcalculation programs. A lot of these forward computation models compute stresses, strains and displacements based on the following assumptions:

- Surface load is uniformly distributed.
- All layers are homogeneous, isotropic, and linearly elastic.
- Upper layers extend horizontally to infinity.
- Bottom layer is a semi-infinite half-space.

Examples of some of the forward models are BISTRO, developed by Shell and

modified to BISAR (Peutz, 1968), CHEVRON (Michelow, 1963), and other approximate methods, such as the Method of Equivalent Thicknesses (Ullidtz, 1977; and Lytton, 1989). BISAR can handle horizontally applied loads and also allows for variation in strain transfer at pavement interfaces. CHEVRON (Michelow, 1969), ELSYM5 (Ahlborn, 1972) and WESLEA (Van Cauwelaert *et al.* 1989) which were developed later solve the same formulation as in BISAR. Currently, to obtain a Burmister type solution, it is necessary to perform integration using digital computers:

$$\text{Deflection} = F \left[ \int_0^{\infty} f(e^{2mh}, e^{-2mh}, h) \cdot J_0(mr) \cdot J_1(mr) \cdot dm \right] \quad (2.13)$$

where,

F = Bessel's functions of  $J_0(mr)$ ;

f = Bessel's functions of  $J_1(ma)$ ;

m = parameter;

R= radial distance from the load axis;

a = loading radius; and

h = largest layer thickness considered.

Sivaneswaran *et al.* (1991) developed a technique based on the use of nonlinear least squares to achieve convergence between the measured and calculated deflection basin. Their backcalculation procedure is capable of backcalculating both layer thickness and layer moduli simultaneously. The method was adopted to a layered elastic program (Chevron N-layer). In their study, the researchers state four requirements of a backcalculation method. First, the backcalculation process must be able to recognize and correct small errors in layer moduli to develop an accurate solution. Secondly, it must be efficient enough to allow large amounts of data in the shortest possible period of time. Thirdly, the backcalculation method must converge to a correct solution, even under difficult circumstances. Finally, the fourth requirement is that the backcalculation method should be versatile. The nonlinear least squares optimization method was used to minimize the sum of the squared relative differences to solve the following problem:

$$f(E, h) = \frac{1}{n} \sum_{i=1}^n \left\{ \frac{d_i^c(E, h) - d_i^m}{d_i^m} \right\} \quad (2.14)$$

The error location  $i$  is defined as follows:

$$r_i(E, h) = \frac{d_i^c(E, h) - d_i^m}{d_i^m} \quad (2.15)$$

The above function can be expressed, after multiplying by the constant  $n$  simply for convenience, as follows:

$$f(E, h) = \sum_{i=1}^n (r_i(E, h))^2 = r^T r \quad (2.16)$$

where,

$r = \{r_1, r_2, r_3, \dots, r_n\}$  the relative error (residual); and

$T$  = transpose function.

The gradient of the criterion function is  $\nabla f = 2Ar$ ; where  $A = \{\nabla r_1, \nabla r_2, \dots, \nabla r_n\}$ ; and

the Hessian can be written as follows:

$$H = \nabla^2 f = 2AA^T + 2 \sum_{i=1}^n r_i \nabla^2 r_i. \quad (2.17)$$

The gradient and Hessian are the respective multi-dimensional equivalents of the slope and curvature of a one-dimensional function. In this formulation, the first part of the Hessian is known as soon as the gradient  $\nabla f$  has been evaluated. Since  $r^T r$  is being minimized, the relative errors are often too small. A good approximation to the Hessian may be made by neglecting the second part, in which case it is approximated by

$$H \approx 2AA^T. \quad (2.18)$$

A solution can then be obtained iteratively by incorporating the approximated Hessian into the Levenberg-Marquardt algorithm. This nonlinear squares approach has two main advantages: it converges faster than other methods, and since  $2AA^T$  is always positive, it indicates that the criterion function is convex and will have a unique minimum.

This advanced backcalculation procedure was applied to actual deflection basins

obtained from the Washington State Department of Transportation FWD. Conventional backcalculation software (ELMOD, ELSDEF, EVERCALC 2.0, ISSEM4, MODCOMP2) were used. Measured HMA and base thicknesses were utilized to backcalculate moduli of each of the three layers; HMA, base and subgrade. The average RMSE at convergence for the five software was 2.7%. The RMSE for the advanced backcalculation procedure was 0.8%. The backcalculated thicknesses and the backcalculated moduli were in good agreement with those backcalculated by the conventional programs. The results of analysis are shown in Table 2.2.

**Table 2.2** Backcalculated Moduli.

<b>Method</b>	<b>HMA</b>	<b>Base</b>	<b>Subgrade</b>	<b>RMSE (%)</b>
ELMOD	518	28	23	1.9
ELSDEF	550	27	25	5.8
EVERCALC 2.0	761	23	27	1.2
ISSEM4	592	25	28	n.a
MODCOMP2	686	22	29	1.8
Average	621	25.0	26.4	2.7
EVERCALC 4.0	656	22	27	0.8

The BOUSDEF (Zhou *et al.* 1988) and ELMOD backcalculation software are based on the method of equivalent thicknesses and modified Boussinesq equations. They also consider nonlinearity of pavement materials and overburden pressure. The method of equivalent thicknesses (Ullidtz and Peattie, 1980) assumes that any two layers with similar structural stiffness will distribute loading the same way. This assumption allows the conversion of a multilayered structure to one layer with an equivalent stiffness by using the following relationship:

$$D = \frac{E h^3}{12(1-\nu^2)} \quad (2.19)$$

where,

D= stiffness;

H= layer thickness;

E = modulus of elasticity; and

$\nu$  = Poisson's ratio.

For a two layer system, the equivalent thickness of a layer with modulus  $E_2$  and Poisson's ratio  $\nu_2$  relative to a layer of thickness  $h_1$ , modulus  $E_1$ , and Poisson's ratio  $\nu_1$ , may be expressed by equating the stiffness of both layers:

$$D_1=D_2 \quad (2.20)$$

or,

$$D = \frac{E_1 h_1^3}{12(1-\nu_1^3)} = \frac{E_2 h_2^3}{12(1-\nu_2^3)} \quad (2.21)$$

Rearranging the equation gives:

$$h_2 = h_1 \left[ \frac{E_1(1-\nu_2^2)}{E_2(1-\nu_1^2)} \right]^{1/3} \quad (2.22)$$

A general form of the equation can be written as follows:

$$h_{ei} = \sum_{i=1}^{n-1} h_i \left[ \frac{E_i(1-\nu_{i+1}^2)}{E_{i+1}(1-\nu_i^2)} \right]^{1/3} \quad (2.23)$$

where,

$h_{ei}$  = equivalent thickness for ith layer;

$h_i$  = thickness of ith layer;

$E_i$  = modulus of ith layer; and

$\nu_i$  = Poisson's ratio for ith layer.

Using the equivalent thickness method, the Boussinesq equation for calculating deflection at a depth  $z$  and radius  $r$  in an elastic half-space can be applied to a multilayer elastic system. The general equation for deflection due to a point load is the following:

$$d_{z,r} = \frac{(1+\nu)P}{2\pi R E} \left[ 2(1-\nu) + \cos^2 \theta \right] \quad (2.24)$$

where,

$d_{z,r}$  = deflection at depth  $z$  and radius  $r$ ;

$P$  = point load;

$R$  = distance from point load to the location where deformation occurs;

$E$  = modulus of elasticity; and

$\theta$  = angle between centerline of load and location of analysis.

For a uniformly distributed load, integration yields

$$d_z = \frac{(1+\nu)\sigma_0 a}{E} \left[ \frac{1}{[1+(a/z)]^{1/2}} + (1-2\nu) \left\{ \left[ 1+(z/a)^{1/2} - \frac{z}{a} \right] \right\} \right] \quad (2.25)$$

where,

$d_z$  = deflection on the load axis;

$\sigma_0$  = stress under the loading plate;

$a$  = radius of the loading plate; and

$z$  = depth where deformation occurs.

The equation 2.25 is valid only for calculation of deflections on the load axis. For points off the axis of the load, the integration cannot be carried out analytically. However for layered systems with a stiff top layer, Boussinesq's equation for a point load will give satisfactory results. Boussinesq also formulated equations for calculating stresses for a homogeneous, isotropic, linear, elastic semi-infinite space. For uniformly distributed load, the normal stresses can be determined using the following equations:

$$\sigma_z = \sigma_0 \left\{ 1 - \frac{1}{[1+(a/z)^2]^{3/2}} \right\} \quad (2.26)$$

$$\sigma_r = \sigma_t = \sigma_0 \left\{ \frac{1+2\nu}{2} - \frac{1+\nu}{[1+(a/z)^2]^{1/2}} + \frac{1}{2[1+(a/z)^2]^{3/2}} \right\} \quad (2.27)$$

where,

$\sigma_z$  = vertical stresses; and

$\sigma_r = \sigma_t$  = horizontal stresses.

The above equations are used to calculate stresses induced by loadings. These

equations are approximate. To obtain better agreement with exact theory of elasticity, Ullidtz and Peattie (1980) suggest that correction factors should be applied to the equivalent thicknesses. For the simple case of calculation on the axis of a uniformly distributed load, equation 2.22 is modified to:

$$h_{ei} = f \sum_{i=1}^{n-1} h_i \left[ \frac{E_1 (1 - \nu_{i+1}^2)}{E_{i+1} (1 - \nu_i^2)} \right]^{1/3} \quad (2.28)$$

where,  $f$  is a correction factor; for a 2-layer system,  $f = 0.9$ ; for a multilayer system (greater than 2 layers),  $f = 0.8$ .

The resilient properties of pavement materials, especially those that are unbound are stress dependent. The resilient moduli are usually approximated by the following relationships:

$$M_R = k_1 \theta^{k_2} \text{ for coarse grained materials} \quad (2.29)$$

$$M_R = k_1 \sigma_d^{k_2} \text{ for fine grained materials} \quad (2.30)$$

where,

$M_R$  = resilient modulus;

$\theta$  = bulk stress;

$\sigma_d$  = deviator stress; and

$k_1, k_2$  = regression coefficients that depend on material properties.

The BOUSDEF software takes into consideration the stresses in the pavement structure, the overburden stresses, and the load induced stresses. The total vertical stress  $\sigma_{vt}$  is the sum of the load-induced stress  $\sigma_{vl}$  and overburden pressure,

$$\sigma_{vt} = \sigma_{vl} + \sum_{i=1}^n h_i \gamma_i \quad (2.31)$$

where,

$h_i$  = the thickness of  $i$ th layer; and

$\gamma_i$  = density of  $i$ th layer.

The total horizontal stress  $\sigma_{ht}$  is a function of the load-induced horizontal stress  $\sigma_{hi}$  plus the horizontal stress due to overburden pressure:

$$\sigma_{ht} = \sigma_{hi} + K_o \sum_{i=1}^n h_i \gamma_i \quad (2.32)$$

where  $K_o$  is the coefficient of at-rest earth pressure.

Since pore water is a function of depth to ground water, its influence was not included. It was assumed that the ground water table is at a depth below the top of the subgrade and therefore does not affect the results. The software starts its run by reading data sets that include NDT load force and radius, pavement layer thicknesses, Poisson's ratio, minimum, maximum, and initial modulus, density of pavement materials, deflection data, percent tolerance to stop the deflection matching process, and number of iterations. By calling the subroutine DEFLECTION, which uses solution techniques described earlier, the initial modulus and layer thickness information are used to determine the equivalent thicknesses. Deflections for the given NDT load and load radius are calculated and then compared to measured deflections. If the sum of the differences is greater than the tolerance specified by the user, the program will start iterations by changing the moduli to compute a new set of deflections.

This process repeats until the sum of the differences is less than the tolerance or the maximum number of iterations has been reached. The moduli determined from each set of deflection basin data are used to calculate normal stresses induced by load. Stresses under the deadload of the upper pavement materials are also determined. For the base layer, bulk stresses in the middle of the layer are calculated. For the subgrade, deviator stresses on the top of subgrade are determined. These stress values and moduli are then regressed to find coefficients  $k_1$  and  $k_2$  for the both base layer and subgrade. The program has the capability of determining the following:

- (a) Resilient modulus for each pavement layer;
- (b) Bulk stresses and deviator stresses induced by both load and deadload of upper-layer pavement materials;
- (c) Coefficients  $k_1$  and  $k_2$  for base and subgrade layers appearing in the equations 2.29 and 2.30.

The BOUSDEF software (1988) was evaluated by comparing backcalculated results with hypothesized theoretical values. The comparison was done by assuming a set of pavement structures with different combinations of layer thicknesses and different resilient moduli. The surface deflections were calculated using the method of equivalent thicknesses together with the Boussinesq equations. An initial comparison of the

surface deflections calculated using Boussinesq equations, ELSYM5, and BISAR was made beforehand. The evaluated pavement structures included two cement treated base (CTB) systems and three Portland cement concrete (PCC) pavement structures. The comparison showed that deflections calculated from the Boussinesq equations, ELSYM5, and BISAR were similar for conventional and PCC pavements, but not as good for pavements with a stiff base (CTB). The closeness of the backcalculated moduli for all structures to the theoretical values indicated the BOUSDEF software has the capability of backcalculating the layer moduli from known deflections, layer thicknesses, and load data.

Lytton *et al.* (1979) developed another form of the equivalent layer method that uses a more general form of Odemark's assumption to convert a multilayered pavement into a single layer above a rigid base. Instead of the exponent of the modulus ratio ( $E_i/E_0$ ) being 1/3, a power  $n$  is used and is found by nonlinear regression analysis to depend on the thickness of the stiff upper layers. The deflection data used for this analysis were measured with a Dynaflect to provide the load and horizontal and vertical accelerometers to measure the displacement vectors at points on the pavement surface and with depth on each one of the 27 pavement sections at the Texas Transportation Institute Pavement Test Facility.

Lytton *et al.* (1979) modified the equation for the surface deflection derived from original work by Vlasov and Leontev (1966) to give the following expression:

$$w(r, z) = \frac{CP(1 + \nu_0)(2m + 1)}{\pi E_0 H'} K_0(\alpha r) \left( \frac{H' - z}{H'} \right) \quad (2.33)$$

and

$$\alpha = \frac{mB}{H'} \left[ \frac{2(2mb + 1)}{(2mB - 1)(1 - \nu_0)} \right]^{1/2} \quad (2.34)$$

where,

$H'$  = the transformed depth of the multilayered pavement above a rigid layer;

$z$  = the transformed depth of a point below the pavement surface where the vertical deflection is calculated;

$K_0(\alpha r)$  = the Bessel function of the second kind order, with argument,  $\alpha r$ ; and

B, C, m, n, H' = empirical constants to be found by nonlinear regression analysis on the measured deflection patterns on each pavement section.

The starting values of the constants B, C, m, n were all determined from field measurements. It was reported that experimentation showed that a good set of moduli could be determined in about one thousandth of the computer time required for backcalculation.

A backcalculation program PADAL (Brown *et al.* 1987; Tam, 1987) was developed in Nottingham, UK for the backcalculation of the elastic stiffness of pavement layers from deflection data measured using the FWD. In PADAL, the pavement is represented by a series of linear elastic layers. The nonlinear properties of the subgrade were incorporated by dividing the subgrade into five sub-layers, each with a different stiffness based on a stress-dependent elastic model derived from the results of laboratory testing. The limitations affecting the performance of PADAL included the modeling of subgrade nonlinearity in the vertical ignoring the stiffness variation with the radius. The PADAL does not consider the nonlinear behavior that unbound granular layers are known to exhibit, however since the iterative algorithm for the adjustment of layer moduli during backcalculation does not consider all the deflections measured, the final solution was affected.

The subgrade is divided into five sublayers of thicknesses increasing with depth, and stresses at the mid-depth of each sub layer and directly beneath the load center are considered for the calculation of subgrade elastic stiffness using the equation below:

$$E_r = A \left( \frac{p_o'}{q_r} \right)^B \quad (2.35)$$

where,

$p_o'$  = effective mean normal;

$q_r$  = deviatoric stress due to wheel loading; and

A, B = material constants.

The backcalculation software LEAD (Layered Elastic Analysis of Deflections) and FEAD (Finite Element Analysis of Deflections) have addressed some of these shortcomings. Both software use Gauss-Newton minimization techniques.

For describing the nonlinear response of unbound granular layers and coarse grained soils, the k- $\theta$  model presented in equation 2.29 (Hicks and Monismith, 1971) is

adopted by the LEAD software. Two parameters  $k_1$  and  $k_2$  are considered in the definition of the material behavior, while other models generally involve a greater number of constants. This property is very important in backcalculation, where the number of material constants to be determined influences the speed and convergence of the iterative process. Furthermore, the  $k$ - $\theta$  model assumes a constant value for Poisson's ratio.

The LEAD software (de Almeida *et al.* 1994) utilizes an approximate procedure to make the layer stiffness variable with radius. This new approach computes the surface deflection at a certain radial position using a set of stiffnesses for the nonlinear materials corresponding to the stresses at that same radial position. The subgrade and granular layer stiffness used for the calculation of the surface deflection at a distance  $r$  from the load center are obtained from the subgrade resilient moduli equations and the  $k$ - $\theta$  model equation when the stresses existing at the mid-depth of each sublayer at radius are considered. The FEAD backcalculation software was implemented because it produced more accurate results than the LEAD software since it could easily accommodate changes in material properties, allowing for variations in both the vertical and horizontal directions. In all these backcalculation software, PADAL, LEAD and FEAD, the Gauss-Newton minimization algorithm was used. Using the concept of least squares method, an error function  $f$  requiring the minimization shown below is used:

$$f = f(X) = \frac{1}{2} \sum_{K=1}^n W_k (dm_k - dc_k(X))^2 \quad (2.36)$$

where,

$k$  = sensor index;

$n$  = number of measured deflections (usually 7 for the FWD);

$W$  = weighting coefficient or weight;

$dm$  = computed deflection.

If all weights  $W_k$  are equal to 1,  $f$  represents half of the sum of the squares of the absolute deflection errors. If the weights  $W_k$  equal the inverse of the squares of the measured deflections  $dm_k$ , then  $f$  represents half of the sum of the squares of the relative deflection errors. There are several mathematical techniques for determining the minimum of a multi-variable nonlinear function, such as  $f(X)$ .

Given an estimate for a set of unknown parameters ( $X$ ), the adjustment vector  $\{\Delta X\}$  to be added to that set so as to minimize the error function defined by Equation

2.36 is obtained by solving the following simultaneous equations:

$$\{S\}\{\Delta X\}=\{R\} \quad (2.37)$$

where,

$\{S\}$  = sensitivity matrix, with a generic term given by:

$$S_{ij} = \sum_{K=1}^n w_k \frac{\partial dc_k}{\partial x_i} \frac{\partial dc_k}{\partial x_j} \quad i=1,\dots,m \quad j=1,\dots,m \quad (2.38)$$

$\{R\}$  = vector of residuals with a generic term given by:

$$R_i = \sum_{k=1}^n w_k (dm_k - dc_k) \frac{\partial dc_k}{\partial x_j} \quad j=1,\dots,m \quad (2.39)$$

This procedure is iterative; i.e. at step p of the computation, after Equation 2.37 has been solved, the unknown parameters are updated by using

$$\{X\}^P = \{X\}^{P-1} + \{\Delta X\} \quad (2.40)$$

The process is repeated until the variations in the unknown parameters become very small (lower than a predefined limit). At this stage, computation stops and the system is said to have converged at an optimal point.

Nonlinear materials, being stress dependent, exhibit variable moduli according to the level of stress (Almeida *et al.* 1994). This results in changes in moduli during backcalculation and, hence, changes in stress distribution. This interdependency between stiffness and stress makes convergence extremely difficult unless appropriate assumptions are formulated.

The backcalculation of nonlinear parameters, such as A and B in Brown's model (Equation 2.35) was accomplished using the Gauss-Newton method for backcalculation. These parameters can be treated as additional unknowns in the same way as the layer stiffness are considered for linear elastic materials. However, it was found that special provisions are needed to ensure convergence when nonlinear relationships are adopted. For unbound materials, numerical instability was overcome by use of correlations proposed by Rada and Witczak (1981) between coefficients  $k_1$  and  $k_2$  of the  $k$ - $\theta$  model. Based on a comprehensive set of laboratory tests, Almeida *et al.* (1994) concluded that

a relationship between the two parameters could be defined and regression analysis could be performed to work out the  $k_1$ - $k_2$  relationship.

In dealing with the subgrade, an evaluation of the nonlinearity of the subgrade is usually performed to simplify the tasks of backcalculating nonlinear parameters. The equivalent or composite elastic modulus at a certain radius is defined as that of a linear elastic half-space that yields the same surface deflection as the one measured at that radius. For distances corresponding to the furthest geophones of the FWD, these deflections depend almost exclusively on the subgrade and consequently the equivalent modulus becomes practically equal to the subgrade modulus. For linear elastic subgrades, a plot of composite modulus versus the radius shows the outer branch of the curve to be approximately flat. In the case of the nonlinear subgrade, this branch is not horizontal thereby indicating the variation of stiffness with the radius.

In addition to input data needed in pavement backcalculation, LEAD and FEAD require values of unit weight, suction, and the coefficient of lateral pressure ( $K_0$ ) for each pavement layer. These quantities were needed for the evaluation of the initial stresses in the pavement, when computing stress dependent elastic stiffnesses. The initial states of stress, due to overburden, pore pressure, compaction, and other residual effects often play an important role in the structural behavior of paving materials (Brown, 1979; Stewart *et al.* 1985).

Deflection data was collected during the FWD survey in Wakefield, UK. Deflection bowls representative of average pavement conditions, i.e. the ones closest to the theoretical 50<sup>th</sup> percentile bowl for each section were selected for backcalculation and analyzed using LEAD. The subgrade was modeled as nonlinear elastic using Brown's relationship for grained soils (1979). The subbase was modeled as linear elastic. The backcalculated moduli of the HMA layers and subbase from LEAD were compared to values obtained from PADAL as a means for assessing both programs. Resilient moduli were also determined in the laboratory using the repeated load indirect tensile test. Results of the testing program showed that moduli values from the laboratory were far lower than the backcalculated moduli from PADAL and LEAD. This could be explained by the fact that laboratory moduli were obtained using longer loading times than those of the FWD. The results from the LEAD software, however, compare better with the laboratory values. Software using the aforementioned concept have been utilized in this study. They are ELMOD, EVERCALC, MICHBACK and PEDMOD. Details about these software are presented in Chapter 5.

### 2.3 FACTORS AFFECTING BACKCALCULATED MODULI

Nazarian and Boddapati (1995) studied the effects of the plate-pavement interaction in light of the dynamic nature of the FWD load. To assess the significance of a non-uniform pressure distribution under dynamic loading on the measured and backcalculated parameters, they used two models. In the first model, the typical composite FWD loading plate on the pavement system was “discretized” in a finite element mesh. In the second, a uniform load distribution was assumed on top of the pavement. Deflection basins from three sets of numerical cases were compared to those measured in the field. The first set, designated as the control, corresponded to the elastostatic case with a uniform load applied to the pavement surface. The second set corresponded to the case where the dynamic nature of the load is considered, but the interaction between the FWD and the pavement is ignored. In the last set, both the FWD-pavement interaction and the dynamic nature of the load were considered.

The sensitivity analysis utilized as the control pavement section, a standard pavement section, was assumed to have three layers, an HMA layer over a granular base over a subgrade. Large variations between the deflections from the static and dynamic algorithms were observed. The variation is small for a sensor located 30 mm from the load, but increases to about 50% for a sensor located about 180 mm from the load. These difference emphasized the importance of considering the dynamic nature of the FWD loads. Based on the results of their study, the following conclusions were drawn:

- Deflections measured on flexible pavements could be significantly influenced by the FWD pavement interaction.
- The dynamic nature of the load significantly affected the deflections measured away from the load.
- The depth to bedrock and the duration of impulse interact to produce significantly different static and dynamic deflections, and both factors should be considered. If dynamic FWD pavement interaction is not considered, the remaining life may be significantly overestimated.

However, based on the results of other researchers (Sebaaly *et al.*, 1986, Stolle *et al.*, 1989), it appears that an overwhelming support exist for the practice of backcalculating pavement moduli using static analysis with FWD data.

### **2.3.1 Inertial Forces**

It has been implicitly assumed that the response of pavement to static or impact loading is similar to response of a moving load. However, with the use of high speed trucks and new giant aircraft, ignoring the inertial forces may not be appropriate. A special and crucial case where inertial forces must not be ignored is when there is frozen subgrade or shallow bedrock. Sebaaly and Mamlouk (1985) developed a set of differential equations for steady-state (harmonic loading) to compute stresses and strains in addition to displacements. Mamlouk *et al.* (1997) considered the effect of damping in the pavement materials. Damping is the internal energy dissipation (viscous effect) which occurs in real material subjected to dynamic loading. This dissipation in the ground occurs because the dynamic waves encounter increasingly larger volumes of material as they travel outwards. The damping ratio of the pavement materials was obtained in the laboratory by subjecting the specimen to harmonic loading and measuring the phase lag in the material response. In order to evaluate the accuracy of the theoretical analysis, field deflection measurements were compared to the computed values at different truck speeds at the AASHO Road Test for different truck types traveling at different speeds. Close agreement between the measured and computed deflections was found. This accurate prediction of stresses and deflections due to moving wheel loads may not be obtained using static analyses, however detailed examination of wide range of frequencies used for dynamic phenomena incorporating inertial damping suggests that no simple correlation between dynamic and static deflections can be developed at this time. The use of three dimensional dynamic finite element software has been advocated as the best means to incorporate inertia and damping effects but the computation time can be very long from 8 to 12 hours. Tam and Brown (1989) also concluded that inertial effects of the pavement were insignificant and a static model could be used, which is also consistent with research by Hardy (1990), who found that increasing the density of the layers in a dynamic layered elastic analysis had virtually no effect on the horizontal strain response at the base of the asphalt layer.

### **2.3.2 Spatial Variations**

Using a light weight deflectometer from tests completed directly on a subgrade material, Ullitdz (1987) found that the coefficient of variation of a normalized surface modulus was 50% over a 3 m interval with minimum and maximum values of 6.5 and 46 MPa,

respectively. The coefficient of variation was found to be less than 10% based on the subsequent analysis of the FWD data collected from tests on the pavement after its completion. The important point Ullidtz's tests make is the information on local variations in properties is usually lost when estimating properties from field data. Spatial variations are known to be due to the heterogeneous nature of the pavement materials and non-uniform layer thicknesses and it is present in all pavements and its magnitude depends to a great extent on such factors as construction quality. Spatial variations are incorporated into the pavement evaluation process through the selection of design values (deflections or predicted layer moduli) based on statistical variation. The use of the 85<sup>th</sup> percentile predicted layer moduli for evaluation of major roads and 50<sup>th</sup> percentile deflection values for low volume roads is done to eliminate factors that cause high degree of variability of moduli along the length of the road.

### **2.3.3 Effect of Thickness Variation**

In the structural evaluation process, pavement layer thickness is a variable whose variation and standard deviation cannot be easily measured even though these have a tremendous impact on the accuracy of the backcalculated material properties of the constituents of the pavement layers. Pavement layer thickness data is obtained principally from two sources: (i) plan sheets and (ii) measurements taken during material sampling activities at test pit locations. There are major disadvantages to both methods. Often the plans do not reflect variations in layer thickness resulting from construction activities. Deviations from the plans that become necessary during the construction are not shown on the drawings.

In 1990, the Texas Department of Transportation sponsored research projects with the Texas Transportation Institute with the objective of developing a swift, accurate, nondestructive method for measuring pavement layer thickness and their variations along the roadway (Briggs *et al.* 1991). Ground penetrating radar (GPR) was used to survey selected SHRP LTPP sites near College Station, Texas in order to determine how closely the GPR apparatus could predict HMA and base thicknesses and measure the moisture content of the base material. The results showed that differences between the thicknesses assumed from the SHRP database and those of the GPR measured approached 100 to 125 mm in some of the test sections. This finding raised the question of how these variations in pavement structure could affect the backcalculated

moduli of the paving materials if the pavement structure is assumed to be that stored in the SHRP data base. Falling weight deflectometer deflections were obtained from the four sections and pavement layer moduli were backcalculated using SHRP layer thicknesses and the thicknesses obtained with the GPR. Only the midlane deflections were used in the comparison to avoid the effects of any distresses that may have been present in the wheel paths. The MODULUS software was used for the backcalculation process. For the MODULUS runs using the assumed layer thicknesses, the software was run iteratively with the goal of achieving an average error of 2% or less per geophone.

Briggs *et al.* (1991) who conducted the study concluded that variations found in layer thicknesses on SHRP sites were large enough to cause up to 100% in backcalculated moduli of the surface modulus of the surface layer of the pavement. The variations also resulted in up to 80% error in base materials. The variations did not appreciably affect the backcalculated modulus of the subgrade. For reliable backcalculation results on pavement sections, some method of identifying and quantifying layer thickness variation must be used before the backcalculation process. Since the results also showed that it was possible to obtain small error terms with inaccurate moduli values, the success with which a calculated deflection basin is matched with a measured basin is not a good indicator of the accuracy of the backcalculated moduli.

#### **2.3.4 Effects of Pavement Discontinuities**

Pavement discontinuities such as cracks and/or joints, and subsurface conditions such as voids beneath rigid pavements lead to higher deflection readings and lower moduli. The magnitude of the deflection increase is dependent on the degree and severity of the cracks and joint spacing. However, while pavement discontinuities significantly affect measured deflections and backcalculated moduli, avoidance of testing over cracked areas would introduce measurement bias into the analysis. The effective layer moduli would not be representative of the overall pavement condition. Deflection testing at cracked areas only would also result in unrealistically low effective moduli.

### **2.4 CALIBRATION OF THE FALLING WEIGHT DEFLECTOMETER**

The three main error resulting from collection of the FWD data are seating errors, random

errors, and systematic errors. Irwin *et al* (1989) showed that deflection errors on the order of 2  $\mu\text{m}$  or less can have a large effect on backcalculated moduli. Random errors from the FWD data acquisition system is reduced or eliminated by repeating the test several times and using the average. Calibration of FWD has been developed by the Strategic Highway Research Program (SHRP) to reduce systematic error up to  $\pm 2\%$  of the load and deflection readings by calibrating FWDs to a reliable reference standard. This is to ensure that the SHRP owned FWDs have not drifted out of calibration and to certify state owned FWDs for SHRP LTPP data collection. These quality assurance practices are considered vital in determining accurate moduli of the pavement layers. This systematic error does not vary from time to time, but its magnitude varies from one transducer to another. The second source of error, which is a random error, comes from the analog to digital (a/d) conversion in the data acquisition system, typically with a range that is not more than  $\pm 2$  bits. Concern about the systematic error in the indicated load is relatively small; however, the consequence of errors in the indicated deflections is of greater concern. Using elastic layer theory, the deflection basin for a medium-strength 4-layer pavement system was calculated simulating the data that might be obtained from an FWD. They produced 30 sets of deflection basins. Since the moduli that were used to generate original deflections were known, they could be compared with the 30 sets of backcalculated moduli. The study showed that the influence of random deflection error is greatest for the first layer (ranging between  $-35$  to  $+45\%$ ) and least for fourth layer (almost nil). The results were based solely on the  $\pm 2 \mu\text{m}$  random error. If a  $\pm 2\%$  systematic error had also been incorporated, the effects would have been more dramatic. The finding shows that the importance of FWD calibration cannot be overemphasized.

## **2.5 VERIFICATION OF FIELD BACKCALCULATION WITH LABORATORY VALUES**

Resilient modulus can be determined by means of laboratory testing. Therefore, attempts have been made by researchers to verify backcalculation results from the field (from the FWD) with results from the laboratory testing.

There has been the general observation that two of the accepted methods for characterizing material properties (laboratory testing and backcalculation based on nondestructive testing) do not produce results that are in general agreement. Anderson and Wood (1975) found that moduli from laboratory testing are normally less than the in

situ results by 10 to several hundred percent. Harold and Killingsworth (1998) also conducted a comparison between laboratory and insitu moduli from the LTPP sites. They could not develop a relationship between laboratory and backcalculated moduli. They agreed that some correction for backcalculated moduli is required if a design procedure (such as that inherent in the AASHTO Guide for Design of Pavement Structures) is based on laboratory determined modulus values. Loulizi *et al.* (2002) showed that FWD load pulse simulated by a haversine wave with a time of 0.03 secs equivalent to the resultant pulse obtained from a truck traveling at 25 km/hr at a depth of 190 mm. Current laboratory testing procedures of HMA cores utilize a load pulse simulating a haversine wave of magnitude 0.01 secs. More research is needed to close the gap between laboratory-based resilient modulus and backcalculated resilient modulus to develop an appropriate correction factor (Mikhail *et al.*, 1999).

## **2.6 TEMPERATURE CORRECTIONS OF FWD TESTING**

Structural capacity (deflections and modulus) of the HMA layer is strongly influenced by ambient and pavement temperatures. In order to accurately determine the HMA moduli, a two step correction procedure has to be applied: Predicting temperature of the HMA layer and adjusting the FWD deflections or computed modulus to a reference temperature using a correction factor. The 1986 AASTHO Guide for Design of Pavement Structures presents a temperature correction protocol for FWD deflections. In the AASHTO procedure, the use of the average air temperature for the previous five days is used to predict pavement temperature at selected depths. Several practitioners suggested that the AASHTO procedure is inaccurate, especially at temperatures over 38°C (Johnson *et al.* 1992). Pavement engineers have also challenged its accuracy and practicality since this procedure does not take into account temperature gradient effects due to heating and diurnal heating cooling cycles. These cycles have a significant effect on the effective pavement temperature and its relationship with the HMA modulus and surface deflections (Stubstad *et al.* 1994, Kim *et al.* 1995).

Several researchers have developed models for temperature-modulus correction by addressing the issues enumerated, however, many of these models have been based on a statistical analysis of data obtained from a limited range of mixture types or pavement profiles. For example Johnson and Baus (1992) have recommended the following temperature correction formula based on an approximation from the Asphalt

Institute;

$$\lambda_E = 10^{-0.0002175(70^{1.886} - T^{1.886})} \quad (2.41)$$

where,

T = temperature in °F; and

$\lambda_E$  = the correction factor.

Other researchers, including Ullidtz (1987), have developed a model based on results from the AASHTO Road test data. Ullidtz's correction model is the following:

$$\lambda_E = \frac{1}{3.177 - 1.673 \log T} \quad (2.42)$$

for  $T > 1^\circ\text{C}$ .

Baltzer and Jansen (1994) and Kim *et al.* (1995) developed a correction model based on statistical analysis of backcalculated moduli and measured HMA temperatures in the following form:

$$\lambda_E = 10^{m(T-20)} \quad (2.43)$$

where,

m = 0.018 by Baltzer and Jansen and 0.0275 by Kim *et al.* (1995).

Kim *et al.* (1995) model was developed using data from North Carolina sites and also validated at different sites other than the test sites. The procedure they used was found to greatly improve the accuracy of temperature deflection correction procedures. However, the data, used to develop the model, was obtained from a limited number of pavements in fairly good condition.

Park *et al.* (2001) also developed a new temperature prediction model for HMA temperatures using six selected test sites in Michigan. The model was validated using temperature from the test sites and several other sites from the LTPP Seasonal Monitoring Program. Validation results for their model suggested that the model could be adapted to all seasons and other climatic and geographical regions. The model developed in Michigan also requires fewer parameters than other published models. Future research efforts is being focused on accurately predicting the mid-depth temperature from the air or surface temperature. In addition the accuracy of developed

models for pavement in different climatic regions and pavements with different damage states need to be quantified.

## **2.7 CASE STUDIES OF FIELD INSTRUMENTATION TO VERIFY FWD RESULTS**

Although attempts comparing responses (stresses, strains, and deflections) predicted by mathematical models used in backcalculation software to those measured in real pavements have been made over the years, no conclusive verification of a specific mathematical model have been introduced. It is clear from the literature review presented on some of the various backcalculation approaches that they cannot be verified by theoretical means only. Even the most sophisticated theoretical models such as dynamic, three dimensional viscoelastoplastic finite element approaches are based on simplifications. Infact, no theoretical model can constitute the “truth”, because they are all simplified models in reality (Ullitdz *et al.* 1988). One of the main purposes of backcalculation is to determine layer moduli that can be used in a forward calculation model to predict truck strains within the pavement. Laboratory testing has also been conducted extensively on pavement layers to supplement FWD procedures, but perfect agreement has never been attained. Laboratory testing has generally been performed under simulated stress conditions expected in the pavements under repeated vehicular loadings.

The research community tends to think the most promising method of backcalculation appears to be comparison of stresses and strains predicted or calculated to actual values measured in pavements. Although the measurement of stresses and strains is a complicated process, nevertheless, it could be the only solution. Pavement instrumentation serves as the key providing an accurate comparison of stresses and strains. However, the few cases of pavement instrumentation in parts of the United States and the world, notably Sweden and Denmark, have produced only partial success. The agreement between the measured and predicted strains was far from satisfactory and further studies have been recommended using other mathematical models.

Case studies on FWD testing done on instrumented sections have been carried out in different parts of the world, including four instrumented test sections, one in the Danish Road Testing Machine and the other three in southern Sweden. Layer moduli were backcalculated using different methods, and the stresses and strains in the

different layers were calculated and compared to the stresses and strains measured at the same locations with pressure and strain gauges. The instruments used in the experiments were believed to be reasonably accurate. The strain gages in the HMA layer had a low stiffness, but could under predict by about 10-20  $\mu$ strain. Three different response models were used.

The models based on the Odemark-Boussinesq approach; the elastic layer theory (such as MODULUS, WES5), and the Finite element method.

Ullidtz *et al.* (1994) briefly discussed the above models. In the first instance, deflection basins were measured with the FWD on the instrumented sections and, secondly, FWD testing was carried out on an hydraulic pad to ensure uniform stress distribution under the loading plate. The stresses and strains in the pavement structures were recorded. Stresses and strains were also measured under 11.5 ton axle load at different speeds. The moduli of pavement layers were then calculated using the three models, and the stresses and strains in the pavement were calculated with the corresponding moduli and models and compared to the measured values. The instrumented pavement in Denmark had a thin HMA layer of 64 mm on a 130 mm thick granular base course on 390 mm of granular subbase on a sandy moraine subgrade. The temperature during testing was around 8 °C.

The three sections in Sweden had HMA ranging from 135 to 190 mm, Macadam ranging from 120 mm to 600 mm, and a subbase ranging from 540 to 560mm. In situ testing was done at about 0 °C. In the Road Testing machine, the horizontal strains at the bottom of the HMA layer, base layer, and subbase layer were measured at various locations where there were strain gages, together with the vertical stresses at the top of the subgrade. The measured responses of the strain gages and pressure cells were compared to stresses and strains from the Odemark-Boussinesq approach, the MODULUS software, and a Finite Element programs. The results of the analysis showed both measured and computed values had a high degree of variation with coefficient of variation values of 20% and more. In one particular section, the predicted strain from the MODULUS was one-fifth the measured strain. The agreement between the measured and predicted strain was far from satisfactory and further studies using other mathematical models were recommended. Some of the strain gages were known to under register strain measurements by as much as 10-30 $\mu$ strain ( $10^{-6}$ m/m), and the presence of pressure cells could cause changes in the stress distribution in the layers. In an effort to verify modulus backcalculation procedures, Scullion *et al.* (1989) carried

out studies on pavement sections instrumented with Multidepth Deflectometers (MDD) at the Texas Transportation Institute. The MDD developed by the National Institute for Transportation and Road Research in South Africa, measures the transient deflection between a particular location in the pavement and an anchor located at 2.18 m below the surface. By placing MDD's in each pavement layer, procedures are developed to independently calculate the resilient modulus of each pavement layer. The response of the MDD instruments is measured under FWD loading, and two independent procedures were available for backcalculating layer moduli, one with the FWD sensor readings and the other with the MDD output. A measuring unit of the MDD is a linear variable differential transducer (LVDT) that is mounted inside a module that can be expanded to clamp onto the sides of the hole at the required depth. The MDD's are installed vertically at various depths in the pavement, usually at the interfaces of the pavement layers. At the surface of the pavement, the MDD is sealed with a brass surface cap and lid unit embedded in a polyurethane bedding compound. The top of the surface cap is installed flush with the surface of the pavement. The surface cap is removed during the measuring operation to enable a cable to be connected from the MDD to a computerized data acquisition system. The MDD's have proven to be extremely durable, with some installations being in operation for over five years. Maree *et al.* (1980) has reported that surface deflections measured independently with a deflection beam correlated very well with the deflections measured by the MDD modules.

A summary of the description and installation procedures of the MDD was done by De Beer *et al.* (1989). On the pavement test sections, the distance from the edge of the FWD load plate to the center for the MDD hole was fixed at 1140 mm. The FWD load was dropped at a range of load levels and both the FWD maximum surface deflection and the MDD depth deflections were recorded. The FWD geophones were located at 0, 304, 609, 1219, 1524, and 1829 mm from the center of the loading plate. There was close agreement between the measured and calculated deflection with depth. A generalized procedure for layer backcalculation developed by Uzan *et al.* was modified and used to calculate layer moduli from MDD deflection data. The BISAR linear elastic software was also used. Falling Weight Deflectometer surface deflection data was also analyzed with BISDEF, ELSDEF and the generalized procedure developed by Uzan (1989). Pavement temperatures were recorded at the middepth of the surface and base, respectively.

The FWD results (from the three programs) and MDD analysis produced similar

subgrade stiffness ranging from 138 to 165 MPa, when a finite subgrade depth was used. A semi-infinite assumption resulted in an overestimate of subgrade stiffness by 50%. Multidepth Deflectometer and FWD data produced comparable moduli at high load levels. At lower load levels, the base and subbase moduli were significantly higher. The ESLDEF program with the finite subgrade assumption also produced base and subbase results which were comparable with those from the MDD. Due to the partial success in interpreting the strength of pavement layers and verifying backcalculation techniques, future tests were planned to monitor MDD response under truck wheel loadings at different tire pressures.

In 1995, a full-scale HMA pavement test section was built through the collaboration of the University of California-Berkeley, the University of Washington, and PACCAR, Inc. The foil strain gage was used to measure the various strain responses. An Australian made MDD together with linear variable differential transformers, were also installed to measure pavement layer deflections. Strain gages were installed in the pavement section, and were also installed in axial cores to measure longitudinal and transverse strains at the top and bottom surfaces of the HMA layer were measured. Strain gages were also installed along the wheel paths at 300 mm intervals. To collect temperature data, a multi sensor temperature probe was used. All gages were installed by cutting/coring the existing pavement, because there was no new construction for the purpose of conducting tests. The pavement cross-section consisted of 130 mm HMA layer and 330 mm of crushed stone base.

The elastic moduli for each of the layers in the pavement structure was obtained by the backcalculation of FWD deflection data. The EVERCALC software was used. Two sets of moduli were used for the HMA layer. The first was the frequency dependent HMA properties since HMA is a visco-elastic material and its properties (modulus, damping ratio and Poisson's ratio) have been shown to be frequency dependent. For the frequency independent set, the value for the HMA modulus was backcalculated from FWD deflection. Dynamic analysis based on linear viscoelastic layer theory of the HMA layer was also carried out using the SAPSI finite element software. The FWD load was modeled as a haversine pulse with a duration of 30 ms. Using effective layer thicknesses from the axial cores and backcalculated layer properties, theoretical transient strains were calculated by SAPSI. The measured strains (from the gages) were compared to the calculated static strains from CHEVRON and dynamic strains from SAPSI.

Very good agreement existed between measured and predicted strains. During the earlier stages of the project, all the measured strains were within  $\pm 10\%$  of the calculated values. In 18 months, only 70% of the measured strains were within  $\pm 20\%$  of their calculated values. Time, temperature fluctuations, exposure to moisture, and refitting of the cores into pavement sections caused the sensitivity and reliability of the strain gages to decrease. The results constituted a good field verification for CHEVRON's closed form solution and SAPSI's finite element formulation. The EVERCALC backcalculation software uses linear elastic solution based on the CHEVRON software. The results of the testing also implied that static analysis of pavements using statically backcalculated layer moduli seems to be sufficient for an accurate prediction of the field response under stationary dynamic FWD pulse loads and is summarized by Chatti *et al.* (1995). Since data from MDD could not be obtained, there was no analysis of the MDD's.

The effect of truck speeds on the response of HMA pavements was significant. Increasing truck speeds from 0 to 64 km/hr reduced the peak tensile strain in the HMA layer to between 25 to 40%. Decreasing the tire pressure from 620 to 207 kPa reduced the tensile strain in the HMA layer by about 25 to 40%. Agreement between SAPSI's prediction and field measurements was not as good in the truck tests as in the FWD testing.

Two HMA test sections (I and II) built by Bryan and Caldwell in Texas were instrumented with MDD's (Akram *et al.* 1989). Surface deflection data was collected from the FWD data and from the MDD's and the truck loadings. To determine the transverse position of the truck tires relative to the MDD location, a grid was painted on the pavement surface next to the MDD hole. In the analysis of the field data by Akram *et al.* (1989), the FWD deflection data and the MDD data were matched using the linear elastic model. The moduli backcalculated were compared with those from laboratory testing. The modulus obtained was used to characterize the pavement structure, and the vertical compressive strains at the top of the subgrade from a known tire load was determined. The predicted subgrade strains were compared with those measured under the actual truck loads. Laboratory testing was also carried out by means of indirect tension tests on HMA cores and a resilient modulus test on remolded samples of the base. The tests were performed at 0.4, 5, and 10 Hz loading frequencies.

The backcalculated HMA moduli were considerably less than the laboratory results. There was reasonably good agreement between the laboratory and the

backcalculated results in the lower half of the base layer. The laboratory results indicated that the subgrade modulus on all the test sections to be frequency sensitive. The laboratory modulus increased with an increase in loading frequency and confining pressure. For comparing the measured and predicted subgrade strains under truck loadings, theoretical predictions under truck loadings were obtained from BISAR software using the backcalculated layer moduli and static axle loads. The calculated vertical compressive subgrade strains were compared with measured ones under the truck loadings. Akram *et al.* (1989) concluded from their testing (for both thin and thick sections) that using the FWD deflection resulted in over prediction of the subgrade modulus and an underestimation of the truck induced subgrade vertical compressive strains by 15 to 18%.

This review of the literature on FWD and case studies on instrumented test sections reveal a continuing need for reliable method for the verification of FWD backcalculated moduli results. A brief summary of the problems, limitations and adequacy of existing test methods have been presented. Many of these limitations and failures are addressed in greater detail in the subsequent chapters that seek to verify responses of instruments in the pavement sections.

## REFERENCES

AASHTO (1986). "American Association of State Highway and Transportation Official." Guide for Design of Pavement Structures, Washington, D.C.

Akram, T., Scullion T., and Smith, R. E. (1994). "Comparing Laboratory and Backcalculated Layer Moduli on Instrumented Pavement Sections." *Nondestructive Testing of Pavements and Backcalculation of Moduli*, Von Quintas, H. L., Bush, A. J. III, and Baladi, G. Y., Eds., ASTM STP 1198, American Society for Testing and Materials, Vol. 2, Philadelphia, PA, pp. 170-200.

Ali, N. A., and Khosla, N. P. (1987). "Determination of Layer Moduli Using a Falling Weight Deflectometer." *Transportation Research Record 1117*, National Research Council, Washington, D.C., pp. 1-10.

Anderson, D. G., and Wood, R. D. (1975). "Comparison of Field and Laboratory Shear

Modulus." Proceedings, In-situ Measurement of Soil Properties, ASCE, Vol.1, Raleigh, NC.

Baltzer, S., and Jansen, J. M. (1994). "Temperature Correction of Asphalt-Moduli for FWD-Measurements." Proceedings of the 4<sup>th</sup> International Conference on Bearing Capacity of Roads and Airfields, Vol. 1, Minneapolis, MN, pp. 753-768.

Bonitzer, J., and Leger, P. (1967). "CPC Studies on Pavement Design." Proceedings of the 2<sup>nd</sup> International Conference on Structural Design of Asphalt Pavements, Univ. of Michigan, Ann Arbor, MI, pp. 781-788.

Bohn, A., Ullidtz, P., Stubstad, R., and Sorensen, A. (1972). "Danish Experiments with the French Falling Weight Deflectometer." Proceedings of the 3<sup>rd</sup> International Conference on Structural Design of Asphalt Pavements." Ann Arbor, Univ. of Michigan, MI, pp. 1119-1128.

Boussinesq, J. (1885). Application des potentiels a l'etude de l'equilibre et du mouvement des solides elastique, Gauthier-Villard, Paris, France.

Briggs, C. R., Scullion T., and Maser, K. R. (1991). "Asphalt Thickness Variation on Texas Strategic Highway Research Program Sections and Effect on Backcalculated Moduli." *Transportation Research Record 1377*, National Research Council, Washington, D.C., pp.115-127.

Brown, S. F., and Pappin, J. W. (1985). "Modeling of Granular Materials in Pavements." *Transportation Research Record 1022*, National Research Council, Washington, D.C, pp. 45-51.

Brown, S. F., Tam, W. S., and Brunton, J. M. (1987). "Structural Evaluation and Overlay Design: Analysis and Implementation." Proceedings of the 6<sup>th</sup> International Conference on Structural Design of Asphalt Pavements, Vol. I, Ann Arbor, MI, pp. 1013-1028.

Burmister, D. M. (1943). "The Theory of Stresses and Displacements in Layered Systems and Applications to the Design of Airport Runways." Proceedings, *Highway*

*Research Record 23*, National Research Council, Washington, D.C., pp. 126-144.

Daleiden, J. F., Killingsworth, B. M., Simpson, A. L., and Zamora, R. A. (1994). "Analysis of Procedures for Establishing In Situ Subgrade Moduli." *Transportation Research Record 1462*, National Research Council, Washington, D.C., pp. 102-107.

De Almeida, J. R., Brown, S. F., and Thom, N. H. (1994). "A Pavement Evaluation Procedure Incorporating Material Non-linearity." *Nondestructive Testing of Pavements and Backcalculation of Moduli*, Von Quintas, H. L., Bush, A. J. III, and Baladi, G. Y., Eds., Vol. 2, ASTM STP 1198, American Society for Testing and Materials, Philadelphia, PA, pp. 58-62.

De Beer, M., Horak, E., and Visser, A. T. (1989). "The Multidepth Deflectometer (MDD) System for Determining the Effective Elastic Moduli of Pavement Layers." *Nondestructive Testing of Pavements and Backcalculation of Moduli*, Von Quintas, H. L., Bush, A. J. III, and Baladi, G. Y., Eds., ASTM STP 1026, American Society for Testing and Materials, Philadelphia, PA, pp. 70-89.

Frazier, P., Jr. (1991). "Estimation of Paving Materials Design Moduli from Falling Weight Deflectometer Measurements." *Transportation Research Record 1293*, National Research Council, Washington, D.C., pp. 42-51.

Hicks, R. G., and Monismith, C. L. (1971). "Factors Influencing the Resilient Response of Granular Materials." *Highway Research Record 345*, National Research Council, Washington, D.C., pp. 15-31.

Hardy, M.S.A. (1990). *The Response of Flexible Pavements to Dynamic Tire Forces*. Ph.D. dissertation, University of Cambridge, England.

Huang, Y. H. (1967). "Stresses and Displacements in Viscoelastic Layered Systems Under Circular Loaded Areas." *Proceedings of the 2<sup>nd</sup> International Conference on the Structural Design of Asphalt Pavements*, Ann Arbor, MI, pp. 225-242.

Huang, Y. H. (1968a). "Stresses and Displacements in Nonlinear Soil Media." *Journal of*

the Soil Mechanics and Foundation Division, ASCE, Vol. 94, No. SM1, pp. 1-19.

Irwin, L. H. (2002). "Backcalculation: An Overview and Perspective." Proceedings of the Pavement Evaluation Conference 2002, Al-Qadi, I. L. and Clark, T. M., Eds., Roanoke, VA.

Irwin, L. H., Yang, W. S., and Stubstad, R. N. (1989). "Deflection Reading Accuracy and Layer Thickness Accuracy in Backcalculation of Pavement Layer Moduli." Nondestructive Testing of Pavements and Backcalculation of Moduli, Von Quintas, H. L., Bush, A. J. III, and Baladi, G. Y., Eds., ASTM STP 1026, American Society for Testing and Materials, Philadelphia, PA, pp. 229-244.

Isada, N. M. (1966). "Detecting Variations in Load-Carrying Capacity of Flexible Pavements." NCHRP Report No. 21, Highway Research Board, National Research Council, Washington, D.C.

Johnson, A. M. and Baus, R. L. (1992). "Alternative Method for Temperature Correction of Backcalculated Equivalent Pavement Moduli." *Transportation Research Record 1355*, National Research Council, Washington, D.C., pp. 45-58.

Kim, Y. R., Hibbs, B. O., and Lee, Y. C. (1995). "Temperature Correction of Deflections and Backcalculated Moduli." *Transportation Research Record 1473*, National Research Council, Washington, D.C., pp. 55-62.

Loulizi, A., Al-Qadi, I. L., Lahouar, S., and Freeman, T. E. (2002). "Measurement of Vertical Compressive Stress Pulse in Flexible Pavements and Its Representation for Dynamic Loading." Transportation Research Board 81st Annual Meeting, Paper # 02-2376, Washington, D.C., pp. 1-21.

Lytton, R. L. (1989). "Backcalculation of Pavement Layer Properties in Nondestructive Testing of Pavements and Backcalculation of Moduli." Nondestructive Testing of Pavements and Backcalculation of Moduli, Von Quintas, H. L., Bush, A. J. III, and Baladi, G. Y., Eds., Vol. 2, ASTM STP 1026, American Society for Testing and Materials, Philadelphia, PA, pp. 7-38.

Lytton, R. L., and Michalak, C. H. (1979). "Flexible Pavement Deflection Equation Using Elastic Moduli and Field Measurements." Research Report 207-7 F, Texas Transportation Institute, Texas A&M University, College Station, TX.

Michelow, J. (1963). "Analysis of Stresses and Displacements in an N-Layered Elastic System under a Load Uniformly Distributed in a Circular Area." California Research Corp., Richmond, CA.

Mikhail, M., Seeds, S., Alavi, S. H. and Ott, W. C. (1999). "Evaluation of Laboratory and Backcalculated Resilient Moduli from the WesTrack Experiment." *Transportation Research Record 1687*, National Research Council, Washington, D.C., pp. 55-65.

Nazarian, S., and Boddapati, K. M. (1995). "Pavement–Falling Weight Deflectometer Interaction Using Dynamic Finite-Element Analysis." *Transportation Research Record 1482*, National Research Council, Washington, D.C., pp. 33-43.

Park, S. W., and Kim, Y. R. (1997). "Temperature Correction of Backcalculated Moduli and Deflections Using Linear Viscoelasticity and Time-Temperature Superposition." *Transportation Research Record 1570*, National Research Council, Washington, D.C., pp.108-117.

Park, D., Buch, N., and Chatti, K. (2001). "Effective Layer Temperature Prediction Model and Temperature Correction Via Falling Weight Deflectometer." *Transportation Research Record 1764*, National Research Council, Washington, D.C., pp. 97-111.

Per Ullidtz, Krarup, J., and Wahlman, T. (1994). "Verification of Pavement Response Models." Nondestructive Testing of Pavements and Backcalculation of Moduli, Von Quintas, H. L., Bush, A.J. III, and Baladi, G.Y., Eds., ASTM STP 1198, American Society for Testing and Materials, Vol. 2, Philadelphia, PA, pp. 218-232.

Peutz, M. G. F., Van Kempen, H. P. M., and Jones, A. (1968). "Layered Systems under Normal Surface Loads." *Highway Research Record 228*, National Research Council, Washington, D.C., pp. 34-45.

Press, W. H., Flannery, B. P., Teukolsky, S. A. and Vetterling, W. T., (1989). Numerical Recipes, The Art in Scientific Computing, Cambridge University Press, UK.

Rada, G., and Witczak, M. W. (1981). "Comprehensive Evaluation of Laboratory Resilient Moduli Results for Granular Material." *Transportation Research Record 810*, National Research Council, Washington, D.C., pp.23-33.

Roesset, J. (1987) Computer Program UTFWIBM, The University of Texas at Austin, Austin, TX.

Sebaaly, B., Davis, T. G., and Mamlouk, M. S. (1986). "Dynamics of Falling Weight Deflectometer." *Transportation Research Record 1022*, National Research Council, Washington, D.C., pp. 63-68.

Sebaaly, P. E., Siddharthan, R., and Javaregowda, M. (1992). "Evaluation of FWD Data for NDOT Overlay Design Procedure." Research Report No. 410-3, Nevada Department of Transportation, Carson City, NV.

Sivaneswaran, N., Kramer, S. L., and Mahoney, J. P. (1991). "Advanced Backcalculation Using a Nonlinear Least Squares Optimization Technique." Paper No. 910362, Transportation Research Board, 70<sup>th</sup> Annual Meeting, Washington, D.C.

Stewart, H. E., Selig, E. T., and Norman-Gregory, G.M. (1985). "Failure Criteria and Lateral Stresses in Track Foundations." *Transportation Research Record 1022*, National Research Council, Washington, D.C., pp. 59-64.

Stolle, D. (1992). "Analysis and Interpretation of the Falling Weight Deflectometer Data." MTO Project 21230, Ministry of Transportation of Ontario, Ontario, Canada.

Stolle, D., and Hein, D. (1989). "Parameter Estimates of Pavement Structure Layers and Uniqueness of the Solution." Nondestructive Testing of Pavements and Backcalculation of Moduli, Von Quintas, H. L., Bush, A. J. III, and Baladi, G. Y., Eds., ASTM STP 1026, American Society for Testing and Materials, Vol. 2, Philadelphia, PA, pp. 313-322.

Tam, W. S. (1987). Pavement Evaluation and Overlay Design. Ph.D. Dissertation, University of Nottingham, Nottingham, U.K.

Tam, W.S. and Brown, S.F. (1989). "Back-analysed elastic stiffnesses: Comparison between different evaluation procedures." *Nondestructive Testing of Pavements and Backcalculation of Moduli*, Von Quintas, H. L., Bush, A. J. III, and Baladi, G. Y., Eds., ASTM STP 1026, American Society for Testing and Materials, Vol. 2, Philadelphia, PA, pp. 189-200.

Torpunuri, V. S. (1990). "A Methodology to Identify Material Properties in Layered Viscoelastic Half Spaces." M.S. Thesis, Texas A&M University, College Station, TX, pp. 112-120.

Ullidtz, P. (1987). Pavement Analysis. Elsevier Science, Amsterdam, The Netherlands.

Ullidtz, P. and Peattie, K. R. (1980). "Pavement Analysis by Programmable Calculators." *Journal of the Transportation Engineering Division, ASCE*, Vol. 106, No. TE5, pp. 581-597.

Ullidtz, P. (1977). "Overlay and Stage by Stage Design." *Proceedings of the 4<sup>th</sup> International Conference on the Structural Design of Asphalt Pavements*, Vol. 1, Ann Arbor, MI, pp. 722-735.

Uzan, J. (1994). "Advanced Backcalculation Techniques." *Nondestructive Testing of Pavements and Backcalculation of Moduli*, Von Quintas, H. L., Bush, A.J. III, and Baladi, G.Y., Eds., Vol. 2, ASTM STP 1198, American Society for Testing and Materials, Philadelphia, PA, pp. 3-37.

Van Cauwelaert, F. (1989). "Les bases essentielles des modèles de dimensionnement." *Journée Technique LAVOC*, Ecole Polytechnique Fédérale de Lausanne, France.

Vlasov, V. Z. and Leont'ev, N. N. (1966). Beams, Plates, and Shells on Elastic Foundations, (translated from Russian), Israel Program for Scientific Translations, Jerusalem, Israel.

## CHAPTER THREE

### ESTIMATION OF MODULI OF UNBOUND MATERIAL USING FALLING WEIGHT DEFLECTOMETER DEFLECTIONS MEASURED WITH SMALL AND LARGE PLATES

#### Abstract

The purpose of this Chapter is to examine the capability of the falling weight deflectometer (FWD) in estimating the in-situ moduli of unbound material. The FWD was used at the Virginia Smart Road after the construction of each layer, and the results were analyzed using different backcalculation procedures to provide initial estimates of the effective in-situ material elastic moduli. The analysis of the deflection measured over the subgrade was initially used to determine the combination of the subgrade modulus and depth to bedrock that produced the deflection bowls that best match those measured with the FWD. The “as-built” in-situ modulus of the second layer, 21-B, was determined using the measured layer thickness and the subgrade properties determined in the previous step so that the deflections measured over this layer matched the computed deflections. The modulus of a combined subgrade and granular subbase was also obtained.

A total of five loads configuration (22, 30, 40, 49 and 58 kN) was dropped on each of the layers and the deflections at seven sensors were recorded in all cases. The average of three drops was determined after a seating load drop to minimize the effects of random errors and for backcalculation analysis. Two plate sizes were used for the subgrade and granular 21-B layer with diameters 300 mm and 457 mm for the small and large plates, respectively. A complete analysis of the subgrade and the 21-B layer is presented in this Chapter. Four types of approaches were used in analyzing the deflections over the subgrade. The average moduli obtained utilizing the large plate were higher than those obtained utilizing the small plate for the four approaches. Nonlinear subgrade behavior was detected in some of the sections (E, F, G, J, K and L) together with the presence of a stiff layer or bedrock. The accuracy of the FWD's estimation of the moduli of unbound material was determined. The significance of the use of large and small plates and the differences in the estimations produced by them are highlighted in the different types of analysis used. Utilizing deflections away from the first two sensors with the large plate resulted in the most appropriate subgrade moduli. In addition, the depth to bedrock from the large plate analysis produced the best estimation to depth of stiff layer.

### 3.1 INTRODUCTION

The Virginia Smart Road in southwest Virginia is a unique, state-of-the-art, full-scale research facility for pavement and Intelligent Transportation Systems (ITS) research. It is the first facility of its kind to be built from the ground up with its infrastructure incorporated into the roadway.

The flexible pavement portion of the Virginia Smart Road includes 12 different flexible pavement designs. Each section is approximately 100m long. Seven of the 12 sections are located on a fill, while the remaining five sections are located in a cut. All 12 sections are closely monitored by a complex array of sensors embedded during construction that are located beneath the roadway and embedded during constructions. Table 3.1 shows the structural composition of the 12 flexible pavements. Deflections using FWD were measured during construction of the subgrade and unbound subbase to estimate their moduli.

**Table 3.1** Layer Structure of the Experimental Pavement Sections.

<b>Section.</b>	<b>Surface (38 mm)</b>	<b>BASE BM-25.0</b>	<b>BASE SM-9.5A</b>	<b>OGDL</b>	<b>21-A Agg. Cem.Stab.</b>	<b>21-B Agg.</b>	<b>Total Thickness</b>
A	SM-12.5D	150	0	75	150	175	588
B	SM-9.5D	150	0	75	150	175/GT	588
C	SM-9.5E	150	0	75	150	175/GT	588
D	SM-9.5D	150	0	75	150	175/GT	588
E	SM-9.5D	225	0	0	150	75/GT	488
F	SM-9.5D	150	0	0	150	150	488
G	SM-9.5D	100	50	0	150	150/GT	488
H	SM-9.5D	100	50	75	150	75	488
I	SM-9.5A*	100/MM <sup>#</sup>	50	75	150	75	488
J	SM-9.5D	225	0	75	0/SR <sup>&amp;</sup>	150	488
K	OGFC <sup>^</sup>	244	0	75	0	150	488
L	SMA-12.5 <sup>+</sup>	150/MB	0	75	150	75	488

GT: Woven geotextile/separator;

\* High lab compaction;

MM<sup>#</sup>: Reinforcing mesh placed underneath BM-25.0 layer;

SR<sup>&</sup>: Stress relief geosynthetic (on top of aggregate in section J);

MB<sup>></sup>: Reinforcing mesh placed on top of OGDL;

OGFC<sup>^</sup>: Open-graded friction course. This layer is placed on 19mm SM-9.5 and 244mm BM 25.0; SR is placed within the BM 25.0.

The FWD is used to provide load drops onto the pavement system because of its ability to impose on the pavement dynamic loads similar to those imposed by truck traffic. It consists of a drop weight mounted on a vertical shaft and housed in a trailer that can be towed by most conventional vehicles. The FWD applies an impulse loading to a circular plate in contact with the pavement surface. Variation in the applied load levels is achieved by changing the magnitude of the dropping mass and the height of the drop. The drop weight is hydraulically lifted to predetermined heights ranging from 50 to 510 mm. The applied load is of impulse type and is recorded by a load cell. Since the FWD signature (magnitude: ~40 kN; pulse duration: ~40 ms) is similar to that of a standard (40 kN) half-axle traveling at typical highway speeds, the measured pavement response is considered to be a realistic measure of the pavement response to real traffic.

The Dynatest model 8000 FWD unit, owned by the Virginia Department of Transportation and shown in Figure 3.1, was used for testing at the Virginia Smart Road. This system consists of three main components:

- Dynatest 8002E FWD Trailer. The impact of the falling weight is capable of producing impact loads approximately half-sine wave in form, and having a loading time of between 25 and 40 msec. Two loading plate sizes may be used, a 300 mm plate and a 457 mm plate. A ribbed rubber sheet is used to improve uniformity of loading stress distribution over the whole loading plate area. A suitable hole is provided in the center of the loading plate, to allow the measurement of the center deflection. Seven to nine sensing transducers (geophones) register the peak deflections caused by the applied load. The geophones are mounted in movable holders along a 2.45m raise/lower bar. All transducers (i.e. the load cell and seismic deflection transducers) are connected to sockets in a weather-protected "Trailer Connection Box" on the trailer. The geophones and the Trailer Connection Box are connected to the 8600 System Processor.
- Dynatest 8600 System Processor: It is a microprocessor based control and signal processing unit that interface the FWD trailer with the computer. It controls the FWD operation, performs scanning, conditioning and further processing of the geophone signals and monitors the status of the FWD unit to ensure correct measurements. The operator (driver) remotely controls the application of the load.
- Hewlett-Packard HP-85B laptop computer: This allows the control of the unit through the use of proprietary Dynatest software.



**Figure 3.1** Falling Weight Deflectometer (FWD) Unit.

### **3.2 SUBGRADE MODULI DETERMINATION**

The subgrade is known to usually contribute 60 to 80% of the total center deflection, therefore, a small error in the determination of the subgrade modulus will lead to very large errors in the moduli of other layers.

A detailed analysis of the deflections resulting from FWD drops on the subgrade layer provided the basis for estimating the “as-built” structural capacity of this layer. Potential load-dependent behavior was studied by computing the apparent surface modulus using only the maximum surface deflection ( $D_0$ ) and considering the subgrade as a semi-infinite linear elastic homogenous half-space (one-layer system). Next, the apparent surface moduli, using all sensors and assuming a point load on a single-layer system, were computed to detect any possible non-linearity problems. A two-layer system (modeled with ELSYM5 software) was used to determine both the subgrade modulus and depth to bedrock, if present.

#### **3.2.1 Maximum Deflection ( $D_0$ ) Analysis**

Assuming a semi-infinite space, the theoretical pressure distribution under a rigid plate (used in FWD) can be expressed as follows (Ullidtz, 1998):

$$q(r) = \frac{q a}{2(a^2 - r^2)^{0.5}} \quad (3.1)$$

where,

$q$  = applied pressure

$a$  = radius of the plate; and

$r$  = distance from the center of the plate.

If the solution for a point load on a homogenous half-space is integrated over the area of the rigid plate, such as that of the FWD, with the distribution of pressure given by equation 3.1, the maximum deflection is given by the following equation:

$$D_0 = \frac{\pi(1-\nu^2)qa}{2E} = \frac{(1-\nu^2)P}{2aE} \quad (3.2)$$

where,

$E$  = modulus of elasticity;

$\nu$  = Poisson's ratio; and

$P$  = applied load.

Similarly, if a uniform pressure is applied, the maximum deflection is given by the following equation (showing deflection under a rigid plate is 79% of that under flexible plate):

$$D_0 = \frac{2(1-\nu^2)qa}{E} = \frac{2(1-\nu^2)P}{\pi aE} \quad (3.3)$$

Thus, if the maximum deflection,  $D_0$ , under a rigid plate is known from the FWD test, the elastic modulus ( $E$ ) can be computed using the following equation:

$$E = \frac{\pi(1-\nu^2)qa}{2D_0} \quad (3.4)$$

Tables 3.2 and 3.3 show the subgrade moduli for all the experimental sections computed using equation 3.4. The average applied load and deflection at the center of the loading plate were used for each load level and plate size. The tables include the average modulus, standard deviation, and coefficient of variation for each section, as well as the average modulus computed for each load level (and its standard deviation). The range of moduli of all the experimental sections computed for different loading levels and plate sizes are shown graphically in Figure 3.2. In general, the coefficients of variation (COV) within the sections were lower than 15%, except for a couple of sections. It is notable that the moduli estimated for section I, using all load levels, are very high. This anomaly could

be attributed to the presence of a large rock or stiff material below the first few sensors at that specific loading spot.

To examine a possible load-dependent behavior, the moduli computed using  $D_0$  for all loads are plotted against the applied pressure in Figure 3.3 (without section I). Although the coefficient of determination ( $R^2$ ) for the trend line indicates no statistically significant correlation between the modulus and the applied pressure, the modulus appears to increase with the magnitude of pressure applied (positive coefficient in the regression equation). This increase appears to indicate a mild load-dependent behavior of the subgrade. However, the coefficient of determination ( $R^2$ ) indicates that the statistical correlation between the modulus and the pressure applied is not significant.

**Table 3.2** Moduli Computed Utilizing the Large (457 mm) Plate (MPa).

Section	Load (kN)					Average	St. Dev.	COV (%)
	22	31	40	49	58			
A	242	270	284	322	284	280	29	10
B	283	266	327	331	298	301	28	9
C	216	228	214	231	270	232	23	10
D	178	206	235	226	235	216	25	11
E	178	176	194	224	223	199	24	12
F	215	251	145	175	227	203	42	21
G	174	195	189	202	223	196	18	9
H	319	289	332	248	315	301	33	11
I	955	936	954	953	944	948	8	1
J	354	370	390	408	414	387	25	7
K	384	374	370	362	354	369	12	3
L	154	166	176	183	190	174	14	8

**Table 3.3** Moduli Computed Utilizing the Small (300 mm) Plate (MPa).

Section	Load (kN)					Average	St. Dev.	COV (%)
	22	31	40	49	58			
A	280	329	345	343	353	330	29	9
B	360	323	391	372	351	359	25	7
C	315	335	304	285	338	315	22	7
D	253	269	289	308	325	289	29	10
E	221	270	253	255	287	257	24	10
F	216	279	247	282	263	257	27	10
G	203	217	247	302	308	255	48	19
H	441	294	331	289	356	342	61	18
I	974	1000	1018	1039	1036	1013	27	3
J	277	309	397	347	359	338	46	14
K	264	299	286	297	297	289	15	5
L	206	225	236	243	224	227	14	6

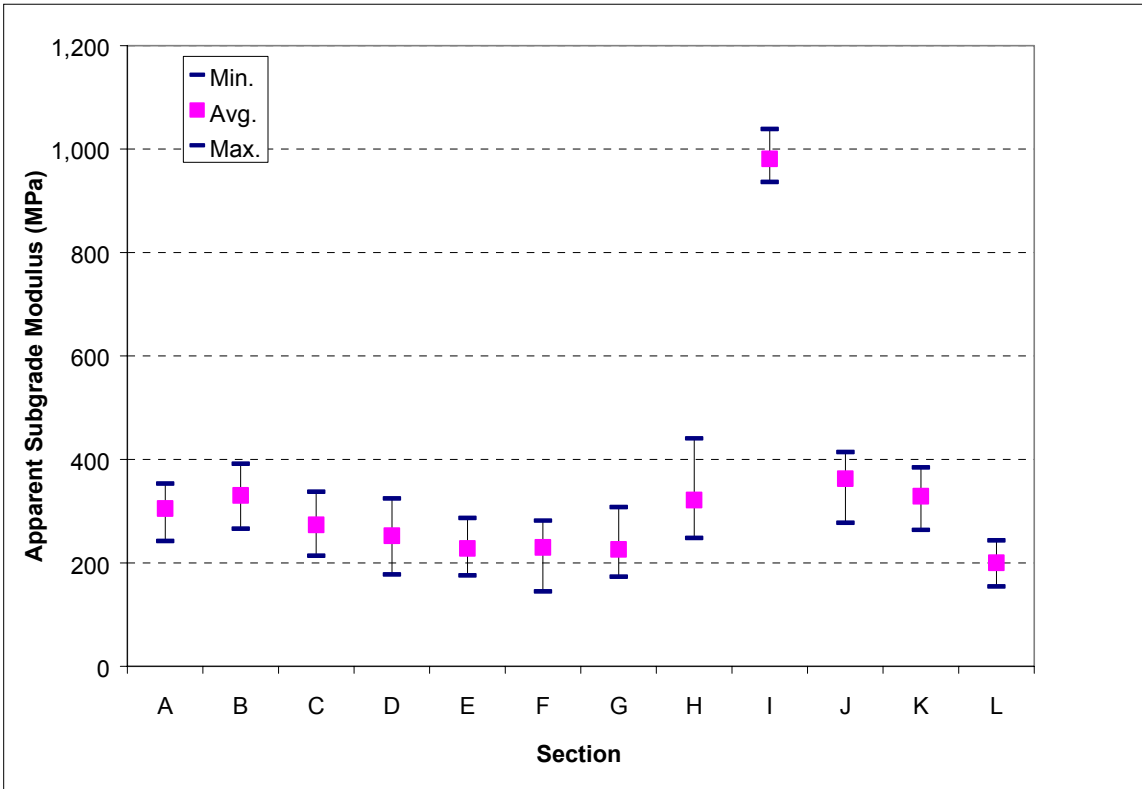


**Figure 3.2** In situ Subgrade Moduli Using  $D_0$ .

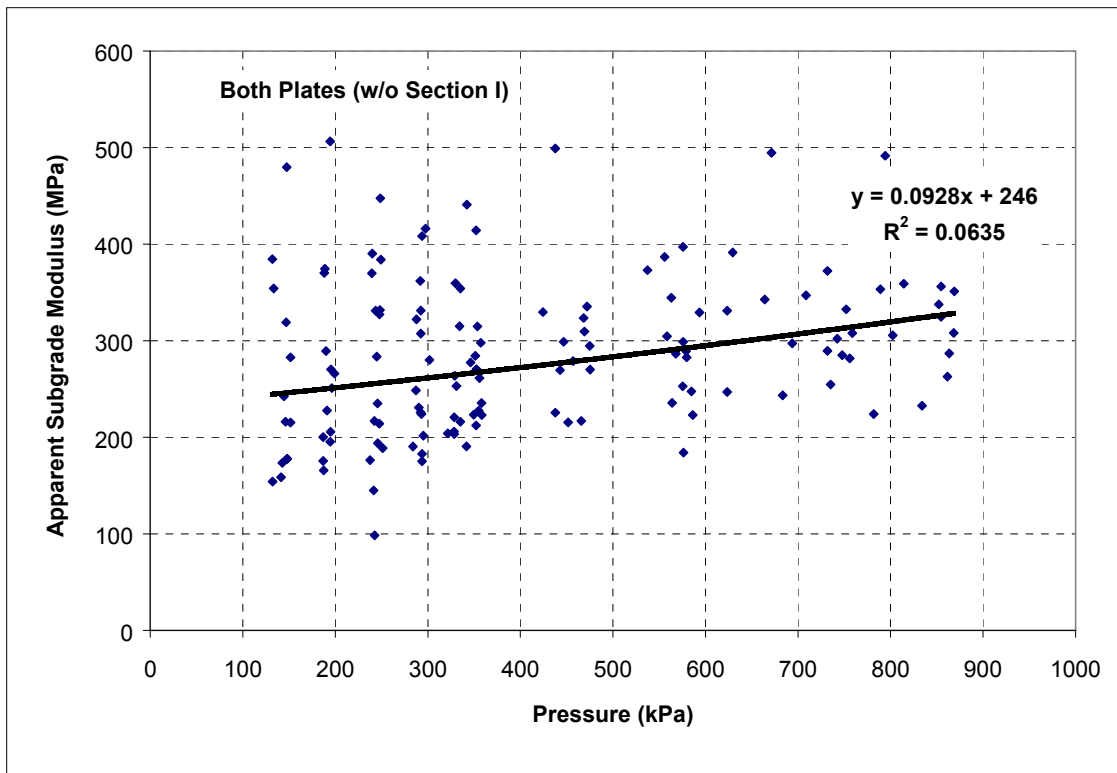


**Figure 3.3** Subgrade Moduli Versus Applied Pressure.

### 3.2.2 Surface Modulus Using All Deflections ( $D_i$ ) and a Point Load

The second approach investigated potential non-linearity in the subgrade modulus. Nonlinearity influences are often encountered in backcalculation analyses, resulting in overestimated subgrade moduli that are compensated for by assigning a lower modulus for the layer on top of the subgrade. Nonlinearity is identified by a greater apparent subgrade modulus at the outer sensor location than the expected value at that point or modulus directly underneath the loading plate. The average apparent surface modulus for all sensors is plotted as a continuous line in Figure 3.4. On average, the subgrade appears to show some non-linear behavior, because the computed modulus tends to increase as the distance from the point of load application increases. This increase of the surface modulus with the increased distance from the load center could be an indication of an increase in the resilient modulus with depth and/or the presence of a stiff layer at a shallow depth beneath the surface.

This possibility is illustrated in Figure 3.5, which shows the apparent surface modulus computed based on synthetic deflection basins obtained using a 345 MPa modulus and a variable depth to a stiff layer. The apparent surface moduli for all sensors

were computed and plotted against the distance of sensors to the applied load (Figure 3.5).

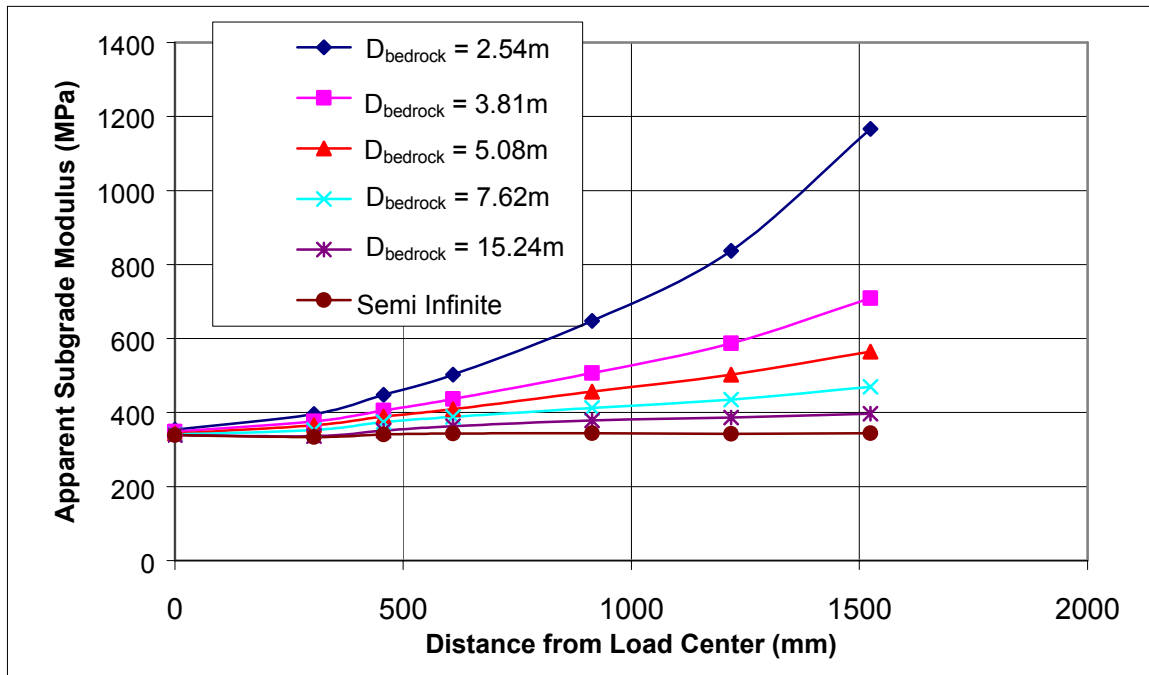


**Figure 3.4** Surface Moduli Using Synthetic Deflections Basins.

The equation for surface deflection on a linear-elastic homogenous half-space subjected to a point load was used for this purpose:

$$D_r = \frac{(1-\nu^2)P}{\pi r E} \quad (3.5)$$

where,

$P$  = applied load;

$r$  = distance to the load center; and

$D_r$  = deflection at a distance  $r$  from the load center.

Ullidtz (1998) has demonstrated that equation (3.5) gives results that match closely with those using a uniform circular load for points located more than two radii from the center of the applied load. Thus, the modulus was computed using this equation for all sensors and drops, and averaged per section. The values for  $D_0$  were computed using equation 3.4, as indicated in the previous section. The results are presented in Tables 3.4 and 3.5 for the large and small plates, respectively. The pressure from the loading of the small plate is higher than that obtained with the larger plate. Therefore, the resultant bulk stress

developing within the subgrade is greater, when the bulk stress equation for granular materials is used, for the same  $K_1$ ,  $K_2$  values. This results in higher resilient moduli or  $M_R$ .

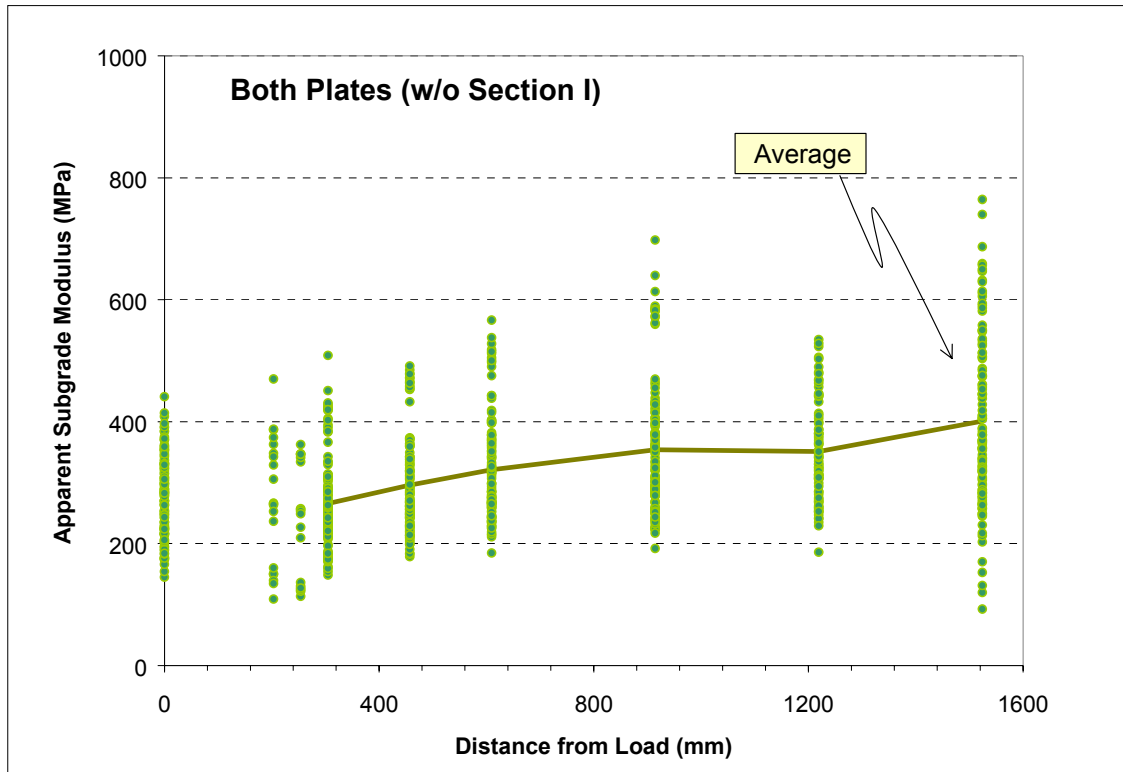


**Figure 3.5** Subgrade Moduli Using All Loads.

**Table 3.4** Subgrade Moduli Using All Sensors for the Large Plate (MPa).

Section	Distance from Load Center (mm)								Average	Average $D_{305} - D_{1524}$
	0	254	305	457	610	914	1219	1524		
A	281	-	272	308	332	364	400	405	337	362
B	301	-	293	349	374	401	447	482	378	411
C	232	-	231	244	264	320	328	341	280	299
D	216	-	222	226	244	285	340	323	265	284
E	199	-	200	233	259	282	279	275	247	266
F	203	-	213	236	261	261	307	317	257	276
G	194	-	230	313	348	370	462	501	345	399
H	301	-	248	227	222	232	244	241	245	233
I	971	875	826	712	671	620	-	448	732	613
J	387	346	425	455	508	580	-	628	476	543
K	349	242	255	260	304	378	-	491	325	358
L	181	126	161	194	229	259	-	265	202	237

**Table 3.5** Subgrade Moduli Using All Sensors for the Small Plate (MPa).

Section	Distance from Load Center (mm)								Average	Average $D_{305} - D_{1524}$
	0	254	305	457	610	914	1219	1524		
A	330	-	291	308	319	344	379	355	332	341
B	360	-	336	368	388	455	466	504	411	436
C	315	-	257	280	307	332	326	321	306	313
D	289	-	241	268	280	310	323	356	295	307
E	257	-	229	271	286	290	264	291	270	280
F	257	-	241	276	291	303	305	365	291	308
G	255	-	273	341	348	399	423	474	359	397
H	342	-	254	255	264	293	309	322	291	289
I	1,032	942	874	835	800	714	-	600	828	737
J	337	367	403	474	485	593	-	700	480	563
K	295	275	306	311	383	367	-	566	358	407
L	220	141	182	220	242	243	-	174	203	220

The moduli estimated using the small plate are consistently higher than those estimated with the large plate. The average moduli calculated using all sensors for section I are much higher than those obtained without including the first two sensors in both small and large plate analysis. This supports the hypotheses of the presence of a stiff spot under the first two sensors in section I. Furthermore, the type of assumed loading (flexible versus rigid plate) significantly affects the response of the first two sensors (within two radii from the center of load application). Therefore, the average values obtained utilizing deflection measurements by sensors two through six were computed to have representative subgrade moduli. Those moduli were used in the analysis of the subsequent layers, as presented in the last column of Tables 3.4 and 3.5.

Figure 3.6 and 3.7 present the apparent surface moduli computed using deflections measured on top of the subgrade for the 40kN load using the large and small plates, respectively. Consistent with the results presented in Figure 3.5, several plots seem to indicate some nonlinear behavior in the subgrade, because the apparent surface modulus significantly increases for the outer sensors, which are pronounced in some sections.

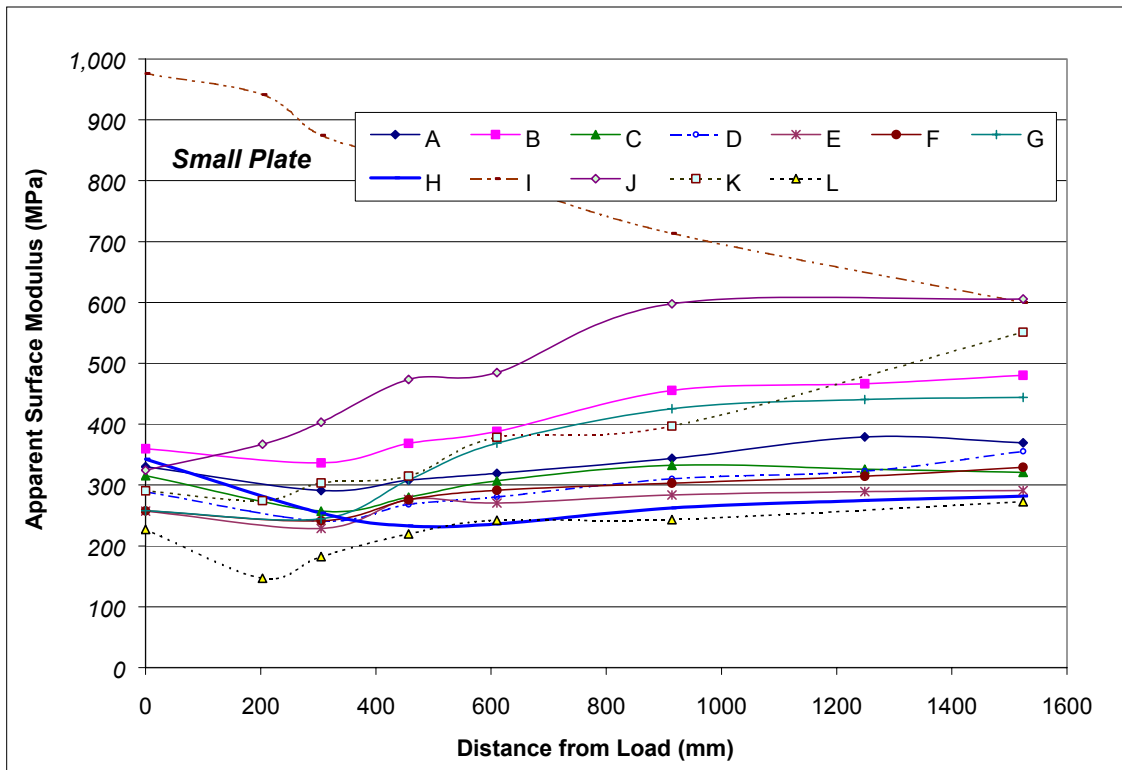


**Figure 3.6** Computed Surface Moduli Using Deflections Measured Utilizing the Large Plate on Top of the Subgrade.

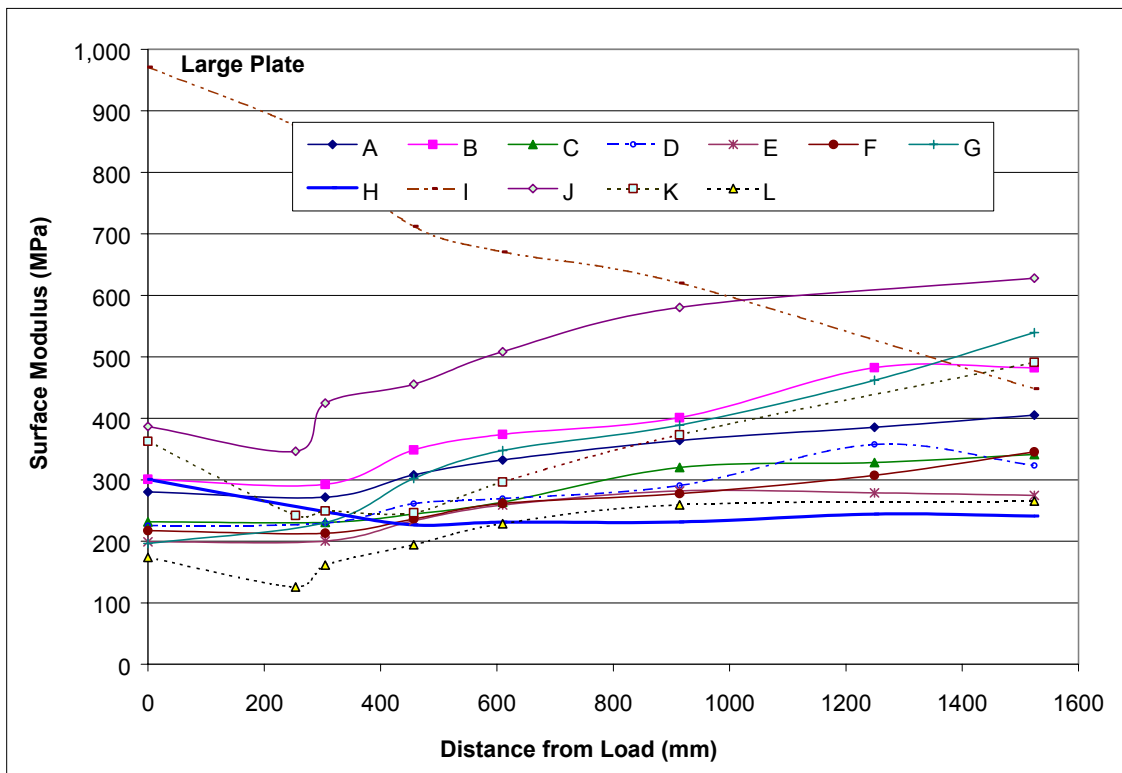


**Figure 3.7** Computed Surface Moduli Using Deflection Measured Utilizing the Small Plate on Top of the Subgrade.

De Almeida *et al.* (1994) suggested that a difference greater than 10 in moduli obtained at different sensor locations should be attributed to nonlinearity and not simply to inaccuracies in the measured deflections. However, based on the variability observed in surface moduli computed at the same locations with different loads (Tables 3.2 and 3.3), the 10 threshold may be too low. If the 10 percent criterion is applied to the plots shown in Figure 3.7, then the subgrade shows nonlinear behavior for most sections. Using a less strict criterion, the plots indicate that Sections G, J, and K appear to show significant nonlinear behavior (moduli increases by more than 50). Sections B, C, D, F, and L also display some nonlinear behavior. The increase in apparent surface modulus could also be due to the presence of a stiff layer, rigid foundation or bedrock in the subgrade or a high ground water table. Please note that the first seven sections were built on a granular fill.

### 3.2.3 Two-Layer System Analysis Of Subgrade

Because of the apparent presence of a stiff layer, the subgrade was further analyzed as a two-layer system using elastic multilayer analysis software, ELSYM5. The ELSYM5 is a linear elastic software that handles up to five layers above the subgrade (Kopperman *et al.* 1986) and is loaded with one or more identical uniform circular loads applied vertically to the pavement surface.

The subgrade was modeled as a finite-thickness, homogenous, linear-elastic layer placed on top of a very stiff half space (bedrock). Synthetic deflection basins were obtained by computing the deflections at the seven geophone locations using a variable subgrade depth with an average modulus of 345 MPa and 40kN loads distributed over circular areas of 300-mm and 457-mm radius to simulate the small and large loading plates, respectively. Large plate is usually recommended for subgrade testing. The modulus of the stiff layer (second layer) was assumed to be 6,900 MPa and its Poisson ratio 0.5. The thicknesses of the subgrade (first layer) used were 0.25, 0.76, 1.8, 2.5, 3.8, 5.1, 7.6 and 15.2 m. A Poisson's ratio of 0.35 was assumed for the subgrade (granular). The deflections obtained for each model (depth to bedrock) were normalized using the following equation:

$$D_{in} = \frac{D_i}{D_0} \quad (3.6)$$

where,

$D_{in}$  = Normalized deflection in sensor  $i$ ;

$D_i$  = Deflection in sensor  $i$ ; and

$D_0$  = Center load deflection (sensor 0).

The normalized synthetic basins are shown in Figure 3.8. Since the material is being considered linear elastic, the normalized deflections are independent of the subgrade modulus. Although the modular ratio between the subgrade and rigid foundation has some influence on the deflection in the two layer system, in this case, it is negligible. The difference between the subgrade modulus and rigid foundation was much higher than the variations in the subgrade modulus.

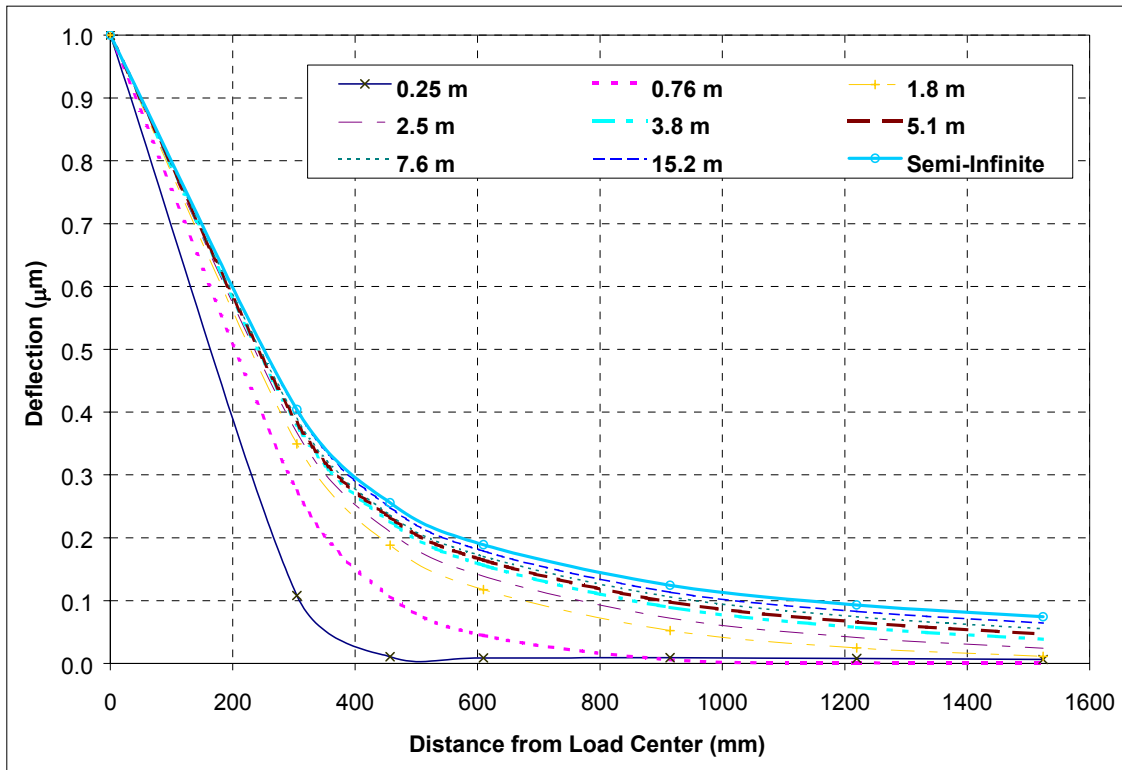


**Figure 3.8** Synthetic Normalized Deflection Basins for the Large Plate on Top of the Subgrade.

The depth to bedrock was determined by comparing the measured normalized basins from the large and small plates with the synthetic ones. The absolute mean square error (MSE) between the synthetic and field measured basins was obtained for each model. The model with the least MSE was selected for each section. As an example, Figure 3.9 shows the measured deflection basin for Section E superimposed with the synthetic ones. It can be observed that the measured deflection approximately follows the trend

for the model with a 7.6-m deep rigid foundation. For some sections, it was necessary to remove the deflection measured by the first (center of the load) and second sensors from the analysis to obtain a good overall fit between the measured and synthetic basins.

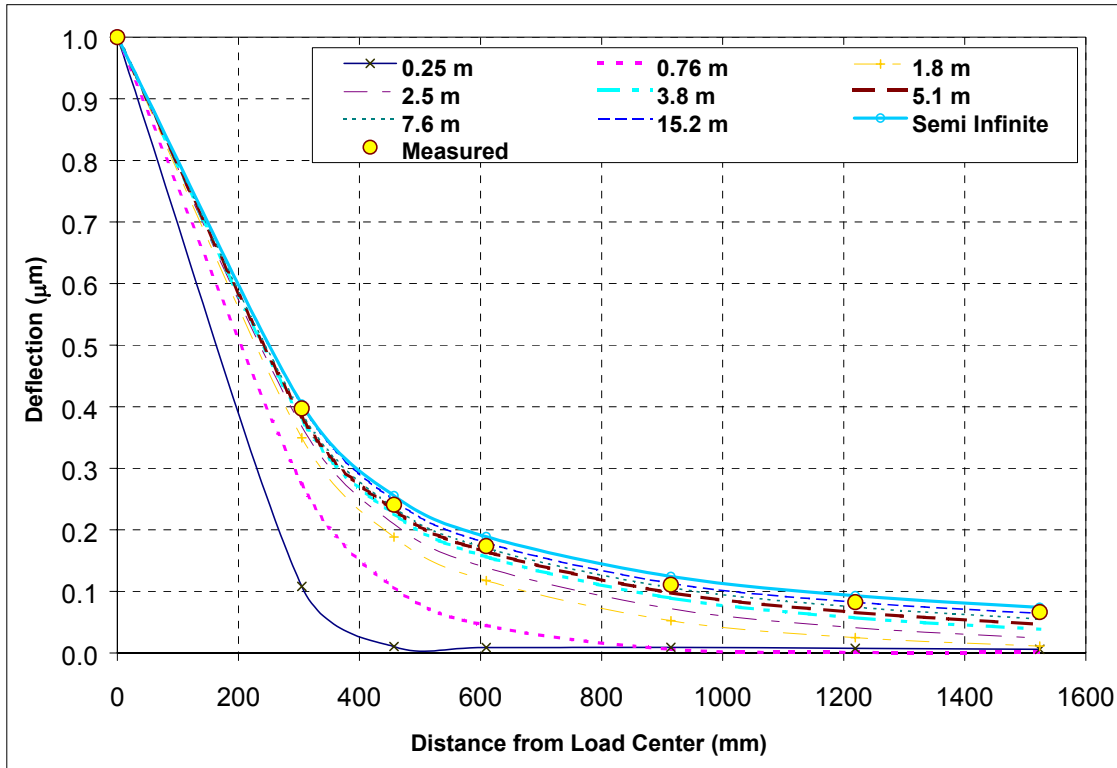


**Figure 3.9** Synthetic and Measured Normalized Basins for the Large Plate on Top of the Subgrade (Section E).

Once the depth to rigid foundation was determined, the modulus of the subgrade layer was varied in increments of 35 MPa and the value that resulted in the lowest MSE between the measured and computed deflections was selected as the average or “effective” subgrade modulus. The results are summarized in Table 3.6.

Results obtained when using the small and large plates are not in full agreement; however, the results appear to indicate the presence of a shallow stiff layer (or nonlinearity) in several Sections (E through H and J through L). The apparent shallow stiff layer could also be due to an increase in moduli with depth because of increased confining pressure or the presence of stiffer materials. Large rocks were used in initial lifts of the fill for Section E through G.

**Table 3.6** Subgrade Modulus Based on ELSYM5 Analysis (40 kN).

Section	Large Plate			Small Plate			Average
	M <sub>R 40 KN</sub> (MPa)	D <sub>bedrock</sub> (m)	RMS (μm)	M <sub>R 40 KN</sub> (MPa)	D <sub>bedrock</sub> (m)	RMS (μm)	
A	345	inf.	2.1	345	inf.	3.0	345
B	414	inf.	2.2	345	inf.	1.6	379
C	276	inf.	2.0	310	inf.	6.5	283
D	276	inf.	9.1	286	inf.	0.9	281
E	241	7.6	0.3	241	15.2	5.3	241
F	172	7.6	5.3	241	7.6	7.2	207
G	241	3.8	6.5	345	5.1	0.5	293
H	207	inf.	1.2	207	inf.	0.5	207
I	1,034	inf.	3.4	966	inf.	0.7	1,000
J	379	2.5	0.9	310	1.8	5.1	345
K	241	5.1	0.5	276	3.8	2.8	259
L	172	3.8	1.3	172	3.8	1.9	172
Avg.	333		2.9	336		3.0	335
Std. Dev.	234		2.7	206		2.4	219

### 3.2.4 Nonlinear Analysis

Depth to a stiff layer and material nonlinearity are two important factors which when neglected would result in inaccurate moduli calculation. The subgrade material was primarily crushed rock. Since experimental data show that the response of some of these materials depends strongly on the prevailing state of stress (Uzan, 1985), knowledge of the correct in-situ stress conditions is vital for the rational approach to design and structural evaluation of type of pavement of interest.

The subgrade was modeled to take into account the change of its modulus with the change of stress or nonlinear behavior. The infinite layer was divided into six layers and the state of stress was calculated at the midpoint of each layer. The last point was located 30 m from the surface of the subgrade layer. The behavior of the subgrade materials is described by nonlinear stress-strain characteristics where the resilient modulus of the subgrade materials is related to the bulk stress. Mathematically it is expressed as follows:

$$M_r = K_1 \theta^{k_2} \quad (3.7)$$

where,

$$\theta = \sigma_1 + \sigma_2 + \sigma_3 \quad (3.8)$$

Inserting the weight of the layered system gives

$$\theta = \sigma_x + \sigma_y + \sigma_z + \gamma z(1+2K_0) \quad (3.9)$$

where,

$\sigma_x, \sigma_y, \sigma_z$  = three normal stresses;

$\gamma$  = the average unit weight;

$z$  = the distance below surface at which the modulus is determined; and

$K_0$  = coefficient of earth pressure at rest.

The values of nonlinear exponential constants  $K_1$  and  $K_2$  were varied within reasonable limits expected for crushed rock material. A Poisson's ratio of 0.49, unit weight of 22 kN/m<sup>3</sup>, and a coefficient of earth pressure at rest of 0.6 were used. The deflections resulting from the seven sensor spacings (0, 305, 452, 609, 914, 1219 and 1524mm) were calculated using the KENLAYER software.  $K_1$  varied between 7500 and 10,000 and  $K_2$  varied from 0.5 to 0.75. The calculated deflections were matched with the measured deflections. A nonlinear relationship with  $K_1$  of 8000 and  $K_2$  of 0.6 resulted in the best match. The deflection bowl resulting from ELSYM5 software which uses a linear elastic analysis was obtained for each of the Sections. Plots of selected sections (Sections A through F, J and K) using the small and large plates, are shown in Figures 3.10 through 3.19. For Sections A and B, the measured deflections fell between the calculated deflections from the nonlinear and linear-elastic behavior for both the small and large plates shown in Figures 3.10 and 3.15. The moduli used for the ELSYM5 analysis for the large and small plates was obtained from Table 3.5. Some of the sections have the same moduli and this resulted in the same calculated values for linear elastic analysis and shown as "Calculated Linear" in the plots. The nonlinear model used was  $M_R = 8000\theta^{0.6}$  and is shown as "Calculated Nonlinear" in the plots. Results indicate that for most of the sections, after the second sensor spacing (305 mm), the measured deflections fall between the calculated linear and nonlinear values for the small and large plate. The only exception was Section F, which shows more nonlinearity when using the large plate.

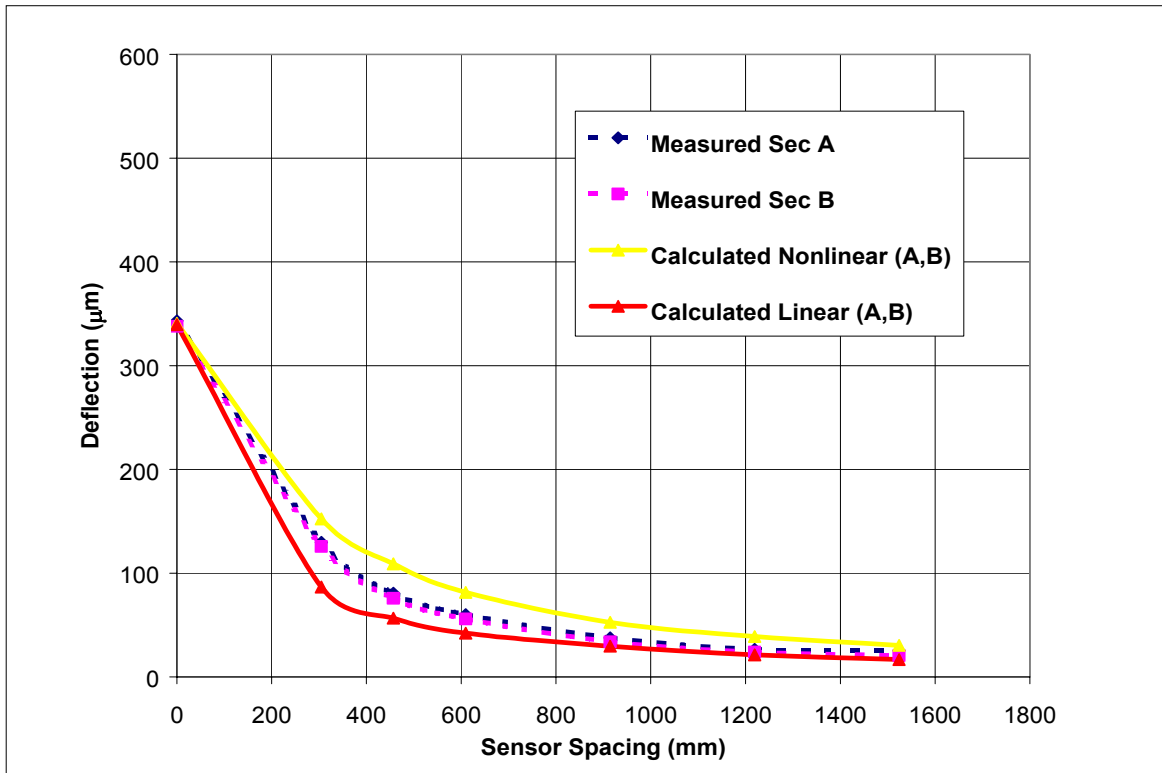


Figure 3.10 Measured and Computed Deflections for Sections A and B from Small Plate.

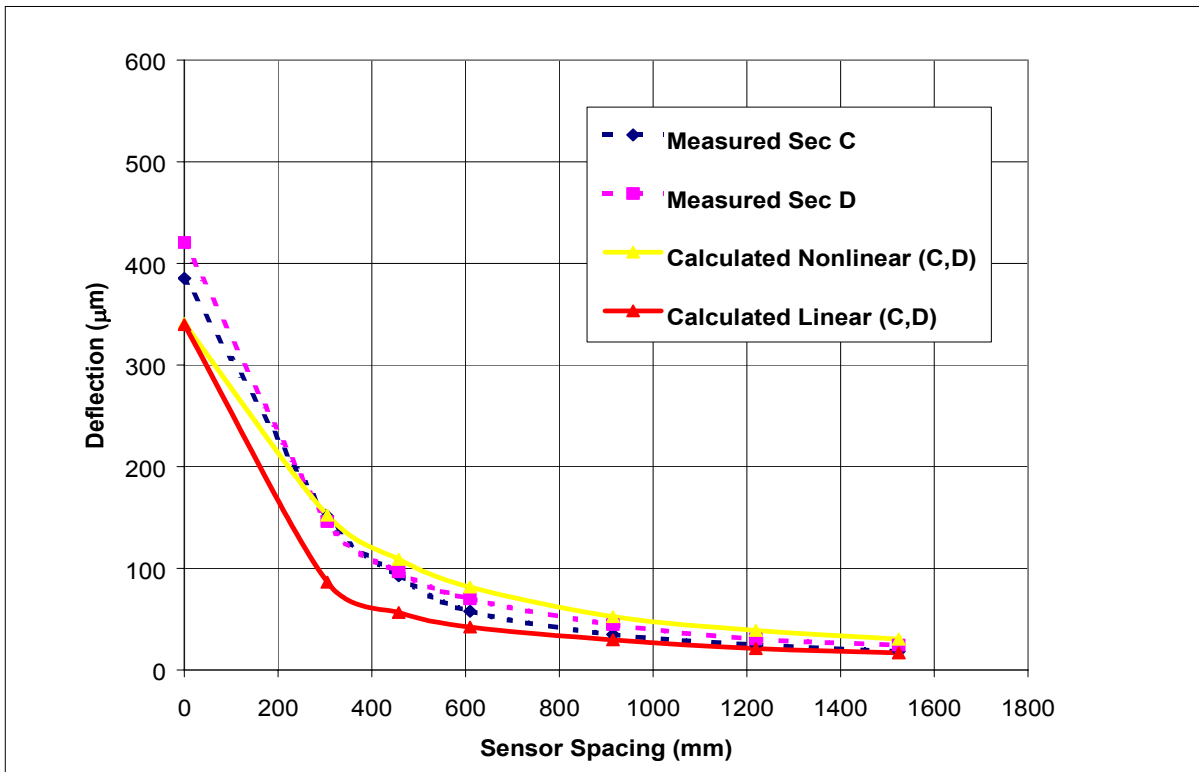


Figure 3.11 Measured and Computed Deflections for Sections C and D from Small Plate.

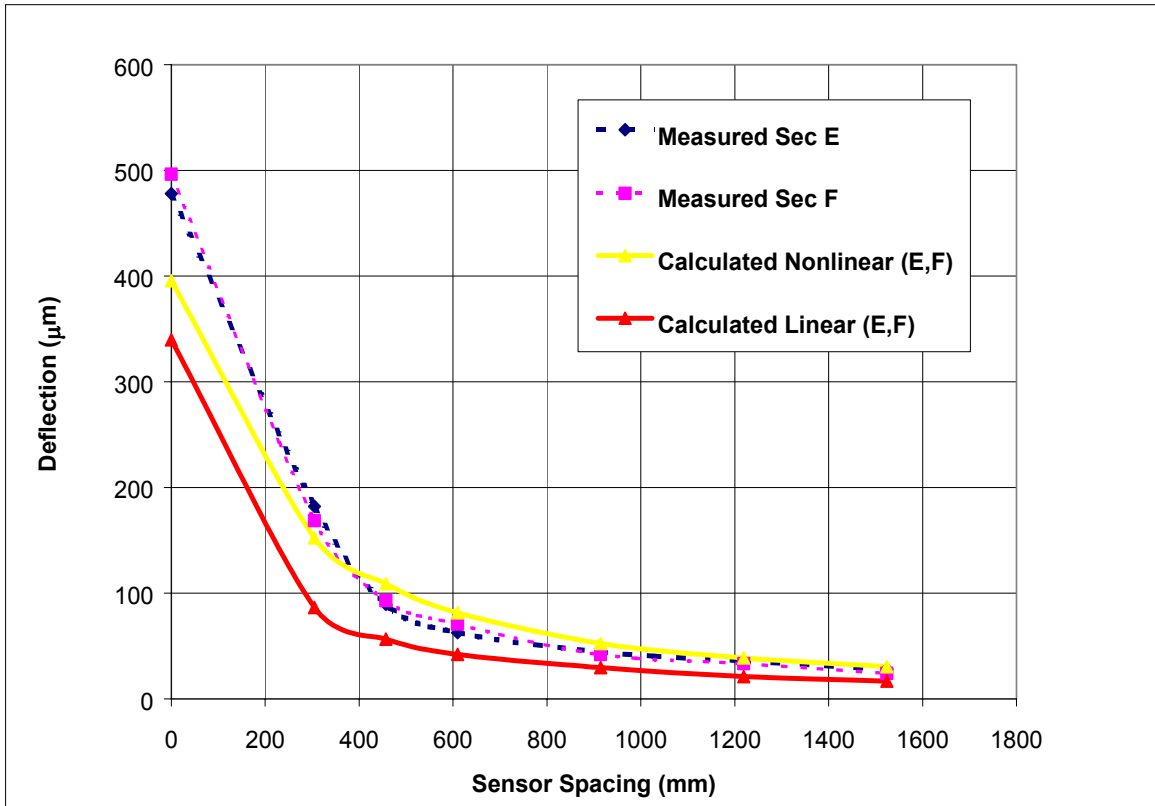


Figure 3.12 Measured and Computed Deflections for Sections E and F from Small Plate.

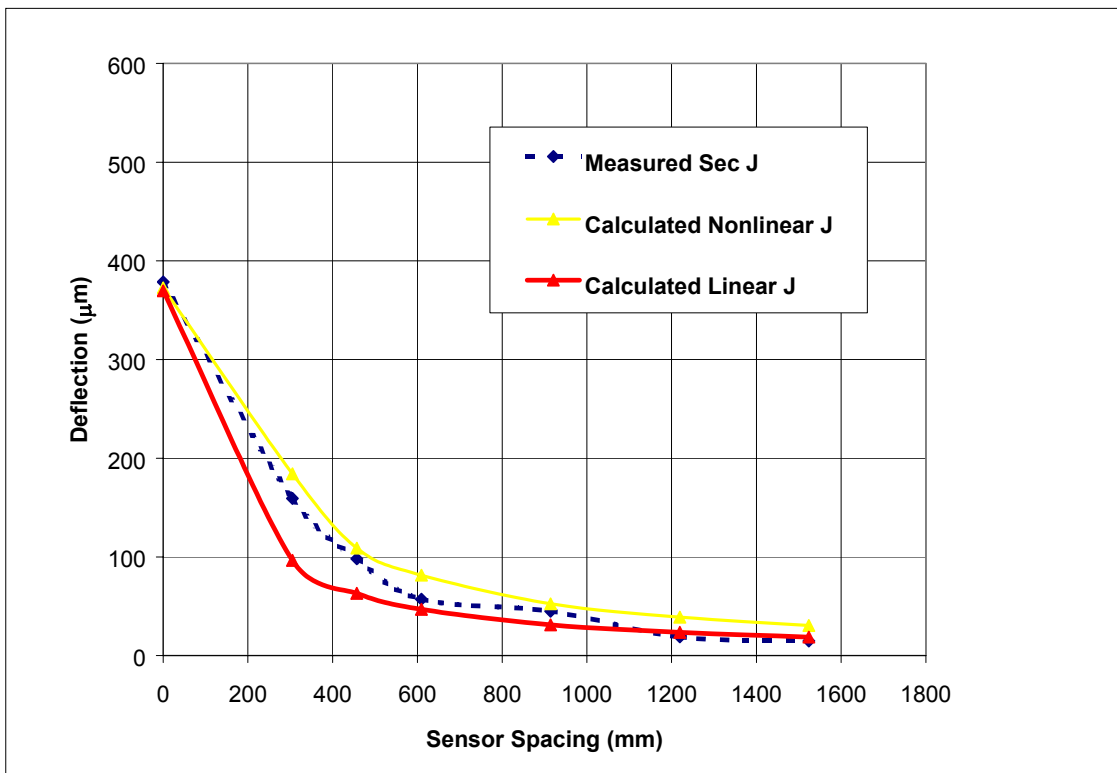


Figure 3.13 Measured and Computed Deflections for Section J from Small Plate.

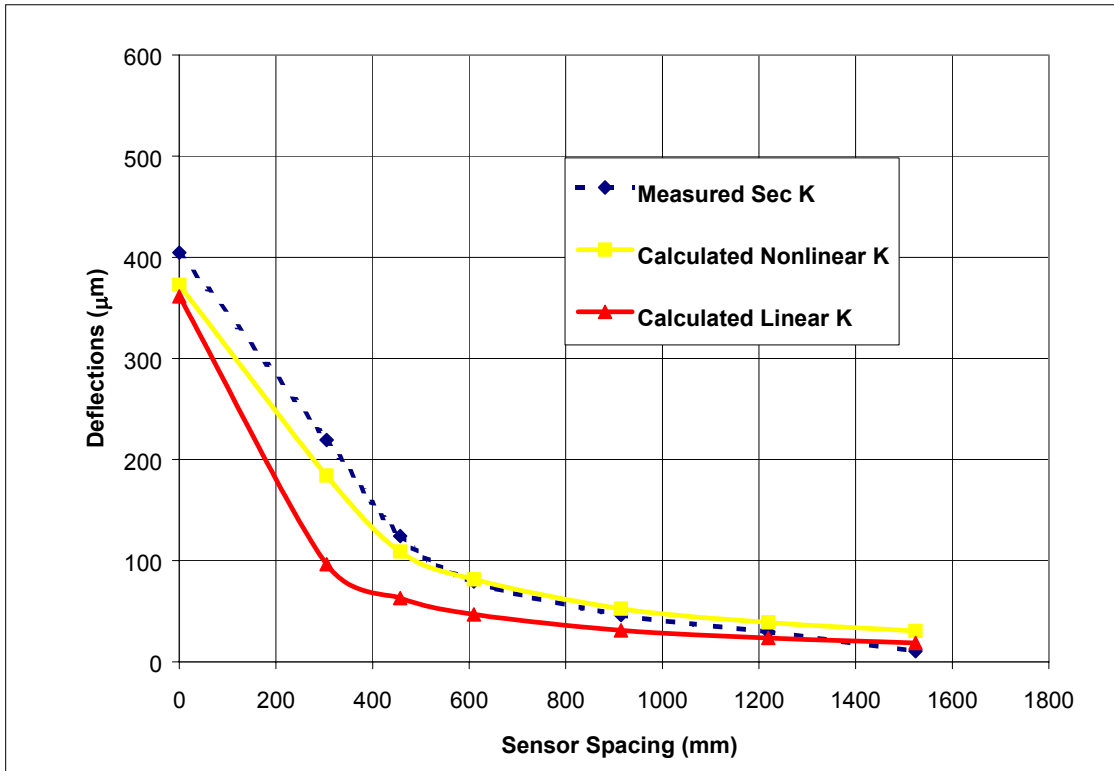


Figure 3.14 Measured and Computed Deflections for Section K from Small Plate.

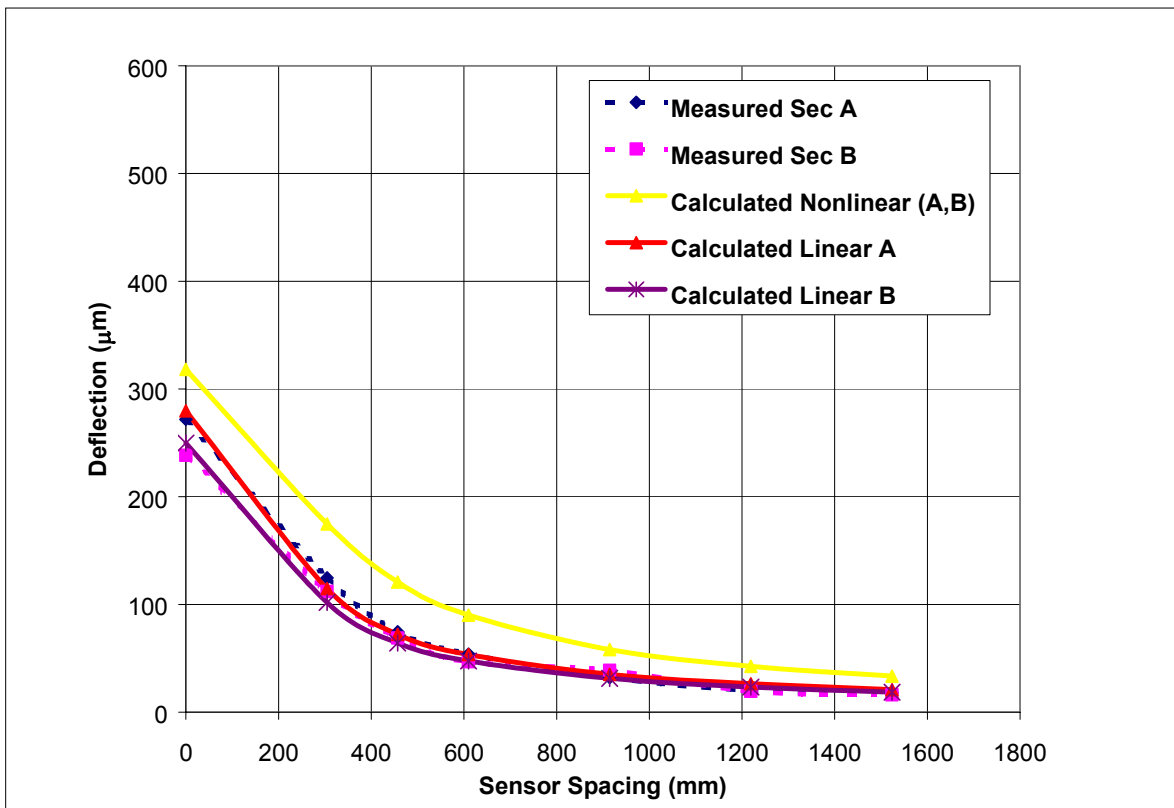


Figure 3.15 Measured and Computed Deflections for Sections A and B from Large Plate.

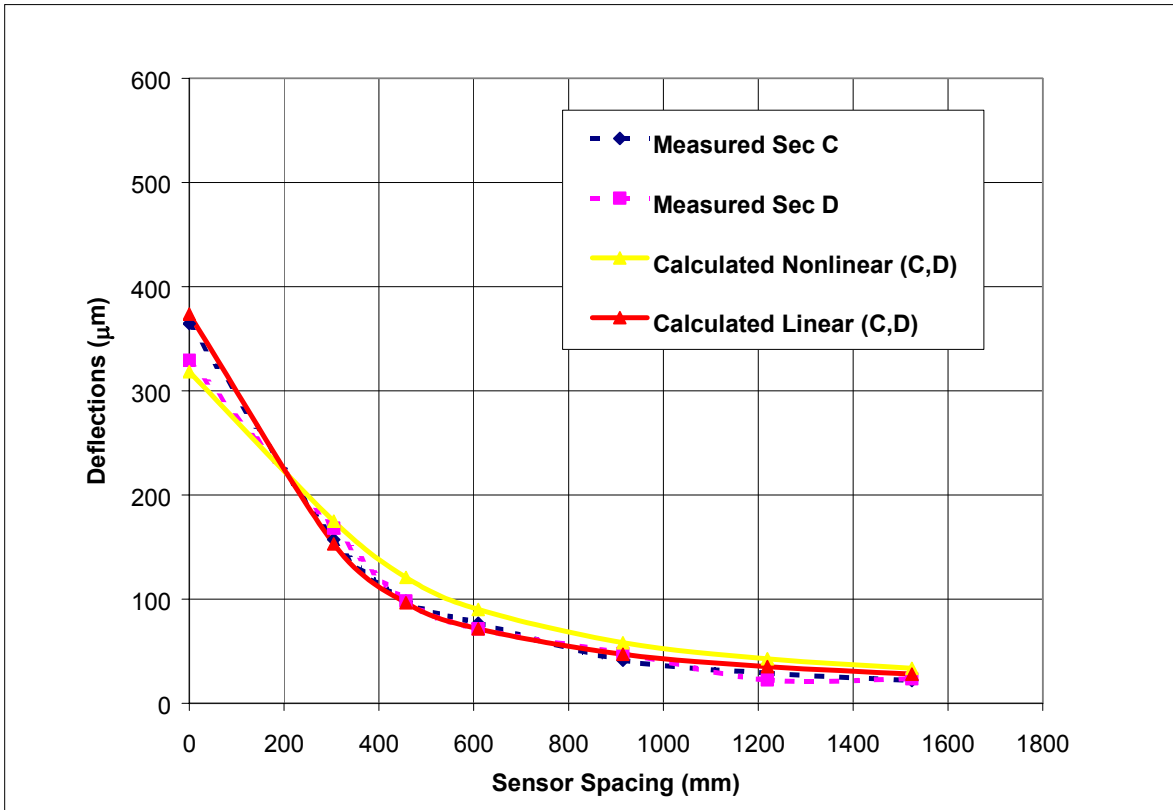


Figure 3.16 Measured and Computed Deflections for Sections C and D from Large Plate.

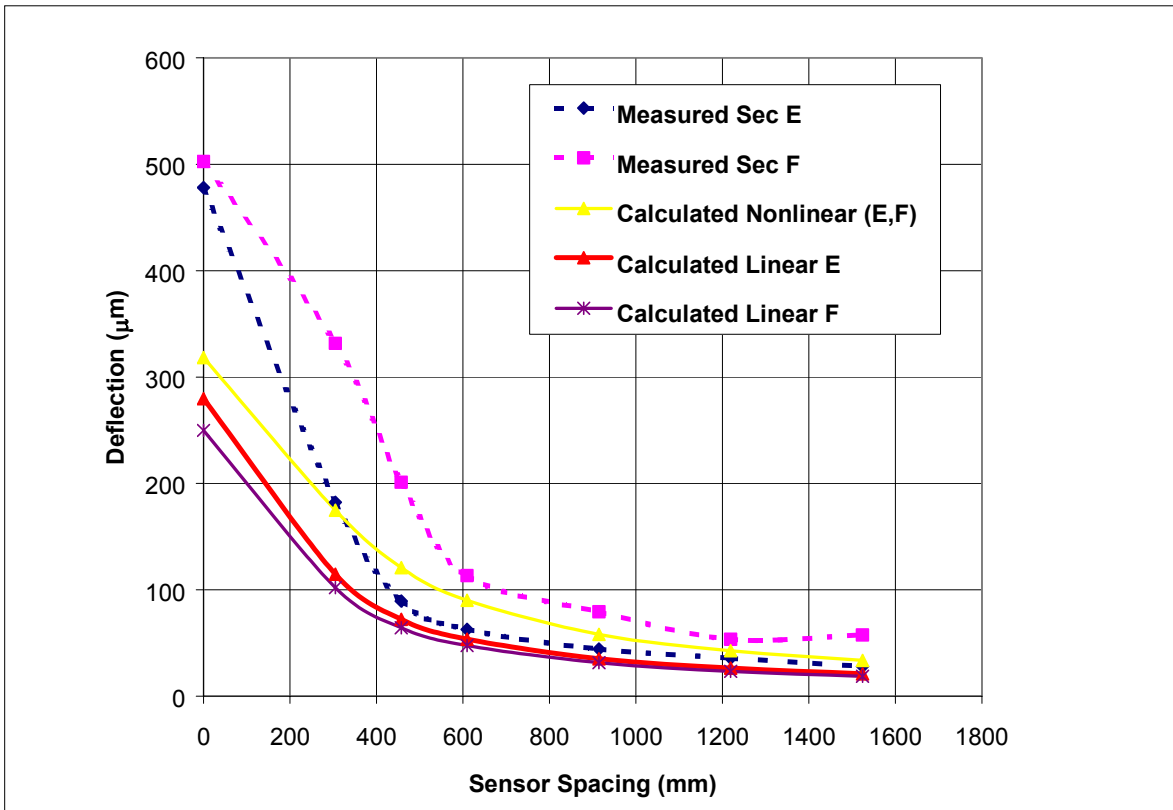
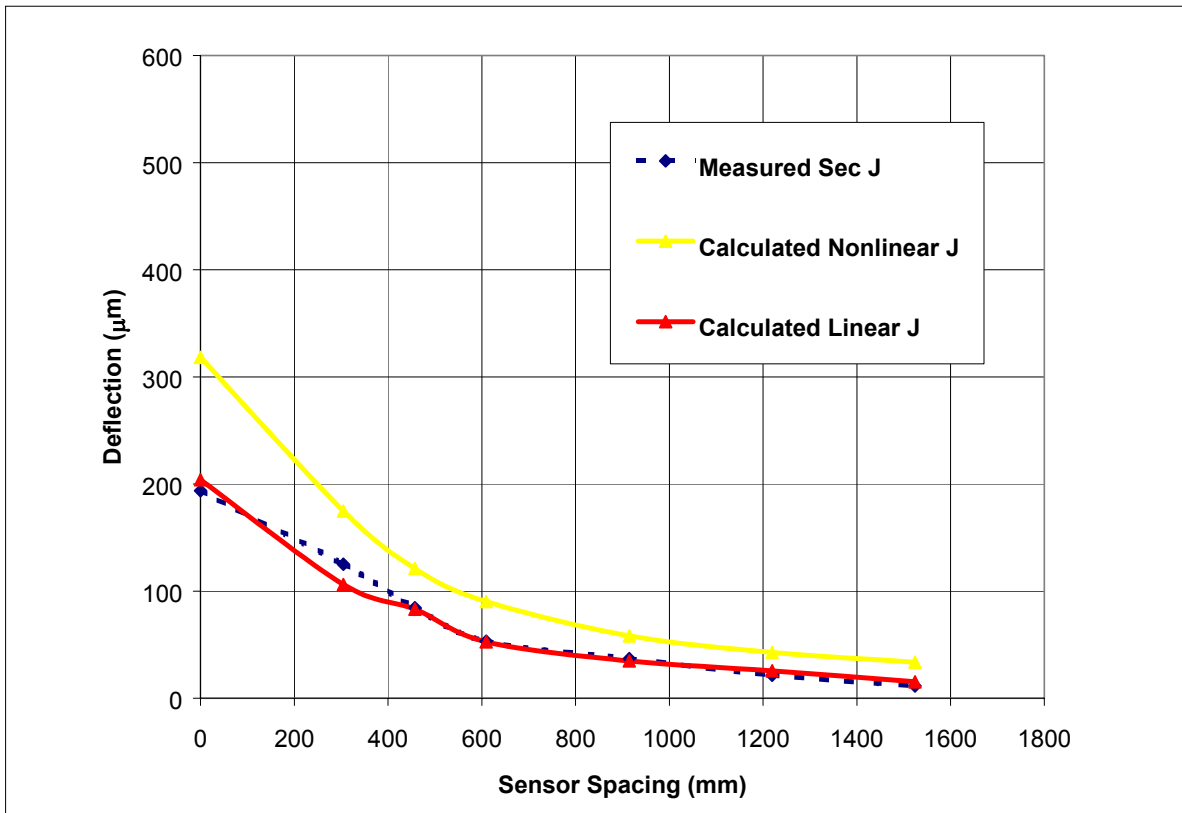
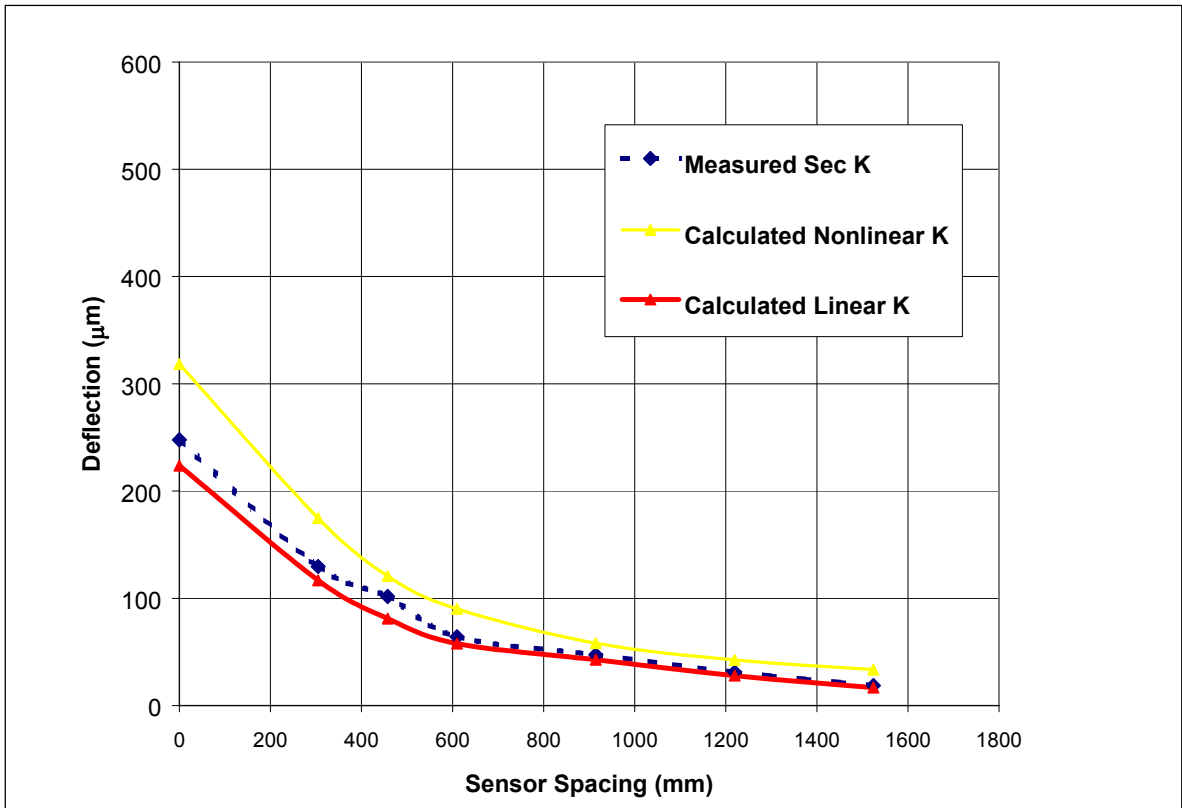


Figure 3.17 Measured and Computed Deflections for Sections E and F from Large Plate.



**Figure 3.18** Measured and Computed Deflections for Section J from Large Plate.



**Figure 3.19** Measured and Computed Deflections for Section K from Large Plate.

### 3.2.5 Ullidtz Method For Estimating The Depth To Bedrock

The procedure proposed by Ullidtz (1988) to determine the presence of a stiff layer and its depth when present was also investigated. This procedure is based on plotting the deflection ( $D_i$ ) versus the inverse of the distance from the load center ( $1/r_i$ ). If there is no rigid layer, the curve will approximately pass through the origin. If the projection of the curve intercepts the 0 deflection axis at a positive  $1/r$ , there is probably a rigid layer at a distance  $r$  below the surface.

The procedure was first tested with the synthetic deflections. Figure 3.20 shows the plots for all the basins and Figure 3.21 shows the comparison between the actual depths used to simulate the synthetic deflections and those estimated using Ullidtz method. It can be observed that the methods produced very close results for depths up to approximately 3 m, but tends to underestimate the depth for lower stiff layers. However, since only shallow stiff foundations (less than 2 m deep) have a significant effect on the backcalculation procedure, the procedure should produce appropriate results. The results with the measured deflection were also reasonably consistent with the previous analysis when the ELSYM5 software was used in detection of a shallow foundation.

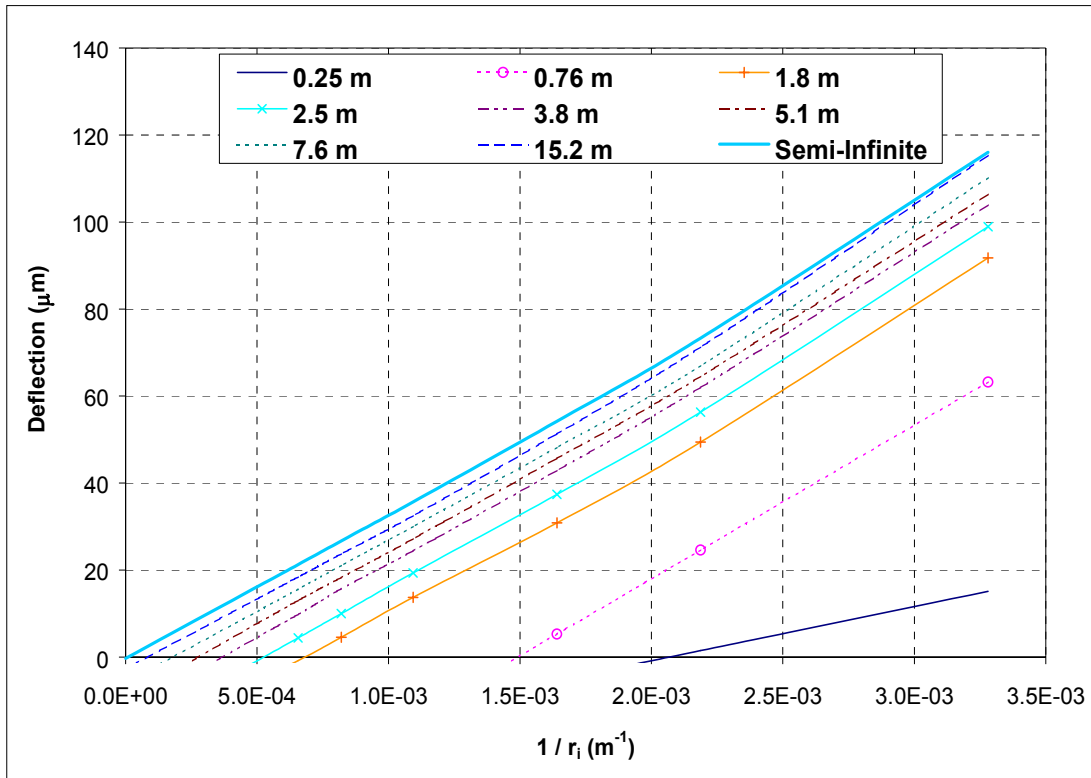
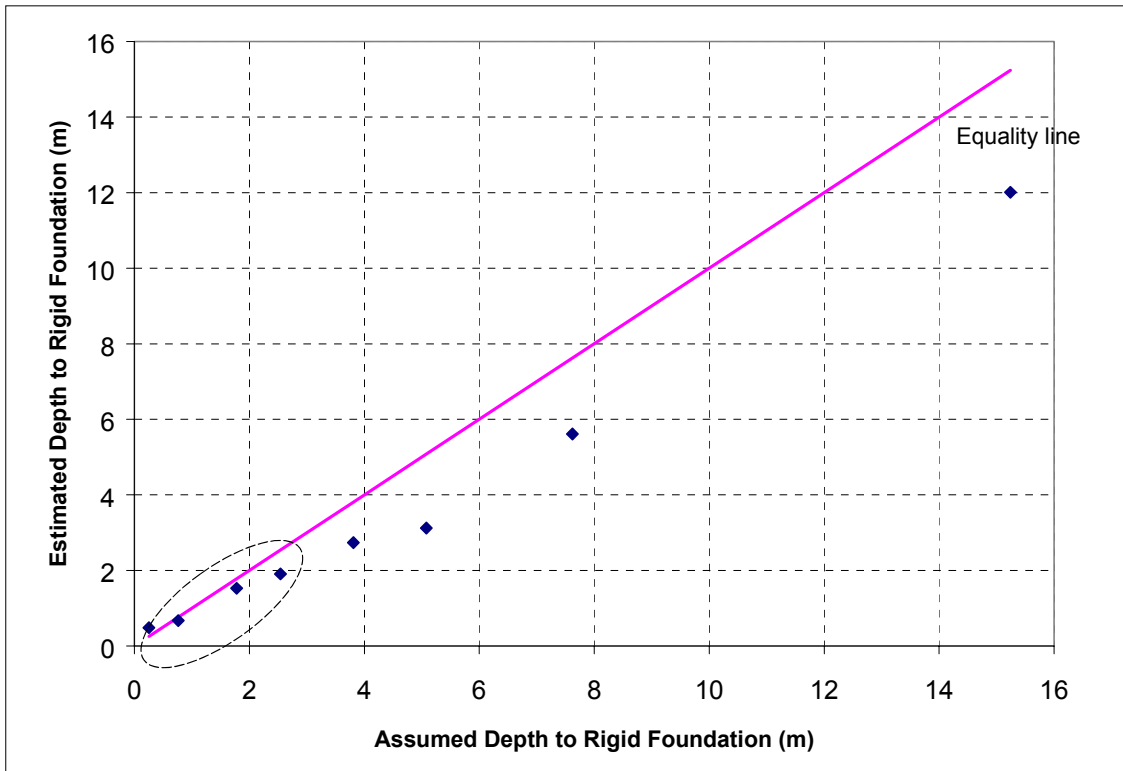
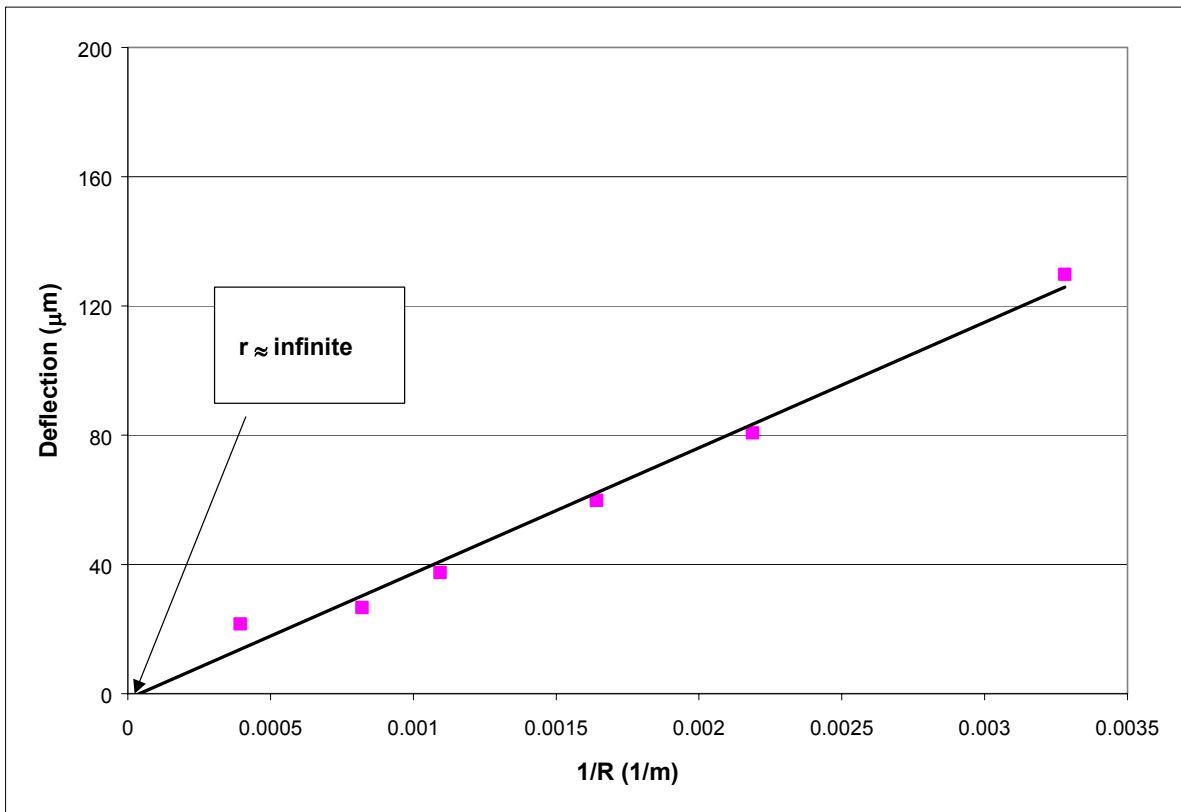


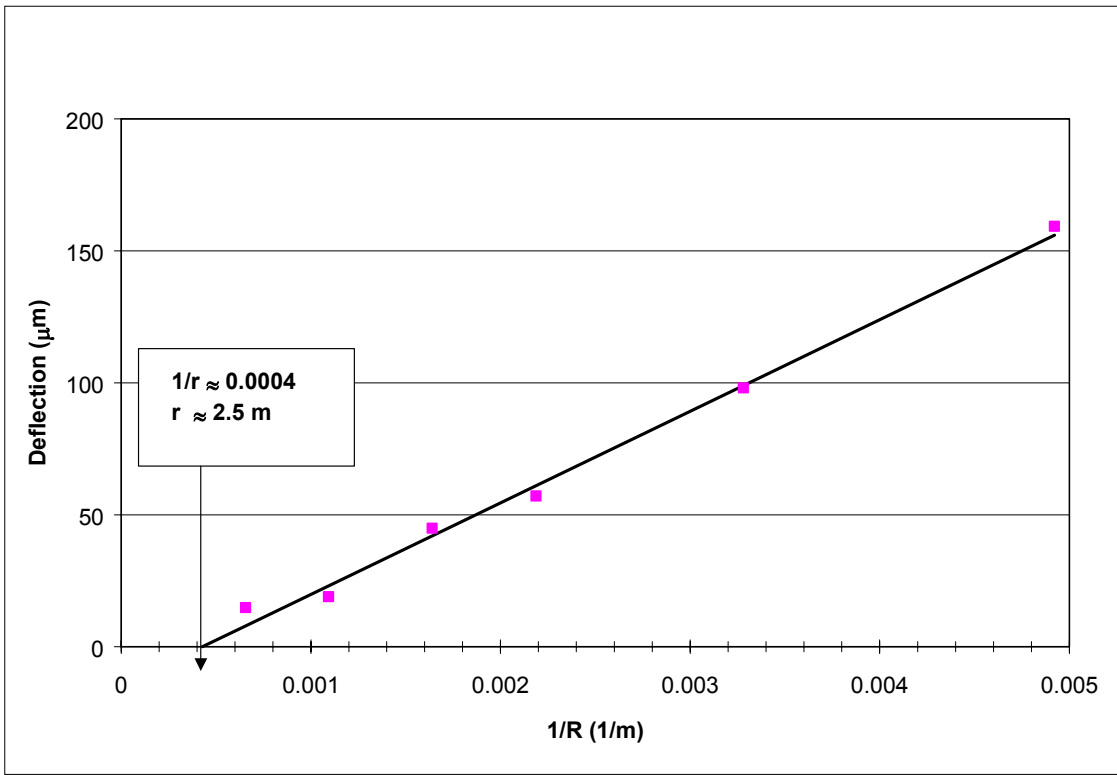
Figure 3.20. Depth to Bedrock Estimation for the Synthetic Basins (Large Plate).



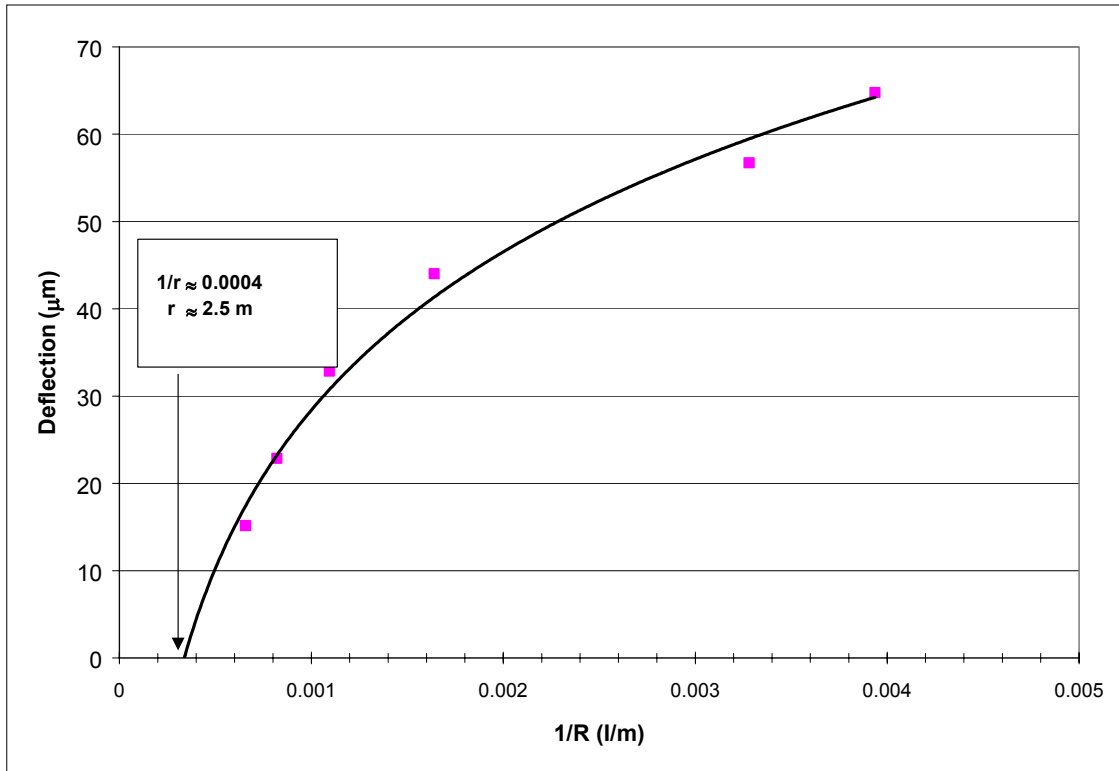
**Figure 3.21.** Comparison between Assumed and Estimated Depth to Rigid Foundation Using Synthetic Basins (Large Plate).



**Figure 3.22** Depth of Stiff Layer Estimation for Section A.



(a)



(b)

**Figure 3.23** Depth of Stiff Layer Estimation for Section J using Deflection from Subgrade and Wearing Surface respectively.

As an example, this procedure was applied to the deflections on top of the subgrade for Section A as shown in Figure 3.22), the plot does not indicate the presence of a stiff layer, it is also known that Section A was built on a fill. For Sections J, shown in Figure 3.23, the results were consistent using deflections on top of the subgrade and the wearing surface, which suggests that there is a stiff layer approximately 2.5 m below the surface. This finding is also consistent with the results of the two-layer analysis with ELSYM5 discussed in the previous section.

### **3.2.6 Summary of The Subgrade Analysis**

A summary of the results using the aforementioned approaches is presented in Table 3.7. Although the results of the different approaches are generally in agreement, differences were observed in some sections, in particular Sections F and G from the linear elastic analysis method. The percentage differences for these sections are 40 and 43% for the linear elastic analysis respectively, the average of the large and small plates results obtained from the layered elastic analysis do not differ much from results using the apparent subgrade formulae as shown in Figure 3.24. They show a similar trend, with Section I having the highest moduli and Section L having the lowest moduli. However, from Table 3.8, the differences in subgrade moduli when utilizing the large and small plates using the deflections from the first sensor ( $D_0$ ) is very high when compared to other analysis approaches. The average difference is 22%. Since the resulting bulk stress for the small plate is larger than that of the large plate, the resultant subgrade modulus is less when utilizing the large plate.

Section I differs from the other sections, it has a subgrade modulus of 675 to 1000 MPa, which is more than twice the moduli of the other sections (Table 3.7). This very high moduli could be due to measurements conducted on a singular (very hard) spot, as noted earlier. The moduli using all sensors are much higher than those obtained without including the first two sensors (Tables 3.4 and 3.5). After careful review of the measurements, the average values obtained without considering the first two sensors were adopted for use in the subsequent analysis for determining the moduli of the overlying pavement layers. In the sections where a stiff layer was detected to be present, the moduli may need to be adjusted to account for the actual thickness of the subgrade. Results presented in Table 3.8 also show the analysis done without considering the first two sensors have the lowest percentage difference (7%) between the moduli obtained

**Table 3.7.** Summary of Subgrade Moduli Computed Using Different Methods (MPa).

Section	Layered Elastic Analysis ELSYM5 (40 kN)				Apparent Surface Modulus Analysis									
	Stiff Layer	Large Pl.	Small Pl.	Average	Non- Lin. <sup>(1)</sup>	D <sub>0</sub> & All Loads			All Sensors & Loads			D <sub>2</sub> -D <sub>6</sub> & All Loads		
						Large Pl.	Small Pl.	Average	Large Pl.	Small Pl.	Average	Large Pl.	Small Pl.	Average
A	No	345	345	345	No	281	328	304	337	332	335	362	341	351
B	No	414	345	379	Possible	301	358	329	378	411	395	411	436	423
C	No	276	310	293	Possible	232	310	271	280	306	293	299	313	306
D	No	276	276	276	Possible	216	282	249	265	295	280	284	307	296
E	Possible	241	241	241	No	199	254	226	247	270	258	266	280	273
F	Possible	172	241	207	Possible	203	261	232	257	291	274	276	308	292
G	Possible	241	345	293	Probable	197	248	222	345	359	352	399	397	398
H	No	207	207	207	No	301	342	321	245	291	268	233	289	261
I	No	1034	966	1000	No	949	1011	980	732	828	780	613	737	675
J	Possible	379	310	345	Probable	387	332	360	476	480	478	543	563	553
K	Possible	241	276	259	Probable	369	286	327	325	358	341	358	407	382
L	Possible	172	172	172	Possible	174	228	201	202	203	203	237	220	228
Average		333	336	335		317	353	335	341	369	355	357	383	370
(w/o I)		270	279	274		260	293	277	305	327	316	333	351	342
Std. Dev.		234	206	219		211	211	209	144	161	152	120	143	131
(w/o I)		80	59	65		73	43	54	77	74	75	93	94	93
COV		70	61	65		66	60	62	42	44	43	30	38	34
(w/o I)		30	21	24		28	15	19	25	23	24	26	27	27

<sup>(1)</sup> Indication of nonlinear behavior or stiff layer while analyzing the change in subgrade modulus with distance to the load center.

**Table 3.8.** Summary of Percentage Differences between Moduli Utilizing Large and Small Plates.

Section	Layered Elastic Analysis ELSYM5 (40 kN)			Apparent Surface Modulus Analysis								
	Large Pl.	Small Pl.	Difference (%)	D <sub>0</sub> & All Loads			All Sensors & Loads			D <sub>2</sub> -D <sub>6</sub> & All Loads		
				Large Pl.	Small Pl.	Difference (%)	Large Pl.	Small Pl.	Difference (%)	Large Pl.	Small Pl.	Difference (%)
A	345	345	0	281	328	17	337	332	2	362	341	6
B	414	345	17	301	358	19	378	411	9	411	436	6
C	276	310	12	232	310	34	280	306	9	299	313	5
D	276	276	0	216	282	31	265	295	11	284	307	8
E	241	241	0	199	254	28	247	270	9	266	280	5
F	172	241	40	203	261	29	257	291	13	276	308	12
G	241	345	43	197	248	26	345	359	4	399	397	1
H	207	207	0	301	342	14	245	291	19	233	240	3
I	1034	966	7	949	1011	7	732	828	13	613	737	20
J	379	310	18	387	332	14	476	480	1	543	563	4
K	241	276	14	369	286	23	325	358	10	358	407	14
L	172	172	0	174	228	31	202	203	0	237	220	7
Average Difference (%)			13			22			8			7

utilizing the small and large plates. The depth to stiff layer was also investigated with ELSYM5 software and Ullidtz (1988) method. A stiff layer is possible in Sections E, F, G, J, K and L. Analysis of FWD deflection data using the small and large plates showed the measured deflections plots fell between linear elastic analysis and deflections resulting from using the nonlinear relationship of  $8000\theta^{0.6}$ . Measured deflections after the second sensor spacing (300 mm) showed the subgrade could be adequately modeled as linear elastic for most of the sections.

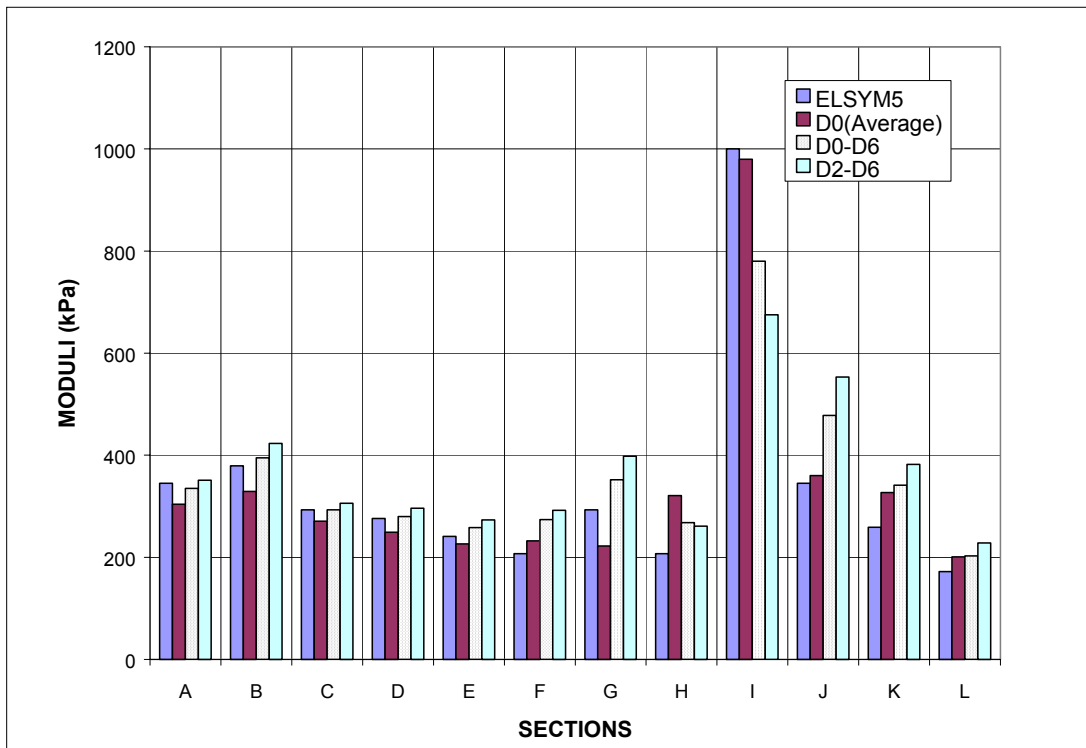


**Figure 3.24** Average Subgrade Moduli Determined Using Different Analysis Methods Summarized in Table 3.7.

### 3.3 GRANULAR SUBBASE (21-B) ANALYSIS

The computation of the subgrade moduli made it possible to compute the in-situ resilient modulus of the granular subbase layer (21-B) utilizing the deflections measured over that layer. The small and large plate was used for FWD testing over the 21-B layer. Using the subgrade moduli computed in the previous section, the pavement was modeled as a two-layer system: a subbase layer and a half-space subgrade. In addition, combined subgrade-subbase moduli

were also determined using the deflections measured over the 21-B assuming a uniform half-space.

### **3.3.1 Two-layer Linear Elastic System**

In this approach, the pavement on each section was modeled as a two-layer system, consisting of a granular course of finite thickness placed on top of a uniform half-space, with the elastic modulus listed in the last column of Table 3.6. Additional considerations were taken in those sections where a potential shallow stiff layer was identified in the previous section. The 21-B elastic modulus was estimated using ELSYM5 and several backcalculation software packages (Table 3.9). The 21-B result with the lowest MSE for each section was selected.

Most of the calculated moduli for the thin 21-B layers (75 mm) are unreasonably high. However, this was expected, because thin layers (75 mm or less) usually cause problems in all backcalculation procedures. Since the subbase material has properties similar to the subgrade, these thin layers were combined with the subgrade for the analysis of the subsequent layers. The three software backcalculation packages used, ELMOD, PEDMOD and MICHBACK, were also used in estimating the moduli of the 21-B layer. ELMOD backcalculates the modulus of each layer in two, three, or four-layered pavement systems using an Odemark-Boussinesq transformed section (method of equivalent thickness). PEDMOD95 is a Windows-based shell that integrates different pavement analysis software (e.g., BISAR and WESDEF) in a mechanistically based pavement analysis and design system (McQueen, 1999). MICHBACK version 1.0 is a public domain, menu-driven software package that estimates the pavement layer moduli, unknown layer thickness, and/or depth to a stiff layer (if present).

The results from the different software packages are similar. PEDMOD provided the most consistent results. MICHBACK apparently overestimated the 21-B moduli. Both ELMOD procedures, radius of curvature (default procedure) and deflection basin fitting, were tested. The modulus of the subgrade ( $E_2$ ) was fixed in the basin fit procedure. The ELMOD program modifies it, if needed, to improve the fitting between the computed and measure deflections. However, the deflection basin fit procedure produced more consistent results for all the sections.

**Table 3.9.** 21-B Moduli Considering a Two-Layer System (MPa).

Section	21-B Thick. (mm)	Subg. Moduli (MPa)	21-B Moduli (MPa)					
			ELSYM5	MICHBACK <sup>(1)</sup>	PEDMOD	ELMOD4 (All Loads, SP)		
			(MPa, 40 kN load, Small plate)			RC*	DBF <sup>+</sup> <sup>(2)</sup>	
A	178	351	138	204 (18)	216	187	212 (294)	
B	178	423	207	280 (18)	267	230	292 (305)	
C	178	306	207	351 (18)	275	246	319 (224)	
D	178	N/A	N/A	N/A N/A	N/A	N/A	N/A	
E	76	273	103	430 (18)	259	186	254 (240)	
F	152	292	207	297 (9)	314	314	384 (209)	
G	152	398	103	246 (18)	217	136	268 (179)	
H	76	261	1034	360 (6)	>690	376	229 (294)	
I	76	675	--	>690 (5)	>690	675	1351 (287)	
J	152	553	--	>690 (2)	275	150	649 (132)	
K	152	381	--	>690 (6)	265	127	421 (122)	
L	76	228	--	>690 (2)	>690	54	1095 (81)	
Average A-C			184	278	253	221	274	
Average F-G			155	272	266	225	326	
Average J-K			--	--	270	138	535	

<sup>(1)</sup> Depth to stiff layer (m) provided between brackets. \*Radius of Curvature

<sup>(2)</sup> Computed moduli for the subgrade are between brackets. + Deflection basin fit

### 3.3.2 Single-Layer System

The subbase and subgrade may be dealt with as one layer, given the great variability in the results obtained in the previous section, the use of the 21-B leveling layer underneath the 21-B subbase, and the similarity between 21-B and the fill material (mostly 21-B) properties. Table 3.10 presents a summary of the apparent surface moduli computed using the maximum deflection (equation 2.4) and the average of all sensors, as well as the average results for both plates for each section. Section B was tested using the small plate only, and one test load (22 kN) was conducted on section D, when both sections were under construction. The average combined moduli computed for each sensor (all drops) for the deflections measured over the subbase (combined layers) are in general comparable to those computed for the subgrade only with Section I producing the highest moduli.

**Table 3.10.** Combined Subbase-Subgrade Moduli (MPa).

Section	Using $D_0$ & All Loads				All Sensors & Loads			
	Large Pl.	Small Pl.	Average	Difference (%)	Large Pl.	Small Pl.	Average	Difference (%)
A	200	189	195	6	314	333	323	6
B	N/A	230	230	N/A	N/A	328	328	N/A
C	160	207	183	29	211	241	226	14
D	129	N/A	129	N/A	192	N/A	192	4
E	137	188	162	37	244	254	249	6
F	155	233	194	50	313	333	323	3
G	110	166	138	51	234	242	238	3
H	345	346	342	0	304	295	299	3
I	1,034	1,139	1,086	10	740	753	746	2
J	454	434	444	4	381	401	391	5
K	391	348	369	11	324	349	336	8
L	174	232	203	33	200	219	210	10
Average	299	337	306	23	314	341	322	6
w/o I	225	257	235		272	299	283	
Std Dev.	270	279	265		154	148	147	
w/o I	123	88	103		64	59	63	
COV	91	83	86		43	49	46	
w/o I	55	34	44		20	23	22	

### 3.4 SUMMARY AND CONCLUSIONS

The deflections obtained from the FWD using two testing plate sizes were analyzed to estimate the in-situ resilient modulus of the subgrade and subbase materials. The analysis of the deflection measured over the subgrade was initially used to determine the combination of subgrade modulus and depth to bedrock. Four approaches were used: (1) using only the maximum surface deflection ( $D_0$ ) over a semi-infinite linear elastic homogenous half-space (one-layer system); (2) using all sensors (assuming a point load) on a single-layer system; (3) using measured deflections from the sensors on an assumed nonlinear elastic subgrade; and (4) using a two-layer system to determine both the subgrade modulus and depth to bedrock.

The results of the approaches (1), (2), and (4) are in reasonable agreement. However, significant differences were observed for some of the sections. In particular, for Section I, the moduli obtained is more than twice the moduli of the other layers. The differences probably occurred because the measurements were conducted on a singular (very hard) spot.

The average apparent subgrade moduli utilizing the small and large plates without the first two sensors range from 273 to 675 MPa. This variation is attributed to the fact that seven

sections were built on a fill that its backcalculated modulus ranges from 261 to 423 MPa, while the other five sections were built on a cut and its backcalculated modulus ranges from 228 to 675 MPa. A coefficient of variation of approximately 27% was observed for moduli computed using measurements at different loads within a specific section.

Plots of the computed surface moduli against the distance of the sensors from the center of the applied load indicated mild non-linear behavior of the subgrade. In particular, Sections G, J, and K appeared to show relatively significant nonlinear subgrade behavior. The increase in apparent surface modulus could also be due to the presence of a stiff layer (bedrock) in the subgrade or large rocks (possibly in Section G). Analysis of FWD data using a small loading plate indicates that the modulus of the subgrade can also be described by a nonlinear relationship given by  $8000\theta^{0.6}$  for nonlinear behavior.

The results of the two-layer system analysis utilizing the FWD data from the small and large plates were close with a difference ranging from 6 to 10%. It was decided to use the moduli obtained from the large plate for subsequent analysis since the results of the depth to bedrock estimation was closer to Ullidtz analytical method with the large plate.

The "as-built" in-situ modulus of the granular subbase layer 21-B was determined based on the deflections measured over that layer. Using the computed subgrade moduli, the pavement was modeled as a two-layer system: a subbase layer and a half-space subgrade. The 21-B elastic modulus was estimated using ELSYM5 and three backcalculation software packages. The backcalculated resilient moduli of thin 21-B layers (75 mm) were found to be very high, but this was expected because thin layers (75 mm or less) usually cause problems in all backcalculation procedures. PEDMOD software provided the most consistent results. MICHBACK software apparently overestimated the 21-B moduli, while ELMOD results were more variable.

Combined subgrade-subbase moduli were determined using the deflections measured over the 21-B layer, assuming a uniform half-space. Results from analysis using all sensors produced a difference of 6% in moduli when utilizing the large and small plates, while 23% was resulted when only the first sensor deflection was used for all loads.

It is clear that Boussinesq's equation using deflections after two radii away from the FWD large plate produces more satisfactory results when analyzing the subgrade in both cut and fill sections at the Virginia Smart Road and the 21-B layer. This approach produced the least difference between the moduli utilizing large and small rigid plates. It also produced the least coefficient of variance (30%) for all the sections. The depth to bedrock was determined with ELSYM5 software using the maximum surface deflection ( $D_0$ ) from the FWD large plate and

analytically verified for Sections A and J using method recommended by Ullidtz (1988). Perfect agreement was resulted between the two methods.

This study has concluded that the moduli of the subgrade and the granular 21-B layers can be estimated using the FWD small and large plates. Analysis of the results for these layers from both plates showed that the large plate produced lower coefficient of variation and better depth to bedrock estimation, hence, the results from the large plate was used in subsequent backcalculation analysis in determining the moduli of the other layers in all the sections of the Virginia Smart Road.

## REFERENCES

De Almeida, J. R., Brown, S. F., and Thom, N. H. (1994). "A Pavement Evaluation Procedure Incorporating Material Non-linearity." *Nondestructive Testing of Pavements and Backcalculation of Moduli*, ASTM STP 1198, Vol. 2, Von Quintas, H. L., Bush, A. J. III, and Baladi, G. Y., Eds., American Society for Testing and Materials, Philadelphia, PA, pp. 218-232.

Kopperman, S., Tiller, G., and Tseng, M. (1986). "ELSYM5 Interactive Microcomputer Version, User's Manual." Report No. FHWA-TS-87-206, Federal Highway Administration, Washington, D.C.

McQueen (1999). *PEPMOD95 User's Guide and PEPMOD95 Documentation*, Roy D. McQueen and Associates, Ltd., Sterling, VA.

Ullidtz, P. (1988). *Pavement Analysis*, Elsevier Science." New York, NY.

Uzan Jacob (1985). "Characterization of Granular Material." *Transportation Research Record 1022*, National Research Council, Washington, D.C., pp. 52-59.

## **CHAPTER FOUR FWD SPATIAL AND TEMPORAL VARIABILITY WITHIN AND BETWEEN PAVEMENT SECTIONS**

### **Abstract**

Falling weight deflectometer measurements were conducted on 12 sections at the Virginia Smart Road in order to quantify within and between test sections variability. Measurements were taken on the instrumented and noninstrumented lanes every 10 m from May 2000 through October 2002, while temperature data was collected every time FWD testing was conducted. Analysis of the deflection measurements and temperature data resulted in the development of an exponential model between deflection versus temperature with very good coefficient of determination for all 12 sections. An exponential relationship was also developed to correct deflections for temperatures within the range of temperatures at the bottom of the wearing surface during testing. Analysis of Variance (ANOVA) of the sensor deflections showed significant statistical differences between mean deflections of the different sections. Sensor spacing with the exception of the last sensor had no influence on the results. A temperature correction model was developed and compared to an independently developed correction model. Both models produced the same trend when used for all the test sections. After correction to a standard temperature of 25 °C, Sections K and L produced the highest deflections, while Sections B and D produced the lowest deflections. Results indicate that lowest coefficients of variation (COV's) are produced during the coldest temperatures of the wearing surface, while testing at intermediate temperatures produced the highest COV's. Deflection results from the outermost sensor produced the highest COV values. Analysis of deflection results from the first sensor ( $D_0$ ) is found to be enough in assessing variability among sections at the Virginia Smart Road. This study has concluded that temporal and spatial variations exist in the deflections within and between sections at the Virginia Smart Road. The COV ranged from as low as 7% to as high as 42% for the FWD center deflections. These variations are temperature dependent as well as dependent on the material properties used in the construction of the pavement.

#### 4.1 BACKGROUND

Deflection results from the FWD can be used in a backcalculation analysis procedure to give information on the in-situ stiffness moduli of the various pavement layers as well as to predict pavement structural capacity.

Several studies have focused on the spatial and temporal variability of FWD measurements, because the estimated structural capacity of existing pavements is known to be affected by the spatial variability of the measured deflections. Spatial variations are known to be due to the heterogeneous nature of the pavement materials while temporal variations in material properties are caused by temperature changes. Mamlouk *et al.* (1988) concluded from the results of extensive studies on test sections in Arizona that the variability caused by the equipment was insignificant compared to the spatial variability. Siddharthan *et al.* (1991) analyzed data from six sites approximately 300 m in length, where thickness of the hot-mix asphalt (HMA) material varied from 75 to 200 mm. Deflection testing was undertaken at 15 m intervals. The coefficient of variation (COV) of the measured deflections varied from 9 to 48%, with generally higher values occurring at sensors farthest away from the load plate.

Rauhut and Jordal (1992) found FWD deflection COV's ranging from 4 to more than 40% in 132 flexible and 88 rigid Long Term Pavement Performance (LTPP) sections. The backcalculated stiffness moduli COV's ranged from 13 to 67% for the sections in the United States. Variability in backcalculated moduli for base layers were much higher than for the HMA layers and the subgrade. The researchers also found that COV's for backcalculated HMA moduli were proportional to those for measured deflections at the center of the load. Statistical analysis showed that pavement structure, air temperature during testing, moisture, and annual precipitation contributed significantly to the variability of deflections.

Hossain *et al.* (1992) studied the effect of FWD deflections on the variability of the remaining service life of the pavement estimated in terms of equivalent single axle loads (ESAL's) to cause fatigue failure. The study found high variabilities in this process which were related to the variabilities in FWD input deflection data, which is used in the backcalculation scheme. The study also suggested that the FWD sensor readings showed more variability on a long section of roadway than on a short section. For a mile long section, five FWD tests were found to be a viable choice for estimating the remaining service life of the pavement. Hossain *et al.* (2000) reported that extreme test

temperatures, both high and low, resulted in high variation of measured deflections and subsequently backcalculated subgrade moduli across a site.

Kestler (1997) who studied the use of spatial variability deflection measurements to determine the optimum number and location of the FWD tests to optimize the cost of overlay design and pavement design costs, conducted FWD tests on 71 test points on top of each of the layers composing a pavement system. A geostatistical semi-variogram analysis, used to model the degree of correlation between the data at any two test points, showed that as the distance between test points increases, corresponding data become decreasingly dependent upon each other, until at some appreciable distance, they are independent of each other. Analysis of baseline FWD data with this technique could provide valuable and cost saving information. With the efficiency of future FWD testing maximized, optimum FWD test point spacing can be determined for evaluation and overlay design. As a result there could be a reduction in testing at unnecessary locations and greater use of representative coverage of any pavement section for pavement evaluation and overlay design.

This study analyzes FWD deflection measurements on the Virginia Smart Road using the deflections from the first sensor position and other sensors in order to assess the variability within and between test sections. Temperature and deflection data collected during the course of the project is used to develop a deflection temperature correction model to a standard temperature so that all the sections can be compared. The model developed is also validated with other deflection data at different temperatures.

## **4.2 SITE TESTING**

The flexible pavement test facility has an approximate total length of 1.4 km. Twelve different flexible pavement designs have been included in the Virginia Smart Road with the lengths varying from 76–117m. Sections A to D have the same structural properties, Sections E to G have varying thickness in the underlying layers of the BM 25.0, while sections H to L have special designs. The profile of the Virginia Smart Road is shown in Figure 4.1.

A Dynatest model 8000 FWD unit was used to monitor the structural capacity of the pavement system. Initially, FWD testing was conducted after the construction of each layer in one location in each section, and these locations were then used for each successive layer. The moisture and temperature of the placed layers were measured at

the time of testing. After construction, FWD testing has been conducted bi-monthly on the same locations to investigate the result of seasonal variation on the layer moduli as part of the periodic monitoring.

Section A	Section B	Section C	Section D	Section E	Section F	Section G	Section H	Section I	Section J	Section K	Section L
SM-12.5D	SM-9.5D	SM-9.5E	SM-9.5A	SM-9.5D	SM-9.5D	SM-9.5D	SM-9.5D	SM-9.5A	SM-9.5D	OGFC SM-9.5D	SMA-12.5
Base BM-25.0 (150mm)	Base BM-25.0 (150mm)	Base BM-25.0 (150mm)	Base BM-25.0 (150mm)	Base BM-25.0 (s25mm)	Base BM-25.0 (150mm)	Base BM-25.0 (100mm) SM-9.5A (50mm)	Base BM-25.0 (100mm) SM-9.5A (50mm)	Base BM-25.0 (100mm) SM-9.5A (50mm)	Base BM-25.0 (s25mm)	Base BM-25.0 (s25mm)	Base BM-25.0 (150mm)
OGDL (75mm)	OGDL (75mm)	OGDL (75mm)	OGDL (75mm)		21-A (CTA) (150mm)	21-A (CTA) (150mm)	OGDL (75mm)	OGDL (75mm)			OGDL (75mm)
21-A (CTA) (150mm)	21-A (CTA) (150mm)	21-A (CTA) (150mm)	21-A (CTA) (150mm)	21-A (CTA) (150mm)			21-A (CTA) (150mm)	21-A (CTA) (150mm)	OGDL (75mm)	OGDL (75mm)	21-A (CTA) (150mm)
21-B Subbase (180mm)	21-B Subbase (180mm)	21-B Subbase (180mm)	21-B Subbase (180mm)	Subbase 21-B Sub (75mm)	21-B Subbase (150mm)	21-B Subbase (150mm)	Subbase 21-B Sub (75mm)	Subbase 21-B Sub (75mm)	21-B Subbase (150mm)	21-B Subbase (150mm)	Subbase 21-B Sub (75mm)

Figure 4.1 Pavement Design for the Virginia Smart Road.

In addition, since May 2000, FWD testing has been conducted periodically every 10 m on both lanes using a 40 kN load and a nine-sensor array (with sensor spacing 0, 203, 305, 457, 610, 914, 1219, 1524, and 1829 mm).

Temperature data was also collected every time FWD testing was conducted on the wearing surface layers. The average pavement temperature for each test was determined as an average of the values measured by thermocouples installed in the bottom of the wearing surface layer. This process made it possible to develop temperature-deflection relationships.

### 4.3 SEASONAL VARIATION

Using 40 kN load at a spacing of 10 m, the seasonal variation on deflection data on Sections A to H (the first eight sections) was monitored to develop seasonal correction models. Four temperature regimes within a period of one year were investigated. The

analysis included testing done in August 2000, January 2001, February 2001 and April 2001. The average HMA temperatures during the testing dates in these months/periods were 35°C, 5°C, 16°C, and 25°C, respectively.

The average deflection bowls for each test are shown in Figures 4.2 through 4.9. As shown in Figures 4.2 and 4.3 the deflection at the center of the FWD loading plate  $D_0$  dropped from a range 60 – 80  $\mu\text{m}$  for the sections A through D in August to about 30 – 45  $\mu\text{m}$  in January which is almost a 50% reduction. Sections A through D have the same structure except for the wearing surface.

Sections E through H have the same overall thickness but a slightly different structural composition. Figures 4.6 through 4.9 show the deflection bowls resulting from 40kN of FWD testing for these sections. The deflection from the center of the loading plate rises in sections E through H from a range of 40-60 $\mu\text{m}$  in January, 2000 to 65-80 $\mu\text{m}$  in August 2001. A rise of almost 25% in deflections for a change in temperature from 5 °C to about 35 °C. The plots also show Sections E and F are stronger than G and H, as would be expected. The effects of temperature on deflections is noticeable, because higher temperatures result in greater deflections. Figure 4.10 shows a plot of center deflections A through L. Random variations are known due to heterogeneous nature of pavement materials and non-uniform layer thickness, whilst stratified variations, on the other hand are due to significant changes in layer thicknesses or materials. Random variations could be due to the presence of bedrock at shallow depths.

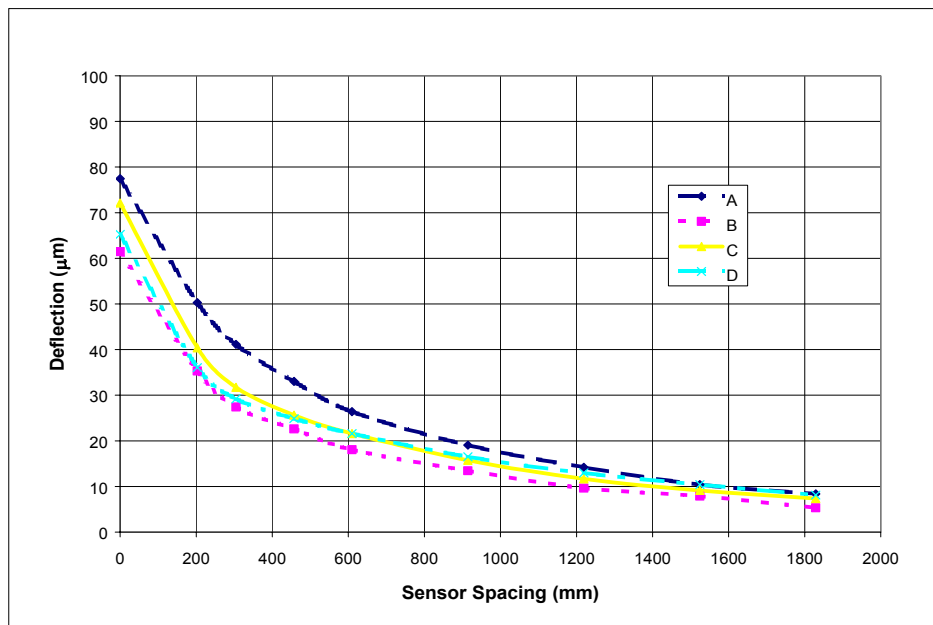


**Figure 4.2** Deflection Bowls for Sections A through D in August 2000.

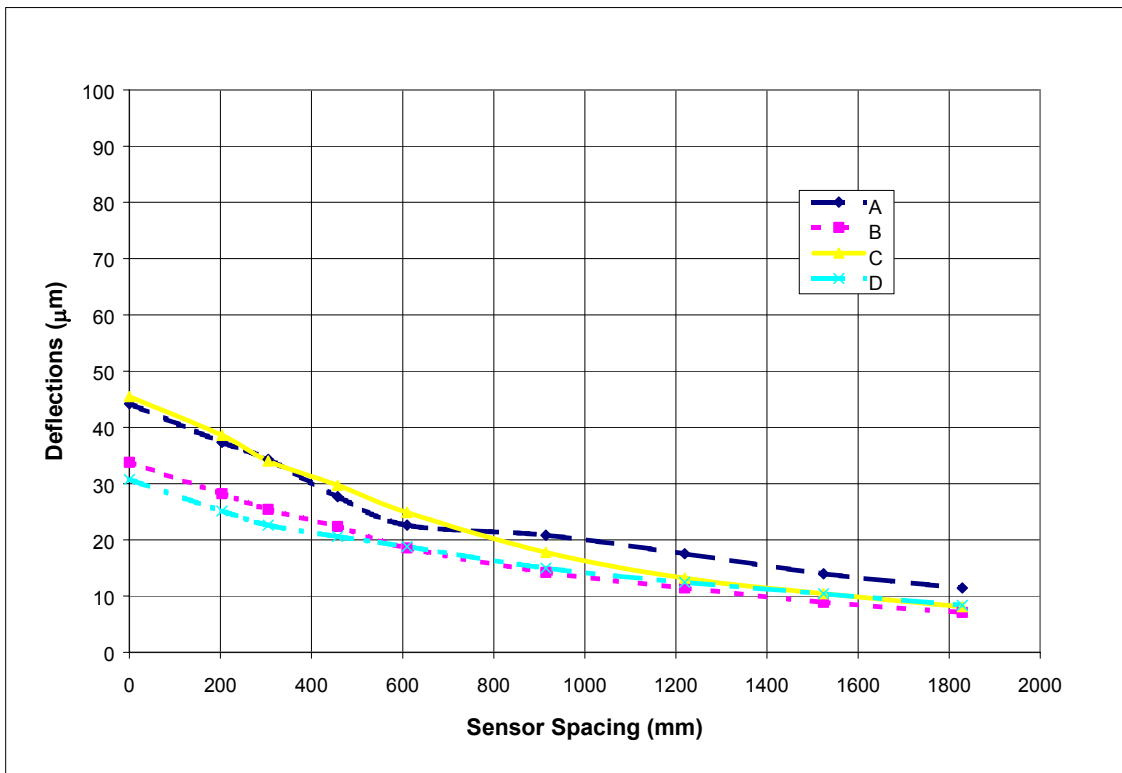


**Figure 4.3** Deflection Bowls for Sections A through D in January 2001.

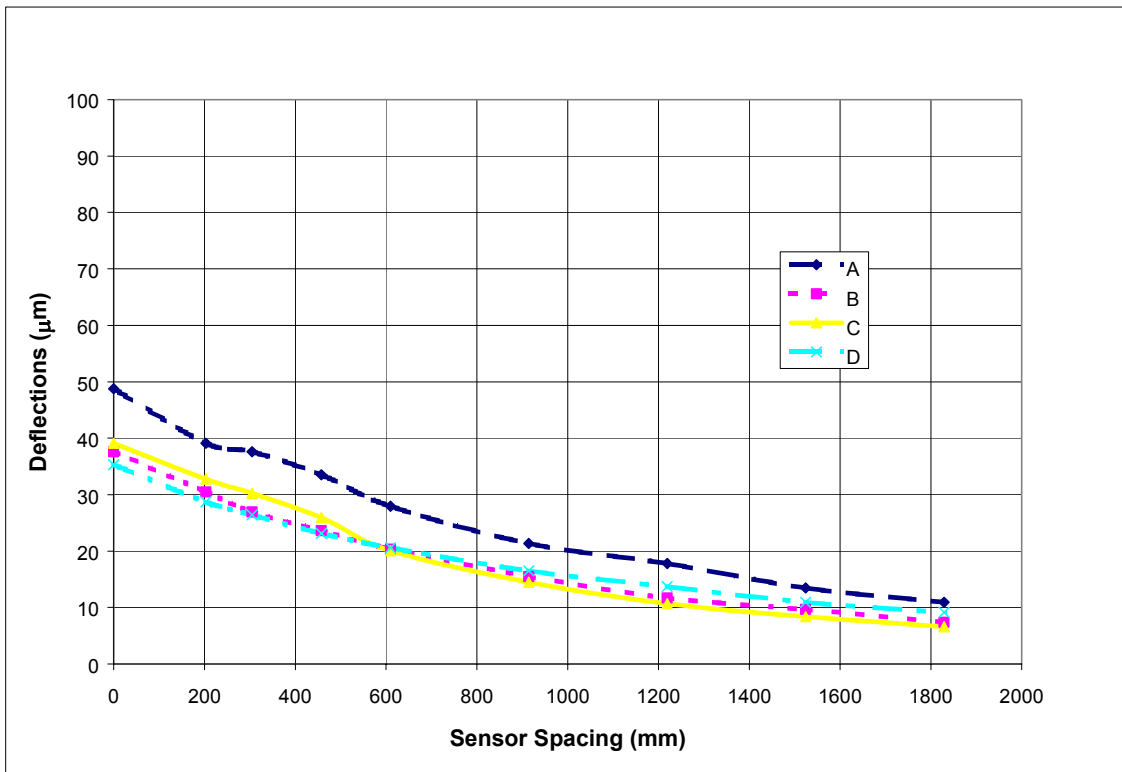


**Figure 4.4** Deflection Bowls for Sections A through D in February 2001.

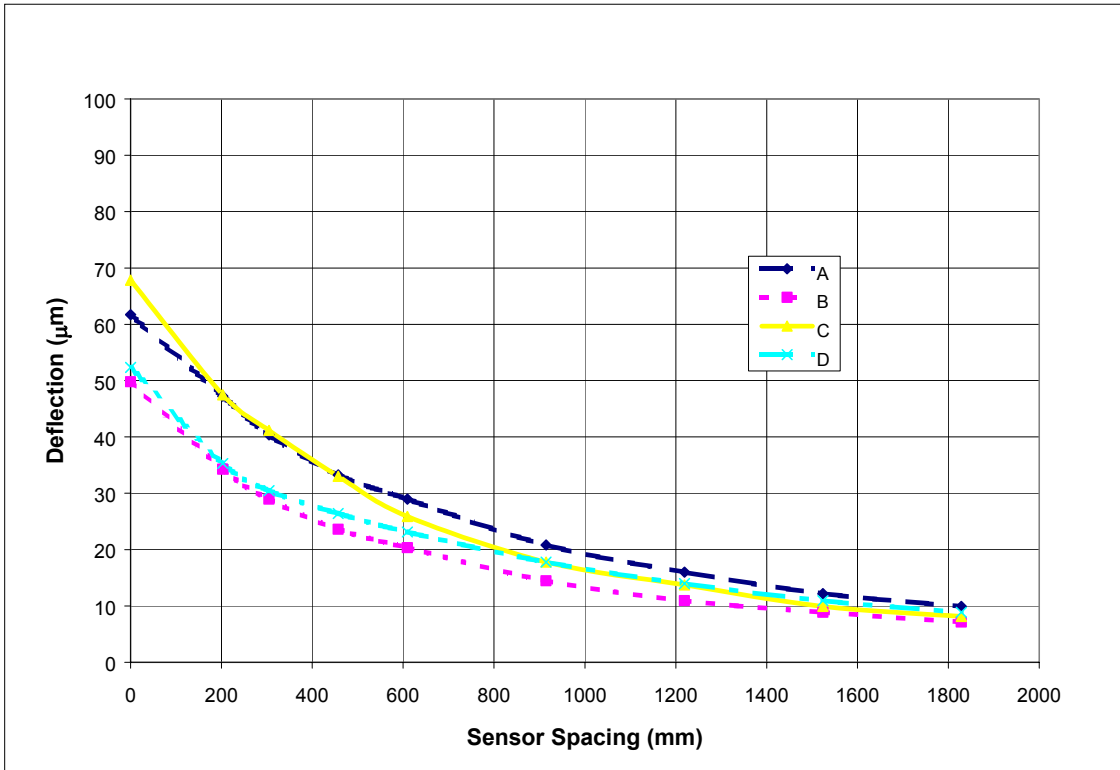


**Figure 4.5** Deflection Bowls for Sections A through D in April 2001.

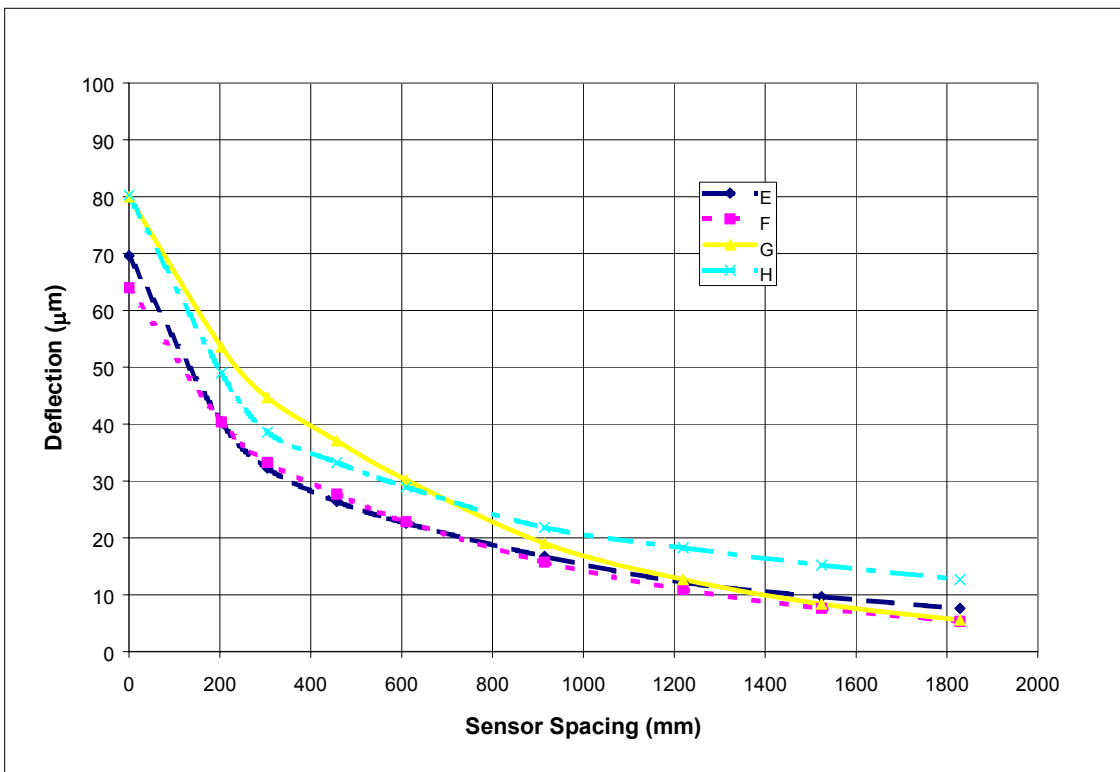


**Figure 4.6** Deflection Bowls for Sections E through H through in August 2000.

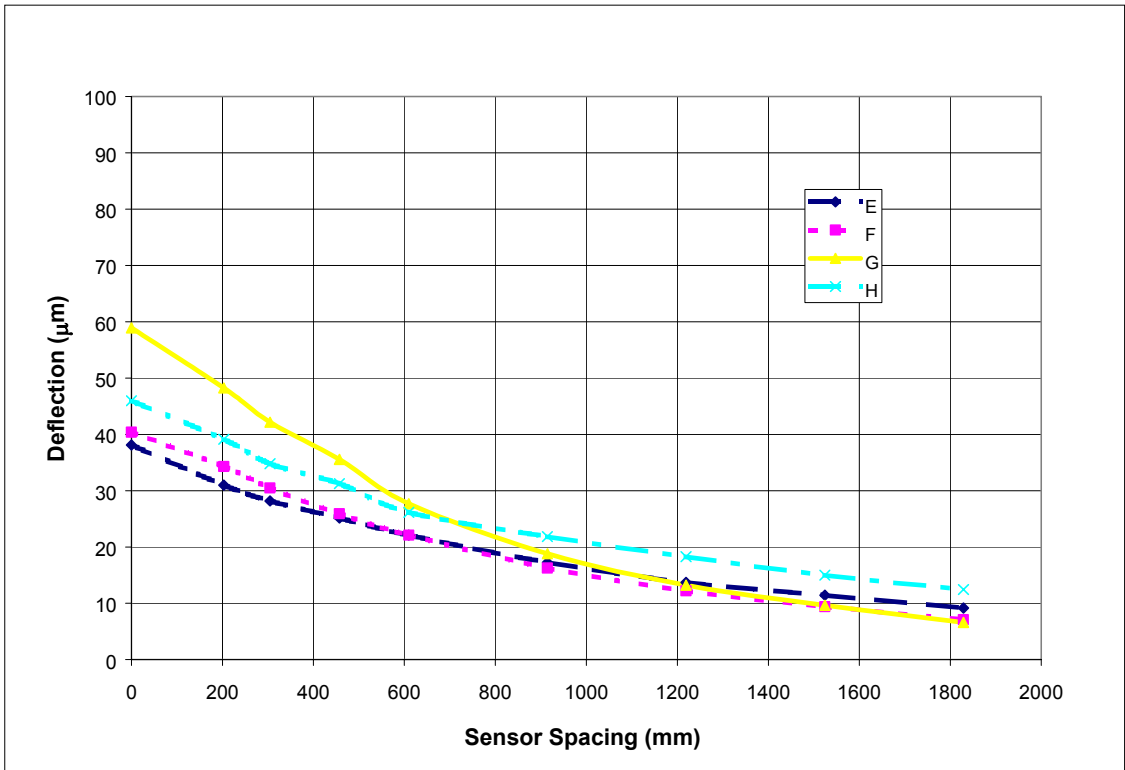


**Figure 4.7** Deflection Bowls for Sections E through H through in January 2001.

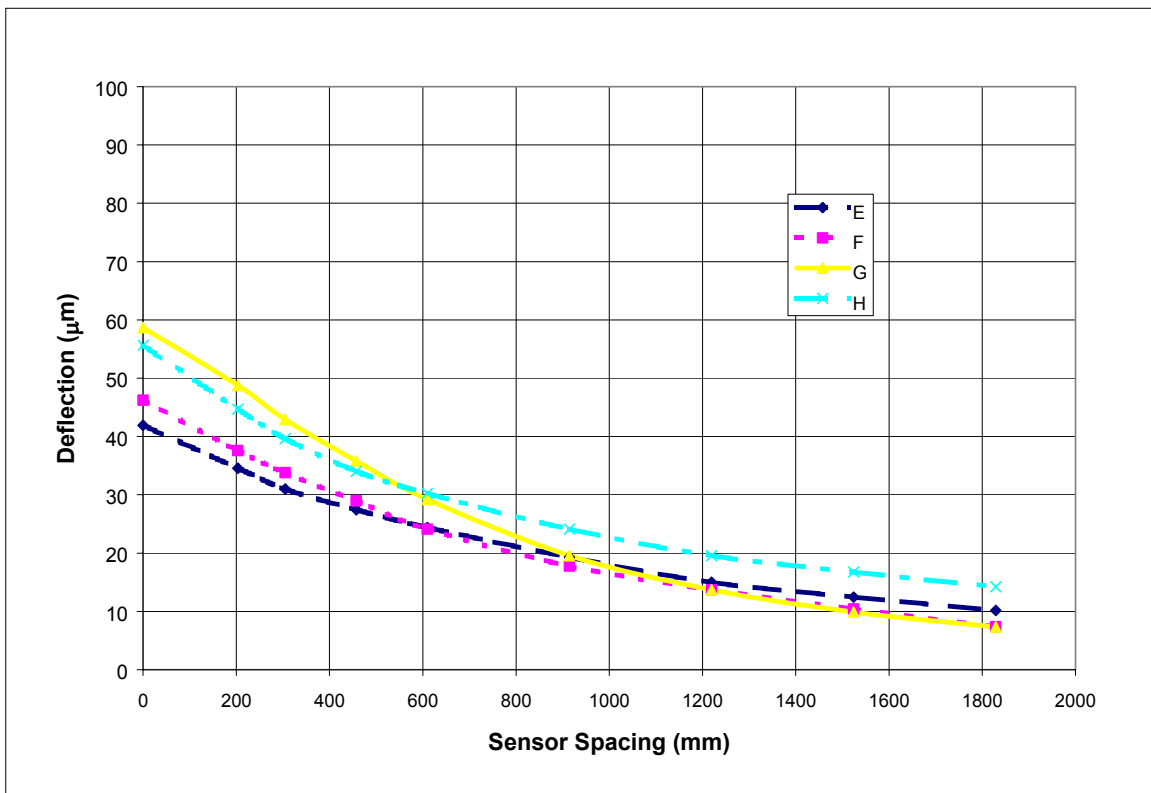


**Figure 4.8** Deflection Bowls for Sections E through H through in February 2001.

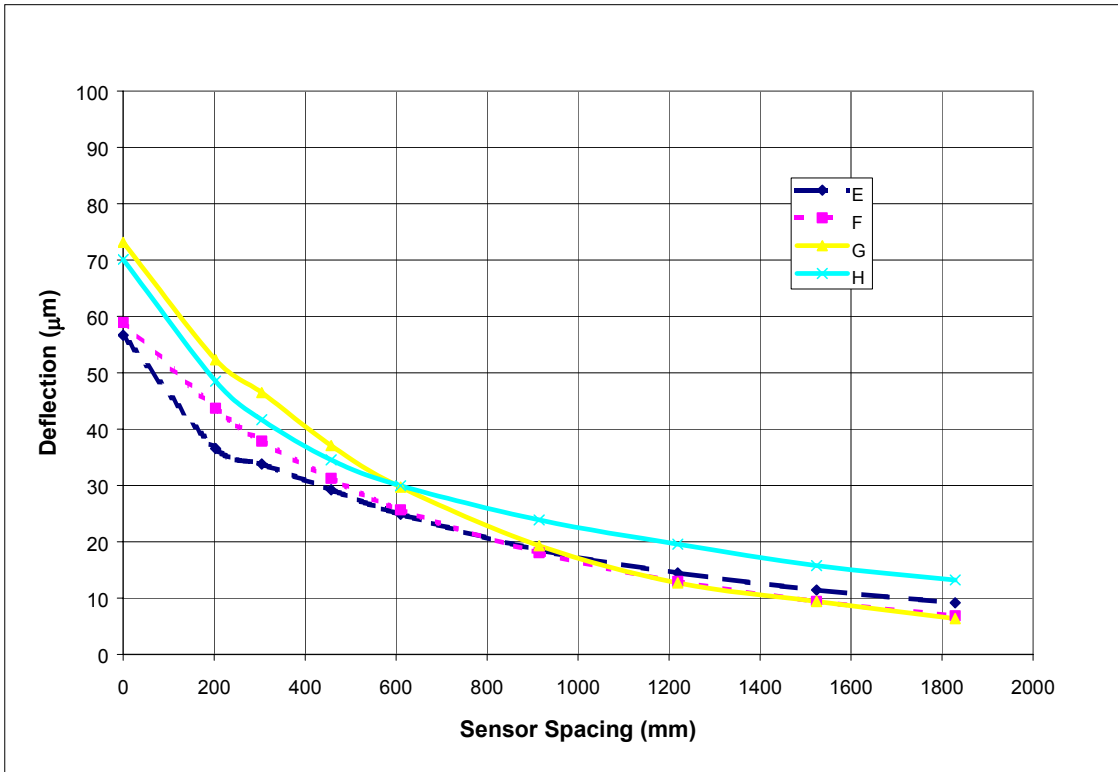


Figure 4.9 Deflection Bowls for Section E through H in April 2001.

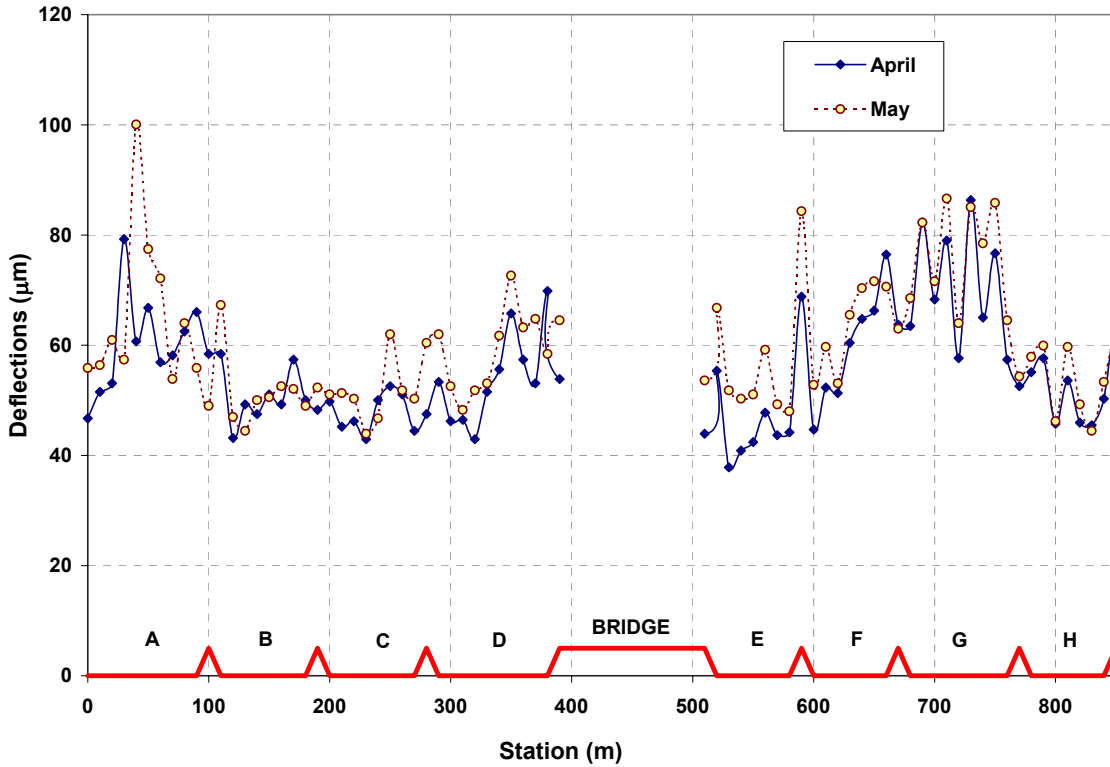


Figure 4.10 Deflections on the Instrumented Lane in April and May 2000.

#### 4.4 VARIABILITY WITHIN-SECTION

The within-section variability was investigated using the 40 kN load deflections measured every 10 m for testing conducted between January 2000 and November 2001. The average standard deviation, and coefficient of variation (COV) of the center and last sensor deflections,  $D_0$  and  $D_8$  (1829 mm from the center) were calculated for sections A through L. From these measurement the coefficient of variance of the deflections of each section was determined.

Plots of the COV of the center deflections for each section of the instrumented and non-instrumented lanes for May, 2000, August, 2000, December, 2000, April, 2001, May, 2001, July, 2001, and August, 2001 are shown in Figures 4.11 through 4.17, respectively. The plots of COV for the last sensor measurements in May 2000 and April 2001 are shown in Figures 4.18 and 4.19, respectively.

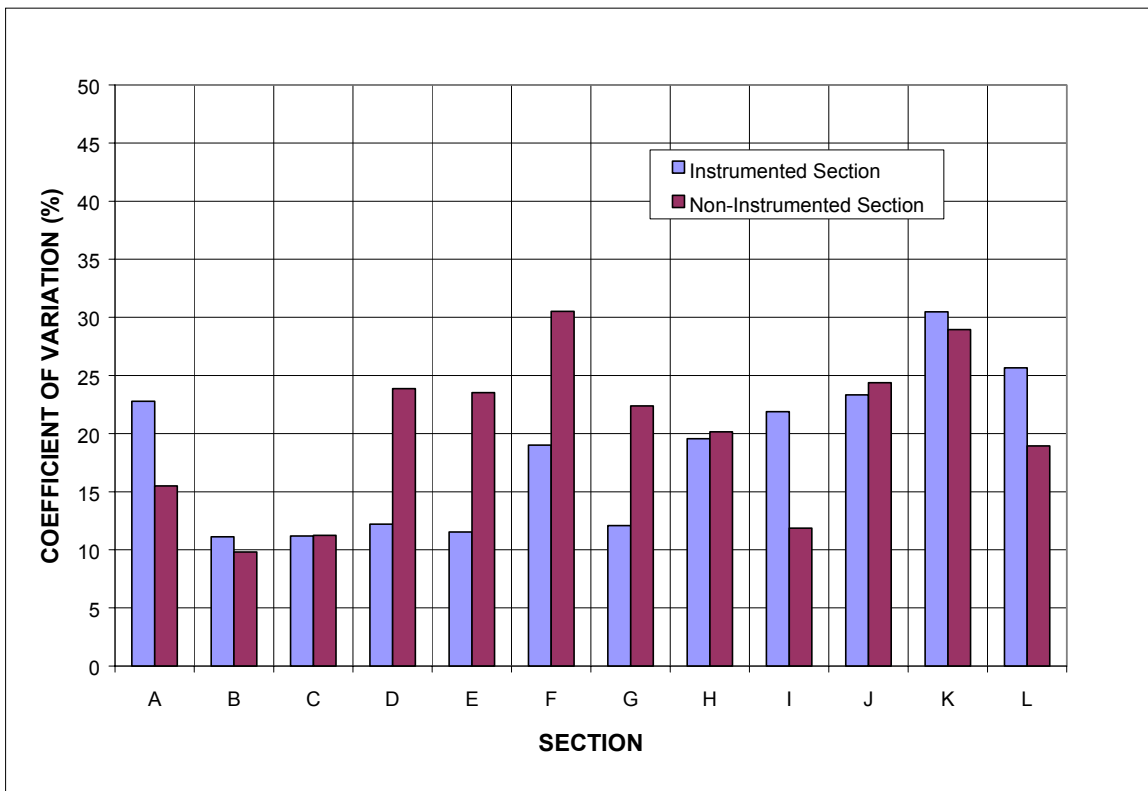
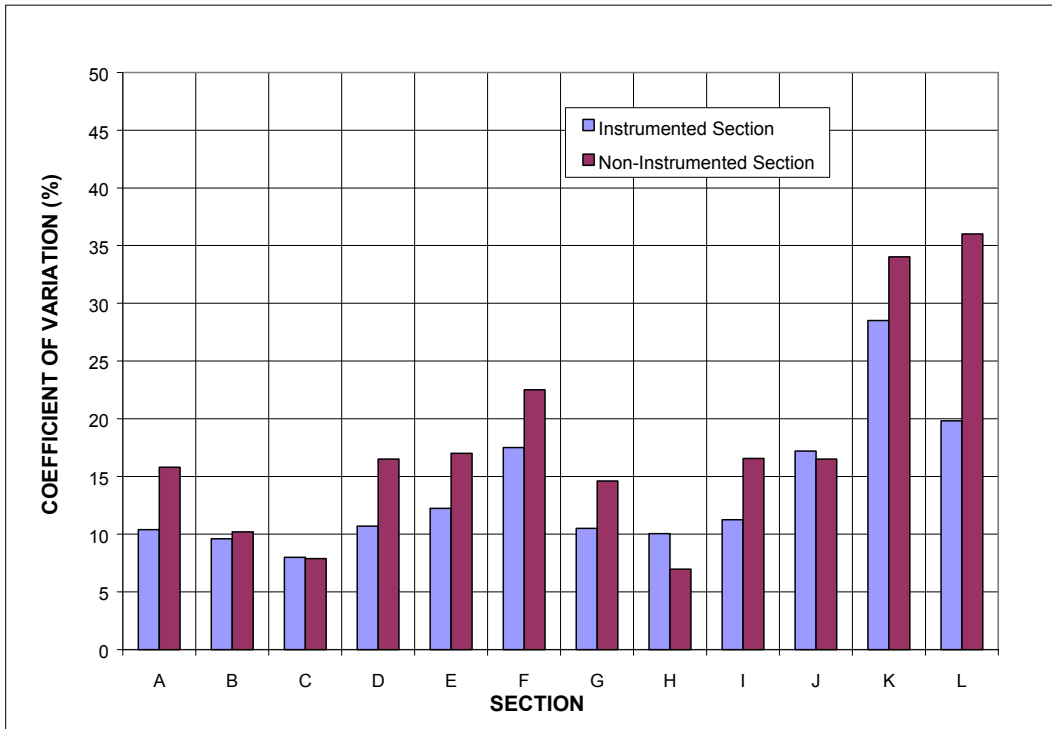
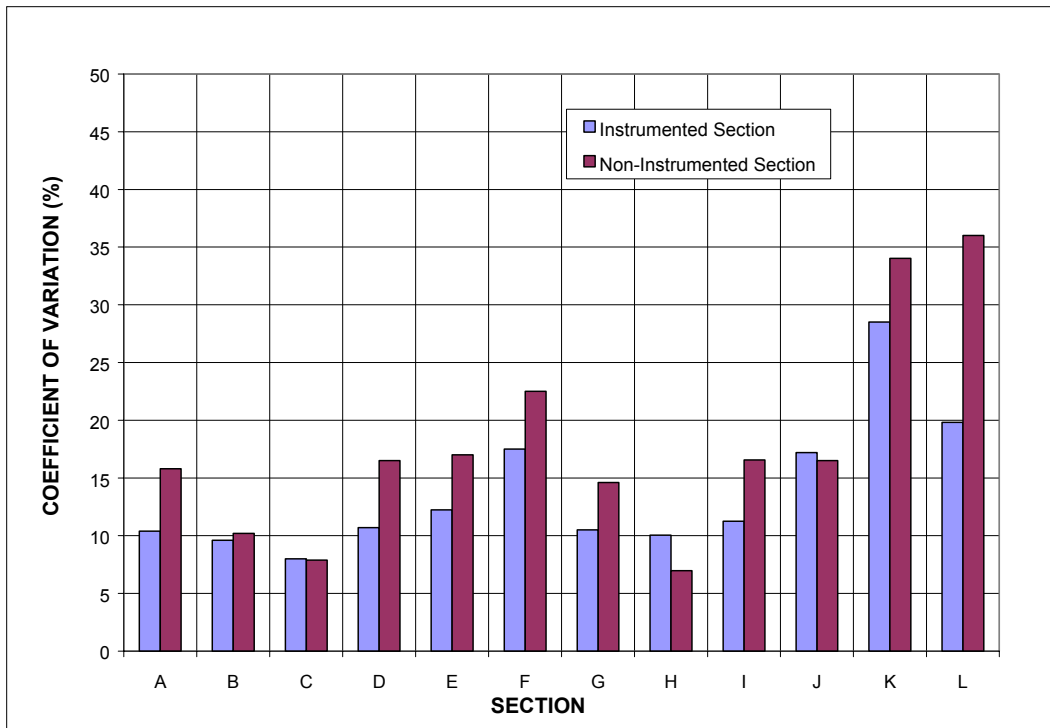


Figure 4.11 Variability of Center Deflections Measured in May 2000.



**Figure 4.12** Variability of Center Deflections Measured in August 2000.



**Figure 4.13** Variability of Center Deflections Measured in December 2000.

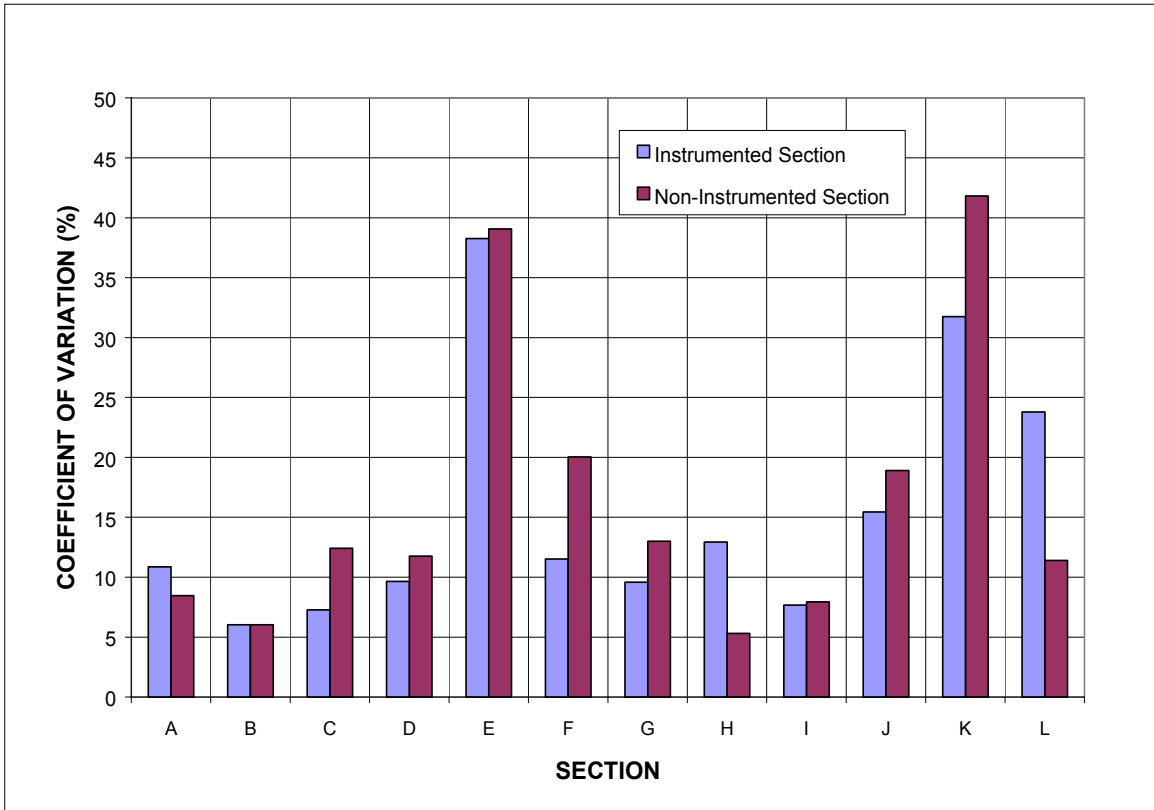


**Figure 4.14** Variability of Center Deflections Measured in April 2001.

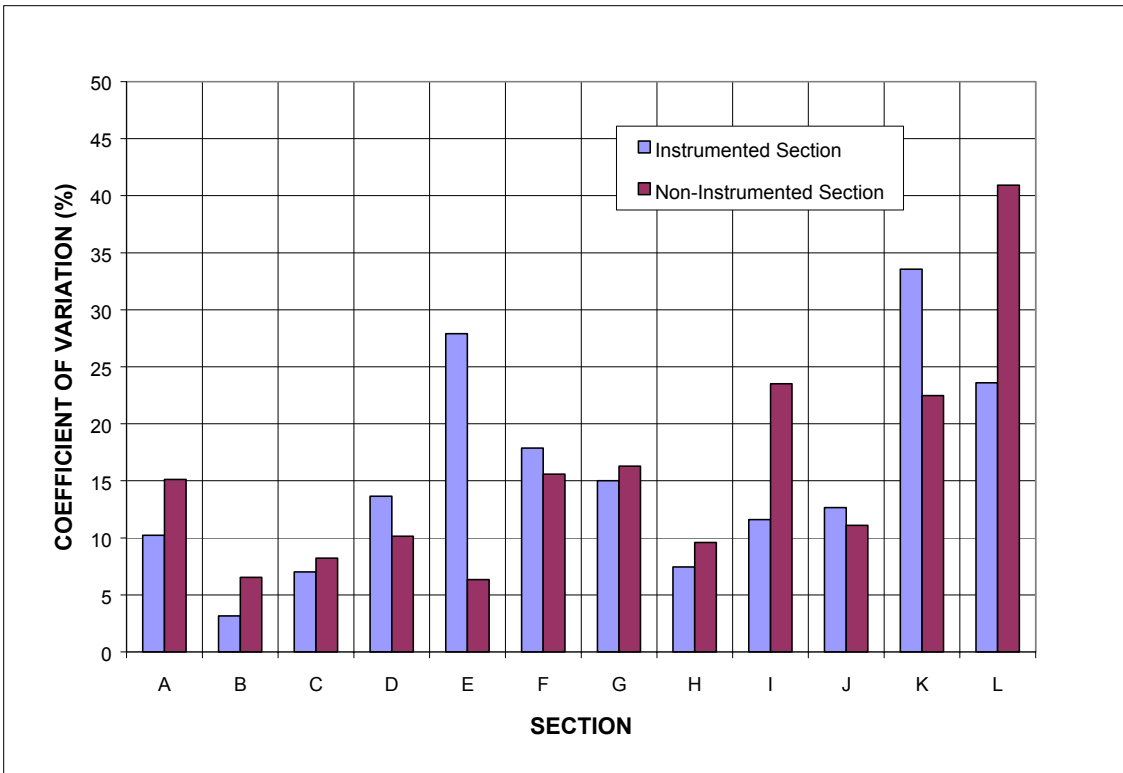


**Figure 4.15** Variability of Center Deflection Measured in May 2001.

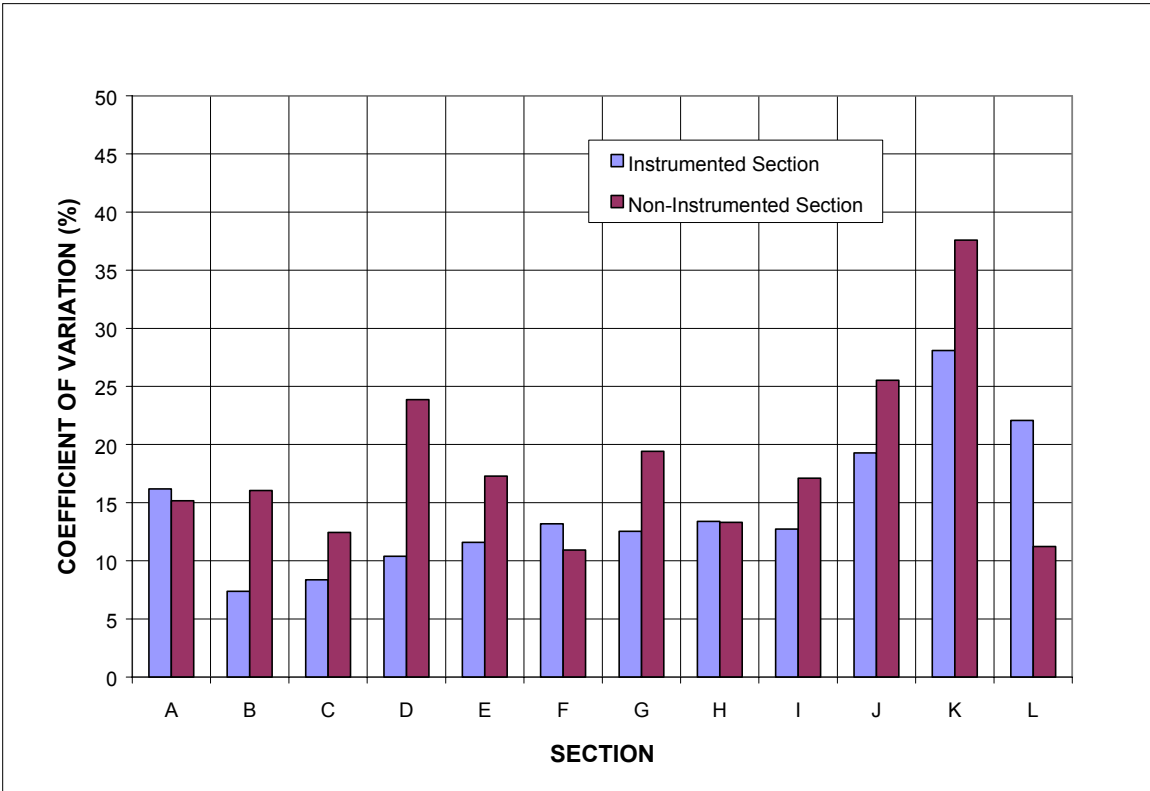


**Figure 4.16** Variability of Center Deflection Measured in July 2001.

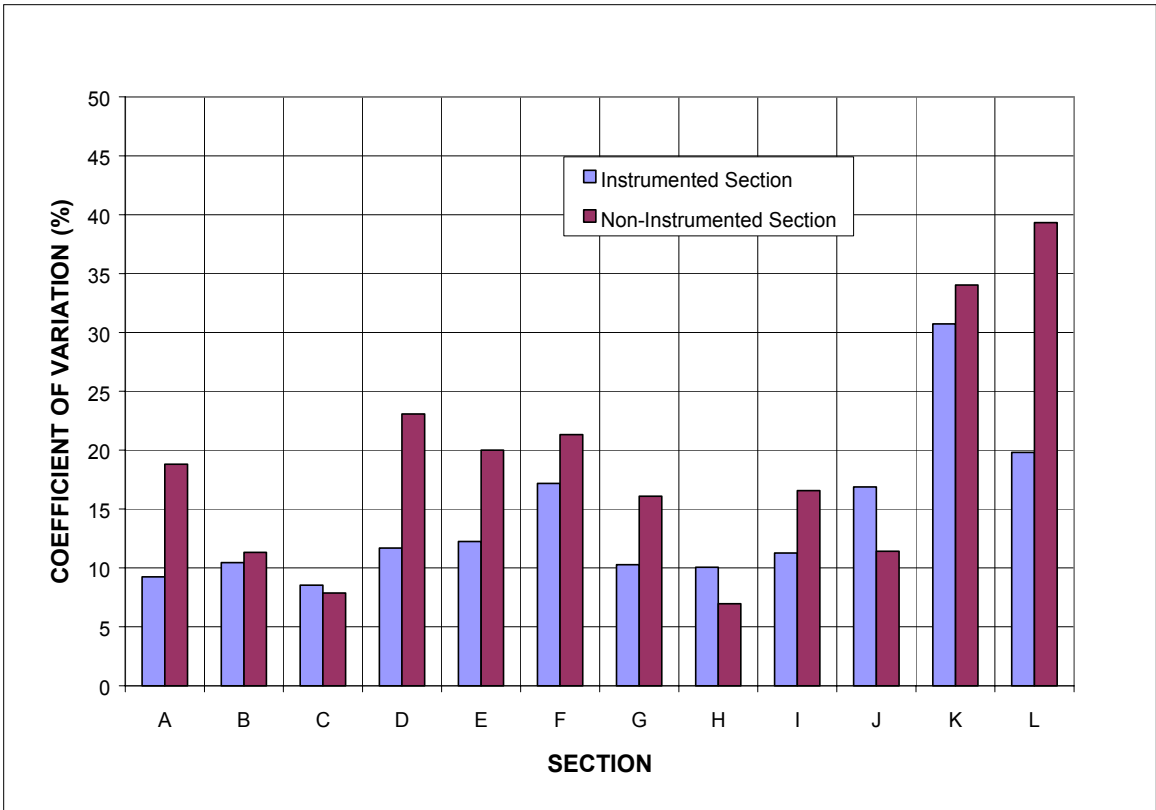


**Figure 4.17** Variability of Center Deflection Measured in August 2001.

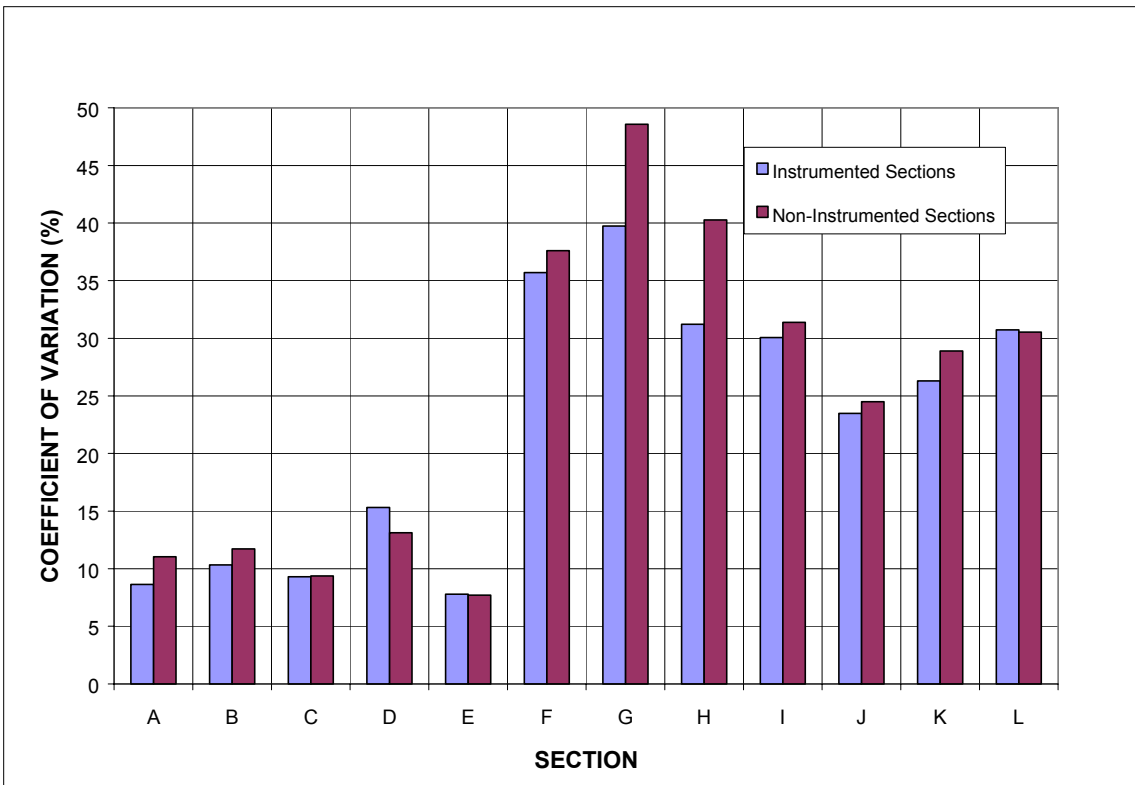


Figure 4.18 Variability of Deflection Measured by Sensor 8 in May 2000.

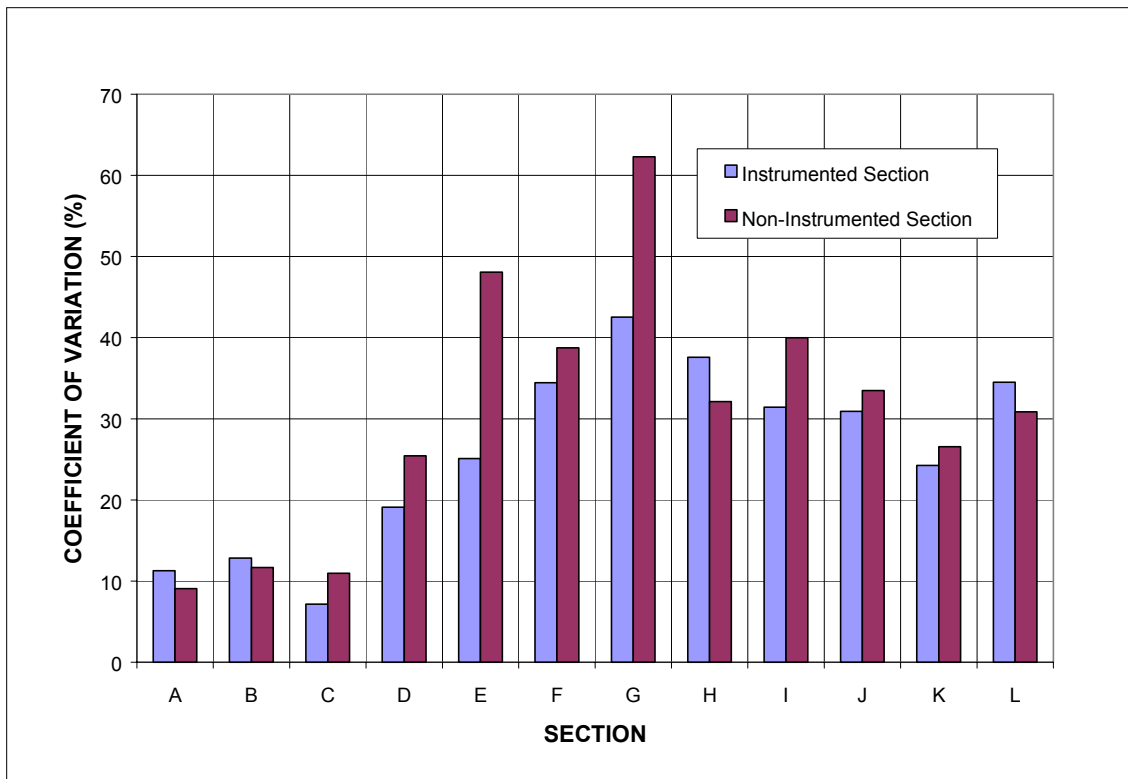


Figure 4.19 Variability of Deflection Measured by Sensor 8 in April 2000.

Table 4.1 shows a summary of the results obtained from the analysis. The lowest temperature in the wearing surface was recorded in December; the resulting range of COV's (7 to 22%) of the deflections was measured at the center of the loading plate. The highest temperatures of the wearing surface were recorded in July and August 2001 and the range of the coefficient of variation was from 10-37% and 7– 39%, respectively. The COV's were recorded in April and May of 2001. These values were up to 42%, where the temperature ranged from 24 to 40 °C.

Overall, Sections K and L had the highest COV's (for both the instrumented and non-instrumented lanes). Sections A and B showed the lowest COV's for the instrumented lane. Section B, however, showed the lowest COV for the non-instrumented lane. Deflection analysis of the data collected in August 2000 and in August 2001, with similar temperatures, produced very similar results.

The deflections obtained by the last sensor produced COV's as high as 47% and 62% in May and April of 2001, respectively. Figures 4.17 and 4.18 show that deflection reading variability increased for the sensor farthest away from the loading plate.

**Table 4.1.** Summary of Deflection Data for Instrumented and NonInstrumented lanes.

Temp (°C)	Testing Date	COV for Instrumented Lane (IL) (%)	COV for Non-Instrumented Lane (NL) (%)	Section with Highest COV (IL)	Section with Highest COV (NL)	Section with Lowest COV (IL )	Section with Lowest COV (NL)
24 - 33	May 2000	10 – 31	9 - 32	K	K	B	B
26 - 39	Aug 2000	7- 28	6 – 33	K	L	C	H
2 – 6	Dec 2000	7 – 22	6 – 26	L	L	A	B
24 - 37	Apr 2001	5- 37	5 – 42	G	G	A	B
33 - 40	May 2001	3 – 32	6 – 42	K	L	B	B
35- 47	Jul 2001	6 – 30	10 – 37	K	K	B	F
29-45	Aug 2001	7 – 30	7 – 39	K	L	C	H

The variability of the analysis for the deflections obtained from FWD loading drops every 10 m was also carried out by isolating the first five sensor (D<sub>0</sub> - D<sub>4</sub>) readings on each of

the seven testing dates for all 12 Sections. The results from the Analysis of Variance (ANOVA) indicated that each of the variables, temperature and sections are significant, with a  $Pr < 0.0001$ . A Randomized Complete Block Design was set up with the temperatures as blocks and sections as treatments using 420 observation points for the 12 sections, seven dates and five deflection readings ( $D_0$ -  $D_4$ ). The Least Square Difference (LSD) means separation procedure was used to find significant differences between the 12 sections. The results from the ANOVA showed that significant differences existed between test sections. Sections L, J and K had the highest deflection of 104, 88.7 and 88.6, respectively; while B, C, and D had the lowest deflections of 53.2, 56.9 and 57.7, respectively. The deflection measured for Section L was about twice that for Section B. The results of the analysis are shown in Appendix B.

#### 4.5 VARIABILITY DUE TO TEMPERATURE

In addition to the influence of pavement structure, deflections are known to be affected by temperature. Therefore to achieve reliable results, it is necessary to correct measured deflections for temperature variation. Kim *et al.* (1995) have suggested that the theoretical determination of deflection-correction factors is more complicated than the modulus-correction factors, because it is necessary to deal with the entire pavement system rather than just the HMA layer properties. Studies have also showed that deflections can be obtained through solving a boundary-value problem that involves material properties and layer thickness of each layer and the loading condition.

Nonlinear regression modeling of deflection measurements as a function of temperature and thickness of the HMA layers was performed with Statistical Analysis Software (SAS). The thickness of the HMA wearing surface and BM-25.0 base HMA layers were combined and used as the input layer thickness as part of this analysis. The two thickness types analyzed were 188 mm (Sections A to D, G, F and H) and 293 mm (Section E). The model used was the following

$$Y = \beta_0 e^{\beta_1 x^t} \quad (4.1)$$

where,

Y = deflection in mils;

x = thickness of the sections in inches;

t = the temperature in °C; and

$\beta_0, \beta_1$  = nonlinear coefficients.

Specifying the Gauss method of convergence, suitable ranges were selected for  $\beta_0$  and  $\beta_1$  to obtain a nonlinear model. The (ANOVA) results showed temperature was more significant in the equation than the thickness of the HMA layers. Thickness had a  $Pr > F$  of 0.097, while temperature showed  $Pr > F$  of 0.0001. This result was expected since the Virginia Smart Road had only two different thicknesses of the HMA layers as compared to other studies where more than four thicknesses were available.

A temperature correction protocol that incorporates the surface deflections and wearing surface temperature was developed. To compare the deflections between sections, a different analysis was used because only four replicate 40 kN drops or tests per section was done and averaged, this was to reduce random errors associated with the drops. Falling weight deflectometer testing was carried out on one location of each section in the traveling lane center approximately 25 m from the beginning/end of the section. There were ten testing dates, May, August, November, and December of 2000, January, February March, April, May and July of 2001; a little more than a one year period in which all 12 sections were tested. Thermocouples installed in the top and bottom of the wearing surface were used to determine the average mid-depth temperatures of the wearing surface. The load was normalized to 40 kN, and the deflection at the center of the loading was calculated. For each section, the relationship between temperature and normalized deflection over the testing period was developed. An exponential relationship produced the best  $R^2$ , which ranged from 0.7134 (for Section A) to 0.9818 (for Section H). From Figures 4.20 to 4.22, using the fitted relationship, the deflections for all sections were all corrected to a standard temperature, 25 °C, as shown in Figure 4.23. Sections K, J, and L show the highest measured deflection, 101, 85, and 84  $\mu\text{m}$ , respectively. Sections B and D showed the lowest deflection, 61 and 59  $\mu\text{m}$ , respectively. The model equations are shown in Table 4.2. The average deflection after temperature correction for each section was compared to the deflection obtained utilizing the correction model developed by Kim *et al.* (1995). The model developed by Kim *et al.* (1995) is based on statistical analysis incorporating the wearing surface thickness:

$$\lambda_w = 10^{-n(T-20)} \quad (4.2)$$

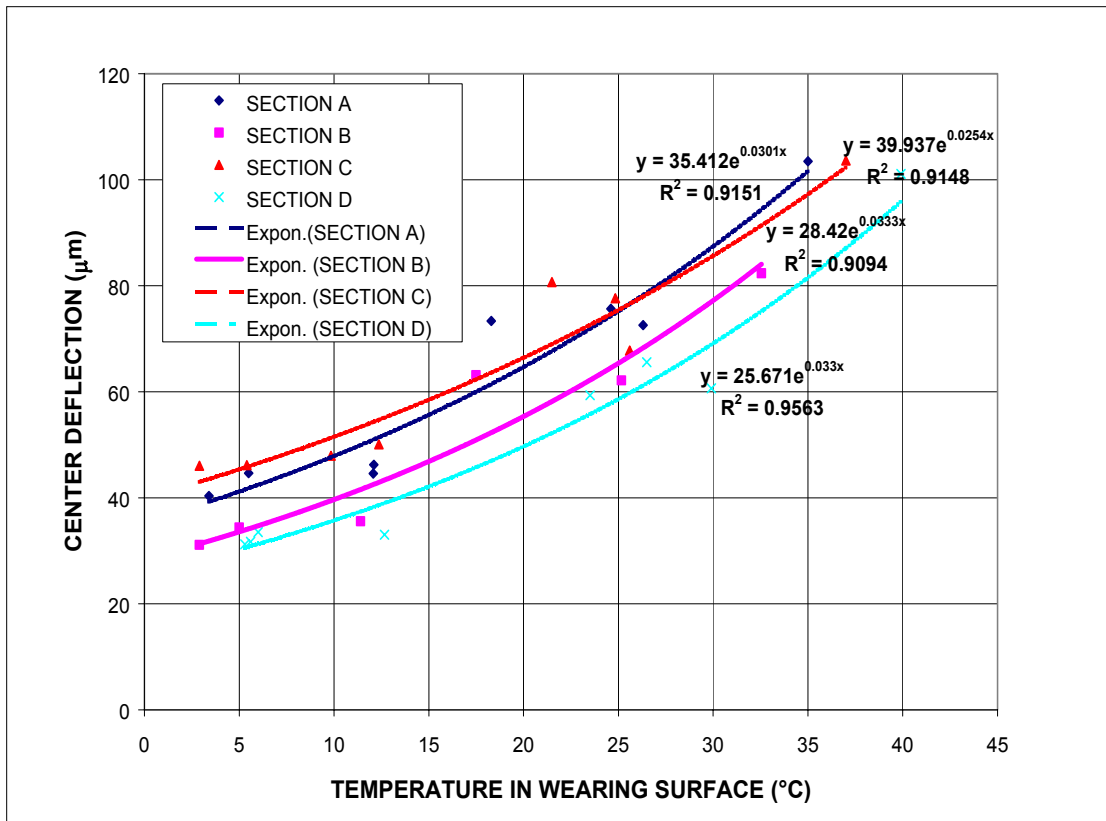


Figure 4.20 Temperature Correction Relations for Sections A through D.

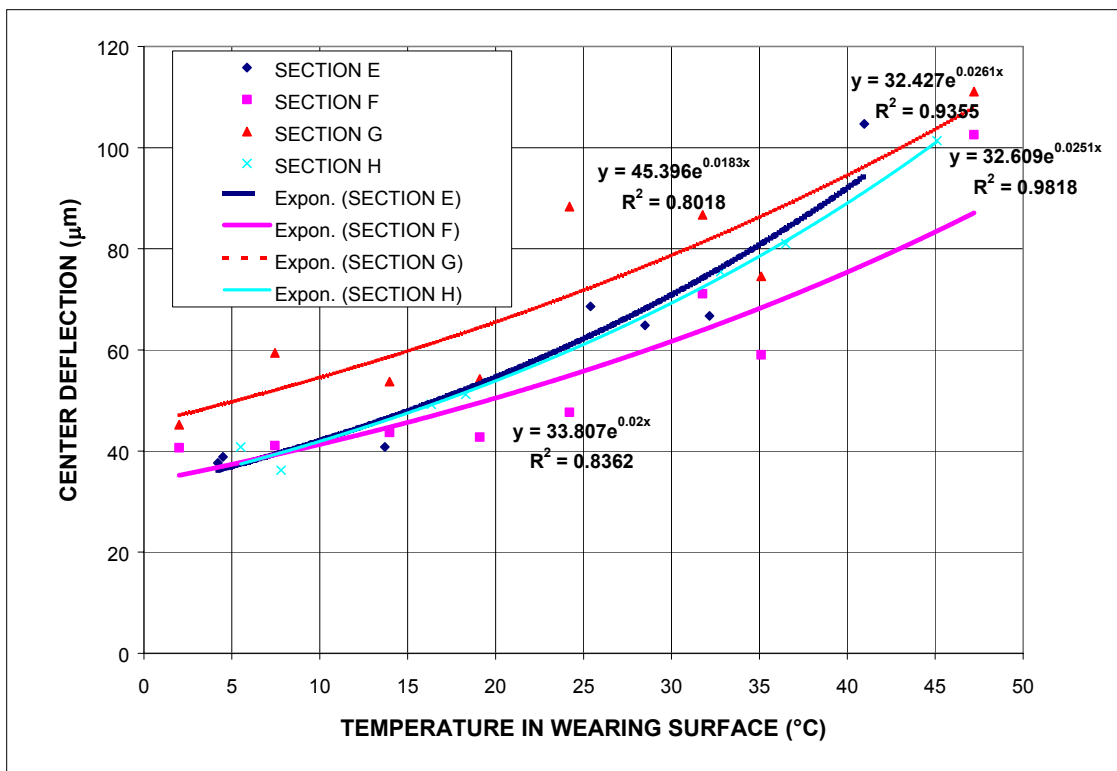


Figure 4.21 Temperature Correction Relations for Sections E through H.

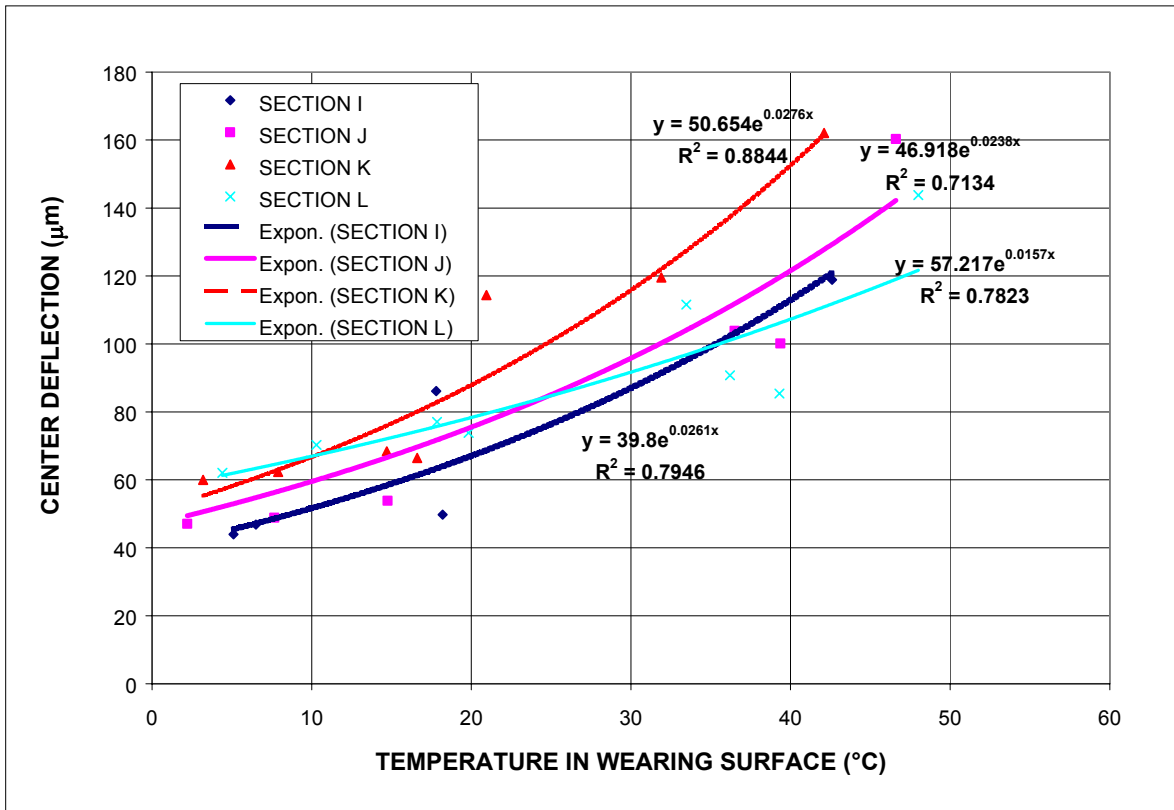


Figure 4.22 Temperature Correction Relations for Sections I through L.

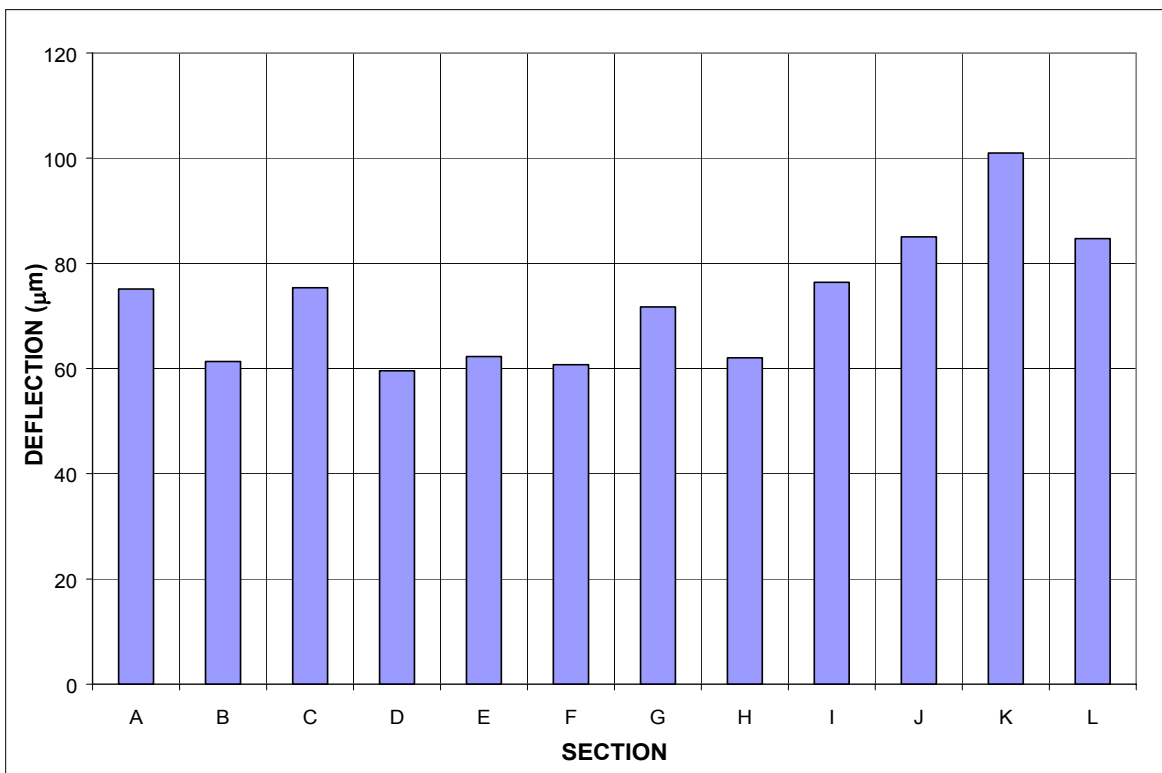


Figure 4.23 Average Section Deflections (after Temperature Correction) for 2000-2001.

**Table 4.2.** Model Equations and R-square for Deflections vs. Temperature for all Sections.

Section	Model Equation of Deflection vs. Temp	R <sup>2</sup>
A	$Y = 35.412 e^{0.0301T}$	0.915
B	$Y = 28.42 e^{0.0333T}$	0.909
C	$Y = 39.937 e^{0.0254T}$	0.915
D	$Y = 25.671 e^{0.0333T}$	0.956
E	$Y = 32.427 e^{0.0261T}$	0.936
F	$Y = 33.807 e^{.02T}$	0.836
G	$Y = 45.396 e^{0.0183 T}$	0.802
H	$Y = 32.61 e^{0.0251 T}$	0.982
I	$Y = 39.8 e^{0.0261 T}$	0.794
J	$Y = 46.92e^{0.0238 T}$	0.713
K	$Y = 50.65 e^{0.0276 T}$	0.884
L	$Y = 57.27 e^{0.0157 T}$	0.782

where,

$\lambda_w$  = deflection correction factor;

n = a function of HMA layer thickness ( $h_{AC}$ );

$n = 0.000005807(h_{AC})^{1.4241}$  for wheel path;

$n = 0.00000656(h_{AC})$  for lane center;

$h_{AC}$  = thickness of HMA in mm; and

T = temperature in °C.

Figure 4.24 shows the plots of the deflection versus the temperature corrected to 20 °C for the models obtained from the Virginia Smart Road and the one developed by *Kim et al.* (1995). Both show the same trend, with K, J, and L producing the highest deflections and B and D producing the lowest deflections. The difference between the two models is greater in Sections G through L than the rest however.

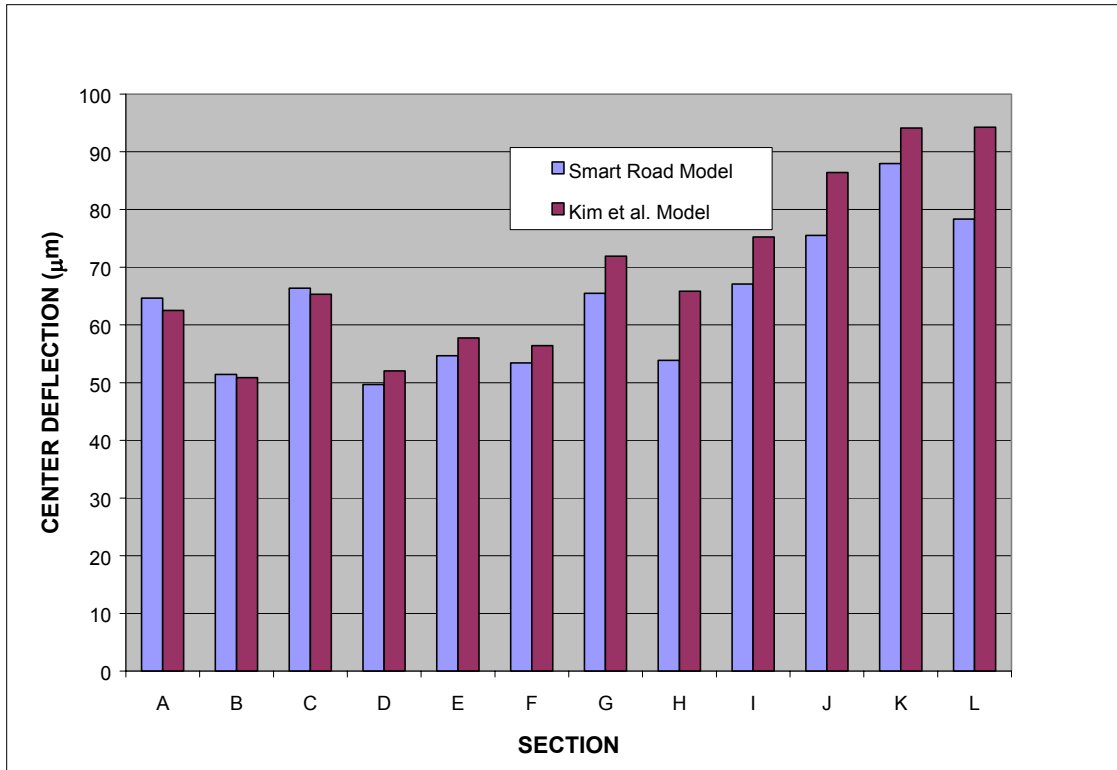


**Figure 4.24.** Comparison of Deflection-Correction Models for Center Deflections Under FWD Load.

Correction factors for the deflections were also obtained by normalizing the exponential equations determined for each section. Each equation was divided by the estimated corresponding deflection at 25 °C. The correction factors determined for all sections are compared in Figure 4.25, where the equation using the average parameters is represented as a solid dark line. The normalized deflection at 25 °C can be determined using the following equation:

$$D(25) = D_0 e^{-0.279(T-25)} \quad (4.3)$$

where,

$D_0$  = Measure center deflection (°C); and

T = Temperature at the bottom of the wearing surface (approximately 38 mm from the surface).

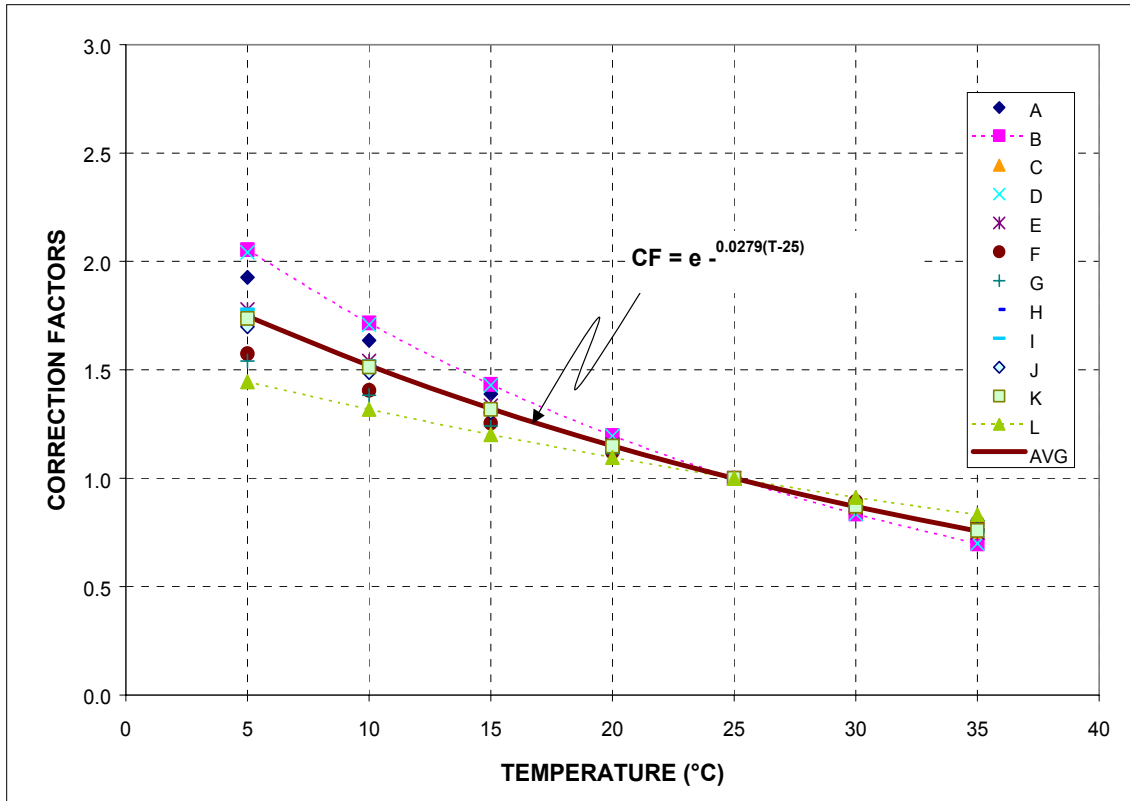


**Figure 4.25** Temperature Correction Factor for the Maximum Deflection.

To validate the equations developed in Table 4.2, the reduction in deflections at selected temperatures were calculated and compared to those measured in the field. The temperature drop from 35 °C to 5 °C (measured in August and December) was input into the exponential model developed for Sections A through D (shown in Table 4.2). The calculated deflection reduction was between 48 to 52%, which is comparable to a 50% drop in deflection measured in the field. However, for Sections E through L, the measured deflection drop was in the neighborhood of 25% within the same temperature drop. Using the model for those sections, an average calculated deflection drop of 25 to 58% was obtained. This drop shows an over prediction by the model for those sections. For the temperature drop from 25 to 15 °C (measured between April and February), calculated deflection reductions and measured reductions are all in the range of 20 to 30%. There was good agreement between model obtained and field measured values. Results presented in Figures 4.26 and 4.27 show the plots for this deflection behavior.

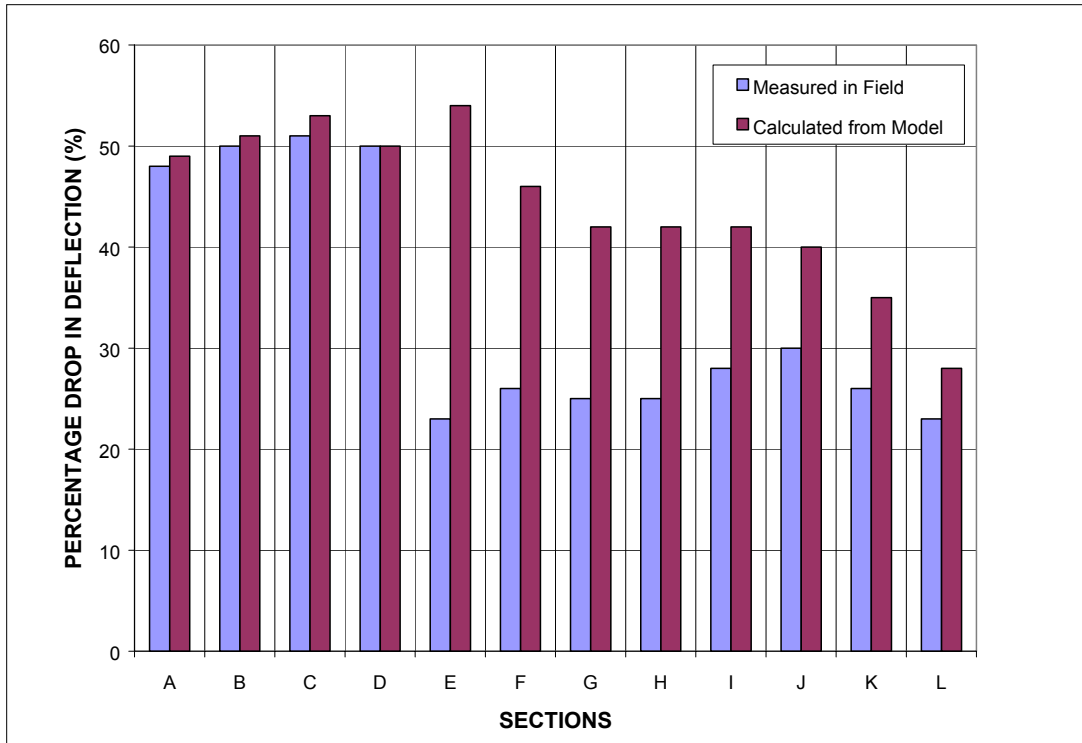


**Figure 4.26** Deflection Reduction (%) from 35 to 5 °C.

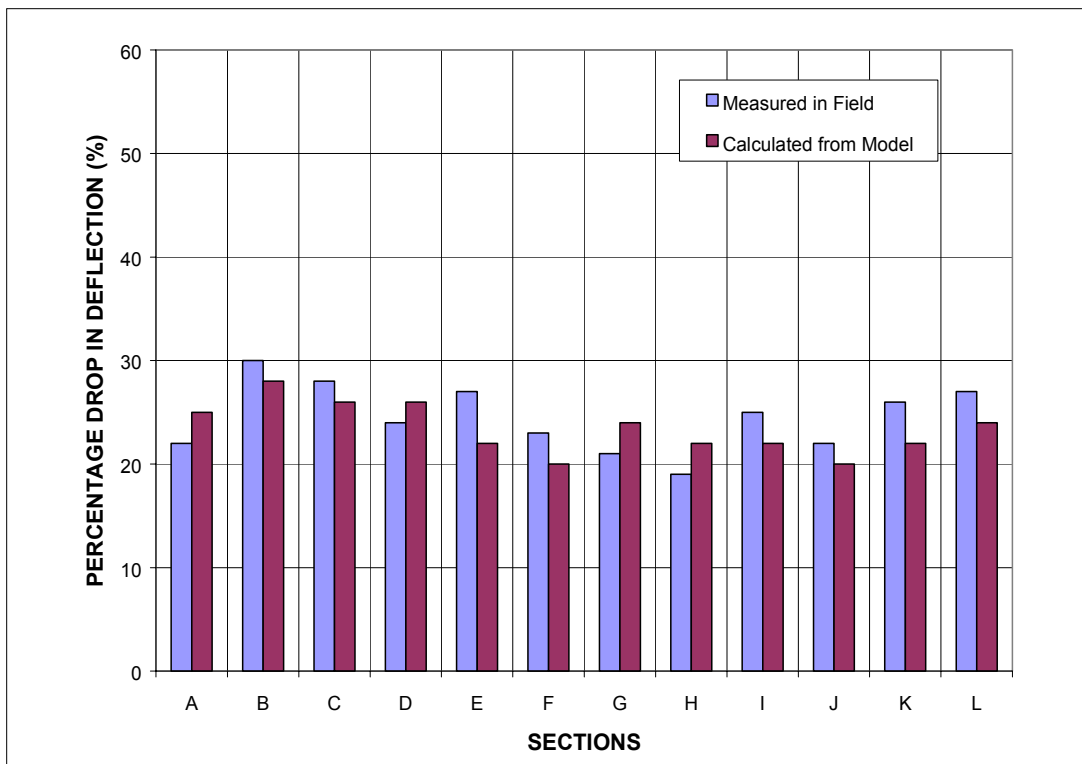


**Figure 4.27** Deflection Reduction (%) from 25 to 15 °C.

#### 4.6 STATISTICAL ANALYSIS

The Randomized Complete Block Designs (RCBD) were set up with the center deflections ( $D_0$ ) as treatments and the temperatures as blocks. To determine whether the differences among the sections were significant, mean separation procedures using the PROC GLM in the SAS software were performed on all deflection and temperature data collected on all the testing dates. The Fisher's Protected Least Square Difference (LSD) was used. Ordinarily such procedures would be carried out only if the ANOVA showed significant differences among the treatment means. A reasonable strategy is to have the mean separation procedures performed with the first analysis by PROC GLM. If no significant difference of means is established, the mean separation procedures may be ignored. The results from SAS showed that means differed significantly in the first run.

The results of the analysis demonstrated that the first sensor deflections ( $D_0$ ) in all the sections and testing temperatures showed significant differences, with a Pr value  $< 0.0001$ , at 5% significance level. The results of the LSD procedure showed that order of highest to lowest deflections are as follows: Sections K and L, followed by Section J, followed by Sections G, I, H and C, followed by Sections A, F, and E. Sections B and D have the lowest deflections and do not show significant difference. Sections with no significant difference between them are grouped. Contrasts tests on some of the selected sections confirmed that deflections resulting from Sections B and D were not significantly different.

The SAS analysis was also performed on the deflections at the fifth sensor ( $D_4$ ) and the last sensor ( $D_8$ ) to determine if similar results would be obtained to make it possible to conclude that sensor spacing or distance did not have influence on which sections produced the highest and lowest deflections, and also did not affect the variability between test sections. The  $D_4$  deflection results demonstrated that the deflection on different sections showed significant differences with a Pr  $< 0.0001$  and results similar to those from the center deflections. Means comparison procedures using the LSD showed Sections K and L produced the highest deflections, representing the weakest pavement sections, while Sections B and D produced the lowest deflections, representing the strongest sections. Higher deflections for the first sensor on the wearing surface is not an indicator of a weaker pavement since it is the shape of the deflection basin which is important for estimating the pavement moduli (McCullough *et*

*a.l.* 1982). Sections K and L were built on cut; results of subgrade data showed Section L had the weakest subgrade among all the sections. Section K has a geocomposite membrane in the HMA layer in one half of the section, which usually produces high deflections due to its low modulus. Section L has a 12.5 stone matrix asphalt (SMA) mix, which is known for its low resilient modulus compared to other SuperPave mixes.

The results of the deflection from the last sensor ( $D_8$ ) were, however, very different. The ANOVA output shows that the means were significantly different and Sections G and K produced the lowest deflections. Deflection values from the last sensor,  $D_8$ , are affected more by the strength of the subgrade layers. Preliminary studies (from ELSYM5 analysis) of the subgrade material after construction indicated the presence of a stiff layer at Section G and K. This could be responsible for results from this sensor ( $D_8$ ) readings being completely different from the other 2 sensor readings ( $D_0$  and  $D_4$ ). Also, the earlier analysis of COV of the deflection results from the sensor readings shows that the last sensor had higher COV values than those of the sensors at the center of the loading plate.

#### **4.7 FINDINGS AND CONCLUSIONS**

The structural design of the flexible pavement sections at the Virginia Smart Road would affect the FWD measured deflections. For example, Section L has a 12.5mm stone matrix asphalt mix, which is known for its low resilient modulus compared to other SuperPave HMA; Section K has a geocomposite membrane in the HMA base layer, the geocomposite membrane produces high deflections due to its low modulus; the wearing surface of Section K has an open graded friction course which after construction had a rough texture and appeared as loose stone gravels at some spots, this could result in seating problems of the FWD load plate. Section J has a geocomposite membrane underneath the open-graded drainage layer (OGDL). Field testing showed that the cold temperatures produced the low COV's (26%) of measured deflections on the wearing surface, while intermediate temperatures produced high COV's (42%). After correction of temperature effect, Sections K and L had the highest COV's in both the instrumented and non-instrumented lanes, while Section B had the lowest COV. In addition, deflections from the outermost sensor ( $D_8$ ) showed higher COV's (as high as 62%) than the deflections from that at the center of the loading plate ( $D_0$ ), which had a maximum COV of 42%.

Results from the exponential model developed for the deflection versus temperature relationship compared well with widely used logarithmic models. After correction to a standard temperature, Sections K and L produced highest deflections, 87 and 78  $\mu\text{m}$  respectively, while B and D, at 49 and 50  $\mu\text{m}$ , respectively, produced the lowest deflections.

The results of the ANOVA procedures using the statistical package SAS were used to show significant differences between the mean deflections in each of the 12 sections, both within the sections and between the sections. The post-ANOVA analysis showed that the section and temperature (testing dates) are significant to the analysis. Sections K, L and J produced the highest deflections, while Sections B and D produced the lowest deflections as measured by  $D_0$  and  $D_4$  sensors. Sections B and D were the strongest with deflections of almost 50% less than those of Sections J, K and L.

The analysis of the deflection results from  $D_8$  showed the presence of a stiff layer in Sections G and K. Since Section G was built on a fill, the presence of large rocks in that section was a strong possibility as reported earlier, confirming the earlier subgrade analysis done using the linear elastic software ELSYM5. Results from  $D_8$  are influenced mostly by the behavior of the underlying subgrade material.

The deflection resulting from correcting to a standard temperature were compared to statistical analysis using ANOVA procedures in analyzing the deflections at the first sensor and other sensor positions together at different temperatures for all the 12 Sections. Statistical analysis of measured deflections at different sensor spacing,  $D_0$ ,  $D_4$ , and  $D_0$ - $D_4$  produced the same trend of deflections results for all the 12 sections.

Analyzing the deflection from the first sensor ( $D_0$ ) appears to be enough for assessing extent of variability within and between the sections at the Virginia Smart Road. Spatial variation are known to be due to the heterogenous nature of the pavement materials while temporal variations in material properties are caused by temperature changes. However for practical purposes a more detailed analysis of the contribution of all the other sensors deflections based on theory incorporating material behavior to the overall pavement system may be needed as part of the long term monitoring.

This study has concluded that variations exist in the deflections within and between every section of the Virginia Smart Road. The coefficient of variation ranged from as low as 7% to as high as 42% (for the center deflections). The FWD measured

deflections and their variations were temperature dependent as well as pavement layer materials dependent.

## REFERENCES

Hossain M., Romanoschi, S., and Gisi, A. J. (2000). "Seasonal and Spatial Variation of Subgrade Response." *Journal of Transportation Engineering*, ASCE, Vol 127, No 1, pp. 150-167.

Hossain M., and Zaniewski J. (1992). "Variability in Estimation of Structural Capacity of Existing Pavements from FWD Data." *Transportation Research Record 1293*, National Research Council, Washington, D.C., pp. 124-132.

Kestler, M. (1997). "Current and Proposed Practices for Nondestructive Highway Pavement Testing." Proceedings of the 4<sup>th</sup> International Conference on the Bearing Capacity of Roads and Airfields, Minneapolis, MN, pp. 317-330.

Mamlouk, M.S., Houston, W.N., Houston, S.L., and Zaniewski, J. P.(1988). "Rational Characterization of Pavement Structures Using Deflection Analysis." Report No. FHWA-AZ88-254, Vol. 1, Arizona Dept. of Transportation, Phoenix, AZ.

McCullough, B.F. and Taute, A. (1982). "Use of Deflection Measurements for Determining Pavement Material Properties." *Transportation Research Record 852*, National Research Council, Washington, D.C., pp. 8-14.

Rauhut, J.B., and Jordahl, P.R. (1992). "Variability in Measured Deflections and Backcalculated Moduli for the Strategic Highway Research Program Southern Region." *Transportation Research Board 1377*, National Research Council, Washington, D.C., pp. 45-56.

Siddharthan, R., Sebaaly, P.E., and Javaregowda, M. (1991). "Influence of Statistical Variation in Falling Weight Deflectometers on Pavement Analysis." *Transportation Research Board 1377*, National Research Council, Washington, D.C., pp. 57-66.

Sun Woo Park, and Kim, Y. R. (1997). "Temperature Correction of Backcalculated Moduli and Deflections Using Linear Viscoelasticity and Time-Temperature Superposition." *Transportation Research Board 1570*, National Research Council, Washington, D.C., pp. 108-117.

## CHAPTER FIVE

### MODULI BACKCALCULATION OF THE VIRGINIA SMART ROAD PAVEMENT SECTIONS

#### **Abstract**

The purpose of this Chapter is to develop a backcalculation procedure for evaluating deflection data on the Virginia Smart Road in order to estimate the in situ elastic moduli of pavement layer materials. The structural capacity of the flexible pavement test sections at the Virginia Smart Road was evaluated using a falling weight deflectometer (FWD) as the pavement was constructed. The surface of each finished layer was tested shortly after placement and periodically after that. The embedded sensors were used to collect temperature and moisture data from various pavement layers. The structural capacity of each section is monitored periodically to assess both seasonal and long-term changes in the material properties. After several backcalculation approaches were evaluated for estimating the moduli of the pavement system layers, a detailed procedure that includes provisions to combine thin pavement layers and criteria to determine the reasonableness of the backcalculated moduli was defined. This procedure also considers the strengthening of the cement treated layer and the stress-dependency of the granular layers.

After the deflections obtained from the FWD testing were analyzed to estimate the “as-built” in situ resilient modulus of each layer, the analysis of the deflection measured over the subgrade was initially used to determine the subgrade modulus and depth to bedrock. The modulus of the granular subbase layer was then determined from deflections measured over that layer. This process was repeated for each subsequent layer to determine the initial moduli of all pavement layers. The measurements over the hot-mix asphalt (HMA) base layer were repeated at different pavement temperatures to evaluate the temperature susceptibility of the HMA layers. Backcalculated moduli for the wearing surface at temperatures below 10 °C produced moduli values sometimes exceeding the upper value of range moduli set for that layer. In an attempt to achieve an overall root mean square error of 25% or less, defined in used backcalculation procedure, and reasonable moduli values for the layer moduli, significant engineering judgment has to be incorporated into the backcalculation algorithm. Some of the extreme variability of the moduli obtained were demonstrated by each of the backcalculation software used. Seasonal variation during freeze-thaw periods were also

observed in the moduli of the HMA layer over a three year period from November 1999 to June 2002 for all the sections. The EVERCALC and ELMOD software were selected as the most appropriate software to be used for performing the backcalculation since a lot of the issues involved in performing the backcalculation are addressed by these software.

## 5.1 INTRODUCTION

Although a complete analysis of the FWD field data may provide estimates of the linear-elastic response of the various materials composing the pavement structure and its supporting medium, such an analysis requires considerable knowledge of the material properties of each layer (elastic modulus, Poisson's ratio, and layer thickness), as well as the characteristics of the pavement system (linearity, isotropy, elasticity, interlayer friction, infinite or finite bottom conditions and so forth). A backcalculation procedure is commonly used to estimate the elastic modulus of each layer and the depth to a rigid foundation, if applicable, based on the deflection basins produced by the load drops. The pavement structure is modeled using assumed layer moduli that are adjusted, using an iterative procedure, until the theoretical and measured deflection basins reach an acceptable match. Unless a perfect match between computed and measured deflection basins is achieved (i.e. approaching zero error), multiple sets of moduli may be generated, depending on the assumptions used in the backcalculation analysis.

Currently, there are many backcalculation software packages in use. Most backcalculation procedures rely on the linear elastic layered theory for basic structural modeling, and the results are evaluated mostly based on the goodness of fit between computed and measured deflections. The goodness of fit has improved over the years due to increased computing power and better search techniques. However, in many cases, improving the goodness of fit does not necessarily mean that the theoretical model better represents actual pavement response. If an existing pavement structure violates some of the fundamental assumptions of the elastic theory, the goodness of fit should not be the determining factor for deciding if a solution is realistic or not. Other possible problems include distress in the pavement layers, variations in layer thickness, nonlinear material response, and presence of bedrock or stiff layers (Ullidtz and Coetzee, 1995).

In general, since backcalculation consists of a laborious process, it requires a high degree of engineering skills, consequently the results are moderately dependent on the individual doing the backcalculation. Based on evaluation performed on the Strategic Highway Research Program Long Term Pavement Performance (LTPP) monitoring program data, Rada *et al.* (1994) highlighted a number of reasons for that and mentioned a lack of consensus for addressing all aspects of the backcalculation process. This chapter, therefore, examines various backcalculation schemes and

programs in an attempt to recommend a standard for addressing all aspects of the process.

## 5.2 BACKCALCULATION SCHEMES AND PROGRAMS

Uzan (1994) analyzed several existing backcalculation procedures and concluded that the main differences among them are related to the following two components:

1. The forward computation model used to predict the pavement response.
2. The error minimization scheme.

Existing packages base their forward computations on either numerical integration methods to solve a multilayer elastic system such as is used in BISAR (Peutz *et al.* 1968) and WESLEA (Van Cauwlaert *et al.* 1989) or on approximation methods, such as the method of equivalent thickness used in ELMOD (Ullidtz, 1977; and Lytton, 1989). Although the approximate methods are considerably faster, they may in some cases lead to unacceptable error in the forward computation of the response of the pavement that would be reflected in the computed backcalculated moduli. For example, the method of equivalent thickness may produce erroneous results when the moduli does not vary in a monotonously decreasing way with depth (Peutz *et al.* 1968).

Common error minimization schemes include the minimization of the absolute or percent mean square error (MSE). The absolute MSE for a problem involving  $n$  deflection measurements on a pavement section of  $m$  layers with an unknown modulus and known thickness can be computed using the following equation:

$$MSE = f(E, h) = \frac{1}{n} \sum_{i=1}^n W e_i \{ D_i^c(E, h) - D_i^m \}^2 \quad (5.1)$$

where,

$D_i^c(E, h)$  = calculated deflection at location  $i$  based on  $E$  and  $h$ ;

$D_i^m$  = measured deflection at location  $i$ ;

$n$  = number of FWD sensors;

$E = \{ E_1, E_2, E_3, \dots, E_m \}$  (unknown moduli of the layers);

$H = \{ h_1, h_2, h_3, \dots, h_{m-1} \}$  (known layer thickness); and

$W e_i$  = weighing factor for sensor  $i$  ( $W e_i = 1$  if all sensors are given the same importance).

Similarly, the percent MSE can be computed using the following equation:

$$MSE(\%) = \frac{1}{n} \sum_{i=1}^n W e_i \left\{ \frac{D_i^c(E, h) - D_i^m}{D_i^m} \right\}^2 \quad (5.2)$$

The absolute MSE which assigns a similar weight to all deflections, is more affected by the deflections close to the center of load application than the outer ones, but the percent MSE puts more weight on the outer deflections, because the differences for the sensors farther from the load are divided by a smaller number ( $D_i^m$ ) than those for the closer sensors. If both the forward computation program and the minimization scheme used by two packages, are appropriate, the backcalculated moduli should be similar (Lytton, 1989).

Four backcalculation software packages, PEDMOD 95 version 1.0, EVERCALC version 5.0, ELMOD version 4.0, and MICHBACK version 1.0 were evaluated utilizing data collected at the Virginia Smart Road test facility.

This test facility includes 12 heavily instrumented 100-m long (approximately) flexible pavement test sections and one continuously reinforced concrete section. The pavement structure of the different sections combines the following layers: subgrade, granular subbase (21-B), cement stabilized base (21-A), open-graded drainage layer (OGDL), hot-mix asphalt (HMA) base (SM-9.5D and BM-25.0), and different HMA wearing surfaces. In addition, the last four Sections (I through L) include geocomposite materials and metallic meshes in different locations in the pavement structure. The structural design of all 12 sections and the thickness of all the pavement layers are presented in Figure 5.1. A complex array of sensors were embedded in the experimental pavement sections during construction. The Virginia Smart Road, therefore provides an ideal laboratory to assess the four backcalculation software packages, which are described in the following subsections.

Section A	Section B	Section C	Section D	Section E	Section F	Section G	Section H	Section I	Section J	Section K	Section L
SM-12.5D	SM-9.5D	SM-9.5E	SM-9.5A	SM-9.5D	SM-9.5D	SM-9.5D	SM-9.5D	SM-9.5A	SM-9.5D	OGFC SM-9.5D	SMA-12.5
Base BM-25.0 (150mm)	Base BM-25.0 (150mm)	Base BM-25.0 (150mm)	Base BM-25.0 (150mm)	Base BM-25.0 (s25mm)	Base BM-25.0 (150mm)	Base BM-25.0 (100mm) SM-9.5A (50mm)	Base BM-25.0 (100mm) SM-9.5A (50mm)	Base BM-25.0 (100mm) SM-9.5A (50mm)	Base BM-25.0 (s25mm)	Base BM-25.0 (s25mm)	Base BM-25.0 (150mm)
OGDL (75mm)	OGDL (75mm)	OGDL (75mm)	OGDL (75mm)		21-A (CTA) (150mm)	21-A (CTA) (150mm)	OGDL (75mm)	OGDL (75mm)			OGDL (75mm)
21-A (CTA) (150mm)	21-A (CTA) (150mm)	21-A (CTA) (150mm)	21-A (CTA) (150mm)	21-A (CTA) (150mm)			21-A (CTA) (150mm)	21-A (CTA) (150mm)		OGDL (75mm)	OGDL (75mm)
21-B Subbase (180mm)	21-B Subbase (180mm)	21-B Subbase (180mm)	21-B Subbase (180mm)	Subbase 21-B Sub (75mm)	21-B Subbase (150mm)	21-B Subbase (150mm)	Subbase 21-B Sub (75mm)	Subbase 21-B Sub (75mm)	21-B Subbase (150mm)	21-B Subbase (150mm)	Subbase 21-B Sub (75mm)

Figure 5.1. Pavement Design for the Virginia Smart Road.

### 5.2.1 PEDMOD

PEDMOD 95 version 1.0 is a user-friendly, windows-based shell that integrates different pavement analysis software (e.g., BISAR and WESDEF) in a mechanistically based pavement analysis and design system (McQueen, 1999). This study evaluates its backcalculation portion, which uses WESDEF (Van Cauwlaert *et al.* 1989) for the backcalculation of the pavement layer moduli. WESDEF, which is based on a multilayer elastic forward computation model, conducts an iterative process to select the set of layer moduli that minimizes the percent MSE between the measured and computed deflection basins. Initially, a set of modulus values is assumed and the theoretical deflection is computed at offsets corresponding to the measured deflections. Subsequently, each modulus is varied individually, and a new set of deflections is computed for each variation. For multiple deflections and layers, the solution is given by the relationship between the deflection and the modulus shown in the following equation (Alexander *et al.* 1989):

$$\log(d_j) = A_{ij} + S_{ij}(E_i) \quad (5.3)$$

where,

$A_{ij}$  = intercept for deflection sensor  $i$ , and layer  $j$ ;

$S_{ij}$  = deflection sensor  $i$ , and layer  $j$ ;

$j = 1, 2, \dots, ND$  ( $ND$  = number of deflections); and

$i = 1, 2, \dots, NL$  ( $NL$  = number of layers with unknown moduli).

Normally three iterations of the program produce a set of modulus values that yield a deflection basin within an average of 3% of each measured deflection. Limiting iteration criteria requires the absolute sum of the percent differences between computed and measured deflections or the predicted change in modulus value is less than 10%.

PEDMOD95's documentation recommends setting the thickness of the subgrade at 6 m unless there is an indication that a shallower depth should be used, is because WESDEF by default incorporates a layer of infinite thickness (having a modulus of 6,900 MPa) 6 m below the subgrade layer. However, Van Deusen (1996) evaluated existing backcalculation software for use in the MnRoad project and concluded that the performance of the WESDEF might be enhanced if this depth is adjusted to reflect actual field conditions, even for stiff layers deeper than 6 m. In this study, the results were considerably more stable when using a 15-20 m stiff layer rather than a 6 m layer. The moduli estimated in this case were also more consistent with the materials used. Van Deusen also found that WESDEF and EVERCALC produced the best results.

## **5.2.2 EVERCALC**

EVERCALC version 5.0 is a mechanistic-based pavement analysis computer program based on the Chevron N-layer program which was developed for Washington State Department of Transportation. This software uses an iterative procedure of matching the measured surface deflections with the theoretical surface deflections calculated from assumed elastic moduli, produces a solution when the summation of the absolute values of the discrepancies between the measured and theoretical surface deflections falls within a preset allowable tolerance (generally 10% or less using five deflection inputs). It estimates the initial "seed" moduli and performs backcalculation of the modulus for each pavement layer and also determines the stress sensitivity coefficient ( $K$  values) for the granular base and subgrade materials when more than two load levels are given at a point. Also the HMA moduli can be adjusted to standard laboratory conditions of 25°C temperature and 100ms load duration. Seed moduli are estimated using internal regression equations, which are algorithms developed using regression relationships

between layer moduli, load and various kinds of deflection basin parameters. In the EVERCALC Ver 5.0 software, the WESLEA layered elastic analysis program is used for forward analysis and a modified Gauss-Newton algorithm for optimization. They are the Newton-Coates closed type or the Gauss integration formula. Options for estimating apparent depth to the stiff layer and temperature correction for the HMA moduli are included.

In the Newton-Coates method, the integral to be transformed is of the following form:

$$\text{Int} = pa \int_0^{\infty} J_0(mr) J_1(ma) f(mz) dm \quad (5.4)$$

where the required integrals include a product of the oscillating Bessel function (made up of the radii,  $a(i)$  of the loads, and distances  $r$  to the coordinate system) multiplied by a function of exponentials related to the geometry of the structure and the depth at which the stresses are calculated. The most utilized formulae are Simpson's rule and Weddle's rule for determining the integration intervals. Conditions for various interface friction conditions based on Coulomb's friction law presented by Van Cauwlaert *et al.* (1986) are also included in the software.

For a semi-infinite layer, calculated deflection from WESLEA is given by the following equation:

$$w(r=0) = -\frac{2(1-\nu^2)}{E} pa \left[ (1+z^2/a^2)^{1/2} - z/a \right] - \frac{1+\nu}{E} pa \left[ z/a - \frac{z^2/a^2}{(1\pm z^2/a^2)^{1/2}} \right] \quad (5.5)$$

where,

- w = deflection;
- r = radius of the axis of symmetry;
- p = the uniform applied pressure;
- z = the distance below the surface;
- a = the radius of the circular load;
- E = the elastic modulus of the half space; and
- $\nu$  = the Poisson's ratio.

### 5.2.3 ELMOD

ELMOD version 4.0 is a windows-based and user-friendly software package. It backcalculates the modulus of each layer in two, three, or four layered pavement systems using an Odemark-Boussinesq transformed section (method of equivalent thickness). The multilayer pavement structure is transformed into an equivalent single layer of equivalent stiffness using the following equation:

$$\frac{h_1 E_1}{(1 - \nu_1)} = \frac{h_2 E_2}{(1 - \nu_2)} \quad (5.6)$$

where,

$E_1$  = modulus of the upper layer;

$\nu_1$  = Poisson's ratio of the upper layer;

$E_2$  = modulus of the bottom (and the transformed equivalent) layer; and

$\nu_2$  = Poisson's ratio of the bottom layer.

Two options are available for performing the backcalculation in ELMOD: the deflection basin fit and the radius of curvature approach (Odemark-Boussinesq approach). The radius of curvature option uses the radius of curvature along with the actual or apparent non-linear subgrade properties to determine moduli within the pavement system. The "radius of curvature" from the central geophones can be used to assess the stiffness of the upper pavement layer. The stiffness of remaining layers is then calculated based on the overall pavement response to the applied load. This ensures that the proposed pavement structure results in the correct central deflection under the measured load. The deflection basin fit option starts with a set of estimated moduli for the pavement structure, and the theoretical deflection bowl for this pavement structure is calculated, the error between the measured and calculated deflections is assessed. The advantage of the Odemark-Boussinesq approach is that nonlinear materials may be considered and the computational process is much faster than "conventional" layered elastic analysis backcalculation computer codes. ELMOD considers possible non-linearity of the subgrade to improve the fit between measured and calculated deflection basins. This feature generally removes the so-called "compensating layer effect," which can introduce large errors if the moduli are computed assuming only linear elastic materials (Ullidtz *et al.* 1994). All materials are assumed to be homogenous, isotropic, and linear elastic,

with the exception of the subgrade, which is assumed to exhibit a non-linear response in accordance with the following equation:

$$\varepsilon_0 = C_0 \left( \frac{\sigma_1}{\sigma} \right)^n \quad (5.7)$$

where,

$\varepsilon_0$  = surface modulus;

$\sigma_1$  = major principal stress;

$\sigma$  = a reference stress; and

$C_0$  and  $n$  = constants ( $n$  is negative).

The influence of the HMA temperature on the layer moduli is accounted for in the analysis. ELMOD uses the Bells equation developed by Baltzer and Jansen (1994) for temperature correction.

The maximum precision is obtained when the structure has only one stiff layer (with a modulus five greater than that of the subgrade) and the moduli are in decreasing order of depth (ratio of at least two). Since these conditions are violated to some extent at the Virginia Smart Road test sections, the applicability of this software package in this study was carefully evaluated.

#### **5.2.4 MICHBACK**

MICHBACK version 1.0 is a public domain, menu-driven software package. It estimates the pavement layer moduli, unknown layer thickness, and/or depth of a stiff layer (if present) and also accounts for a temperature correction for HMA. The pavement response is computed using the layered elastic program CHEVRON. For the backcalculation process, MICHBACK uses a modified Newton method in which a gradient matrix is used to determine how to change the current estimates of the layer moduli (and layer thickness, if needed). In this method, the  $i^{\text{th}}$  incremental corrections to the logarithm of the unknown moduli and layer thickness are obtained by calculating the least-squares solution of the following over-determined system of linear equations (Harichandran *et al.* 1994):

$$[G]^i \left\{ \frac{\{\Delta(\log E)\}^i}{\{\Delta t\}^i} \right\} = \{\log w\} - \{\log w'\}^i \quad (5.8)$$

$$[G]^i = \left[ \begin{array}{cccc} \frac{\partial(\log w_1)}{\partial(\log E_1)} & \dots & \frac{\partial(\log w_1)}{\partial(\log E_n)} & \frac{\partial(\log w_1)}{\partial t_1} & \dots & \frac{\partial(\log w_1)}{\partial t_p} \\ \vdots & & \vdots & \vdots & & \vdots \\ \frac{\partial(\log w_m)}{\partial(\log E_1)} & \dots & \frac{\partial(\log w_m)}{\partial(\log E_n)} & \frac{\partial(\log w_m)}{\partial t_1} & \dots & \frac{\partial(\log w_m)}{\partial t_p} \end{array} \right]_{\{E\} = \{\bar{E}\}^j, \{t\} = \{\bar{t}\}^j} \quad (5.9)$$

where,

$[G]^i$  = gradient matrix of partial derivatives of the logarithm of the m surface deflections, with respect to the logarithm of the n unknown moduli, and p unknown layer thickness, evaluated using the current moduli,  $\{E\}^j$ , and thickness,  $\{t\}^j$ ;

$\{\Delta(\log E)\}^i$  = vector of corrections to the logarithm of the  $i^{\text{th}}$  moduli estimate;

$\{\Delta t\}^i$  = vector of corrections to the  $i^{\text{th}}$  estimate of the thickness;

$\{\log w\}$  = vector of logarithm measured surface deflections;

$\{\log w'\}^i$  = vector of logarithm of surface deflections using the  $i^{\text{th}}$  estimate of the moduli and thickness.

The least-squares problem is reduced to a  $n \times n$  system of normal equations that can be solved by the Newton method:

$$[G]^T [G] \left\{ \frac{\{\Delta(\log E)\}^i}{\{\Delta t\}^i} \right\} = [G]^T \{\{\log w\} - \{\log w'\}^i\} \quad (5.10)$$

Two criteria are used to check the convergence which is assumed to have occurred if one of the two is met:

1. The root-mean square percentage error (RMSE) between the measured and calculated surface deflections is smaller than a specified tolerance (3% in this analysis), as expressed in the following equation:

$$\text{RMSE} = 100 \sqrt{\frac{1}{n} \sum_{i=1}^n \left( \frac{D_i^c - D_i^m(E, h)}{D_i^m} \right)^2} \leq \varepsilon_1 \quad (5.11)$$

where,  $\varepsilon_1$  is the specified tolerance.

2. The percentage error in each successive moduli evaluation is smaller than a specified tolerance (1% in this analysis), as expressed in the following equation:

$$\frac{\bar{E}_k^{i+1} - \bar{E}_k^i}{\bar{E}_k^i} \times 100 \leq \varepsilon_2 \quad \left( \text{or} \quad \frac{\bar{t}^{i+1} - \bar{t}^i}{\bar{t}^i} \times 100 \leq \varepsilon_2 \right) \quad k = 1, 2, \dots, n \quad (5.12)$$

where,

$\bar{E}_k^i$  = estimated modulus of layer k at iteration i;

$\bar{t}^i$  = layer thickness at iteration i; and

$\varepsilon_2$  = specified tolerance.

This last criterion indicates that the iterative scheme has stabilized and that unknown variables (moduli, thickness, and/or stiff layer depth) are not changing significantly from one iteration to another. The RMS criterion often results in no convergence in the iterative process, because the computed deflections cannot match the deflection basins measured in the field. In this case, the backcalculation process relies on the second convergence criteria.

### 5.2.5 Temperature Correction in Backcalculation Software

The stiffness of the HMA is primarily affected by both temperature and loading rate. Correction of backcalculated HMA wearing surface to a standard temperature is done in most of the backcalculation procedures. In the MICHBACK software, the standard temperature for correction is 25 °C and the equation developed by the Asphalt Institute is used:

$$\text{Log } E_0 = \text{log } E + 1.47362 \times 10^{-4} (t^2 - t_0^2) \quad (5.13)$$

where,

$E_0$  = corrected HMA modulus in psi;  
 $E$  = backcalculated uncorrected HMA modulus in psi;  
 $t$  = test temperature in degrees Fahrenheit; and  
 $t_0$  = reference temperature = 25 °C

However, its more desirable to develop a temperature correction model based on the deflection data and temperature data collected in the wearing surface at a specific location. In the EVERCALC software, the temperature correction used is based on a relationship found for WSDOT Class B HMA (a traditional typical dense HMA) and given as follows:

$$\text{Log } E_{ac} = 6.4721 - 1.47362 \times 10^{-4} (T_p)^2 \quad (5.14)$$

where,

$E_{ac}$  = modulus of HMA in psi; and

$T_p$  = pavement temperature in °F or a temperature adjustment factor of

$$10^{0.0000147362(T_p^2 - 77^2)}$$

In the ELMOD software, temperature correction factors have been developed based on temperatures taken over a 2-3 year period and an algorithm developed from the Strategic Highway Research Project (SHRP) database called BELLS (Baltzer, Ertman-Larsen, Lukanen and Stubstad, 1994). One of the BELLS equations (Baltzer and Jansen, 1994) is given below:

$$T_d = 2.9 + 0.935 \times IR + \log\left(\frac{d}{17.8 \text{ mm}}\right) \times \left[ -0.487 \times IR + 0.626 \times (1 - \text{day}) + 3.29 \times \sin\left(\frac{(hr_{11} - 15.5) \times 2\pi}{18}\right) \right] + 0.037 \times IR \times \sin\left(\frac{(hr_9 - 13.5) \times 2\pi}{18}\right) \quad (5.15)$$

where,

$T_d$  = temperature in °C at a depth  $d$ ;

IR = the surface temperature in °C, measured with the infrared sensor on the FWD;

1-day = average air temperature the day of testing;

$hr_{11}$  = a decimal time between 11:00 and 5:00 hrs. If the actual time is outside this time range then  $hr_{11} = 11$ . If the actual time is less than 5:00, add 24. For example if the actual time is 13:15, then decimal time is 13:15; and

$hr_9$  = decimal time between 09:00 and 03:00 hrs. If the actual time is outside the range, use  $hr_9 = 9$ . If the time is less than 03:00 hrs add 24.

A temperature correction model based on moduli obtained from backcalculation from the different software at different temperatures at the Virginia Smart Road was developed and used. The model is presented in Chapter seven.

### **5.3 EVALUATION OF SOFTWARE UTILIZING DATA OBTAINED AT THE VIRGINIA SMART ROAD**

A preliminary analysis was conducted to assess the strengths and weaknesses of the four backcalculation software. In some preliminary runs, the performances of the four software packages were compared in terms of usability and accuracy. The main advantages and disadvantages are summarized in Table 5.1. The moduli of all layers were obtained for Section A using all the software packages. The modulus of each layer was determined based on the deflections measured on top of the layer and fixing the moduli of all underlying layers. Some software packages modified the moduli for the subgrade to improve the fit between measured and calculated deflections. The subgrade modulus presented in the last column of Table 5.2 was used, because there was no indication of the presence of a stiff layer. The results are presented in Table 5.3. These results have not taken into consideration important material properties, such as an increase in the strength of the 21-A layer with time, stress susceptibility of the granular layers, or a change of the strength in the granular layers because of moisture variations. The deflection basin fit procedure in ELMOD4 produced very reasonable results. However, it did not allow fixing the modulus of the subgrade, because it adjusted it automatically to improve the fit. This method produced the most reasonable results for the combined HMA base and wearing surface modulus.

However, it seems to have underestimated the modulus of the cement treated aggregate (CTA) base (21-A) and overestimated the modulus of the OGDG (probably as a “compensating” error).

Both software that use “pure” layered linear elastic forward computation procedures (MICHBACK and PEDMOD) failed to model the very flat deflection bowls measured on top of the wearing surface. In both cases, the maximum value of the admissible range of the HMA layer was assigned by the backcalculation software. Since these tests were conducted in the winter (December, 2000) with temperature of the

wearing surface less than 5°C, the conditions at the time of testing may explain these problems.

**Table 5.1** Main Advantages and Disadvantages of the Software Packages Evaluated.

Software	Operation Principles	Advantages	Disadvantages
PEDMOD95 (v.1.0)	Uses WESDEF. Layered elastic forward computation (WESLEA). Minimizes percent MSE.	Windows-based. User-friendly and easy to use.	Optimization procedure not detailed (only three iterations). Handles one load at a time. Very sensitive to seed values. Does not estimate depth to stiff layer.
EVERCALC (v.5.0)	Layered elastic forward computation (WESLEA). Minimizes percent error.	Windows-based. User-friendly and easy to use. Always converge.	Sensitive to initial seed values.
ELMOD4 (v.4.0)	Approximate forward computation (Equivalent Thickness). Minimizes absolute or percent MSE.	Windows-based. Flexible optimization objective. Handles four pavement layers plus the subgrade. Analyzes several loads and sections at the same time. Considers non-linearity of the subgrade. Considers asphalt temperature correction.	Does not allow fixing the moduli of the subgrade layer (changes it to improve the fit if necessary). Did not detect shallow stiff layer/ non-linearity in many cases. Must be very careful with input format.
MICHBACK (v.1.0)	Layered elastic forward computation (Chevron). Minimizes percent RMS (modified Newton method).	Menu-driven. Allows estimating one unknown layer thickness (or depth of a stiff layer). Considers asphalt temperature correction. Detailed optimization routine (although not always converge).	Dos-Based. Not user friendly. Rigid input data format (must be transformed manually). Handles one load at a time. Sensitive to initial seed values.

The results produced by PEDMOD were extremely sensitive to the user-provided seed values. For example, the modulus of the CTA layer varied from 1,661 to 4,468 MPa when using seed values ranging from 1,380 to 3,100 MPa. However, these may be due to the relative depth of the stiff layer recommended by PEDMOD. When using a deeper stiff layer (1.8 m), the results (last set of rows in Table 5.3) were considerably more stable.

**Table 5.2** Summary of Subgrade Moduli Computed Using Different Methods (MPa).

Section	Two-Layer Analysis. (40 kN)		Surface Modulus Analysis			
	Stiff Layer <sup>(1)</sup>	Modulus	Stiff Layer <sup>(2)</sup>	Using D <sub>0</sub> & All Load	All Sensors & Loads	Using D <sub>2</sub> -D <sub>6</sub> & All Loads
A	No	345	No	313	377	351
B	No	379	Possible	312	395	423
C	No	293	Possible	271	293	306
D	No	236	Possible	253	280	296
E	7.6-15.2m	241	No	236	258	273
F	7.6m	207	Possible	242	274	292
G	3.8-5.1m	293	Yes	233	352	398
H	No	207	No	329	268	261
Average		275		274	312	331
St. Dev.		63		39	54	64
COV		22%		14%	17%	19%

<sup>(1)</sup>Indication of nonlinear behavior or stiff layer while analyzing the subgrade as a two-layer system.

<sup>(2)</sup>Indication of nonlinear behavior or stiff layer while analyzing the change in surface modulus with distance to the load center.

The estimated moduli seem to be more consistent with the materials used. Before conducting the moduli backcalculation, a comprehensive analysis of the FWD measurements on the subgrade had been conducted. Three approaches were used to estimate the “as-built” modulus of the subgrade for all the experimental sections: The first used only the maximum surface deflection (D<sub>0</sub>) over a semi-infinite linear elastic homogenous half-space (one-layer system); the second used all the sensors (assuming a point load) on a single-layer system; and the third used a two-layer system (modeled with ELSYM5). Table 5.2 summarizes the results. All the results indicated the presence of bedrock at 1.8 to 2.5 m below the surface in some sections.

Furthermore, to study the occurrence of nonlinearity in the subgrade modulus, the computed surface moduli were plotted against the distance of the sensors to the center of the load application, as shown in Figure 5.2. The subgrade appears to show mild non-linear behavior, because the computed modulus tends to increase as the distance from the applied load increases.

**Table 5.3** Backcalculated Moduli for Selected Sections Using Different Software Packages in November 2000 and April 2001.

Sect.	Date	Software	Modulus (MPa)					Bed. Depth (m)	RMSE (%)
			WS+BM	OGDL	21-A	21-B	Subgr.		
A	Nov-00	PEDMOD	13,800	1,283	4,551	364	351	--	21
		EVERCALC	10,425	932	10,350	380	552	--	18
		MICHBACK	15,525	1,380	13,800	483	345	--	22
		ELMOD4	11,673	1,473	17,194	296	400	--	11
	Apr-01	PEDMOD	10,812	1,283	4,554	366	370	--	19
		EVERCALC	4,248	1,159	5,520	339	552	--	21
		MICHBACK	12,455	1,083	8,655	414	483	--	36
		ELMOD4	8,197	1,235	6,927	276	379	--	7
B	Nov-00	PEDMOD	13,800	1,653	5,940	358	424	1.8	16
		EVERCALC	12,420	1,704	6,072	338	421	2	22
		MICHBACK	26,910	1,380	10,814	518	380	3	18
		ELMOD4	20,265	1,483	9,731	524	545	--	6
	Apr-01	PEDMOD	9,757	1,656	5,941	359	421	1.8	17
		EVERCALC	5,755	1,339	7,250	345	547	2	26
		MICHBACK	9,757	1,380	12,655	455	380	3	32
		ELMOD4	8,866	2,125	6,210	241	428	--	16
E	Nov-00	PEDMOD	13,800	--	4,944	276	276	--	13
		EVERCALC	7,280	--	5,175	248	414	--	19
		MICHBACK	26,910		13,800	483	345	--	28
		ELMOD4	8,287		15,752	2,594	627	--	2
	Apr-01	PEDMOD	8,287	--	5,361	359	483	--	28
		EVERCALC	5,520	--	13,800	545	552	--	16
		MICHBACK	4,140	--	6,107	311	380	--	37
		ELMOD4	5,872	--	5,313	605	890	--	12
H	Nov-00	PEDMOD	13,800	1,380	5,373	282	355	--	
		EVERCALC	8,280	1,304	5,451	290	455	--	65
		MICHBACK	26,910	1,380	10,800	483	455	--	
		ELMOD4	8,197	787	7,735	368	600	--	2
	Apr-01	PEDMOD	8,970	1,410	5,868	186	400	6	24
		EVERCALC	5,575	--	5,865	207	414	--	56
		MICHBACK	10,219	1,242	9,025	345	332		
		ELMOD4	8,411	--	7,217	283	395	--	6

De Almeida *et al.* (1994) has suggested that a difference greater than 10% in moduli obtained at different sensor locations should be attributed to nonlinearity and not

simply to inaccuracies in the measured deflections. Using a less strict criterion, the plots in Figure 5.2 indicate that Section G seems to show significant nonlinear behavior (moduli increased by more than 50%). Sections B, D, and F also displayed some nonlinear behavior. The increase in apparent surface modulus could also be due to the presence of a stiff layer (bedrock) in the subgrade or the presence of large rocks. The water table is very low in this project; hence, that possibility has not been considered.

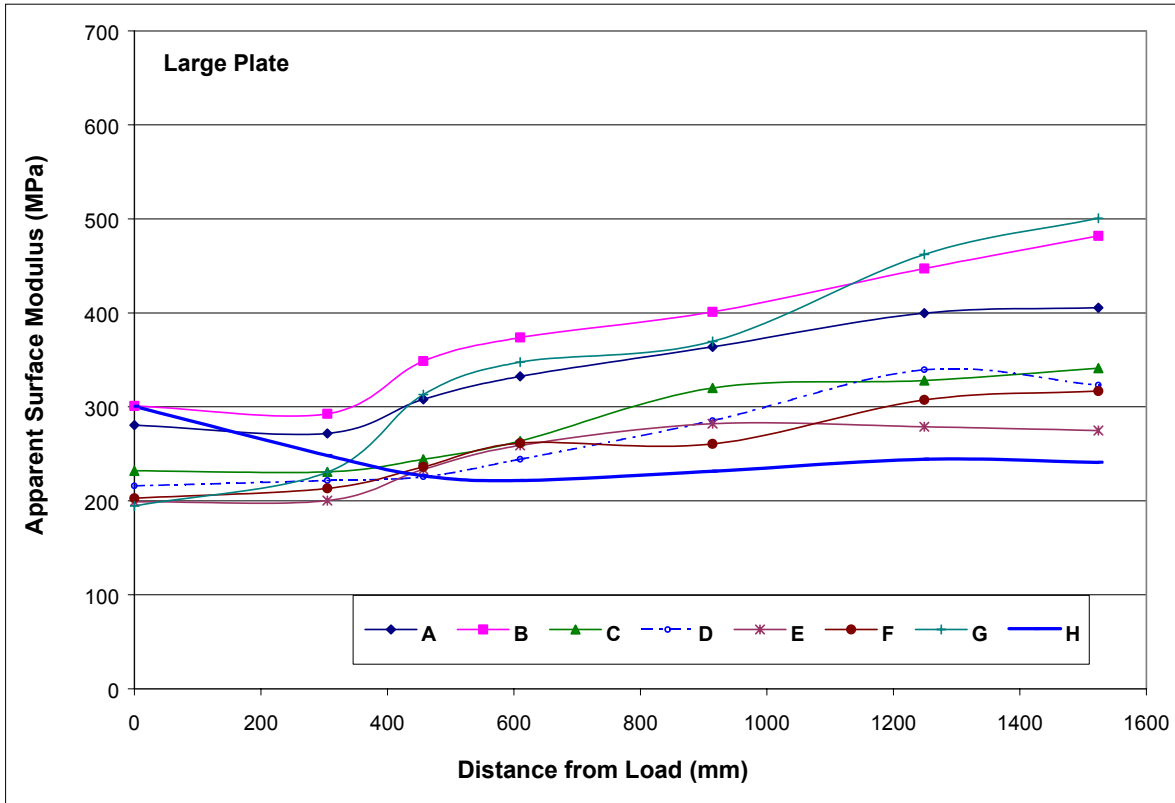


**Figure 5.2** Computed Surface Moduli Using Deflections Measured with the Large Plate on Top of the Subgrade.

For those sections, which indicated the possible existence of a shallow stiff layer underneath the subgrade, the depth to bedrock was estimated using the method proposed by Ullitz (1994). This procedure was based on plotting the deflection ( $D_i$ ) at each sensor versus the inverse of the distance at each deflection from the load center ( $1/r_i$ ), and used the 40kN load for the analysis. If the projection of the curve intercepts the 0 deflection axis at a positive  $1/r$ , there is probably a rigid layer at a distance  $r$  below the surface. This procedure was applied to Section G. The results (Figure 5.3)

suggested a stiff layer at approximately 2m below the surface, which is also consistent with the results of the ELSYM5 analysis.

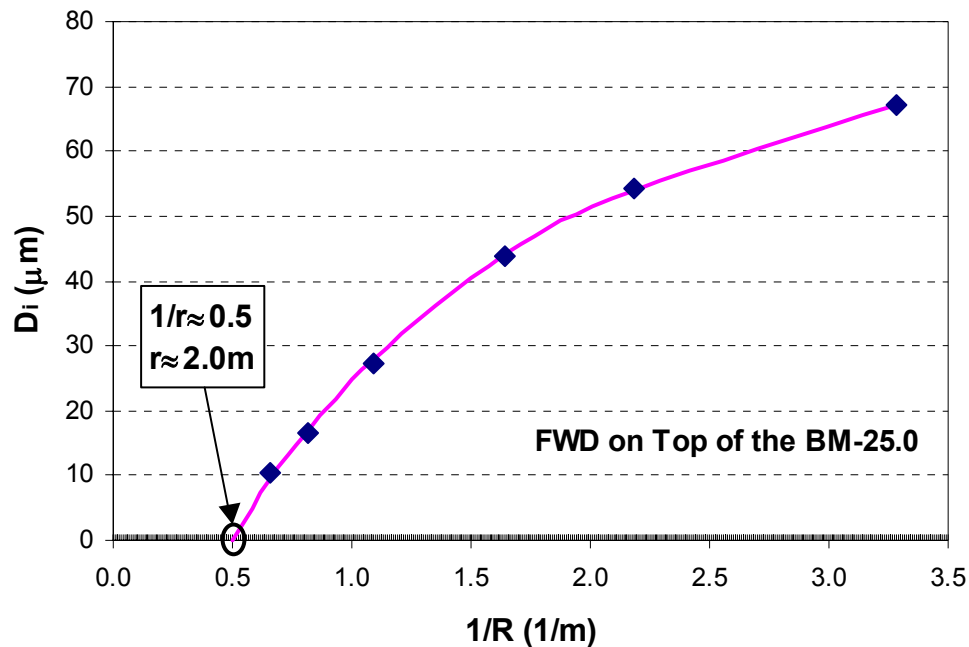


**Figure 5.3** Depth to Stiff Layer Estimation for Section G.

#### 5.4 DEVELOPMENT OF A BACKCALCULATION PROCEDURE

A Dynatest model 8000 FWD unit was used to monitor the structural capacity of the pavement system. FWD testing was conducted after the construction of each pavement layer. One location in each section, in the center of the traveling lane, approximately 25 m from the beginning/end of the section was selected for testing and used for each successive layer. The moisture and temperature of the placed layers were measured at the time of testing. At any given test location and for each FWD drop height, three drops of each load were performed, and the variance of each of these drops was checked to ensure that the loads were within 10% of the target load. The sensor spacing (seven) of the geophones during the initial FWD testing was 0, 203, 305, 457, 610, 914 and 1524 mm from the loading plate center, the recommended long term pavement performance (LTPP) standard sensors spacing. This spacing setup provided closely spaced sensors near the load plate to accurately delineate pavement surface conditions, while still providing sensors far enough out to get accurate subgrade properties. The new sensor spacing (nine sensor spacing) used after March 2000 was 0, 203, 305, 457, 610, 914,

1219, 1524, 1824 mm. This new setup provided sensors far enough out to get accurate subgrade properties without the interference of the pavement section (Sebaaly *et al.* 1999). The first step in the backcalculation process was to obtain the thickness of each layer from the construction records.

Based on the result of the preliminary evaluation of backcalculation software and the subgrade evaluation, the following steps were defined for the backcalculation of the layer moduli:

1. The average apparent surface modulus for the last five sensors (last column in Table 5.2) was adopted for the subgrade modulus. In those cases in which the structure could not be modeled with a RSME of less than 25%, this value was allowed to float in a  $\pm 15\%$  to account for possible moisture and compaction variations.
2. The moduli of the all pavement layers were determined using the deflections measured on top of the layer under study and assuming the moduli computed in previous steps for all the underlying materials. Only one unknown modulus, that of the top layer, was used in each backcalculation step.
3. Each backcalculation step was conducted several times with different seed values to avoid local minima in the error minimization procedure. The set of moduli that resulted in the model with the lowest RMSE was selected in each case.
4. The subbase (21-B) was combined with the subgrade in those sections where the thickness of the 21-B layer was less or equal to 75 mm, i.e. sections E and H. The backcalculation method estimated unreasonable high moduli in these cases.
5. Since the FWD measurements on top of the cement-treated aggregate base (21-A) was conducted, in some cases, just a few days after construction, the modulus of the 21-A was adjusted to account for increased cement hydration in the analysis of the subsequent pavement layers.
6. A default value of 1,380 MPa was used when the backcalculated OGD L moduli were unreasonable; the OGD L thickness is 75 mm.
7. The moduli for the HMA base layers were determined at three different temperatures using deflections measured during different environmental conditions.

## **5.5 BACKCALCULATION RESULTS**

The backcalculated moduli for selected Sections A, B, E and H using PEDMOD, ELMOD, MICHBACK and EVERCALC are summarized in Table 5.3, while detailed analyses for sections C, D, F, and G are presented in Appendix B. Sections I through L are not included in the study using all the software, because the inclusion of steel mesh reinforcement or geocomposite membrane in the pavement system of these sections places them out of the scope of this study. The results for each layer are discussed in the following sections, while the results of the subgrade is reported in Chapter Three.

### **5.5.1 Subbase Moduli**

The backcalculation results of the 21-B layer were reasonably consistent, except for some of the sections with a 75 mm subbase. However, this was expected because thin layers (75 mm or less) usually caused problems in backcalculation procedures. Given the similarity between the 21-B and the fill material (mostly 21-B with some large aggregate), the subbase and the subgrade were combined if the thickness of the 21-B was 75 mm or less. The moduli values determined agree within reason with those measured earlier in the laboratory.

### **5.5.2 Cement-Treated Base Moduli**

Since FWD testing on the 21-A layer was done just days after the material was placed, the strengthening of the layer because of increased cement hydration had to be incorporated in the analysis. The increase in moduli (Table 5.4) was estimated based on unconfined compression tests. Laboratory tests using 100x200mm cylinders, prepared in the field, were conducted after 1, 3, 7, 10, 14, 21, 28, and 50 days of curing in a moisture room. The modulus at each age was estimated using the relationships given in the AASHTO Guide for Design of Pavement Structures (1996). The adjustment factors used for the different layers are summarized in Table 5.5.

### **5.5.3 Combined HMA Base and Wearing Surface Moduli**

Falling weight deflectometer testing of the HMA BM-25.0 layer was conducted in May 1999 and again in June and August 1999 to analyze the moduli variation due to temperature.

**Table 5.4.** Strength Development of 21-A Layer with Time.

<b>Age (days)</b>	<b>Compressive Strength (MPa)</b>	<b>Estimated Resilient Modulus (MPa)</b>
1	0.603	3,100
3	1.207	3,320
7	1.564	3,590
10	1.701	3,660
14	1.865	3,760
21	2.085	3,860
28	2.290	3,930
50	2.370	4,000

**Table 5.5.** Adjustment Factors Used for the 21-A Moduli.

<b>Section</b>	<b>FWD Test on Layer</b>	<b>Age of 21-A (days)</b>	<b>Correction Factor (%)</b>
A – D	21-A	4	--
	OGDL	14	+11%
	BM & WS	>44	+18%
E – H	21-A	1	--
	OGDL <sup>(1)</sup>	14	+18%
	BM & WS	>40	+28%

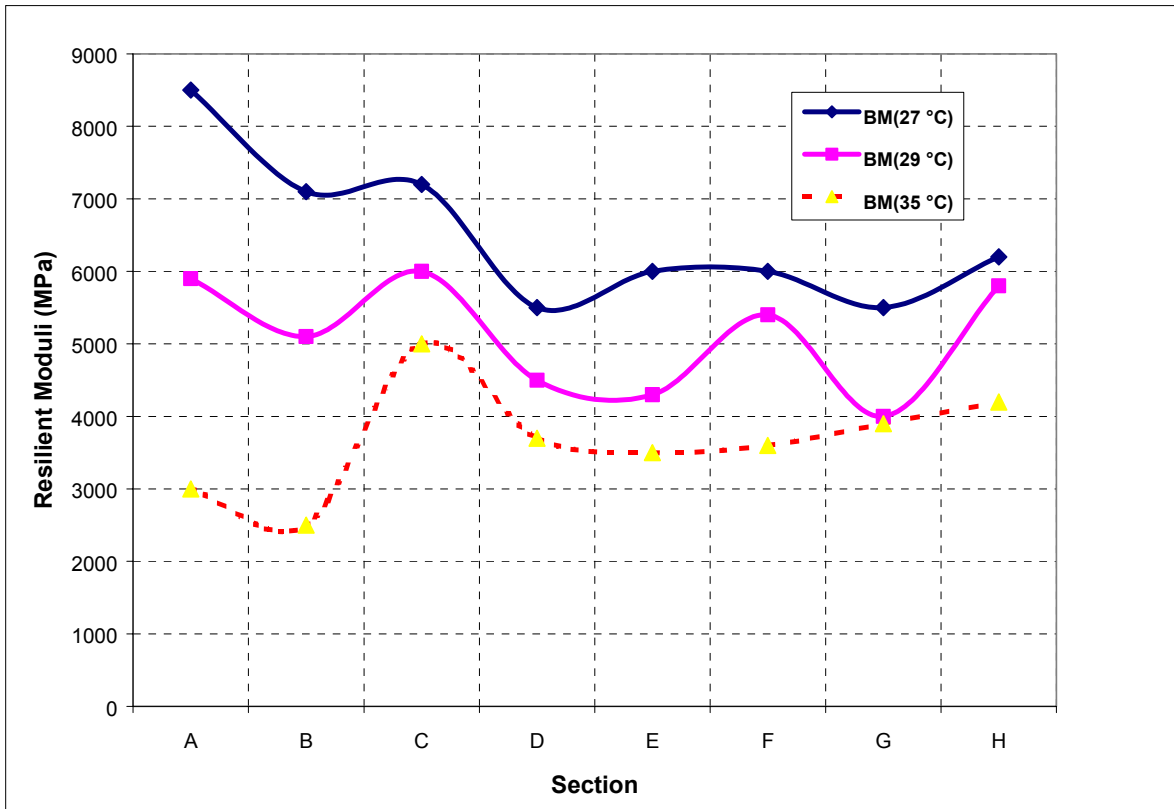
<sup>1</sup> Under Section H only

Figure 5.4 shows the resilient moduli of the BM-25.0 layer corresponding to the three tests. As would be expected, the backcalculated moduli indicate that the HMA BM-25.0 is highly susceptible to temperature. The highest moduli results were obtained for June, 1999 with an average of 6,470 MPa (for all sections). They were followed by those for May, 1999 with an average of 5,140 MPa, and for August 1999 with average resilient moduli of 3,677 MPa.

The moduli of the 38-mm-thick wearing surface layers could not be accurately determined using the software packages. These problems were expected, because backcalculation procedures do not typically work for layers less than 75-mm-thick. Consequently, a combined HMA layer (combining BM-25.0 and wearing surface) was used. The moduli presented are for the combined BM-25.0/wearing surface layer.

A regression equation was fitted to the data to determine and adjust the modulus to a base temperature of 25 °C. The average pavement temperature for each test was determined as an average of the values measured by thermocouples installed at the bottom of the wearing surface and the BM-25.0 layer.

The moduli backcalculated for all the seasonal monitoring tests (thirteen tests over the finished pavement) from November 1999 2000 to December 2002 were used in the developing the temperature-moduli correction model curve. It appears that the model is similar to models presented by other researchers (Kim *et al.*, 1995; Baltzer and Jansen, 1994).



**Figure 5.4** Resilient Moduli of BM-25.0 Layer at Different Testing Periods from FWD.

The following is the resulting equation:

$$E_T = E_{25} e^{-0.031(T-25)} \quad (5.11)$$

where,

$E_T$  = HMA modulus (MPa) at temperature  $T$ ;

$E_{25}$  = HMA modulus (MPa) at 25°C;

$E_0 = 7,125$  MPa for this study; and

$T$  = Temperature of the HMA layer during FWD measurement (°C).

The temperature correction model is shown in Figure 5.5. Values from the temperature

correction model were to be used as part of the comparison of measured and calculated stresses and strains in the pavement layers.

Falling weight deflectometer testing over the two-year period from November 1999 to June of 2002 was done every two months and the moduli of the HMA wearing surface and BM-25.0 layers were combined and backcalculated using the EVERCALC software program. Results of the moduli backcalculation are shown in Figures 5.6 through Figure 5.8 for Sections A through I at the Virginia Smart Road. The seasonal variation of the moduli over the time period of testing was observed.

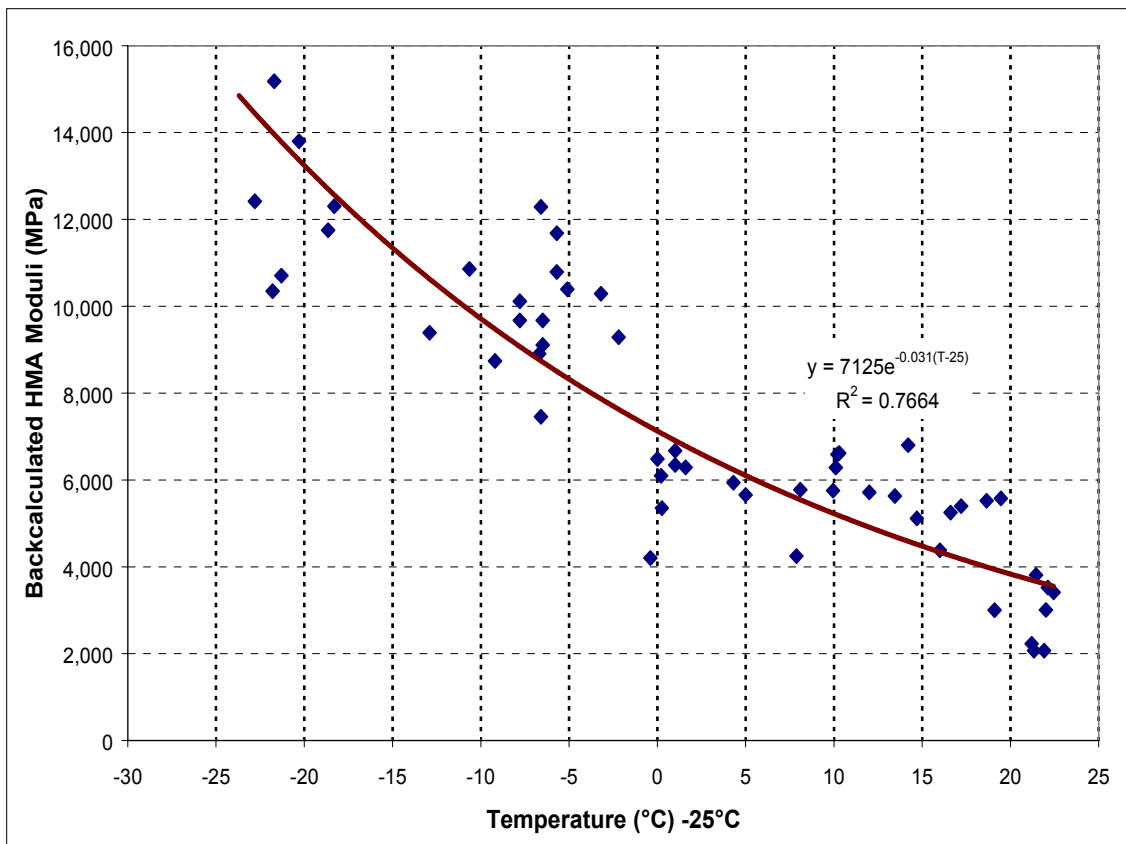


**Figure 5.5.** Backcalculated Resilient Moduli of BM-25.0 Layer Versus Temperature.

Due to freezing temperature between November and February (2 to 10 °C), the HMA moduli increase and decrease during the thawing period. For Sections A through D, the highest moduli were obtained in January and February 2001 with a range between 10,000 to 13,300 MPa. While the lowest moduli was obtained in July of 2001 ranging from 2,070 MPa to 3,808 MPa. For Sections E through H, the highest moduli were backcalculated in January 2001 with moduli of 7,800, 9,100, 11,700 and 15,200 MPa, respectively. The moduli obtained for E through H during December 2001

recorded the next highest moduli. The lowest moduli were obtained during July of 2001 with values between 2,070 and 3,522 MPa.

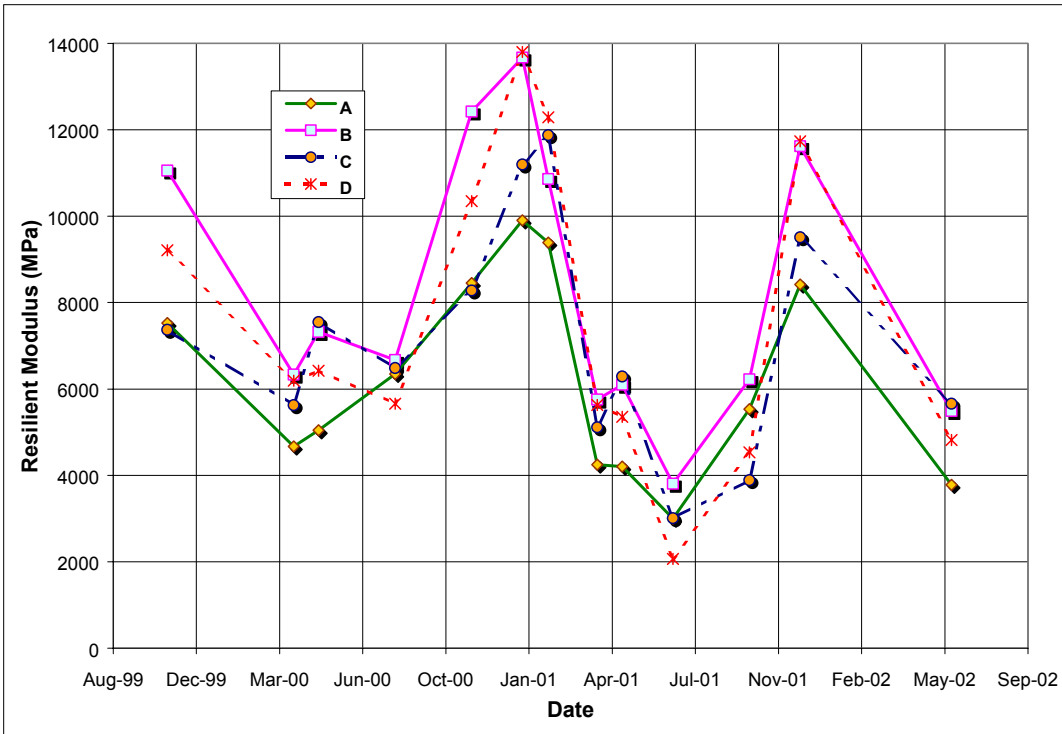


**Figure 5.6** HMA Resilient Moduli for Sections A through D.

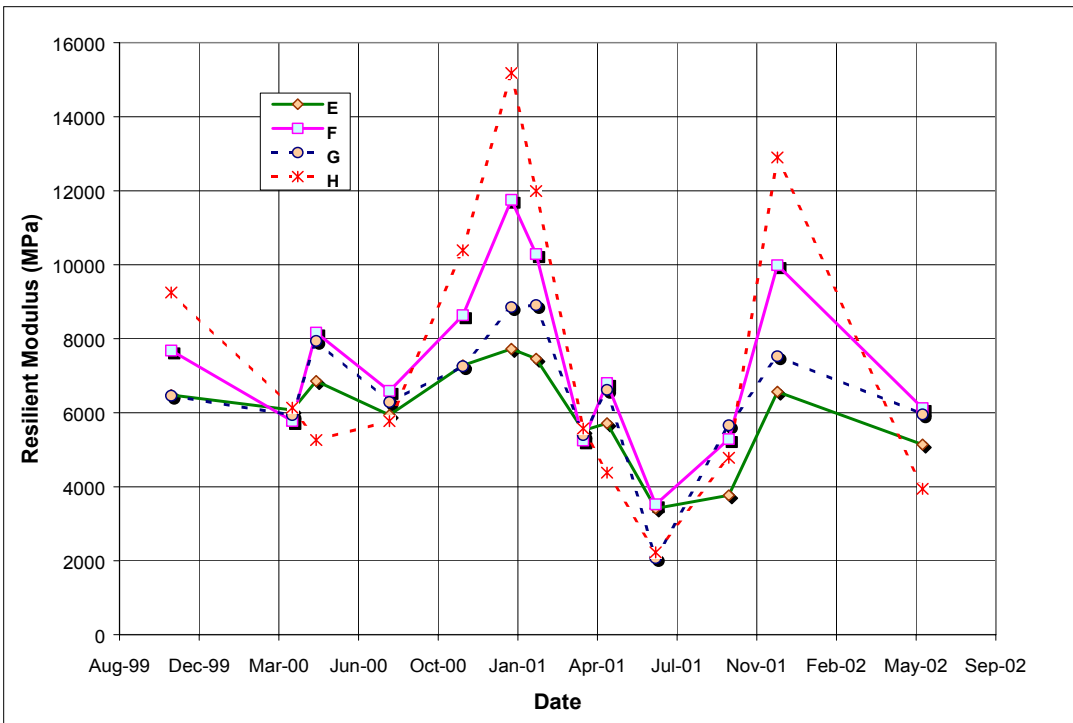


**Figure 5.7** HMA Resilient Moduli for Sections E through H.

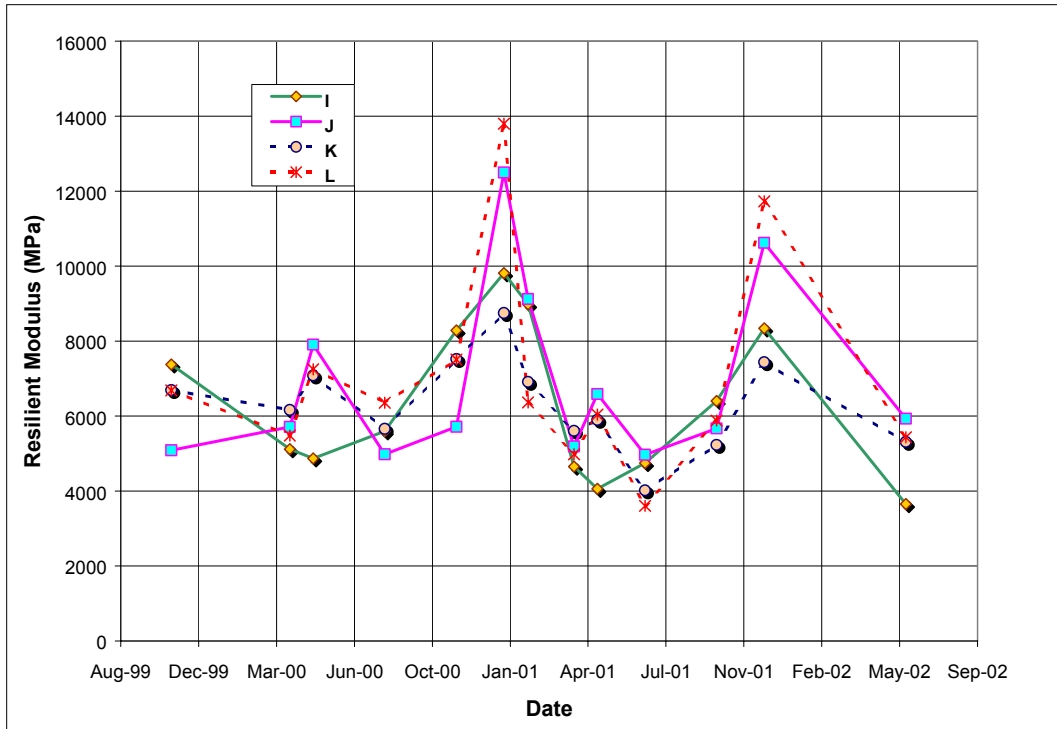


**Figure 5.8** HMA Resilient Moduli for Sections I through L.

Sections I through L showed the same trend with the highest moduli obtained in January 2001 followed by December 2001. The HMA moduli for Sections L and J recorded the highest moduli of 12,500 and 14,000 MPa respectively in January 2001 and 11,900 and 10,800 MPa in December 2001. The lowest moduli were recorded in July 2001 with values of 3600 and 4100 MPa respectively for Sections L and K

## 5.6 DISCUSSION

Falling weight deflectometer testing on the wearing surface was conducted every two months from November 1999 through December 2001. As indicated earlier, a combined HMA layer (combining BM-25.0 and wearing surface) was used. Even with these modifications of combining the BM-25.0 and wearing surface, some of the software packages were not able to produce accurate results. For example, during extreme cold temperatures when the pavement temperatures were less than 5°C, almost all the software produced the highest end of the layer moduli range provided (13,800-27,000 MPa) for the combined BM-25.0/wearing surface layer. A new set of backcalculation procedures or rules were developed to aid in the determination of the moduli of the wearing surfaces using the aforementioned four types of backcalculation software. This procedure addressed three major areas: the first group focused on the definition of the

moduli ranges needed to run each of the selected backcalculation software, because they all gave different expected upper bound of the moduli for each pavement layer selected. For example, MICHBACK gives an upper bound moduli value of HMA up to 27,579 MPa, whereas PEDMOD gives a value up to 13,800 MPa. The second set of rules sought to address the modeling of the pavement structure for purposes of backcalculation and inclusion of depth of rigid layers analytically obtained in the first Chapter, while the third rule focused on the evaluation of the backcalculated results.

Temperature data was collected every time FWD testing was conducted on the wearing surface and the HMA base layers. The average pavement temperature for each test was determined as an average of the values measured by the thermocouples installed at the top and bottom of the BM-25.0 and at the bottom of the wearing surface layer in order to be able to develop a temperature correction model. Excavation of Section C during installation of a weigh in motion in 2001 (two years after construction of the Virginia Smart Road) showed the 21-A layer was as strong as concrete. In addition, the underlying granular and subgrade layers appeared well compacted as shown by the backcalculation results in Appendix B.

In modeling the pavement layer to input into the backcalculation software, the wearing surface (38mm) and BM-25.0 layers were combined into one layer, the OGD, cement stabilized 21-A, granular 21-B layer, and the subgrade were treated as separate layers. For the Sections E, H, I and L with the thickness of the 75 mm for the 21-B layer, the subgrade and 21-B layer were combined.

Although many models are currently available for estimating the modulus of unbound and stabilized subbase materials, a simplistic approach was used to estimate the initial modulus and modulus ranges for these materials types. For example, some of the software such as MICHBACK and PEDMOD do not have the ability to deal with the nonlinear behavior of the granular materials. The EVERCALC software is detailed enough to calculate values of vertical, radial, deviator and bulk stress values at a selected point of interest in the pavement layer. The EVERCALC software detects the existence of nonlinear behavior in the granular layers and calculates the values of  $K_1$  and  $K_2$  (nonlinear constants) and gives the  $R^2$  value of the nonlinear fit produced in the equation it derives. In testing during the coldest temperatures (average temperature of 2 °C in January 2001),  $K_1$  values went as high as 83 MPa with a  $K_2$  value of 0.42. This indicates that the granular layers could have been frozen in these cases, because the

high  $K_1$  value showed the cohesion was unusually strong. ELMOD software also gave the  $n$  value of the nonlinear regression exponent for subgrades in some of the sections.

The ranges shown in Table 5.6 were used in the selected software for determining the moduli of the wearing surface. The table also shows the specified ranges and Poisson's ratios that were used for the materials in the pavement layers. If the temperature was below 10°C, a higher modulus value for the upper range was used. It must be mentioned that deflection data during cold temperatures obtained from drops on the wearing surfaces were in some cases very close to FWD data testing on the concrete sections.

After each backcalculation run, the RMSE was determined and if it was more than 25%, the initial moduli set was modified. The lower and upper bound values of the ranges of the moduli were increased from 10 to 30%, and the backcalculation was rerun until an acceptable RMSE was obtained.

**Table 5.6** Range for Pavement Materials.

<b>Material Type</b>	<b>Initial Moduli (MPa)</b>	<b>Moduli Range (MPa)</b>	<b>Poisson's Ratio</b>
Wearing Surface+ BM-25.0	4140	3450– 20700*	0.30
Open Graded Drainage Layer (OGDL)	828	690- 1380	0.35
Cement Stabilized Base (21-A)	5865	4830-13800	0.15
Aggregate Subbase (21-B)	345	310-517	0.35
Subgrade	345	310-552	0.35

\*Moduli for temperatures below 10°C is 27,600 MPa

If the results of the reruns did not change the resulting backcalculated moduli, they were accepted as the true moduli for the various pavement layers. Results of moduli from the four backcalculation software over the 21-B were fairly repeatable with RMSE results between 12 to 30%. Over the 21-A layer, the results from all the software showed a fairly good repeatability for all the backcalculation software. ELMOD gave a very good fit

(2% RMSE) for the 21-A in Section A. Generally, ELMOD, PEDMOD and EVERCALC gave low RMSE results between 2 to 28%, while PEDMOD gave a high value of 28% for Section B. Table 5.7 shows results of RMSE obtained over the 21-B, 21-A, and OGDL layers in Sections A through H for the four software used. The RMSE values were acceptable for all the Sections during backcalculation.

**Table 5.7** Root Mean Square Error Results for Section A, B, C, D and H for the Backcalculation Software.

Section	Layer	RMSE (%) (Michback)	RMSE (%) (Elmod)	RMSE (%) (Pedmod)	RMSE (%) (Evercalc)	Depth to Stiff Layer (m)
A	21-B	19	12	16	12	6-18
B	21-B	21	23	24	25	6-18
C	21-B	18	15	30	23	6-18
D	21-B	14	6	14	18	6-18
H	21-B	34	15	18	11	6-18
A	21-A	21	2	14	12	6-18
B	21-A	14	22	17	11	6-18
C	21-A	26	8	22	14	6-18
D	21-A	28	22	21	18	6-18
H	21-A	18	6	22	11	6-18
A	OGDL	35	16	26	17	6-18
B	OGDL	29	12	18	11	6-18
C	OGDL	39	19	20	16	6-18
D	OGDL	26	9	14	12	6-18
H	OGDL	16	14	22	25	6-18

The details of the moduli for all the layers using the four backcalculation software and average temperatures of the HMA during the testing are shown in Appendix A. Figures 5.9 through 5.11 present the resilient moduli of sections A through H in January 2001 (average temperatures 5 °C for the wearing surface), April 2001 (average temperature 44 °C for the wearing surface), and October 2001 (average temperature 30 °C for the wearing surface). The COV's for the moduli of the HMA surfaces calculated by

PEDMOD, EVERCAL, MICHBACK and ELMOD during January were 19%, 15%, 35%, and 26%, respectively. The COV's for moduli of the HMA obtained from the backcalculation software in April of 2001 were 11%, 9%, 24%, and 20%, respectively. In October, the COV's were 11%, 8.4%, 24%, and 19%, respectively. In August 2000, the COV's of 35%, 7%, 59% and 10% were obtained for PEDMOD, EVERCALC, MICHBACK and ELMOD, respectively. The EVERCALC, PEDMOD and ELMOD software produced results with much less variability than the MICHBACK software.

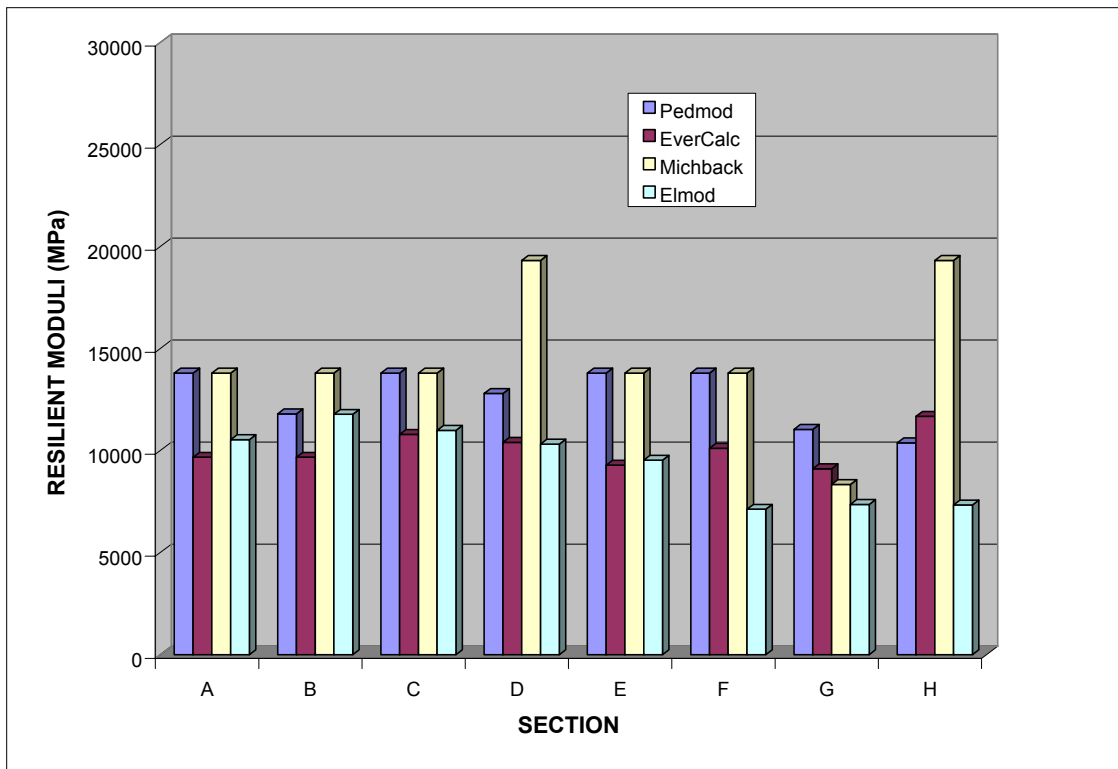


**Figure 5.9** Resilient Moduli of the HMA for Sections A through H in January 2001 from Backcalculation Software.

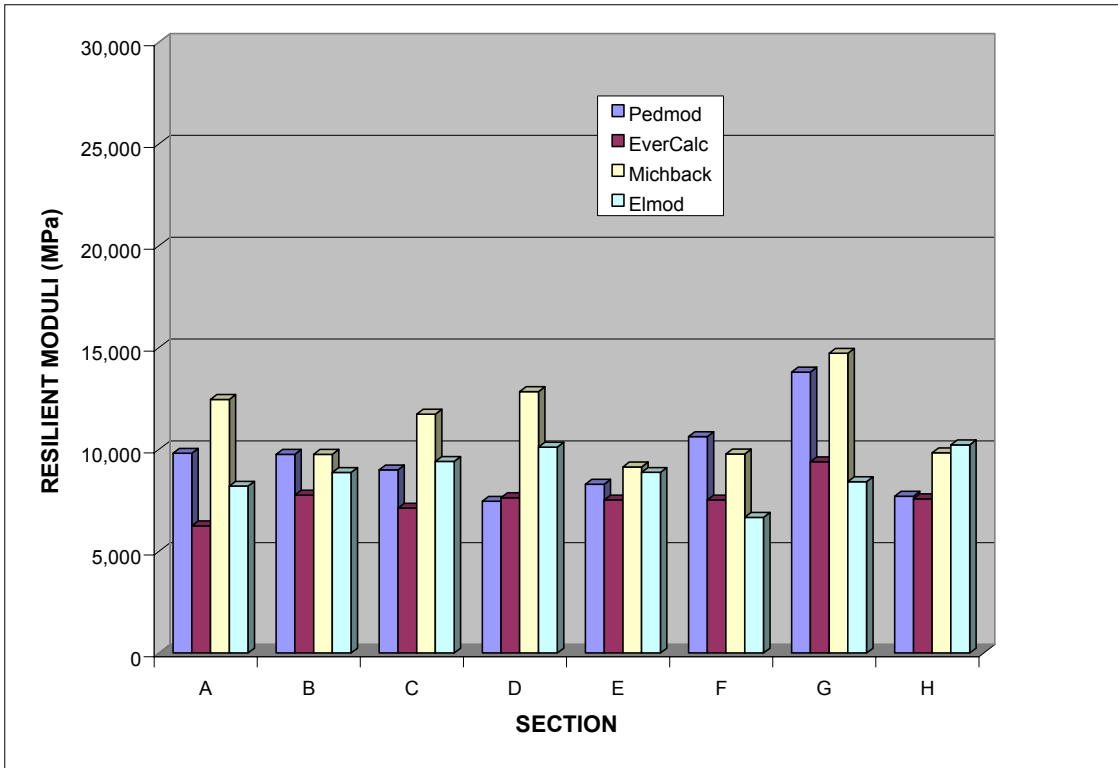


**Figure 5.10** Resilient Moduli of the HMA for Sections A through H in April 2001 from Backcalculation Software.

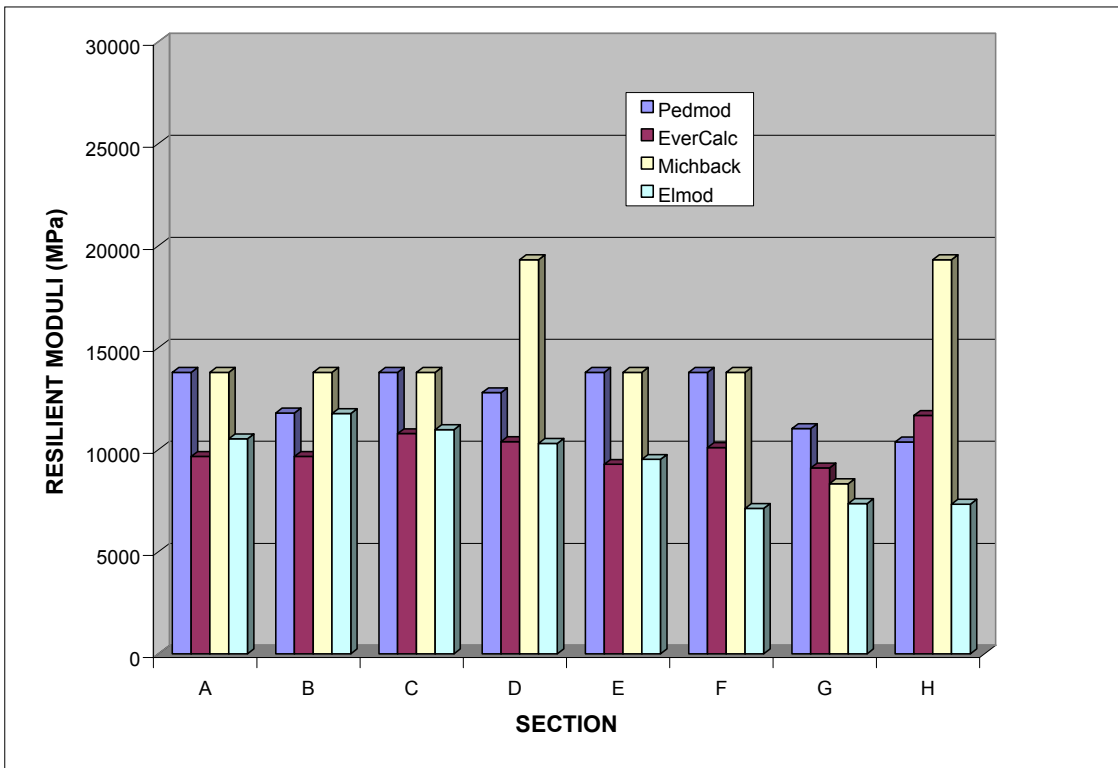


**Figure 5.11** Resilient Moduli of the HMA for Sections A through H in October 2001 from Backcalculation Software.

## 5.7 FINDINGS AND CONCLUSIONS

The determination of the moduli of the pavement layers on sections A through H of the Virginia Smart Road was carried out utilizing four backcalculation software packages: ELMOD, MICHBACK, PEDMOD and EVERCAL. The software packages use different approaches to backcalculate the layer moduli including the forward computation model and error minimization schemes. Based on this study the following were found:

- The backcalculation software packages were successful in determining the moduli of each of the layers at the Virginia Smart Road after defining a rational backcalculation procedure. However, for temperatures less than 5 °C the error per sensor for the PEDMOD and MICHBACK software was in excess of 40%. Hence significant engineering judgment had to be used to achieve reasonable results.
- The highest values of HMA resilient moduli using all backcalculation software packages were recorded when the average temperatures of the HMA were below 5°C.
- The software packages produced similar backcalculation moduli results for the granular 21-B, cement treated 21-A and OGDL layers with very good RMSE values.
- The EVERCALC software was able to detect nonlinear properties ( $K_1$  and  $K_2$ ) of the subgrade and 21-B layer in the final output. It also gave good RMSE values (less than 25%) on all backcalculated moduli of the layers. The deflection basin fit backcalculation mode in ELMOD produced very good RMSE results and reasonable moduli values for data at and below 5 °C.
- The seasonal variation of the moduli of the wearing surface and BM-25.0 combined layers over the three year period from November 1999 to June 2002 was determined. The greatest moduli were backcalculated in January 2001 and December 2001 and the lowest moduli were backcalculated in July 2001 and June 2002.

This study concluded that the EVERCALC and ELMOD software packages were the most suitable among the four software used to backcalculate moduli of the pavement layers for the Virginia Smart Road. EVERCALC particularly produces an output that enabled the user to determine material responses such as bulk stress, tensile strain, vertical strain and stresses at selected depths in the pavement layer. This can aid in providing more information when backcalculation is performed to determine pavement performance. Granular layers of 75 mm or less may need to be combined with other

layers during the backcalculation process. Similarly, thin HMA wearing surface layers may need to be combined with HMA intermediate or base layers.

## REFERENCES

AASHTO (1986). "AASHTO Guide for Design of Pavement Structures." American Association of State Highway Transportation Official." Washington, D.C.

Baltzer, S. and Jansen, J. M. (1994). "Temperature Correction of Asphalt-Moduli for FWD-Measurements." Proceedings of the 4<sup>th</sup> International Conference on the Bearing Capacity of Roads and Airfields, Univ. of Minnesota, Vol. 1, Minneapolis, MN, pp. 753-768.

Baltzer, S., Ertman-Larsen, H. J., Lukanen, S., and Stubstad, R. N. (1994). "Prediction of Asphalt Concrete Material Temperatures for Routine Load Deflection Measurements." Proceedings of 4<sup>th</sup> International Conference on the Bearing Capacity of Roads and Airfields, Univ. of Minnesota, Vol. 1, Minneapolis, MN, pp. 401-412.

De Almeida, J. R., Brown, S. F., and Thom, N. H. (1994). "A Pavement Evaluation Procedure Incorporating Material Nonlinearity." Nondestructive Testing of Pavements and Backcalculation of Moduli, ASTM STP 1198, Von Quintas, H. L., Bush, A. J. III, and Baladi, G. Y., Eds., American Society for Testing and Materials, Vol. 2, Philadelphia, PA, pp. 218-232.

Harichandran, R. S., Mahmood, T., Raab, A.R., and Baladi, G.Y. (1994). "Backcalculation of Pavement Layer Moduli, Thickness and Stiff Layer Depth Using a Modified Newton Method." Nondestructive Testing of Pavements and Backcalculation of Moduli, ASTM STP 1198, Von Quintas, H. L., Bush, A. J. III, and Baladi, G. Y. Eds., American Society for Testing and Materials, Vol. 2, Philadelphia, PA, pp. 68-72.

Huang, Y. J.(1993). Pavement Analysis and Design. Prentice Hall, New Jersey.

Lytton, R. L. (1989). "Backcalculation of Pavement Layer Properties." Nondestructive Testing of Pavements and Backcalculation of Moduli, ASTM STP 1026, Bush, A. J. III,

and Baladi, G. Y. Eds., American Society for Testing and Materials, Philadelphia, PA, pp. 7-38.

McQueen, R. D (1999). PEPMOD95 User's Guide and PEDMOD95 Documentation, Roy D. McQueen and Associates, Ltd., Sterling, VA.

Peutz, M. G .F., Van Kempen, H. P .M. and Jones, A. (1968). "Layered Systems under Normal Surface Loads." *Highway Research Record 228*, National Research Council, Washington, D.C., pp.35-45.

Rada, G.R., Richter, C.A., and Jordahl, P. (1994). "SHRP's Layer Moduli Backcalculation Procedure." *Nondestructive Testing of Pavements and Backcalculation of Moduli*, ASTM STP 1198, H. L. Von Quintas, A. J. Bush, III, and G. Y. Baladi, Eds., American Society for Testing and Materials, Vol. 2, Philadelphia, PA, pp. 38-52.

Ullidtz P., and Coetzee, N.F. (1995) "Analytical Procedures in Nondestructive Testing Pavement Evaluation." *Transportation Research Record 1482*, National Research Council, Washington, D.C., pp.61-66.

Ullidtz, P. (1977). "Overlay and Stage by Stage Design." *Proceedings of the 4<sup>th</sup> International Conference on the Structural Design of Asphalt Pavements*, Eds., Univ. of Michigan, Vol. 1. Ann Arbor, MI, pp. 722-735.

Ullidtz, P. and Ertman Larsen, H.J. (1989). "State of the Art Stress, Strain and Deflection Measurements, State of the Art Pavement Response Monitoring Systems for Roads and Airfields." *Special Report 89-23*, US Army Corps of Engineers, Cold Regions Research & Engineering Laboratory, West Lebanon, NH, pp.148-161.

Ullidtz, P. (1988). Pavement Analysis, Elsevier Science. New York, NY.

Uzan, J. (1994). "Advanced Backcalculation Techniques." *Nondestructive Testing of Pavements and Backcalculation of Moduli*, ASTM STP 1198, H. L. Von Quintas, A. J. Bush, III, and G. Y. Baladi, Eds., American Society for Testing and Materials, Vol. 2, Philadelphia, PA, pp. 3-37.

Van Cauwlaert, F.J., Alexander, D.R., White, T.D. and Barker, W.R. (1989) "Multilayer Elastic Program for Backcalculating Layer Moduli in Pavement Evaluation." Nondestructive Testing of Pavements and Backcalculation of Moduli, ASTM STP 1026, A. J. Bush, III, and G. Y. Baladi, Eds., American Society for Testing and Materials, Philadelphia, PA, pp. 171-188.

Van Cauwlaert, F.J., and Lequeux, D. (1986). "Stresses and Displacements in Four Layered Systems with Fixed Bottom." Cerisic asbl., Mons, Belgium.

Van Deusen, D (1996). "Selection of Flexible Backcalculation Software for the Minnesota Road Research Project." Report No. MN/PR - 96/29, Minnesota Department of Transportation, St. Paul, MN.

## CHAPTER SIX

### RELATIONSHIP BETWEEN BACKCALCULATED AND LABORATORY MEASURED RESILIENT MODULI OF SUBBASE MATERIAL AND HOT-MIX ASPHALT

#### Abstract

In an attempt to establish a relationship between backcalculated and laboratory measured resilient moduli, this Chapter focuses on ascertaining the correlation between backcalculated and laboratory-measured resilient moduli of both the subbase material and hot-mix asphalt (HMA). To achieve this goal, the resilient moduli of the unbound granular subbase (Virginia 21-B) obtained from laboratory testing were compared to those backcalculated from in situ FWD deflections measurements conducted at the Virginia Smart Road. Indirect tensile resilient modulus tests conducted on cored HMA samples, taken from selected sections of the wearing surface of the Virginia Smart Road were compared to backcalculated HMA moduli. Laboratory resilient modulus results confirmed that stress-dependence can be predicted appropriately using the  $k-\theta$  model. Results indicate that the backcalculated moduli are comparable to those obtained in the laboratory using the  $k-\theta$  model if a representative state of stress is used in the model.

Results of laboratory-determined moduli from the indirect tensile tests of cores from the BM-25.0 layer were lower than the moduli obtained from backcalculation at selected temperatures of 5, 25 and 40 °C. The ratios of backcalculated to laboratory determined moduli depend on the temperature of the testing. Lower ratios obtained at low temperatures and higher ratios obtained at high temperatures for all the software. In addition, difference in loading period between laboratory-testing and FWD could affect the resulting resilient modulus.

## **6.1 INTRODUCTION**

Although the rational characterization of pavement layer materials is necessary for any mechanistic-based pavement design methodology, however, the two accepted methodologies (laboratory testing and nondestructive based backcalculation) produce results that are not in general agreement. Some studies have shown that there is a correlation between laboratory measured and backcalculated values. However, it is clear that the differences can lead to potentially large systematic differences in pavement designs (Seeds *et al.*, 1991). The 1993 AAHSTO Guide for Design of Pavement Structures recognizes that the moduli calculated from deflections are not equal to the resilient moduli measured in the laboratory. Anderson and Woods (1975) found that moduli from laboratory testing are normally less than the in situ results by anywhere from ten to several hundred percent. Nazarian *et al.* (1998) have presented the results of a comparison between laboratory tests and backcalculated moduli on Texas unbound granular base materials using a Seismic Pavement Analyzer (SPA). The results from the SPA were typically 70% higher than the FWD moduli. However, the researchers were not able to identify a unique relationship between laboratory and field tests. Von Quintas and Killingsworth (1998) presented a summary of results of a study to determine the magnitude of differences in the resilient moduli of pavement materials and subgrade soils as determined from repeated load tests in the laboratory and backcalculated moduli. Their study did not establish a meaningful relationship between backcalculated and laboratory moduli, however.

This Chapter compares the resilient moduli of an unbound granular subbase, core samples taken from the wearing surface of the Virginia Smart Road, and HMA samples prepared in the laboratory to those backcalculated from in situ FWD deflections obtained from the field. The objective is to establish a relationship between laboratory determined moduli and field determined values from backcalculation. Stress dependency of the moduli of the granular material (Virginia 21-B) was also investigated.

## **6.2 SPECIMEN PREPARATION AND LABORATORY TESTING OF 21-B**

Specimens used for resilient modulus testing consisted of base/subbase material (21-B material) obtained from the Virginia Smart Road project. The test setup requires that preparation of cylindrical specimens that meet the American Association of State Highway And Transportation Officials (AASHTO) specification that the height of the specimen be

twice its diameter. The specimens, therefore, used a 100 mm diameter by 200 mm tall split mold.

Also, since AASHTO requirements do not allow the maximum particle size for triaxial specimens to exceed  $1/16$  of the diameter of the specimen (i.e. approximately 16 mm for the specimen size tested), a 16 mm sieve was used to scalp the 21-B material, which has a maximum aggregate size of 25 mm.

The 21-B specimen material was mixed with water to achieve desired moisture content and compacted into the mold, using a modified Proctor hammer with 2693 KN/m<sup>3</sup> compaction energy. The test specimens were prepared at compacted densities ranging from 2.23 ton/m<sup>3</sup> to 2.36 ton/m<sup>3</sup>, which corresponds to relative field compaction values ranging from 90% to 97% of the Modified Proctor Maximum Dry Density (MPMDD). The average MPMDD for these specimens was 2.46 ton/m<sup>3</sup> and the optimum moisture content was 6.7%.

After compaction, the specimen was placed over the porous stone of the triaxial cell, and another porous stone was placed on the top of specimen. The triaxial cell was assembled and placed on the center of a servo-hydraulic MTS plate. The chamber piston rod was connected with the load cell, which was attached to the MTS machine. The displacement of the top piston relative to the triaxial cell was measured using an extensometer attached to the top of the triaxial cell. Finally, the air pressure line was connected to the cell pressure inlet to apply lateral pressure. Table 6.1 presents soil properties of tested specimen.

### 6.2.1 Test procedure

The resilient modulus is defined as the cyclic deviator stress divided by the recoverable axial strain, as shown in equation 6.1:

$$M_r = \frac{q_r}{\varepsilon_{1r}} \quad (6.1)$$

where,

$q_r$  = repeated deviator stress;

$\varepsilon_{1r}$  = resilient (or recoverable) axial strain; and

$M_r$  = resilient modulus.

**Table 6.1.** Properties of 21-B Specimens.

Specimen ID	Moisture Content (%)	Relative Compaction (%)	Dry Density (ton/m <sup>3</sup> )
1	4.46	96.17	2.36
2	5.54	93.8	2.3
3	5.44	96.11	2.36
4	4.70	97.16	2.38
5	6.22	91.67	2.25
6	5.09	94.83	2.33
7	4.54	96.74	2.37
8	5.06	96.79	2.37
9	6.18	93.06	2.28
10	3.66	91.13	2.28

Since the resilient modulus is a function of the confining pressure and the cyclic deviator stress level, AASHTO recommends carrying out a series of tests with varying confining pressures and cyclic deviator stress levels. The first loading condition corresponds to a conditioning load step, which is applied to eliminate platen bedding effects.

It should also be noted that the specified maximum deviator stress for each sequence has two components: the contact stress and the cyclic stress. The maximum deviator stress is equal to the cyclic stress plus the contact stress. The contact stress is defined as 10% of the maximum deviator stress.

$$\sigma_{\max} = \sigma_{\text{cyclic}} + \sigma_{\text{contact}} \quad (6.2)$$

where,

$$\sigma_{\text{contact}} = 0.1 \times \sigma_{\max}$$

The contact stress ensures that the specimen remains in contact with the top cap. The cyclic load is a haversine applied at a frequency of 1 Hz (1 cycle/sec), consists of two stages: 0.1 sec loading period and 0.9 sec relaxation period. This load pulse shape corresponds to a haversine i.e.  $(1-\cos\theta)/2$ . The procedure of a typical test sequence is as follows:

- The actual load magnitude is calculated by multiplying the desired stress by the actual specimen cross sectional area.
- The upper cap and bottom base valves are opened to ensure atmospheric pressure conditions.

- The confining pressure is raised to the specified value for the given load sequence (e.g. for Sequence No. 0,  $\sigma_3 = 103.4$  kPa).

Once the corresponding contact stress and cyclic stress (e.g. for Sequence No. 0,  $\sigma_{3\text{contact}} = 10.3$  kPa, and  $\sigma_{3\text{cyclic}} = 93.1$  kPa) is set, the cyclic stress is applied for the specified number of load applications (500 times for Sequence No. 0). For Sequence No. 0, if permanent strain is still being recorded after 500 load cycles, another 500 load cycles should be applied. If the permanent strain is greater than 5% during the conditioning stage (i.e., Sequence No. 0), the test is stopped because the specimen could not be compacted appropriately. For Sequence No.1, the contact stress is set at 2.1 kPa, and the cyclic load to 18.6 kPa. One hundred cycles of load are applied and the load and displacement are recorded for the last five cycles. Then, the next sequence is started. The sampling rate of the data acquisition system is 100 Hz (read 100 data points per second). After the test, the weight of the specimen is measured, and the specimen is then dried in an oven for 24 hrs before the water content is measured.

### 6.2.2 Resilient Modulus Model

This research project tested three resilient modulus models. The first was the K- $\theta$  response model, which has been widely used for granular materials and is represented as follows:

$$M_r = k_1 \theta^{k_2} \quad (6.3)$$

where,

$\theta$  = the bulk stress (kPa);

$M_r$  = the resilient Modulus (kPa); and

$k_1$  and  $k_2$  = regression parameters.

Equation 6.3 shows that the resilient modulus is a function of the bulk stress (Hicks 1970; Allen and Thompson 1974; Khedr, 1985). This equation is popular, because it is simple and can be applied to plot resilient modulus versus bulk stress. The constant  $k_1$  and  $k_2$  were found using regression analysis.

The Uzan (1985) model according to which the resilient modulus depends on the bulk stress and deviatoric stress is as follows:

$$M_r = k_3 \cdot \theta^{k_4} \cdot \sigma_d^{k_5} \quad (6.4)$$

where,

$\theta$  = bulk stress (kPa);

$\sigma_d$  = deviatoric stress (kPa);

$M_r$  = resilient Modulus (kPa); and

$k_3$ ,  $k_4$ , and  $k_5$  = regression parameters determined using regression analysis.

In the model proposed by Witczak and Rada (1981), the resilient modulus also depends on the degree of saturation and density. This model, which contains four constant parameters, is given by the following equation:

$$\text{Log}_{10} M_r = C_0 + C_1 \cdot S_r + C_2 \cdot PC + C_3 \cdot \text{Log}_{10} \theta \quad (6.5)$$

where,

$M_r$  = resilient Modulus (kPa);

$S_r$  = degree of saturation (%);

PC = modified relative compaction (%);

$\theta$  = bulk stress (kPa); and

$C_0$ ,  $C_1$ ,  $C_2$ , and  $C_3$  = regression parameters determined using regression analysis.

Ten specimens with different water contents and relative compaction were tested and the resilient modulus vs. bulk stress plots were as performed. The coefficient of determination ( $R^2$ ) in all cases was greater than 90%, indicating that all the models appropriately fit the data. Since each model had an appropriate goodness of fit, the simplest one, K- $\theta$  Model, was selected for comparison. The variation of the resilient modulus as a function of the bulk stress, according to this model for all the specimens, as well as using the average coefficients, is presented graphically in Figure 6.1.

### 6.2.3 Comparison between Field and Laboratory Resilient Modulus Results

The average value for the resilient modulus of the 21-B layer, assuming the stress-dependent behavior given by the K- $\theta$  model, was determined using an iterative process. Pavement Section C was used for illustrating this process. The bulk stresses developed

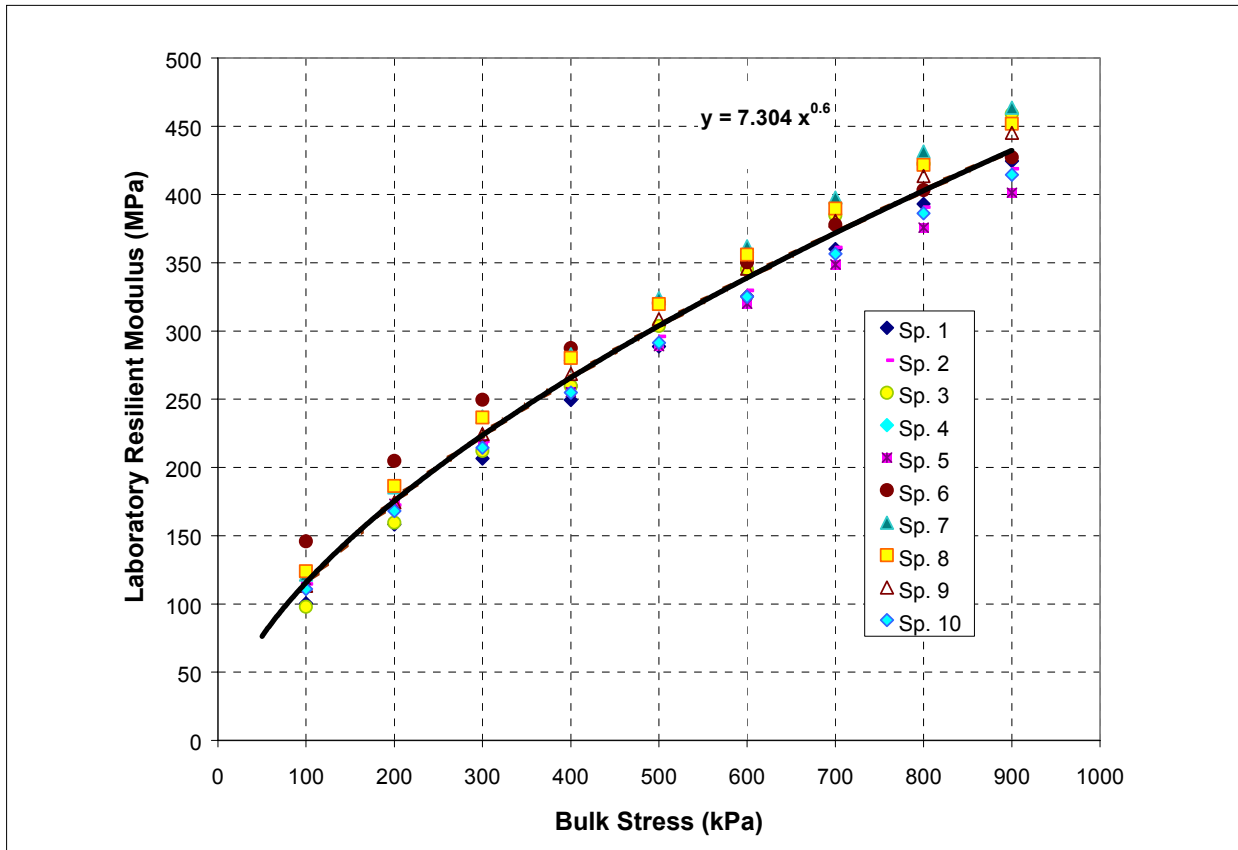


**Figure 6.1** Laboratory Measured Resilient Modulus for 21-B.

at different depths within the pavement were computed using the formula proposed by Huang (1993):

$$\theta = \sigma_1 + \sigma_2 + \sigma_3 + \gamma z(1 + 2K_0) \quad (6.6)$$

where,

$\sigma_1$ ,  $\sigma_2$ , and  $\sigma_3$  = principal stresses due to loading;

$\gamma$  = unit weight of the soil (assumed here 17,267 N/m<sup>3</sup>);

$z$  = depth at which the stresses are calculated; and

$K_0$  = coefficient of earth pressure at rest (assumed 0.6).

The principal stresses were computed using ELSYM5. A 40 kN circular load, and moduli of 207 MPa and 306 MPa for the subbase and subgrade, respectively, were used. The stresses were determined using a grid of points 25 mm apart in the vertical direction and 50 mm apart in the horizontal direction. The computed bulk stresses were then used to compute the moduli distribution based on the K- $\theta$  model (Figure 6.2).

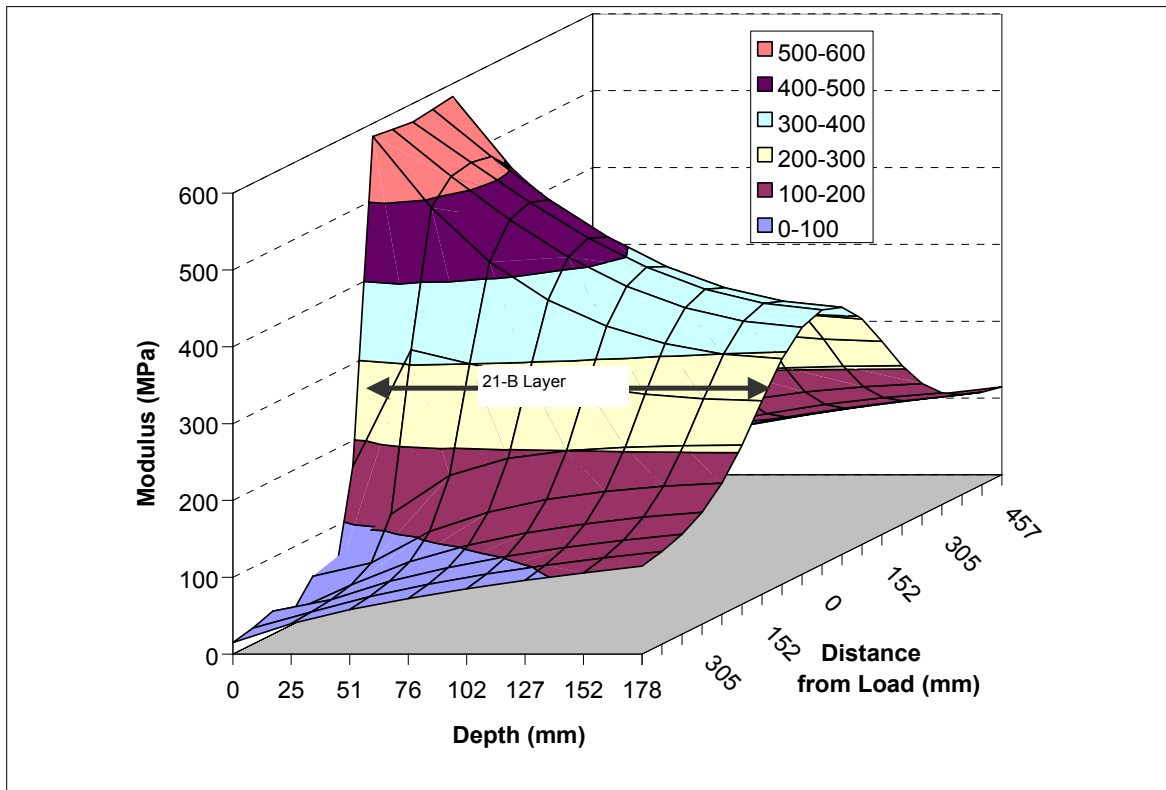


**Figure 6.2** Theoretical Resilient Modulus Distribution.

The average modulus over the area of influence of the load (considering a  $30^\circ$  stress distribution line) within the 21-B subbase layer is 253 MPa. The principal stresses were recomputed using the new 21-B modulus. The bulk stress distribution was determined, and the average modulus recomputed to be 252 MPa, which is very close to the modulus obtained previously. Furthermore, these values are close to the values determined using the different backcalculation methods (246 to 351 MPa), or considering a single-layer system (244 MPa). The values estimated for other subbase thicknesses are presented in Table 6.2. In general, the moduli backcalculated for the other sections were found to be comparable to those obtained at the laboratory; however, that was not the case for thin subbase layers (75mm).

**Table 6.2** Average 21-B Moduli Based on the K- $\theta$  Lab Model (MPa).

Sections	Thickness (mm)	Average Moduli Using 40 kN Load (MPa)
A-D	178	253
E, H, I, L	76	345
F,G, J,K	152	266

### 6.3 FIELD RESILIENT MODULI RELATIONSHIP

The laboratory measured nonlinear behavior of the unbound granular 21-B was used in the KENLAYER program to calculate the measured deflections at the seven-sensor spacing resulting from the FWD small plate. Since it would be possible to establish a relationship between the field behavior and the laboratory results, the sensor spacing of 0, 203, 305, 475, 610, 1219, and 1524 mm was used. Deflection profiles resulting from Hick's relationship (1970) with  $K_1$  values from 3900 to 17320 and  $K_2$  from 0.45 and 0.6, the range recommended for granular materials were generated to simulate the resilient modulus of the granular material in the field using the KENLAYER program (Huang,1987). The deflections resulting from the different stress dependent moduli relationships were compared to the deflections measured in the field, and the RMSE's in percent and microns between the two types of deflections were calculated. Sections A through L were analyzed. The detailed results of the analysis, when all the nine sensor deflection readings were used are shown in Tables 6.3 through 6.8.

Sections A and B, have 178 mm of base layer, Sections E and H, have 76 mm, and Sections J, K, and L, have 152 mm of base layer thickness. Figures 6.3 through 6.10 show plots of deflection versus sensor spacing for some of the sections mentioned earlier.

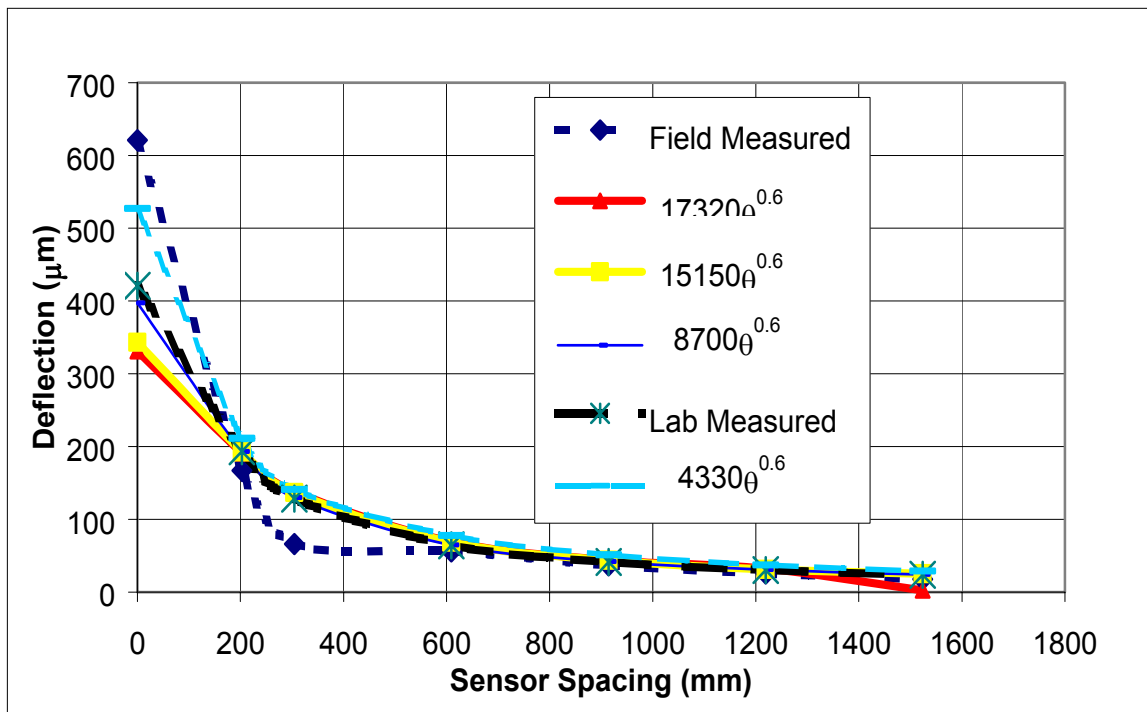


Figure 6.3 Measured and Calculated Deflections for 21-B (Section A).

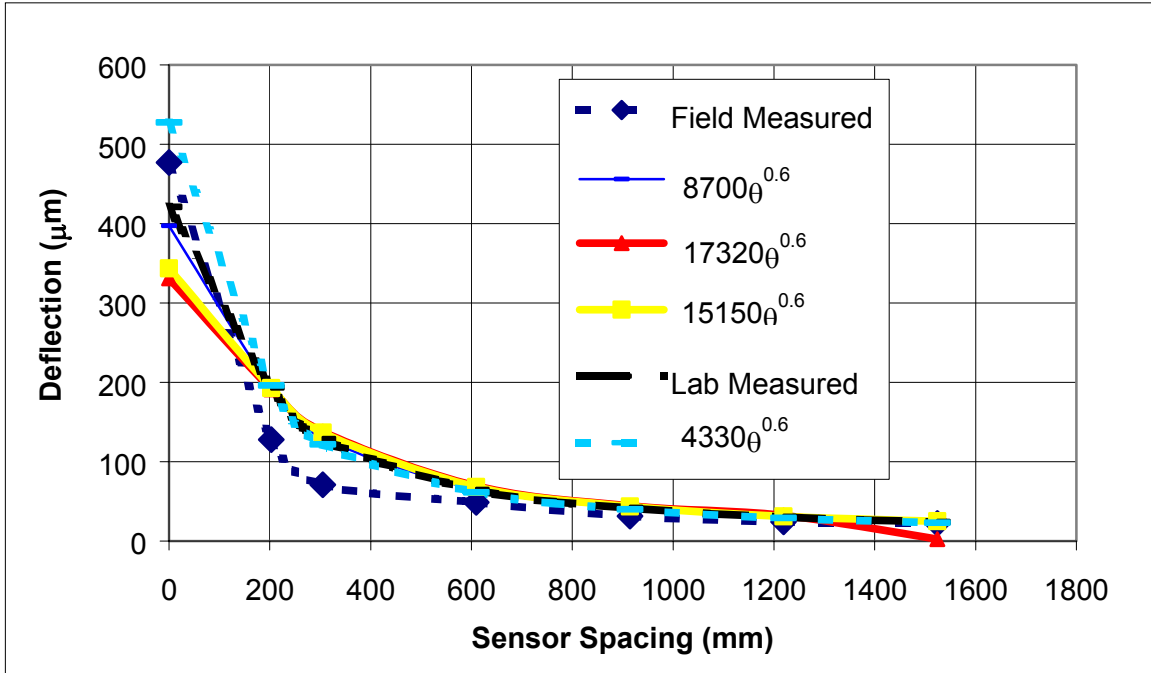


Figure 6.4 Measured and Calculated Deflections for 21-B (Section B).

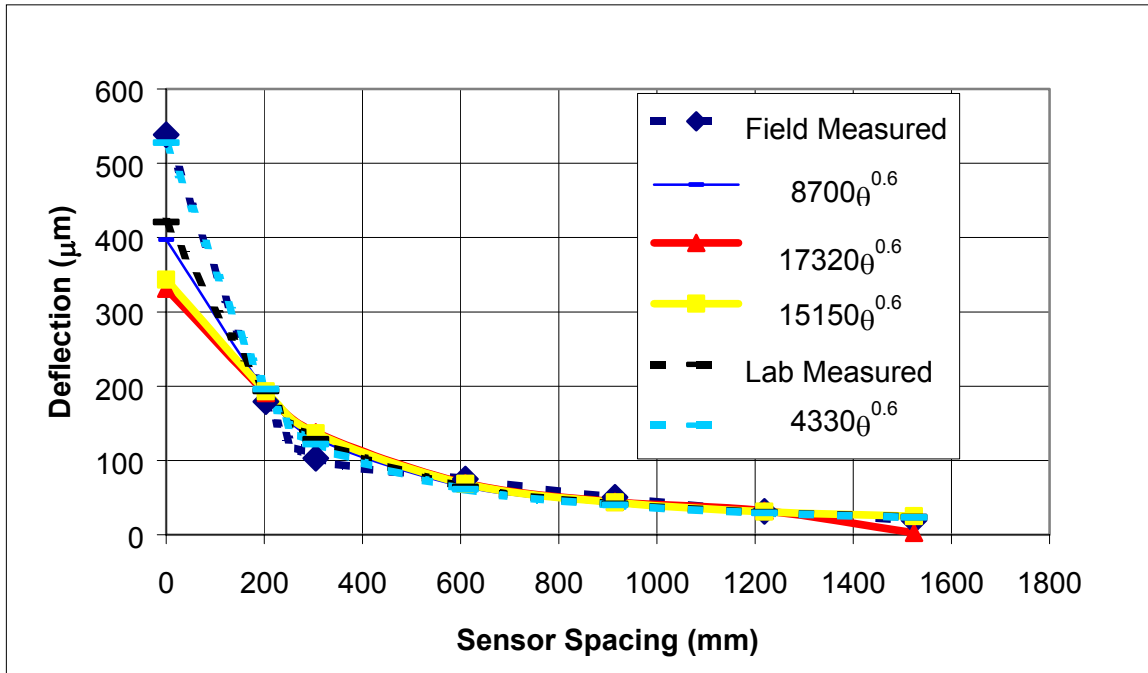


Figure 6.5 Measured and Calculated Deflections for 21-B (Section C).

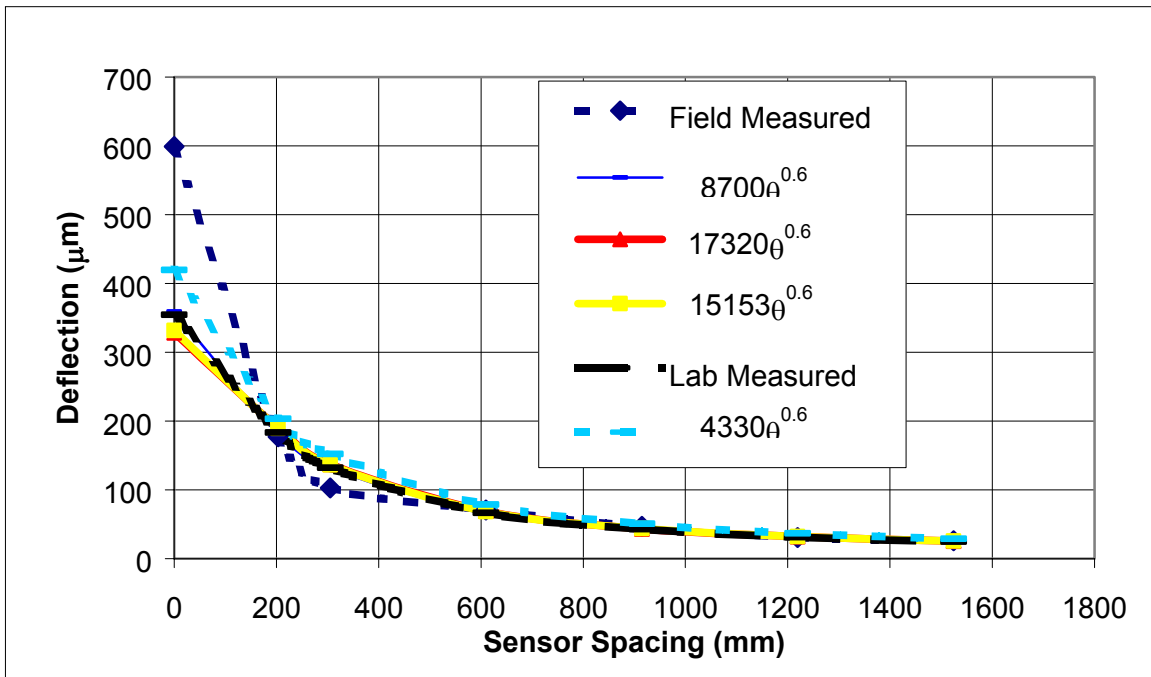


Figure 6.6 Measured and Calculated Deflections for 21-B (Section E).

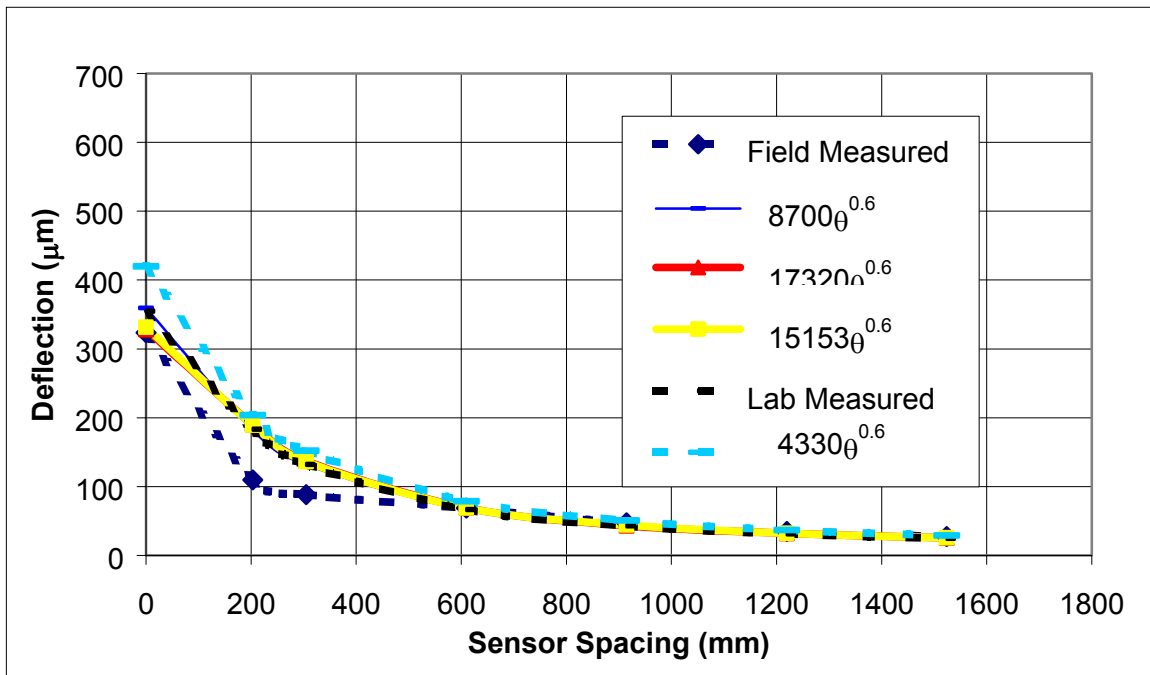


Figure 6.7 Measured and Calculated Deflections for 21-B (Section H).

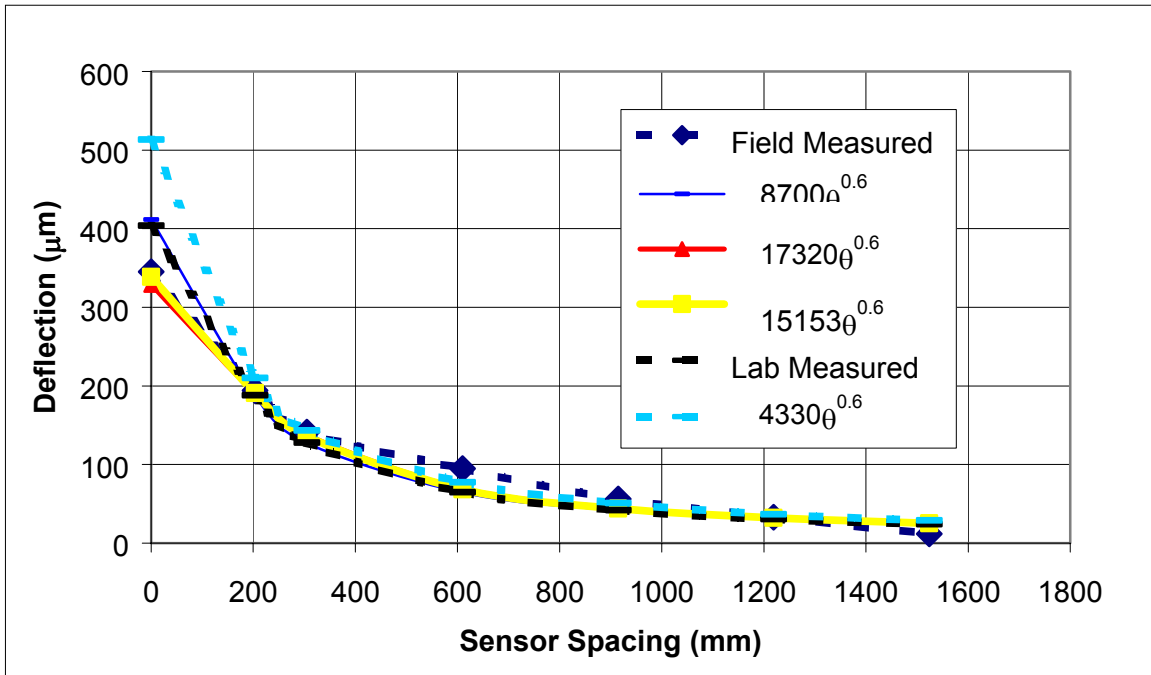


Figure 6.8 Measured and Calculated Deflections for 21-B (Section K).

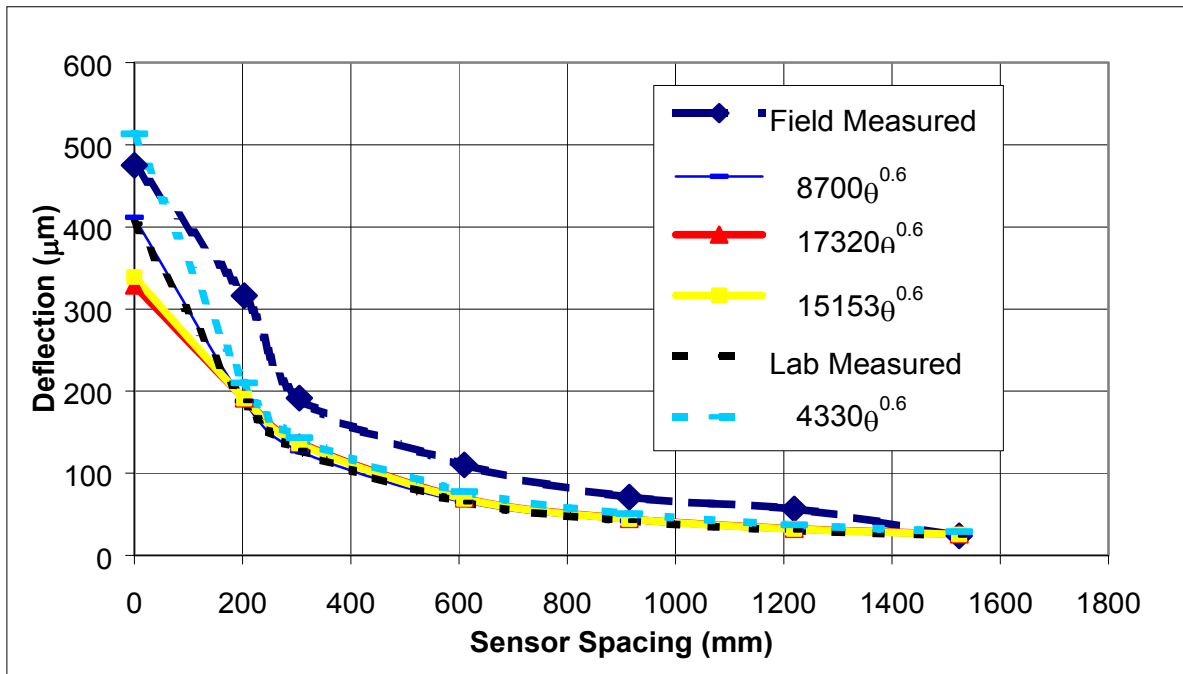


Figure 6.9 Measured and Calculated Deflections for 21-B (Section L).

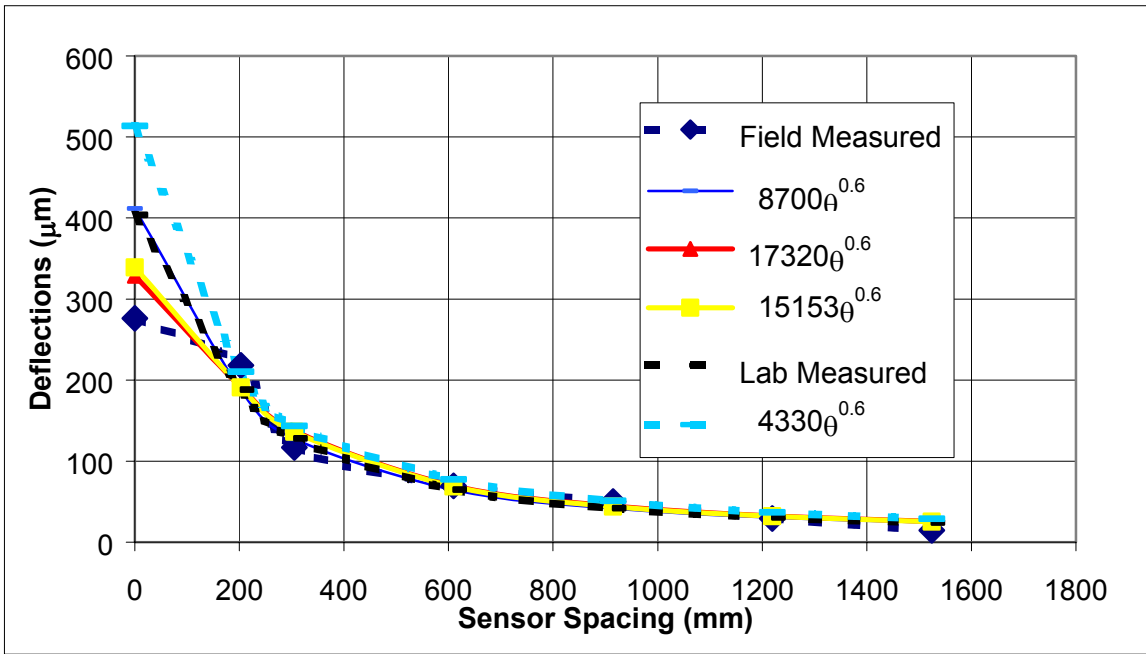


Figure 6.10 Measured and Calculated Deflections for 21-B (Section J).

Table 6.3 Modulus Relationship for the Sections with 176 mm Base Using All Sensors ( $D_0 - D_6$ ).

Section	Relationship	RMSE (%)	RMSE (μm)	Section	Relationship	RMSE (%)	RMSE (μm)
A	$8700\theta^{0.6}$	<b>22.67</b>	8.86	B	$108200\theta^{0.6}$	46.22	5.29
A	$13000\theta^{0.55}$	34.89	9.58	B	$33740\theta^{0.6}$	41.44	3.97
A	$17320\theta^{0.6}$	47.55	11.35	B	$4330\theta^{0.6}$	37.77	3.79
A	$15153\theta^{0.6}$	39.05	10.89	B	$3900\theta^{0.6}$	52.13	6.33
A	$13000\theta^{0.6}$	25.51	10.34	B	$3900\theta^{0.55}$	53.81	8.83
A	$10820\theta^{0.6}$	37.21	9.78	C	$8700\theta^{0.6}$	18.78	5.49
A	$33740\theta^{0.6}$	31.69	8.04	C	$13000\theta^{0.55}$	19.8	6.23
A	$4330\theta^{0.6}$	25.96	4.28	C	$17320\theta^{0.6}$	38.71	7.99
A	$3900\theta^{0.6}$	47.97	4.06	C	$15153\theta^{0.6}$	22.48	7.51
A	$3900\theta^{0.55}$	47.45	4.39	C	$13000\theta^{0.6}$	21.55	6.97
B	$8700\theta^{0.5}$	<b>32.67</b>	4.55	C	$10820\theta^{0.6}$	20.93	6.39
B	$13000\theta^{0.55}$	34.13	5.08	C	$33740\theta^{0.6}$	17.72	4.62
B	$17320\theta^{0.6}$	39.14	2.63	C	$4330\theta^{0.6}$	<b>15.12</b>	1.25
B	$15153\theta^{0.6}$	37.95	6.21	C	$3900\theta^{0.6}$	26.27	3.16
B	$13000\theta^{0.6}$	36.45	5.74	C	$3900\theta^{0.55}$	27.62	5.57

**Table 6.4** Modulus Relationship for the Sections with 75 mm Base Using All Sensors ( $D_0 - D_6$ ).

Section	Relationship	RMSE (%)	RMSE ( $\mu\text{m}$ )	Section	Relationship	RMSE (%)	RMSE ( $\mu\text{m}$ )
E	$8700\theta^{0.6}$	19.17	9.14	H	$8700\theta^{0.6}$	29.22	3.48
E	$13000\theta^{0.55}$	20.24	9.83	H	$13000\theta^{0.55}$	33.12	3.81
E	$17320\theta^{0.6}$	21.71	10.32	H	$17320\theta^{0.6}$	35.07	3.57
E	$15153\theta^{0.6}$	21.33	10.21	H	$15153\theta^{0.6}$	34.59	3.53
E	$13000\theta^{0.6}$	20.98	10.1	H	$13000\theta^{0.6}$	34.11	3.48
E	$10820\theta^{0.6}$	20.41	9.97	H	$10820\theta^{0.6}$	33.49	3.45
E	$7304\theta^{0.6}$	19.41	9.32	H	$7304\theta^{0.6}$	32.39	3.44
E	$4330\theta^{0.6}$	17.44	7.92	H	$4330\theta^{0.6}$	<b>44.21</b>	5.63
E	$3900\theta^{0.6}$	22.83	6.73	H	$3900\theta^{0.6}$	44.28	5.88
E	$3900\theta^{0.55}$	22.92	5.67	H	$3900\theta^{0.55}$	46.06	6.78

**Table 6.5** Modulus Relationship for the Sections with 150 mm Base Using All Sensors ( $D_0 - D_6$ ).

Section	Relationship	RMSE (%)	RMSE ( $\mu\text{m}$ )	Section	Relationship	RMSE (%)	RMSE ( $\mu\text{m}$ )
J	$8700\theta^{0.6}$	32.71	5.29	K	$8700\theta^{0.6}$	<b>34.06</b>	6.91
J	$13000\theta^{0.55}$	30.68	3.64	K	$13000\theta^{0.55}$	44.59	6.57
J	$17320\theta^{0.6}$	31.67	2.42	K	$17320\theta^{0.6}$	47.06	8.35
J	$15153\theta^{0.6}$	31.35	2.73	K	$15153\theta^{0.6}$	46.38	9.26
J	$13000\theta^{0.6}$	31.08	3.03	K	$13000\theta^{0.6}$	45.77	8.87
J	$10820\theta^{0.6}$	<b>30.42</b>	3.47	K	$10820\theta^{0.6}$	44.48	8.71
J	$7304\theta^{0.6}$	32.06	4.99	K	$3374\theta^{0.6}$	43.48	6.51
J	$4330\theta^{0.6}$	51.73	9.06	K	$4330\theta^{0.6}$	59.59	7.62
J	$3900\theta^{0.6}$	53.99	10.02	K	$3900\theta^{0.6}$	60.54	7.31
J	$3900\theta^{0.55}$	59.11	12.23	K	$3900\theta^{0.55}$	62.5	6.71
L	$8700\theta^{0.5}$	34.87	6.35	L	$10820\theta^{0.6}$	34.5	7.83
L	$13000\theta^{0.55}$	34.67	7.11	L	$3374\theta^{0.6}$	34.81	6.43
L	$17320\theta^{0.6}$	33.84	7.83	L	$4330\theta^{0.6}$	<b>27.39</b>	5.15
L	$15153\theta^{0.6}$	33.93	7.59	L	$3900\theta^{0.6}$	27.73	5.74
L	$13000\theta^{0.6}$	34.15	7.41	L	$3900\theta^{0.55}$	28.8	5.67

The nonlinear relationship shown in Table 6.3 for the 176 mm base layer (Sections A, B, and C) shows  $M_R = 4330\theta^{0.6}$  and  $M_R = 8700\theta^{0.6}$  give the lowest RMSE. For Sections E and H (75 mm base layer) shown in Table 6.4, the relationship  $M_R = 4330\theta^{0.6}$  and  $8700\theta^{0.6}$  give the lowest RMSE, respectively. For Sections J, K, and L (the 150 mm base layer) shown in Table 6.5, the following relationships give the lowest RMSE,  $M_R = 10820\theta^{0.6}$ ,  $8700\theta^{0.6}$ , and  $4330\theta^{0.6}$ , respectively.

Since a detailed analysis of the deflection plots showed that, in most of the cases significant differences occurred at the first sensor ( $D_0$ ) between the measured and computed deflections of the nonlinear relationships, the differences were reanalyzed with deflection values using all sensors except the first one. Results are shown in Tables 6.6, through 6.8.

**Table 6.6** Modulus Relationship for the Sections with 176 mm Base Using Sensors  $D_1$  through  $D_6$ .

Section	Relationship	RMSE (%)	RMSE ( $\mu\text{m}$ )	Section	Relationship	RMSE (%)	RMSE ( $\mu\text{m}$ )
A	$8700\theta^{0.6}$	<b>21.01</b>	7.25	C	$8700\theta^{0.6}$	<b>22.21</b>	5.28
A	$13000\theta^{0.55}$	32.38	8.22	C	$13000\theta^{0.55}$	33.43	5.21
A	$17320\theta^{0.6}$	44.78	9.22	C	$17320\theta^{0.6}$	48.28	7.99
A	$15153\theta^{0.6}$	36.04	9.45	C	$15153\theta^{0.6}$	36.27	7.52
A	$13000\theta^{0.6}$	34.74	8.35	C	$13000\theta^{0.6}$	35.27	6.96
A	$10820\theta^{0.6}$	37.74	7.25	C	$10820\theta^{0.6}$	35.49	6.39
A	$3374\theta^{0.6}$	29.87	8.04	C	$3374\theta^{0.6}$	31.2	4.62
A	$4330\theta^{0.6}$	46.94	3.58	C	$4330\theta^{0.6}$	49.92	6.48
A	$3900\theta^{0.6}$	46.65	3.57	C	$3900\theta^{0.6}$	49.84	7.52
A	$3900\theta^{0.55}$	45.84	3.93	C	$3900\theta^{0.55}$	50.09	7.68
B	$8700\theta^{0.5}$	11.96	3.49	B	$10820\theta^{0.6}$	12.21	2.95
B	$13000\theta^{0.55}$	16.29	2.79	B	$3374\theta^{0.6}$	12.68	3.87
B	$17320\theta^{0.6}$	25.87	2.27	B	$4330\theta^{0.6}$	13.09	3.95
B	$15153\theta^{0.6}$	12.83	2.16	B	$3900\theta^{0.6}$	24.85	5.27
B	$13000\theta^{0.6}$	12.44	2.01	B	$3900\theta^{0.55}$	24.76	5.29

**Table 6.7** Modulus Relationship for the Sections with 75 mm Base Using Sensors  $D_1$  through  $D_6$ .

Section	Relationship	RMSE (%)	RMSE ( $\mu\text{m}$ )	Section	Relationship	RMSE (%)	RMSE ( $\mu\text{m}$ )
E	$8700\theta^{0.6}$	11.75	8.41	H	$8700\theta^{0.6}$	<b>21.3</b>	3.04
E	$13000\theta^{0.55}$	12.03	8.14	H	$13000\theta^{0.55}$	29.7	3.81
E	$17320\theta^{0.6}$	13.39	8.98	H	$17320\theta^{0.6}$	29.0	3.26
E	$15153\theta^{0.6}$	13.03	8.57	H	$15153\theta^{0.6}$	29.0	3.37
E	$13000\theta^{0.6}$	12.71	9.16	H	$13000\theta^{0.6}$	29.2	3.03
E	$10820\theta^{0.6}$	12.24	9.49	H	$10820\theta^{0.6}$	29.4	3.24
E	$7304\theta^{0.6}$	11.76	8.53	H	$7304\theta^{0.6}$	30.2	3.25
E	$4330\theta^{0.6}$	19.47	5.53	H	$4330\theta^{0.6}$	25.3	3.41
E	$3900\theta^{0.6}$	19.32	4.31	H	$3900\theta^{0.6}$	25.3	3.24
E	$3900\theta^{0.55}$	19.19	4.71	H	$3900\theta^{0.55}$	25.1	3.16

**Table 6.8** Modulus Relationship for the Sections with 150 mm Base Using Sensors D<sub>1</sub> through D<sub>6</sub>.

Section	Relationship	RMSE (%)	RMSE (μm)	Section	Relationship	RMSE (%)	RMSE (μm)
J	$87000^{0.6}$	<b>26.9</b>	5.19	K	$87000^{0.6}$	32.4	6.88
J	$130000^{0.55}$	28.6	3.43	K	$130000^{0.55}$	34.5	5.40
J	$173200^{0.6}$	28.7	2.33	K	$173200^{0.6}$	40.1	7.11
J	$151530^{0.6}$	29.3	2.65	K	$151530^{0.6}$	36.4	8.24
J	$130000^{0.6}$	28.5	2.98	K	$130000^{0.6}$	42.2	7.29
J	$108200^{0.6}$	30.4	3.34	K	$108200^{0.6}$	34.5	7.35
J	$73040^{0.6}$	28.0	4.89	K	$33740^{0.6}$	38.4	5.22
J	$43300^{0.6}$	38.7	8.21	K	$43300^{0.6}$	52.6	5.13
J	$39000^{0.6}$	49.7	8.04	K	$39000^{0.6}$	52.4	5.11
J	$39000^{0.55}$	52.1	9.33	K	$39000^{0.55}$	55.9	5.34
L	$87000^{0.5}$	34.5	5.88	L	$108200^{0.6}$	25.3	5.74
L	$130000^{0.55}$	33.5	5.78	L	$33740^{0.6}$	34.3	5.85
L	$173200^{0.6}$	31.7	5.55	L	$43300^{0.6}$	27.2	4.69
L	$151530^{0.6}$	32.1	5.58	L	$39000^{0.6}$	27.3	4.68
L	$130000^{0.6}$	32.6	5.64	L	$39000^{0.55}$	28.1	4.44

The resilient modulus-bulk stress relationships for all the sections that have the best RMSE values are marked as “bold” in Tables 6.6 through 6.8. The second type of analysis, without the center deflections, produced lower RMSE values and a more consistent value of  $M_R=87000^{0.6}$  for the granular 21-B layer regardless of the thickness. Hence, it is possible to assume that the nonlinear relationship is not highly affected by the thickness of the granular material layer. The RMSE results for Sections E and H (the 76 mm base layer) are ranging from 11 to 35%. A comparison between the field backcalculated moduli (from the KENLAYER software) and laboratory resilient moduli of the 21-B layer is presented in Figure 6.11. The three dominant field relationships shown by the plots are  $M_R = 43300^{0.6}$ ,  $87000^{0.6}$ ,  $108200^{0.6}$ , represented as Field 2, Field 1, and Field 3, respectively.

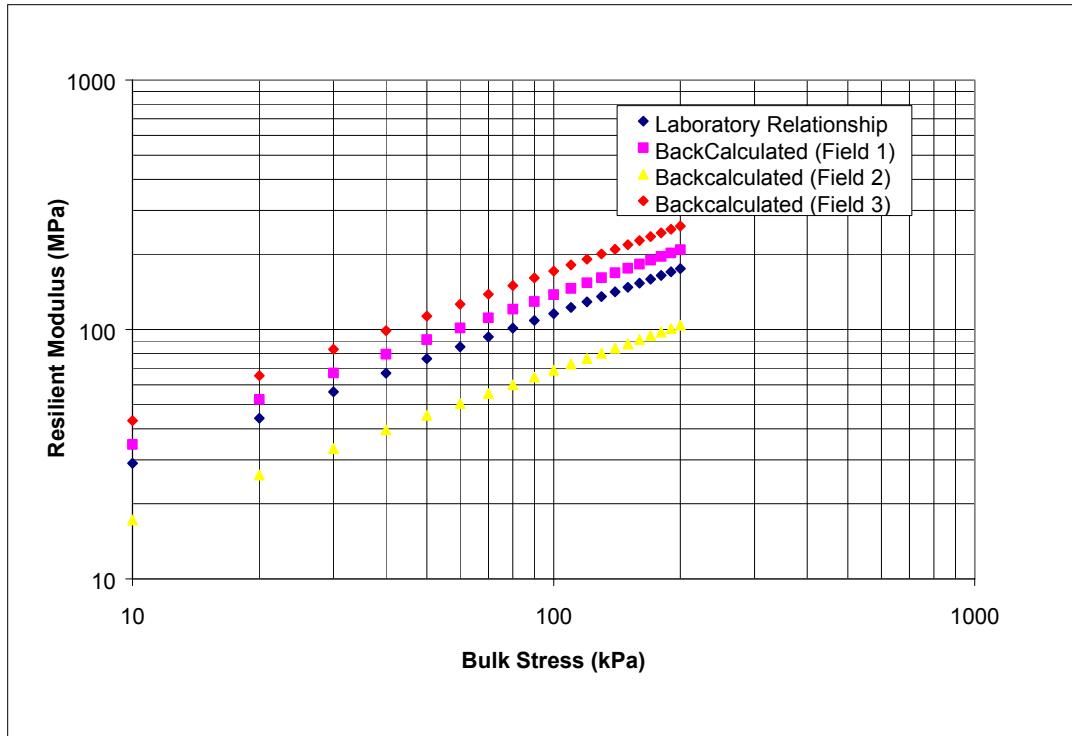


**Figure 6.11** Comparison between Laboratory Tested 21-B and Backcalculated Moduli for All Test Sections

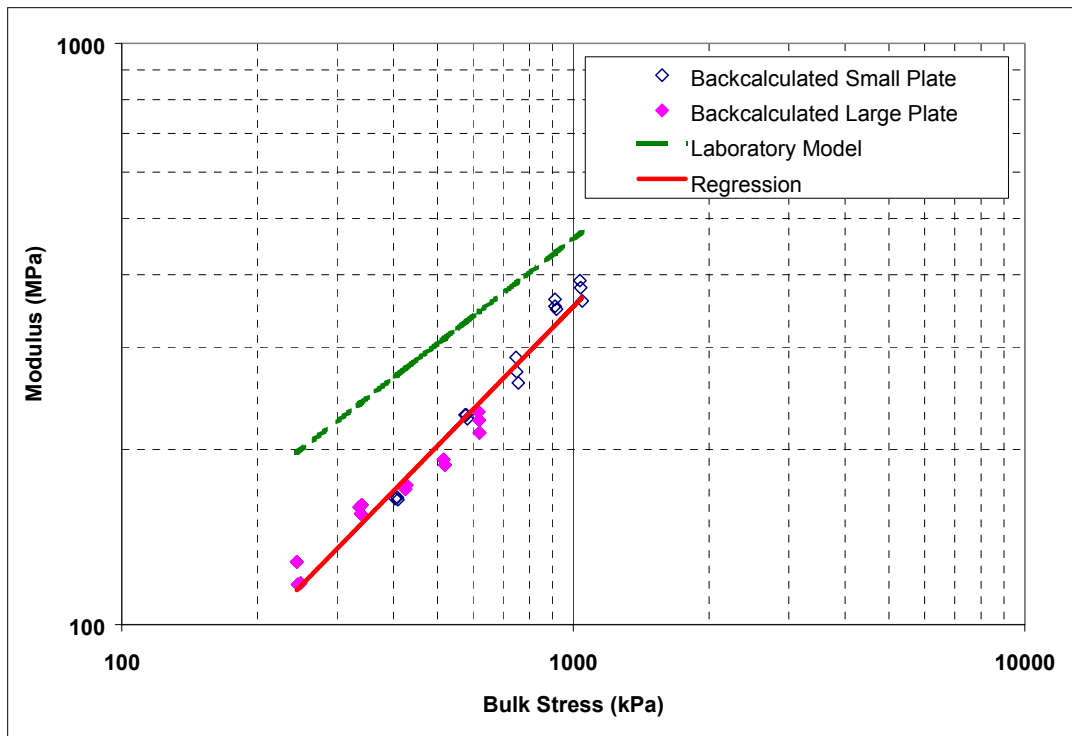


**Figure 6.12** Backcalculated Moduli Using EVERCAL as a Function of the Bulk Stress in the Center of the Layer.

Since the laboratory results indicated stress dependency in the unbound granular subbase, the deflections measured with both plates for one of the sections, Section C, were also analyzed using a backcalculation software package, EVERCAL 5.0. This software which uses a linear elastic forward computation model, has been proven to produce results close to those produced by WESDEF (Van Deusen, 1996). This package computes not only the moduli for the various loads, but also the bulk stress in the center of the subbase layer (under the center of the load). The relationship between the backcalculated layer moduli and the bulk stress in the center of the layer is presented in Figure 6.12. This confirms that in situ modulus is stress dependent. The relationships between the field obtained and laboratory results with bulk stress are different; however strongly correlated (Figure 6.13).

The backcalculated moduli represent an average for the layer; however the stress at the center of the layer is not the average stress in the area influenced by the load applied by the FWD test. In spite of the lack of agreement, these moduli are strongly correlated, as Figure 6.13 shows. Lack of agreement also results from the fact that a compressive stress condition is used in the triaxial test. In the field, materials are subjected to bending. Directly under the load, the bulk stress and confining stress near the bottom of the layers can become tensile.

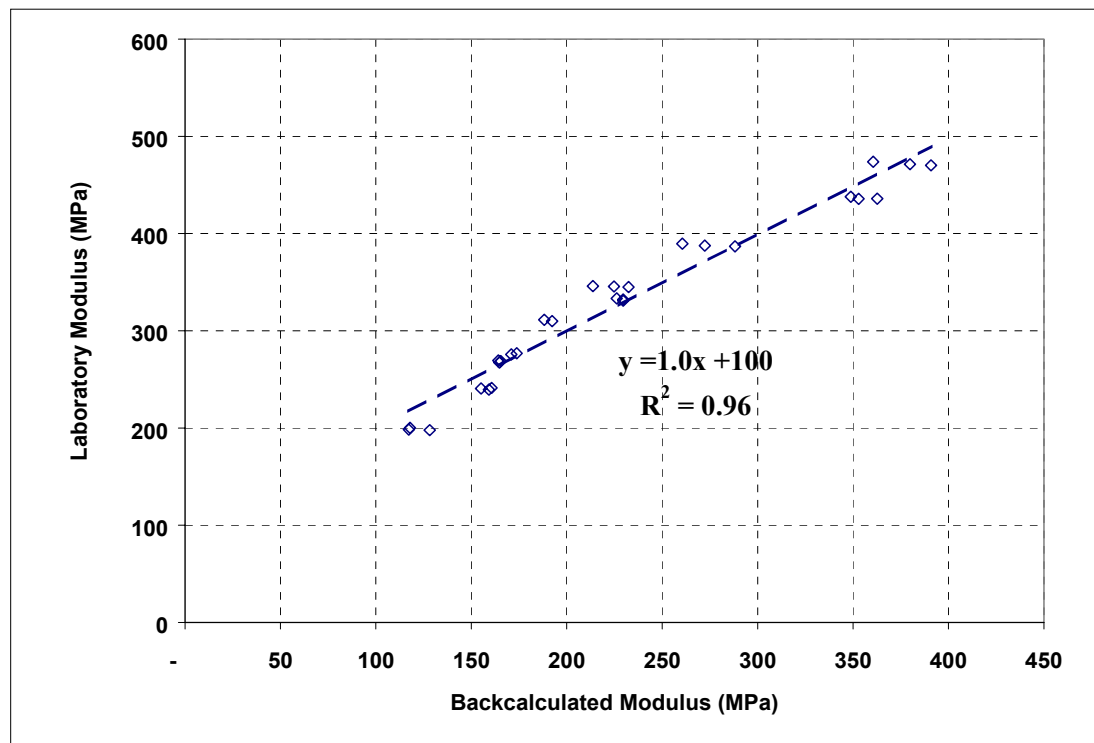


Figure 6.13. Laboratory - Backcalculated (using EVERCAL) Moduli Comparison.

#### **6.4 COMPARISON BETWEEN LABORATORY AND FIELD RESILIENT MODULUS OF HMA**

Von Quintas and Killingsworth (1998) have presented detailed results of comparison between laboratory and in situ moduli from the Long Term Pavement Performance (LTPP) database. The results show adjustment factors or correction ratios between indirect tensile resilient moduli and backcalculated elastic moduli for dense graded HMA wearing surface at different temperatures. In their comparison, they used temperatures measured at the mid-depth of the HMA layer. Zhou (1991) has also presented some comparisons of backcalculated and laboratory measured HMA moduli. He reported that show that backcalculated in situ moduli were generally lower than those determined in laboratory. The differences ranged from 20 to 30%.

The resilient modulus of the HMA wearing surface cores taken from the Virginia Smart Road was measured in the laboratory by means of the repeated-load indirect tensile test. This test, for determining the resilient modulus of HMA, is conducted by applying a haversine, or other suitable wave form, compressive loads. The load is applied vertically in the vertical diametrical plane of a cylindrical specimen. A haversine load of 0.1 sec loading time is applied during all testing with a rest period of 0.9 sec. The test was carried out at three test temperatures, 5 °C, 25 °C and 40 °C. The resulting horizontal and vertical deformations of the specimen is measured and used to calculate the Poisson's ratio. The Roque and Buttlar's method (1992) was used to determine the  $M_R$  and  $\nu$  (resilient moduli and Poisson's ratio). The wearing surface and BM-25.0 layers were made up of different mixes with different SuperPave binders shown in Tables 6.9 and 6.10.

During the field FWD testing, the temperature of the wearing surface and BM-25.0 layer were recorded by means of thermocouples installed at the bottom of the wearing surface. The average temperatures of approximately 5, 25 and 40 °C were recorded for testing done in February 2001, August 2000 and May 2001, respectively. The backcalculated resilient moduli for the first eight sections, A through H, were determined by means of the four backcalculation software, ELMOD44, PEDMOD, MICHBACK and EVERCALC Ver. 5.0. Procedures for performing the backcalculation to produce reasonable values were devised. A standard RMSE per sensor of 25% for the resulting resilient moduli was the limit set for achieving a logical engineering end result. This limit was used by the Strategic Highway Research Program (SHRP) layer moduli backcalculation procedure (Rada *et al.* 1994).

The moduli obtained for laboratory testing of the BM-25.0 layer with the results

**Table 6.9** Mix Properties for HMA (wearing surface) for Sections A through H.

		<b>Section A</b>	<b>Section B</b>	<b>Section C</b>	<b>Section D</b>	<b>Section E</b>	<b>Section F</b>	<b>Section G</b>	<b>Section H</b>
Mix Type		SM-12.5D	SM-9.5D	SM-9.5E	SM-9.5A	SM-9.5D	SM-9.5D	SM-9.5D	SM-9.5D
Binder Grade		PG 70-22	PG 70-22	PG 76-22	PG 64-22	PG 70-22	PG 70-22	PG 70-22	PG 70-22
AC %		5.9	4.7	5.8	6.3	5.9	5.9	5.9	5.9
VTM		5.8	8.6	6.0	1.9	4.8	4.8	4.8	5.8
VMA		18.0	17.1	18.1	15.5	16.2	16.2	16.2	17.3
VFA		68	50	67	88	70	70	70	66
G <sub>mm</sub>		2.422	2.450	2.455	2.440	2.434	2.434	2.434	2.434
G <sub>mb</sub>		2.282	2.239	2.309	2.393	2.317	2.317	2.317	2.292
Sieve Size (mm)	37.5								
	25								
	19	100.0							
	12.5	99.6	98.5	98.0	99.3	97.6	99.4	98.4	98.3
	9.5	98.5	90.3	90.9	92.4	92.9	93.4	95.1	94.3
	4.75	84.2	51.9	55.3	54.9	63.3	56.7	62.3	63.8
	2.36	47.7	35.4	34.3	34.8	42.6	38.6	42.2	43.1
	1.18	37.3	26.7	27.0	25.7	31.5	25.7	28.9	29.3
	0.6	27.0	18.1	19.7	20.4	20.5	18.4	20.9	20.9
	0.3	14.7	11.9	14.1	15.3	13.3	12.1	13.8	13.5
	0.15	10.2	9.4	11.1	11.8	10.4	8.7	10.3	9.6
0.075	5.6	7.8	8.0	9.2	7.6	6.9	8.3	7.6	

**Table 6.10** Mix Properties for HMA Wearing Surface and BM 25.0 Layers for Sections A through H.

	<b>Section I</b>	<b>Section J</b>	<b>Section L</b>	<b>Section A-D</b>	<b>Section E- H</b>	<b>Section I-L</b>
Mix Type	SM-9.5A*	SM-9.5D	SMA-12.5	BM-25.0	BM-25.0	BM-25.0
Binder Grade	PG 64-22	PG 70-22	PG 76-22	PG 64-22	PG 64-22	PG 64-22
AC %	5.4	4.9	6.8	4.5	3.9	5.1
VTM	4.7	10.6	7.3	1.6	3.2	2.7
VMA	16.0	19.7	21.1	12.3	12.3	14.6
VFA	71	46	65	87	74	82
G <sub>mm</sub>	2.467	2.518	2.402	2.596	2.623	2.589
G <sub>mb</sub>	2.350	2.252	2.226	2.554	2.538	2.519
Sieve Size (mm)				100.0	100.0	100.0
				88.8	82.2	97.6
			100.0	75.5	65.9	89.9
	100.0	99.2	99.4	61.6	50.4	76.3
	95.0	91.6	87.7	54.4	44.1	67.7
	51.8	50.5	36.8	45.1	32.4	47.6
	35.0	34.6	25.0	33.9	24.6	32.8
	35.0	34.6	21.4	24.5	19.5	24.5
	20.6	17.9	18.9	18.2	8.7	18.7
	13.9	11.8	16.1	11.7	4.3	11.7
	13.9	11.8	13.9	8.2	2.1	8.2
7.3	6.3	11.2	6.3	0.8	6.5	

**Table 6.11** Laboratory Measured HMA Resilient Modulus (MPa) of Field Cores.

SAMPLE ID	Temperature (°C)		
	5	25	40
A*	9558	3882	2029
B*	9154	3579	1833
C*	8591	2609	1206
D*	11762	2356	986
E*	9862	3729	N/A
H*	10600	4936	1899
I*	12634	4881	2313
L*	5855	2193	N/A
H <sup>+</sup>	8292	3264	1899
I <sup>+</sup>	14381	4075	1594
A-D <sup>x</sup>	10365	4240	N/A
E-H <sup>x</sup>	8229	3964	1159
I-L <sup>x</sup>	11391	3531	1792

\* Wearing surface (100 mm)

+ Fine base (100 mm)

<sup>x</sup> Base mix (150 mm)

obtained from backcalculation using different software. Analysis of deflection basins from the HMA wearing surface and BM-25.0 layers separately at different temperatures showed it was more appropriate to use one HMA than two separate layers.

At 5 °C the backcalculated moduli using four software were in the range of one to two times those obtained from laboratory testing. The relationship between laboratory-measured and backcalculated resilient moduli is presented in Figure 6.14 for 5 °C. At 25 °C, the backcalculated moduli from the backcalculation were in the range of 1.3 to 2.7 times the values from the laboratory testing. At 40 °C, the moduli from software were two to three times the moduli obtained from testing in the laboratory. Figures 6.14 through 6.16 show the resulting laboratory moduli and field backcalculated moduli for Sections A through H. Table 6.12 summarizes the ratios between the backcalculated moduli and the laboratory-measured moduli.

All software shows that the ratio increases when the temperature increases. MICHBACK gave the greatest ratios, while EVERCALC gave the lowest ratios. The variation of temperature gradients measured from thermocouples in the wearing surface and BM-25.0 layer during FWD testing is shown in Figure 6.17. At different temperatures during the FWD testing, the temperature within the wearing surface decreases by a small amount and remains fairly constant throughout the BM-25.0 layer. Results from Table 6.11 show that at 25 °C the average ratio between the backcalculated moduli and laboratory measured moduli was 1.92. Therefore moduli duration of 0.1 sec (from the laboratory testing duration) resulted in approximately 0.53 the resilient moduli at 0.03 sec load duration at 25 °C (from the FWD pulse load).

**Table 6.12.** Ratio between Backcalculated Resilient Moduli and Laboratory Measured Moduli.

	ELMOD	PEDMOD	EVERCALC	MICHBACK
$E_{FWD}/E_{LAB} (5^{\circ}C)$	1.60	1.38	0.97	2.04
$E_{FWD}/E_{LAB} (25^{\circ}C)$	1.95	1.72	1.35	2.65
$E_{FWD}/E_{LAB} (40^{\circ}C)$	2.35	2.22	2.11	2.80

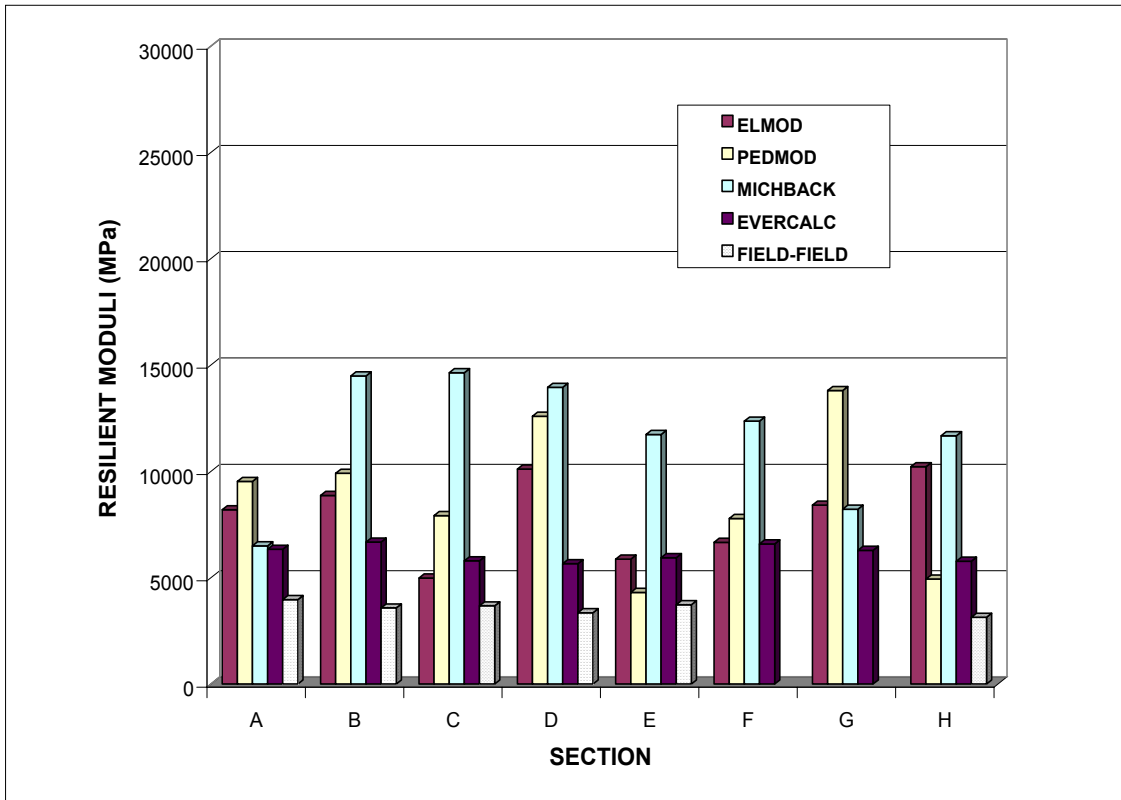


**Figure 6.14** Laboratory Resilient and Backcalculated Moduli at 5 °C.

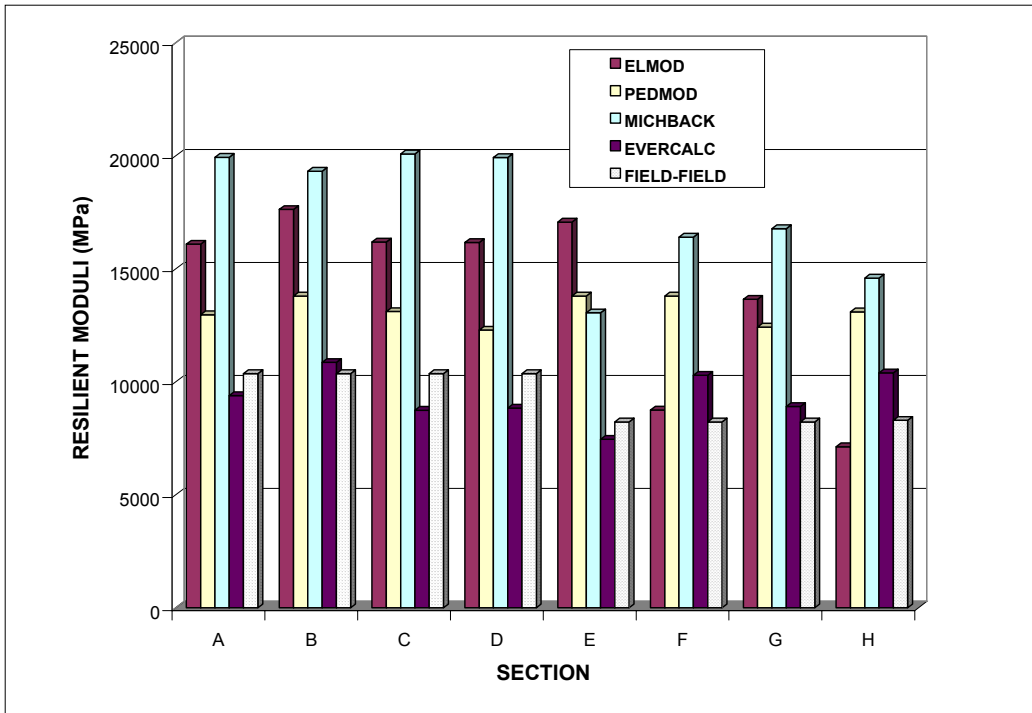


Figure 6.15 Laboratory Resilient and Backcalculated Moduli at 25 °C.

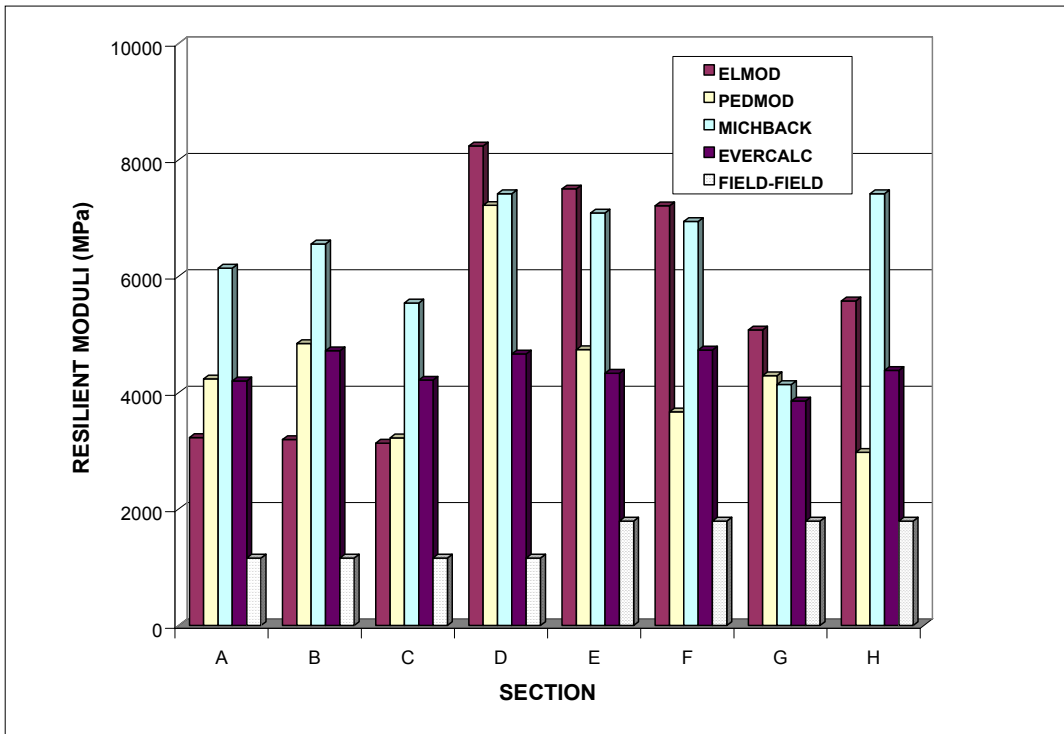
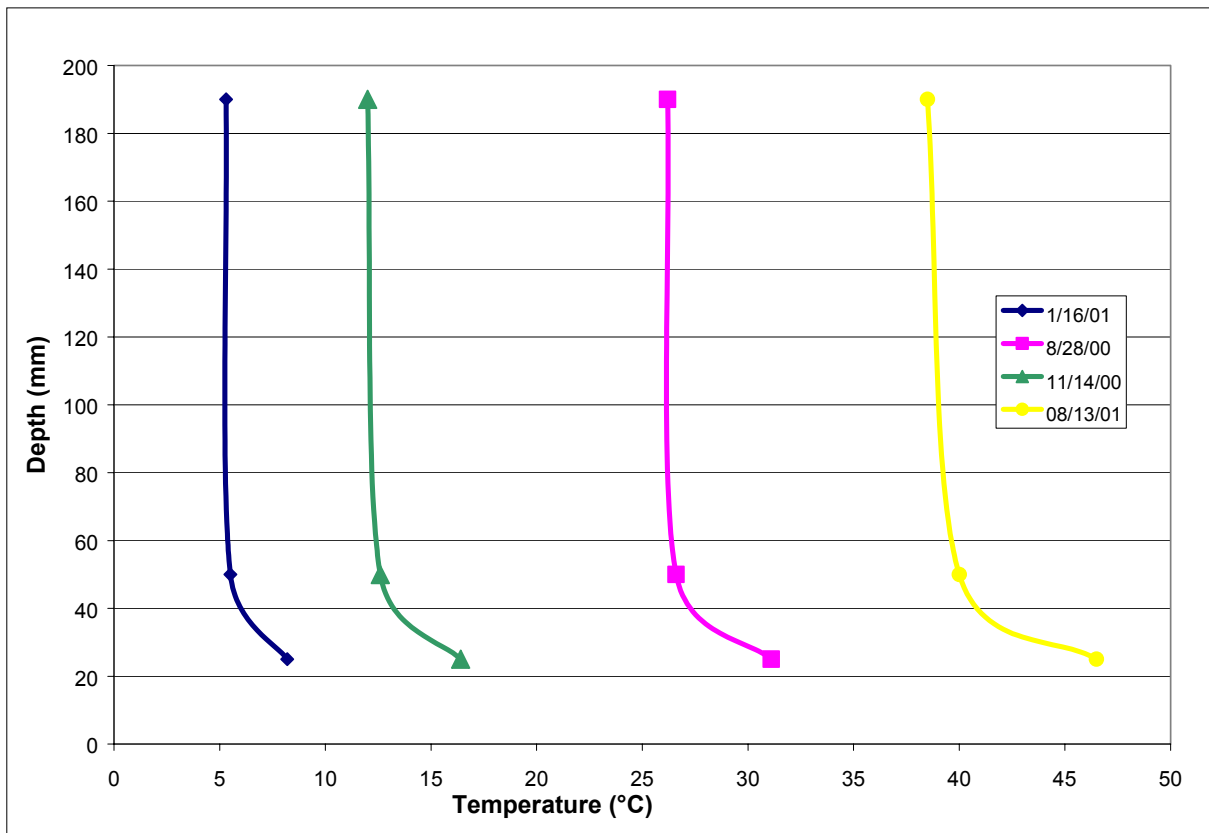


Figure 6.16 Laboratory Resilient and Backcalculated Moduli at 40 °C.



**Figure 6.17** Variation of Temperature with Depth in the Wearing Surface and BM-25.0 Layer for One of the Sections.

## 6.5 SUMMARY AND CONCLUSIONS

The results of the FWD deflection analyses for the unbound granular 21-B subbase layer of the Virginia Smart Road have indicated that the material is stress dependent. The laboratory resilient modulus results confirmed the stress-dependence of the subbase material modulus, whose behavior can be appropriately predicted using a  $k-\theta$  model. The analysis of field backcalculated moduli and laboratory-measured moduli of the granular material show that a correlation between them can be determined, if a representative state of stress is specified.

Comparison between field-backcalculated moduli and laboratory-determined moduli of field cores show that the ratios between the two values of moduli are temperature dependent. The higher the temperature of testing, the greater the adjustment factor. Differences between laboratory and FWD backcalculated moduli could be due to the temperature gradient in the field while temperatures was maintained constant in the testing chamber in the laboratory. The viscoelastic nature of HMA suggests that its response

depends not only on the temperature but also on the duration of applied loading. The average loading time of the FWD pulse load in the field was between 0.03 to 0.04 sec irrespective of temperature. Loulizi *et al* (2002) reported from measurement of vertical compressive stress pulse at the Virginia Smart Road that FWD pulse duration did not vary within the depth of the HMA layer but had tremendous effect on the resilient moduli of the HMA layer. Therefore, a correction factor should be applied to laboratory-measured moduli when compared to FWD determined moduli. Resilient modulus values from the MnRoad project (Baker *et al.* 1994) showed that values obtained from 1s loading duration were approximately 0.6 times the resilient modulus obtained from 0.1s loading duration. Laboratory testing at a duration of 0.03 secs would better simulate the results obtained from FWD testing in the field when comparing laboratory and field resilient moduli results. This could affect the resultant ratio between laboratory-measured and field-backcalculated moduli.

This study concluded that the laboratory-measured field backcalculated resilient moduli are different due to difference in loading mechanism, magnitude, and time. A temperature shift factor that considers these variations should be applied.

## REFERENCES

- Allen, J.J., and Thompson, M.R. (1974). "Resilient Response of Granular Materials Subjected to Time Dependent Lateral Stresses." *Transportation Research Record 510*, National Research Council, Washington, D.C., pp. 1-13.
- Anderson, D.G., and Woods, R.D. (1975). "Comparison of Field and Laboratory Shear Modulus." Proceedings, In Situ Measurement of Soil Properties, ASCE, Vol. 1, Raleigh, N.C.
- Baker, H.B., Buth, M.R., and Van Deusen, D.A. (1994). Minnesota Road Research Project: Load Response Instrumentation Installation and Testing Procedures. Final Report No. MN/PR-94/01, Minnesota Department of Transportation, St Paul, MN.
- Huang, Y. J. (1993). Pavement Analysis and Design. Prentice Hall, Englewood Cliffs, NJ.

Khedr, S. (1985). "Deformation Characteristics of Granular Base Course in Flexible Pavements." *Transportation Research Record 1043*, National Research Council, Washington, D.C., pp 131-138.

Lekarp, F., Ulf, I., and Dawson, A. (2000). "State of the Art. I: Resilient Response of Unbound Aggregates." *Journal of Transportation Engineering*, ASCE, Vol. 126, No. 1, pp. 66-75.

Loulizi, A., Al-Qadi, I.L., Lahouar, S., and Freeman, T. (2002). "Measurement of Vertical Compressive Stress Pulse in Flexible Pavements and Its Representation for Dynamic Loading." Presented at the Transportation Research Board 81st Annual Meetings Paper # 02-2376, Washington, D.C., pp. 1-21.

Nazarian S., Rojas, J., Pezo, R., and Abdallah, I. (1998). "Relating Laboratory and Field Moduli of Texas Base Materials." *Transportation Research Record 1639*, National Research Council, Washington, D.C., pp.1-11.

Roque, R., and Buttlar, W.G. (1992). "Development and Evaluation of The Strategic Highway Research Program Measurement and Analysis System for Indirect Tensile Testing at Low Temperatures." *Transportation Research Record 1043*, National Research Council, Washington, D.C., pp 163-171.

Van Deusen, D. (1996). "Selection of Flexible Backcalculation Software for the Minnesota Road Research Project." Report No. MN/PR - 96/29, Minnesota Department of Transportation, St. Paul, MN.

Von Quintas, H.L., and Killingsworth B.M. (1998). "Comparison of Laboratory and Insitu Determined Elastic Layer Moduli." Presented at the Transportation Research Board 77<sup>th</sup> Annual Meeting, Washington, D.C., pp.1-31.

Uzan, J., (1985). "Characterization of Granular Materials." *Transportation Research Record 1022*, National Research Council, Washington, D.C., pp 52-59.

Witczak, M.W., and Rada, G. (1981). "Comprehensive Evaluation of Laboratory Resilient Moduli Results for Granular Material." *Transportation Research Record 810*, National Research Council, Washington, D.C., pp. 23-33.

## CHAPTER SEVEN

### USING FWD LOADING TO ESTABLISH A COMPARISON BETWEEN IN-SITU MEASURED AND COMPUTED STRESSES AND STRAINS

#### **Abstract**

To compare in-situ measured and computed stresses and strains to establish a measure of accuracy, FWD tests with variable loads were conducted on selected pressure cells and strain gauges between August 2000 and October 2001 at the heavily instrumented Virginia Smart Road. Utilizing the backcalculated moduli, theoretical stresses and strains at the instrument locations were determined using linear-elastic, nonlinear-elastic, and viscoelastic modeling. The calculated stresses compared reasonably well with the field-measured stresses; especially at high temperatures. Computed tensile strains using viscoelastic modeling were found to be comparable to in-situ measured values. The mix properties, temperature of testing, and loading were found to have an effect on the agreement between the measured and computed responses of the strain gages in the wearing surface. Strain gages in surface mix SM-12.5D measured strains that have better agreement with analytical values than the results from SM-9.5D mix. Using a general fatigue damage equation, the number of cycles to failure based on the purely linear elastic case was found to be more than twice the purely viscoelastic case. This difference increases with increasing temperature of the HMA layer.

## 7.1 INTRODUCTION

Over the years, flexible pavement design methods have evolved from purely empirical, based on tests such as Casagrande soil classification, to more rational empirical-mechanistic approaches (Loulizi *et al.* 2001). Full and defensible implementation of mechanistic pavement design methodologies still requires validation of “theoretical” material models versus true performance within a pavement, and a comparison of real pavement performance with design method predictions.

A number of “mechanistic” or “empirical-mechanistic” flexible pavement design methodologies have been developed. They usually rely on fundamental models of vehicular loading, material properties, and structural system response to loading and environmental interaction. The computed pavement responses are then used to predict roughness, rutting, and cracking using empirically determined transfer functions. A more “scientific” approach requires a greater number of material and system parameters to model the pavement system. Such an approach may result in defining the failure mechanisms.

Different analysis approaches are used currently to reach a mechanistic pavement design. These include multilayer elastic analysis, finite element methods, and approximate methods. Pavement materials have been modeled as linear elastic, non-linear elastic, and/or viscoelastic. In the linear elastic approach, all the materials making up the pavement system (hot-mix asphalt [HMA], base, subbase and subgrade) are assumed to be linear, elastic, homogeneous, and isotropic. The modulus of elasticity and Poisson’s ratio of the different pavement materials are needed to characterize the stress-strain relationship. The resilient modulus is defined as the stress dependent ratio of the applied axial stress over the recovered axial strain in a cyclic load triaxial test. At low stress levels, the assumption of linear elasticity may to some extent be adequate in structures, where a bituminous layer constitutes the major structural layer, though it should be emphasized that these assumptions serve only as a rough approximation of pavement response.

In the nonlinear-elastic approach, the behavior of the granular materials and subgrade soils are described by a variety of constitutive equations that depict the change in mechanical properties with the state of stress within the layer (Desai *et al.* 1984 and Chen *et al.* 1990). The elastic moduli of the materials vary with the level of stresses. In general, the resilient modulus of granular materials increases with the

increase in stress intensity while that of fine grained soils decreases with the increase in stress intensity.

In the third modeling approach, the theory of viscoelasticity is applied to multilayer systems and the HMA is treated as a viscoelastic material whose behavior depends on the time of loading and the temperature. The viscoelastic material can be characterized in the laboratory by developing a creep compliance master curve. The elastic-viscoelastic correspondence principle may be used by applying Laplace transform to change a viscoelastic problem into an elastic one.

Creep compliance is defined as follows:

$$D(t) = \frac{\varepsilon(t)}{\sigma} \quad (7.1)$$

where  $\varepsilon(t)$  is the time-dependent strain under a constant stress.

For a generalized model the creep compliance can be expressed as follows (Huang 1993):

$$D(t) = \frac{1}{E_0} \left( 1 + \frac{t}{T_0} \right) + \sum_{i=1}^n \frac{1}{E_i} \left[ 1 - \exp\left( -\frac{t}{T_i} \right) \right] \quad (7.2)$$

where,

$E_0$ ,  $T_0$ ,  $E_i$  and  $T_i$  are viscoelastic constants for a generalized model.

The mechanistic analysis approaches require the knowledge of the mechanical properties of all pavement materials. Material characterization, especially resilient modulus, is normally done in two ways: destructive (laboratory testing of cores) and nondestructive testing. Nondestructive testing uses deflection data generated from a nondestructive testing device, such as FWD, to quantify the response of a pavement structure to known loads. Complete deflection basins are used to estimate in-situ elastic moduli for each pavement layer using a backcalculation approach. The backcalculation procedure involves calculation of theoretical deflections under the applied load using assumed pavement layer moduli. These theoretical deflections are compared to measured deflections, and the assumed moduli are then adjusted in an iterative procedure until the theoretical and measured deflection basins reach an acceptable match.

The backcalculated moduli can be used to calculate stresses and strains in the pavement structure that may be used in distress models to evaluate damage accumulation under traffic and predict pavement failure. They can also be used to evaluate corrective measures, such as overlay thickness.

Accelerated pavement testing may be a useful link between laboratory testing on relatively small samples and the response of in-situ pavements, but they must be interpreted using a theoretical model. Empirical interpretation of results from accelerated pavement testing may lead to values or relationships that cannot be used for real pavements, because the impact of time, ageing, seasonal variations, mixed traffic cannot be ignored.

In recent years, pavement instrumentation has been increasingly used to validate and calibrate the mechanistic design and analysis approaches, such as the ones used for backcalculation of in-situ pavement material moduli. Pavement instrumentation allows for monitoring pavement material performance and quantitatively measuring pavement system response to loading and environment. Ullidtz measured stresses and strains in a homogenous layer and found good agreement between predicted vertical stresses and measured stresses (Ullidtz 1996). However, measurements of stresses and strains were recommended for different loading combinations and materials. Attempts were made by Scullion *et al.* (1989) to verify backcalculation procedures through instrumentation of pavement sections with multi-depth deflectometers (MDD). Some success was achieved with analysis based only on linear elasticity and it was shown that MDD's could provide an excellent tool for validating mechanistic models of pavements under nondestructive testing and truck loading.

In this Chapter, linear and nonlinear elastic and viscoelastic pavement analysis models were examined using field-measured pavement material properties at The Virginia Smart Road (Loulizi *et al.* 2001). The stresses and strains measured by embedded instruments were compared to those computed using the analysis models; the layer resilient moduli used in the models were backcalculated utilizing FWD surface-measured deflections.

## **7.2 FIELD TESTING**

Field testing took place at the Virginia Smart Road, a pavement research facility that has 12 heavily instrumented flexible pavement sections (Figure 7.1). The instruments, including pressure cells, strain gages, thermocouples, moisture sensors, and frost

probes, were embedded during the construction of the road. A Dynatest model 8000 FWD unit was used to monitor the structural capacity of the different pavement systems and materials composing the 12 sections. Several FWD testing schemes were conducted:

Section A	Section B	Section C	Section D	Section E	Section F	Section G	Section H	Section I	Section J	Section K	Section L
SM-12.5D	SM-9.5D	SM-9.5E	SM-9.5A	SM-9.5D	SM-9.5D	SM-9.5D	SM-9.5D	SM-9.5A	SM-9.5D	OGFC SM-9.5D	SMA-12.5
Base BM-25.0 (150mm)	Base BM-25.0 (150mm)	Base BM-25.0 (150mm)	Base BM-25.0 (150mm)	Base BM-25.0 (s25mm)	Base BM-25.0 (150mm)	Base BM-25.0 (100mm) SM-9.5A (50mm)	Base BM-25.0 (100mm) SM-9.5A (50mm)	Base BM-25.0 (100mm) SM-9.5A (50mm)	Base BM-25.0 (s25mm)	Base BM-25.0 (s25mm)	Base BM-25.0 (150mm)
OGDL (75mm)	OGDL (75mm)	OGDL (75mm)	OGDL (75mm)		21-A (CTA) (150mm)	21-A (CTA) (150mm)	OGDL (75mm)	OGDL (75mm)			OGDL (75mm)
21-A (CTA) (150mm)	21-A (CTA) (150mm)	21-A (CTA) (150mm)	21-A (CTA) (150mm)	21-A (CTA) (150mm)			21-A (CTA) (150mm)	21-A (CTA) (150mm)		OGDL (75mm)	OGDL (75mm)
21-B Subbase (180mm)	21-B Subbase (180mm)	21-B Subbase (180mm)	21-B Subbase (180mm)	Subbase 21-B Sub (75mm)	21-B Subbase (150mm)	21-B Subbase (150mm)	Subbase 21-B Sub (75mm)	Subbase 21-B Sub (75mm)	21-B Subbase (150mm)	21-B Subbase (150mm)	Subbase 21-B Sub (75mm)

**BRIDGE**

**Figure 7.1.** Flexible Pavement Design of the Virginia Smart Road.

1. As-Constructed and In-Service Structural Capacity of The Different Layers of The Test Sections: FWD testing was conducted after the construction of each layer. One location in each section, in the center of the traveling lane, approximately 25m from the beginning/end of the section, was selected for testing, and used for each successive layer. The moisture and temperature of the placed layers were measured at the time of testing. Five load levels were used to determine possible nonlinear behavior of the materials.
2. Periodical Monitoring: FWD testing has been conducted bi-monthly on the selected locations after the completion of construction to investigate the effect of seasonal variation on the layer moduli.

3. Structural Capacity Survey: FWD testing has been conducted every 10m on both the instrumented and non-instrumented lanes of each section to assess the within-section variability.

4. Instrument Responses to FWD Loading: FWD testing was carried out on three sections on top of pressure cells and strain gages on four different occasions: August and November, 2000 and April and May, 2001. Loads of 31, 40, 49, 58 kN were used.

### **7.3 INSTRUMENT DESCRIPTION**

The instruments, including pressure cells, the strain gages, thermocouples, moisture sensors, and frost probes, were embedded during construction of the Virginia Smart Road (Loulizi *et al.* 2001). The pressure cells consists of two circular stainless steel plates welded together with the space between them filled with incompressible fluid. A 6-mm stainless steel tube connects the cell to a closed hydraulic transducer. At 204 mm from the plates, the tube was bent at 45° to allow burying the transducer at 50 mm below the plate's level to reduce any disturbance to field measurements. The sensitive plate-side faces downwards to reduce any undesired concentrated stresses due to angular aggregates. The output of the pressure cell is 0-5V, with an excitation of 12V.

Two types of strain gages were considered for the HMA layers, Kyowa and Dyatest. The Kyowa gages were found to be unreliable. The Dynatest H type strain gages consist of an electrical resistance strain gage embedded within a strip of glass-fiber reinforced epoxy surrounded by several protective layers. They had been successfully used in the field on other testing sites, including the Penn State Test track, Mn Roads and Westrack projects, and had a high survivability rate. The sensor (1/4 bridge) has a 120-ohm resistance with a gage factor of 2 and can measure up to 1500 microstrain. Figures 7.2 and 7.3 show the typical pressure cell and strain gages used in the pavement sections.

The embedded thermocouples used to monitor temperature were house-built. They are twisted stranded soldered pair of T-type thermocouple constantat and copper wire. The exposed end was surrounded by 6.4 mm inside-diameter copper tubing. Electrical epoxy grade was used to surround the thermocouple and to serve as a barrier to environmental effects. Two types of moisture measurement instruments were used, CS610 and CS615. CS610 consists of three parallel conducting rods that are 300 mm in

length, with a distance of 22 m separating them. CS615 comprised of two parallel conducting rods that are 300 mm in length with a distance of 22 mm separating them. The frost probes were made from PVC rods with a diameter of 25 mm. The bare copper coils on the gage has to be in actual electrical contact with soil particles over their entire surface area to ensure that a resistivity value is obtained.



**Figure 7.2** Pressure Cell



**Figure 7.3** H-type strain gage

#### **7.4 BACKCALCULATION APPROACHES**

Several backcalculation procedures are currently being used by highway agencies around the world. Most of the software packages estimate layer moduli, unknown layer thickness, and/or depth to a stiff layer (if present). Three backcalculation approaches, which use different forward computation models to predict the pavement response, are evaluated in this Chapter.

The first approach uses numerical integration methods to solve a multi-layer elastic system, such as in BISAR (Peutz *et al.* 1968) and WESLEA (Van Cauwlaert *et al.* 1989), to compute the pavement stresses and strains in the different pavement layers. EVERCALC and PEDMOD, two software packages that use this approach were tested.

These packages use slightly different numerical integration procedures and error minimization schemes, but have been shown to produce comparable results (Van Deusen, D., 1996).

PEDMOD uses WESDEF for the backcalculation of the pavement layer moduli. It uses a multi-layer elastic forward computation model (WESLEA) and conducts an iterative process to select the set of layer moduli that minimizes the percent root-mean square error (RMSE). EVERCALC also uses the forward computation model WESLEA to compute pavement response, but uses the root-mean square error (RMSE) as the convergence criterion. In addition, EVERCALC considers nonlinear stress-dependent granular materials.

In the second approach, the MICHBACK software is used. MICHBACK uses an extended precision version of the CHEVRON elastic program for forward computation, but uses a modified Newton algorithm method (Harichandran *et al.* 1993) to improve the convergence between measured and computed surface deflections. Some of the problems that occurs with most error minimization techniques are the production of several local minima from objective functions that are formulated and the slowness of convergence, because numerous calls are made to mechanistic analysis program.

The third approach uses approximation methods, such as the method of equivalent thickness used in ELMOD (Ullidtz, 1977), to compute the stresses, strains, and deformations in the pavement. Although the approximate methods are considerably faster, in some cases they may result in unacceptable error in the forward computation of the response of the pavement that would be reflected in the computed backcalculated moduli. For example, the method of equivalent thickness may produce erroneous results when the moduli do not vary in a monotonously decreasing way with depth (Ullidtz, 1977). ELMOD uses the Odemark-Boussinesq transformed section approach or the “deflection basin fitting”. The latter is normally used with numerical integration techniques and incorporates nonlinear analysis of the granular layers to improve the fit between measured and calculated deflection basins. A maximum precision is obtained when the structure has only one stiff layer (with modulus five times higher than the subgrade) and the moduli are in decreasing order with depth (ratio of at least two).

For this study, a detailed step-by-step backcalculation procedure was defined in which the modulus of each layer was incrementally computed as the pavement was constructed and is reported in Flinstch *et al.* (2000). The average apparent surface modulus for the last five sensors, using the FWD test conducted on top of the subgrade,

was adopted for the subgrade modulus. Initial (as-constructed) moduli of all pavement layers were determined by using the deflections measured on top of the layer under study and by assuming the moduli computed in previous steps for all of the underlying layers. In cases in which the structure could not be modeled with a percent RSME of less than 25%, the moduli of the existing layers were allowed to float within a range to account for possible moisture and compaction variations, as well as changes due to stress-dependent behavior. Each backcalculation step was conducted several times with different seed values to avoid local minima in the error minimization procedure. The set of moduli that resulted in the model with the lowest RMSE was selected in each case.

The subbase (21-B) was combined with the subgrade in those sections where the thickness of the 21-B layer was less or equal to 75 mm, i.e., Sections E and H. The backcalculation method estimated unreasonably high moduli in these cases. Since the FWD measurements on top of the cement-treated aggregate base (21-A) were conducted just a few days after construction in some cases, the modulus of the 21-A was adjusted to account for increased cement hydration in the analysis of the subsequent pavement layers. The wearing surface and BM-25.0 layers were also combined in the analyses, since the thickness of the wearing surface was only 38 mm. The moduli of the HMA layers were determined at different temperatures utilizing deflections measured during different environmental conditions.

Since asphalt is a viscoelastic material whose behavior depends on the temperature testing and duration of loading, it was necessary to correct the moduli to a standard temperature (25 °C) for experimental purposes. Using moduli backcalculated for all the testing periods on the wearing surface from January, 2000 to December, 2001, (nine testing periods in all), temperature correction models were developed for each backcalculation program. An overall temperature model was also developed using moduli from all four backcalculation programs combined. The average pavement temperature for each test was determined as an average of the values measured by thermocouples installed at the top and bottom of the BM-25.0 layer and at the bottom of the wearing surface layer. Using the backcalculated moduli during different seasons and the average temperature of the HMA layers during testing for all sections, the regression equation was fitted to the data to determine and adjust the modulus to a base temperature of 25 °C. The average pavement temperature for each test was determined as an average of the values measured by the thermocouples at the bottom of the

wearing surface. The moduli backcalculated for all the seasonal monitoring tests (nine tests over the finished pavement) from January 2000 to December 2001 were used in the analysis. It appears the model is similar to models presented by other researchers (Kim *et al.* 1994; and Baltzer *et al.* 1994). The following is the resulting equation:

$$E_T = E_0 e^{-0.031(T-25)} \quad (7.3)$$

where,

$E_T$  = HMA modulus (MPa) at a specific temperature ( $^{\circ}\text{C}$ );

$E_0$  = HMA modulus (MPa) at the reference temperature ( $25^{\circ}\text{C}$ ); and

$T$  = Average temperature of the BM-25.0 layer during FWD measurement ( $^{\circ}\text{C}$ ).

The temperature correction model depicted in Figure 7.4, has a coefficient of determination,  $R^2 = 0.767$ , and an RMSE of 0.27. This temperature correction model is based on a wider range of temperatures than the one presented by Flintsch *et al.* (2000).

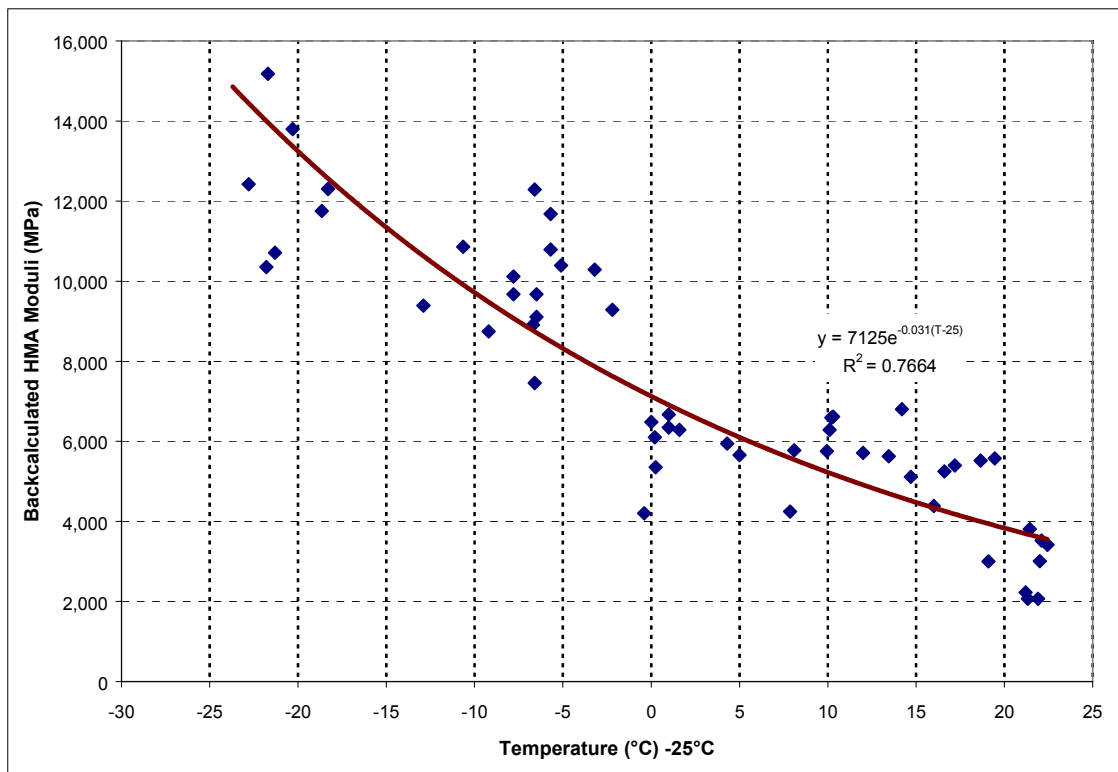


**Figure 7.4** Temperature Correction Model.

The backcalculated moduli were used as input in the KENLAYER software to determine stresses and strains at selected depths of interest. KENLAYER is layered elastic analysis software that considers nonlinearity in the granular layers and variable friction between the layers. It allows the HMA to be considered as viscoelastic. The

KENLAYER software is based on Burmister layered theory and can handle up to 19 layers.

## 7.5 PAVEMENT MODELING

The studied test sections were modeled using KENLAYER. The main models considered were linear elastic and nonlinear for granular materials. For the linear elastic analysis model, all of the layers including granular layers, were assumed to be linear elastic with constant corresponding backcalculated resilient moduli. The theoretical stresses and strains at the instrument location due to FWD loading were calculated using the linear elastic model.

The theoretical stresses, tangential strain, and deflections incorporated in the KENLAYER software are based on multilayer systems under a circular loaded area, and, as in the classical theory of elasticity, has a stress function  $\phi$  that satisfies the governing differential equation.

$\nabla^4\phi = 0$  is assumed for each of the layers and is given below.

$$\sigma_z = \frac{\partial}{\partial z} \left[ (2-\nu)\nabla^2\phi - \frac{\partial^2\phi}{\partial z^2} \right] \quad (7.4)$$

$$\sigma_r = \frac{\partial}{\partial z} \left[ \nu\nabla^2\phi - \frac{\partial^2\phi}{\partial r^2} \right] \quad (7.5)$$

$$\sigma_t = \frac{\partial}{\partial z} \left[ \nu\nabla^2\phi - \frac{1}{r} \frac{\partial^2\phi}{\partial r^2} \right] \quad (7.6)$$

$$\tau_{rz} = \frac{\partial}{\partial r} \left[ (1-\nu)\nabla^2\phi - \frac{\partial^2\phi}{\partial z^2} \right] \quad (7.7)$$

$$w = \frac{1+\nu}{E} \left[ (1-2\nu)\nabla^2\phi + \frac{\partial^2\phi}{\partial r^2} + \frac{1}{r} \frac{\partial^2\phi}{\partial r} \right] \quad (7.8)$$

$$u = -\frac{1+\nu}{E} \left( \frac{\partial^2 \phi}{\partial r \partial z} \right) \quad (7.9)$$

Since most granular materials and subgrade soils exhibit nonlinear behavior as the resilient modulus varies with the level of stress, the granular subbase was treated as nonlinear in the second model analyzed. Mathematical procedures for describing the stress dependence of the resilient modulus, using various stress variables had been formulated (Hicks and Monismith, 1971; Allen and Thompson 1974). Constitutive equations relating the resilient modulus and the first stress invariant, was used in this study. Several constitutive equations were suggested to describe the stress-dependency behavior of the granular materials resilient moduli (Hicks *et al.* 1970; Uzan *et al.* 1985; Witczak and Rada, 1981):

$$M_r = k_1 \theta^{k_2} \quad (7.10)$$

$$M_r = k_3 \theta^{k_4} \sigma_d^{k_5} \quad (7.11)$$

$$\text{Log}_{10} M_r = C_0 + C_1 \cdot S_r + C_2 \cdot \text{PC} + C_3 \cdot \text{Log}_{10} \theta \quad (7.12)$$

where,

$\theta$  = bulk stress or first stress invariant;

$k_1, k_2, k_3, k_4,$  and  $k_5$  = regressions parameters;

$\sigma_d$  = deviator stress;

$S_r$  = degree of saturation (%);

PC = modified relative compaction (%); and

$C_0, C_1, C_2$  and  $C_3$  = regressions parameters determined using regression analysis.

The models in equations 7.10 through 7.12 were considered for the granular subbase material (21-B). Laboratory tests conducted on lab-compacted samples extracted during construction indicated that the model given by equation 7.13 approximately fit the laboratory results and presented in Flintsch *et al.* (2003). The average regression coefficients obtained for this particular material resulted in the following model:

$$M_r = 7304 \theta^{0.6} \quad (7.13)$$

Hence, an average modulus for the granular subbase layer was determined by successive approximations, as proposed by Huang (1968). Laboratory results indicated that the granular subbase showed stress-dependency. Therefore, the FWD field-measured deflections from both plates (300 and 450 mm in diameter) for one of the sections were analyzed using the EVERCALC software. The relationship between the backcalculated moduli and the bulk stresses in the center of the layer is presented in Figure 7.5. It appears that stress dependency also exists in the field. The nonlinear relationship obtained from the laboratory testing results was used in the study.

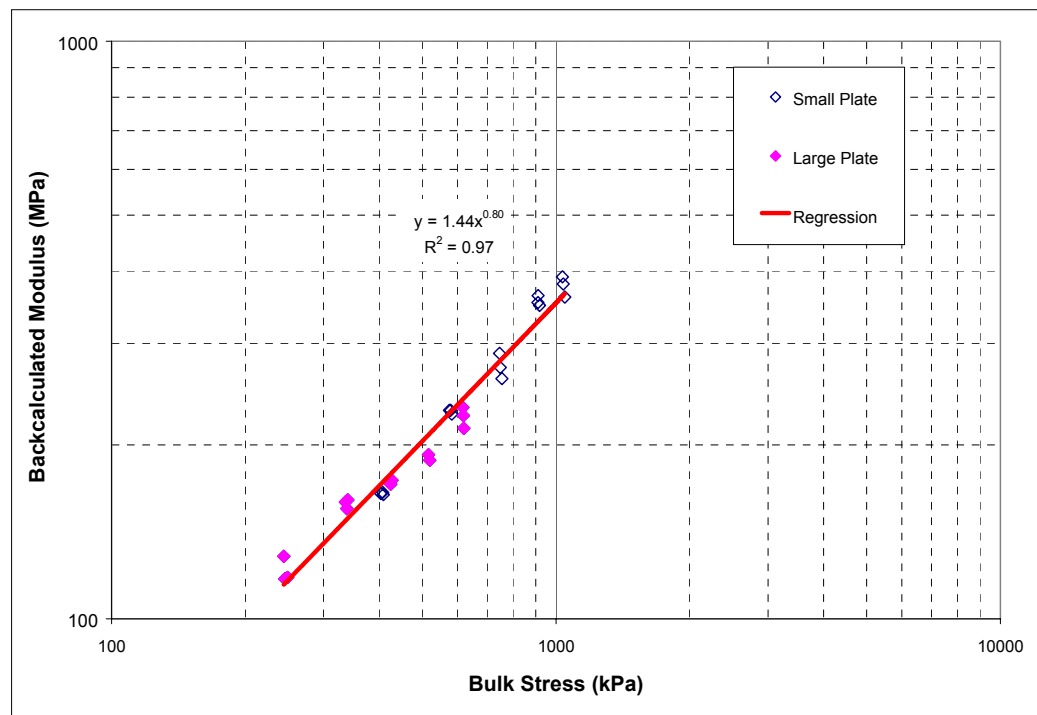


**Figure 7.5** Backcalculated Moduli Using EVERCALC as a Function of the Bulk Stress in the Center of the Layer.

## 7.6 INSTRUMENT RESPONSE AND DATA ANALYSES

The response of the instruments to FWD loading was recorded together with the moisture of the granular layers and the temperature of the HMA layers. A data acquisition software (Smart software) developed at Virginia Tech was used to capture the load response versus time from the pressure cells and strain gauges. Typical examples of the FWD loading of a pressure cell, (AP2-1, located at the bottom of the BM 25.0 layer in Section A) and a strain gauge (DSH1-2L, located at the bottom of the wearing surface in Section D) are shown in Figures 7.6 and 7.7, respectively. Nasser *et al.*(2000) have reported on the use of five FWD loads to determine the pressure

distribution under the BM-25.0 layer on the Virginia Smart Road. The pressure cells produced responses during all tests, but the strain gauges showed responses only when the temperatures were above 20 °C. The triggering value for strains was 20  $\mu$ sec.

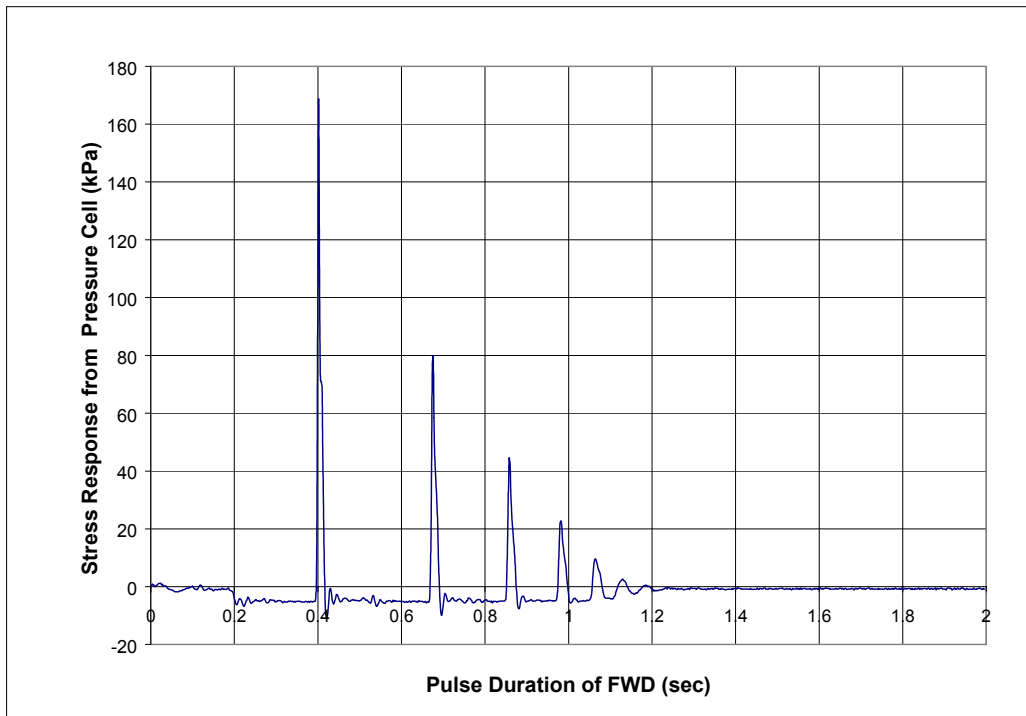


**Figure 7.6** Compressive Stress Response of Pressure Cell AP2-1 from FWD Loading Testing.

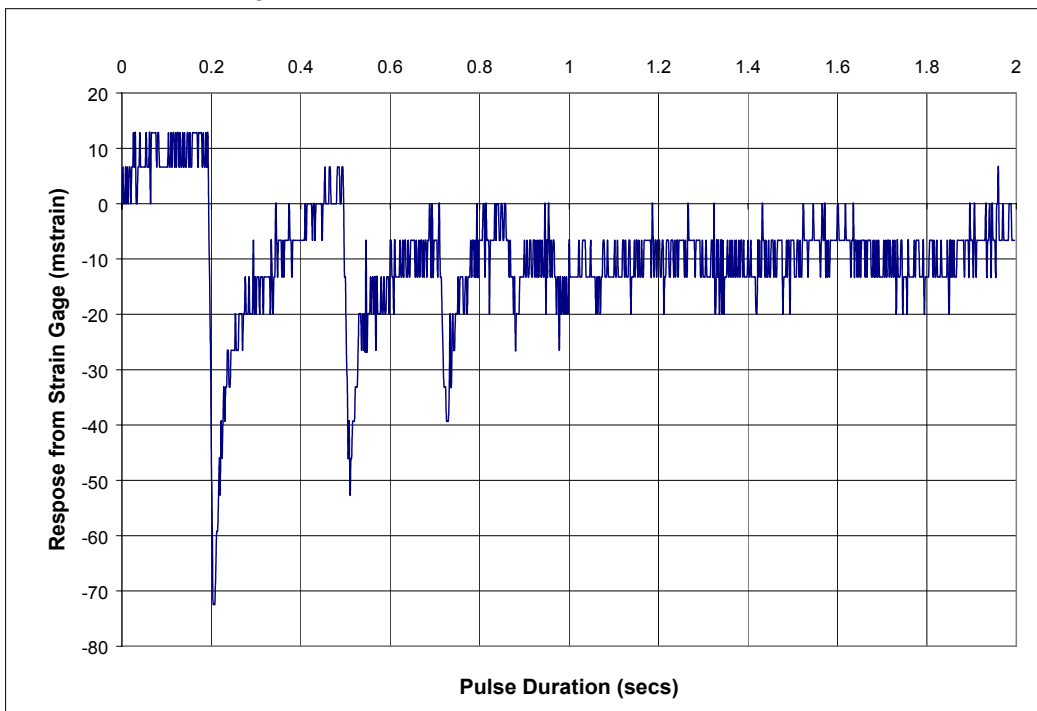


**Figure 7.7** Tensile Strain Response of Strain Gauge DSH1-2L during FWD Testing.

FWD load drops of 31, 40, 49, and 58 kN were applied on selected pressure cells and strain gauges to measure the stresses and strains induced by the loads. The pressure cells selected for the analysis were AP2-1, AP5-3, AP7-2, BP4-2, BP5-3, DP1-2, DP4-1, EP2-2, FP2-2, FP5-3, GP2-2, and HP4-1. The strain gauges selected were ASH1-4L, DSH1-2L, and GSH 2-3L. A labeling system was used to identify each instrument. The first letter refers to the section in which the instrument is placed; the second letter identifies the instrument type (e.g. P- pressure cell, SH- Dynatest strain gage); the first number identifies the layer number where the instrument is placed (e.g. 1 is wearing surface, 2 is HMA base); and the second number identifies the instrument number in that layer, the letter that appears with the second number shows the orientation of the placement of the strain gage.

#### **7.6.1 Analysis of the Pressure Response Data**

The pavement models were first evaluated by comparing the theoretical stresses to the actual stresses recorded by the pressure cells in the pavement layer during the FWD testing. The stresses at the instrument depth were determined in each case using KENLAYER. Figures 7.8 through 7.10 show the stress results at six selected instrument along the depth of the pavement in January, 2001 and August, 2000. The average temperatures in the layers were 12 °C and 28 °C, respectively. Pressure cell AP2-1 is located at a depth of 188 mm from the surface in section A, BP5-3 located at a depth of 413 mm in Section B, DP1-2 located at a depth of 38 mm from the surface in Section D and FP5-3 is located at a depth of 338 mm from the surface in Section F. Pressure cell AP7-2 was located at 610 mm from the surface in the subgrade layer, while DP4-1 was located at 263 mm from the surface in Section D. The linear elastic analysis with a temperature correction produced the stresses that best match those measured in the field for instruments in the HMA layers. The nonlinear elastic analysis with a temperature correction produced the best fit for instruments in the granular layer (or at a deeper level). The EVERCALC software was used for performing the backcalculation analysis to obtain the moduli of the layers, because it produced a better fit and the least RMSE value when compared to the other software.

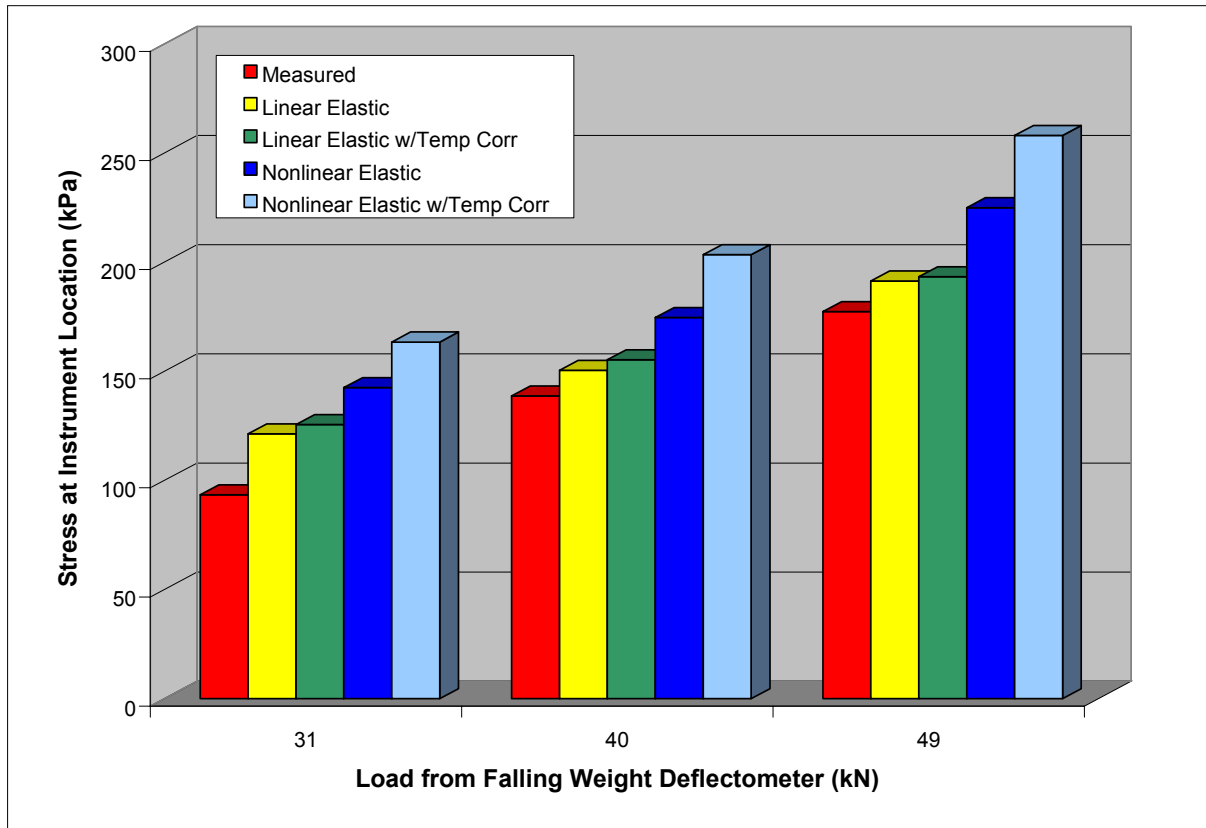


**Figure 7.8** Stress Responses Collected in January 2001 for Instrument AP2-1.

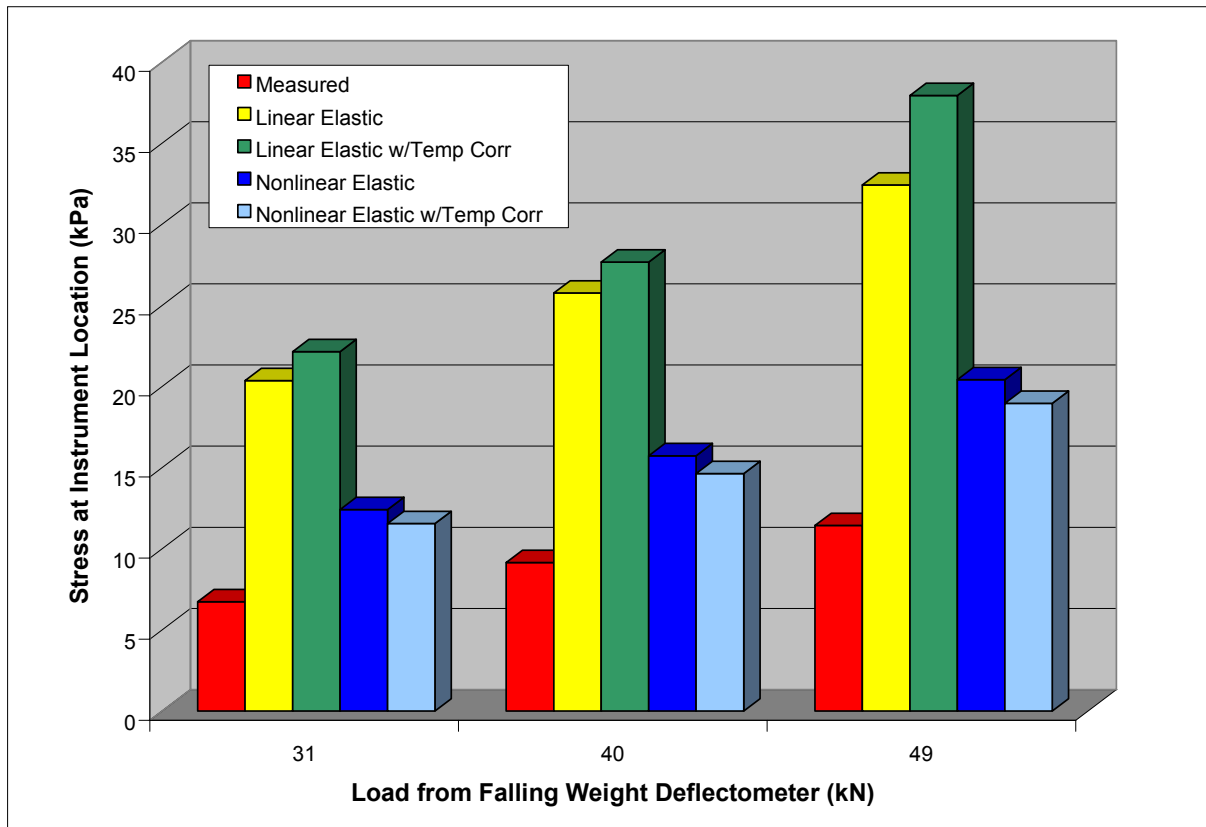


**Figure 7.9** Stress Responses Collected in January 2001 for Instrument BP5-3.

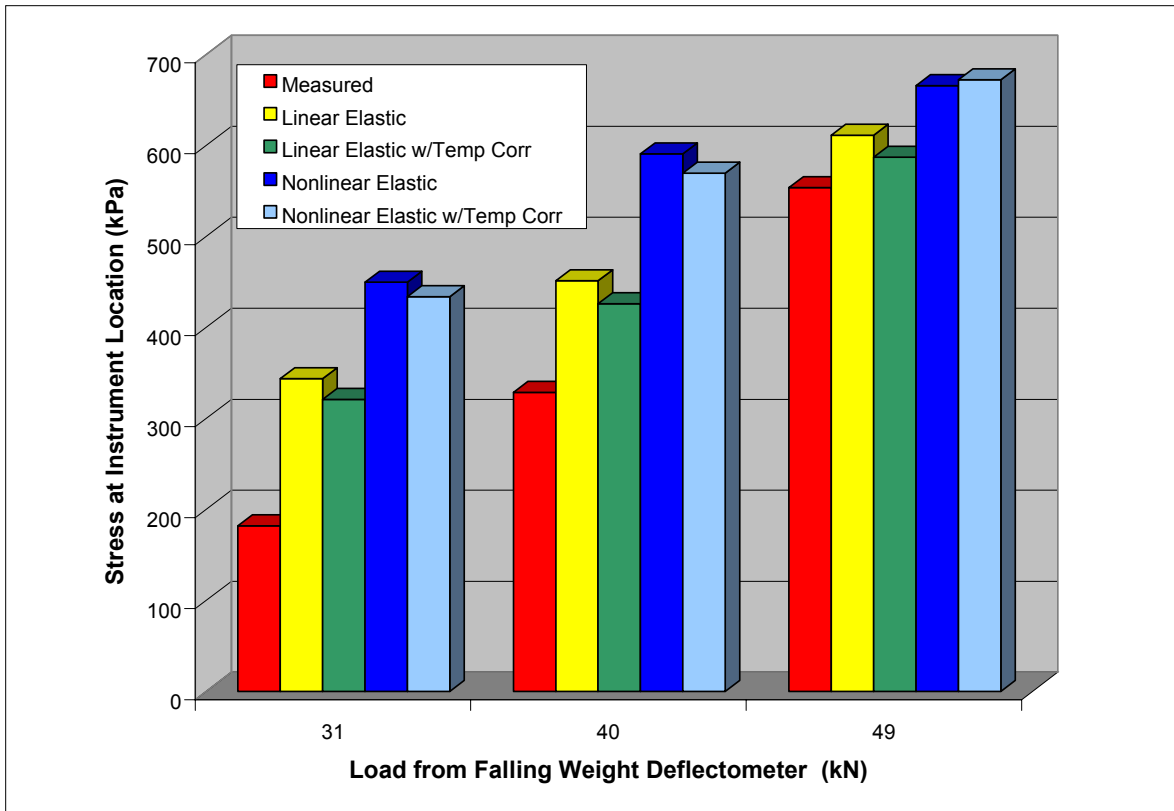


Figure 7.10 Stress Responses Collected in January 2001 for Instrument DP1-2.

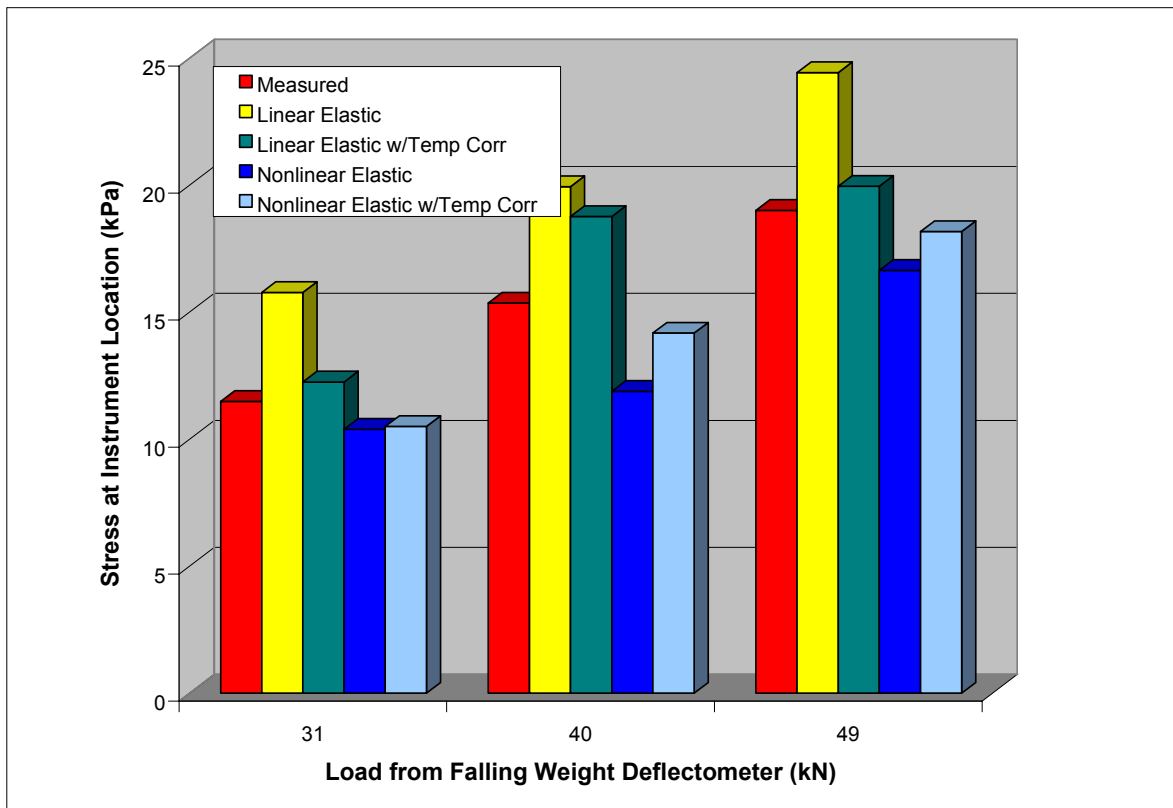
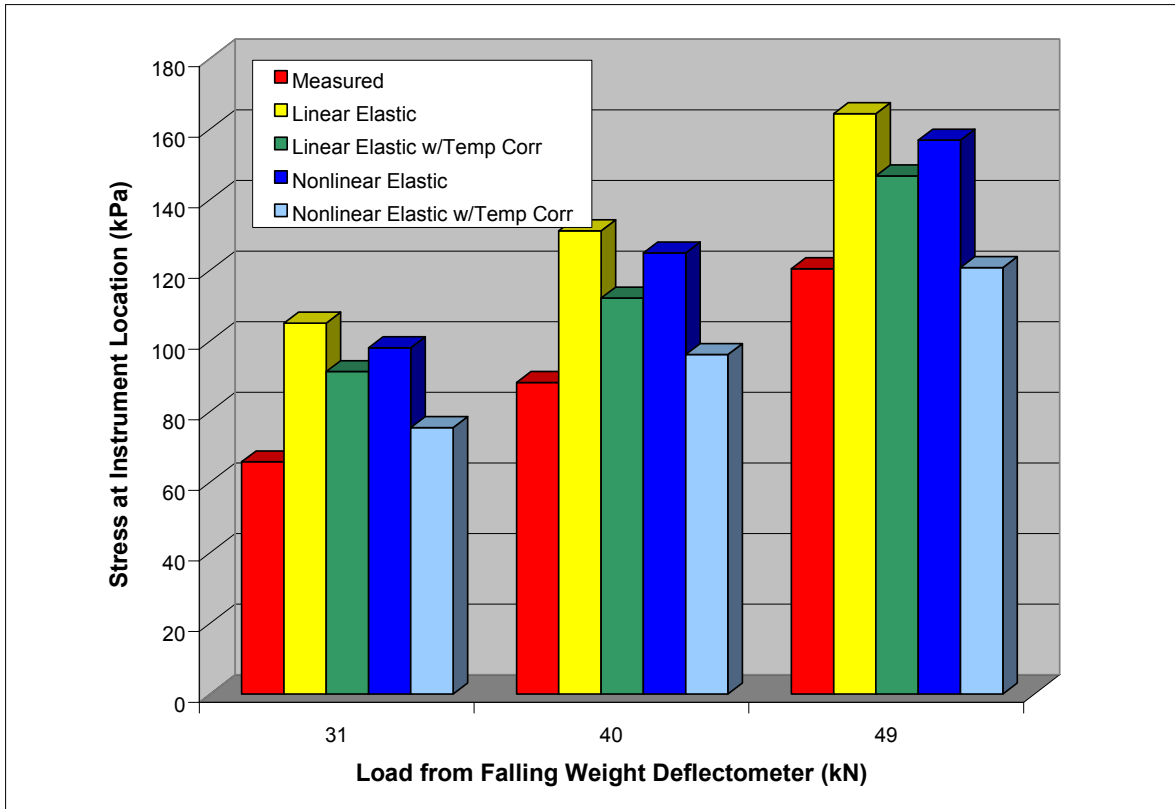


Figure 7.11 Stress Responses Collected in January 2001 for Instrument AP7-2.



**Figure 7.12** Stress Responses Collected in January 2001 for Instrument DP4-1.

Details of the results from all the other instruments using various backcalculation software are shown in the Appendix C. Tables 7.1 and 7.2 show results of the stresses, computed using the moduli from the four backcalculation software packages, and field stress values, obtained from testing during two selected months, November, 2000 and April, 2001, respectively. The average temperature of the wearing surface during November, 2000 was 15 °C, while the average temperature of the wearing surface in April was around 35 °C. The analysis results showed that during warmer temperatures the results of the calculated stresses were in a better agreement with the measured stresses than at in colder temperatures.

The percentage differences between measured and computed stresses in the BM-25.0 layers (AP2-1, DP2-1, FP2-2, GP2-2) during average temperature of 13°C (in November) were higher in most cases than instruments in the lower layers (AP5-3, AP7-2, FP5-3). The only exception was in the Section D where the difference in measured and computed stresses in DP4-1 and DP1-2 were both more than 30%. Instruments in the open graded drainage layer (OGDL), DP4-1 and HP4-1, generally had a high percentage difference between the computed stresses and measured stresses for the 40 kN load.

One of the reasons for the resulting difference of over 30% encountered at low temperatures is the high HMA moduli and the increase in its stiffness. The results obtained in April (average temperature of wearing surface being above 35 °C) are shown in Table 7.2.

**Table 7.1** Computed and Field-Measured Stresses (November 2000).

Instrument	Temp (°C)	LOAD (kPa)	EVERCALC (kPa)	PEDMOD (kPa)	ELMOD (kPa)	MICHBACK (kPa)	Field Response (kPa)
<b>AP2-1</b>	10.5	40	101 (37)*	121 (14)	175 (21)	159 (13)	138
		49	145 (18)	153 (20)	225 (27)	220 (19)	178
<b>AP5-3</b>	10.7	40	13 (13)	15 (1)	24 (38)	25 (40)	15
		49	17 (8)	19 (3)	31 (40)	18 (6)	19
<b>AP7-2</b>	10.4	40	14 (5)	12 (2)	10 (1)	11 (18)	9
		49	17 (34)	16 (28)	13 (15)	17 (35)	11
<b>BP 4-2</b>	13.8	40	106 (2)	89 (17)	96 (8)	98 (6)	104
		49	134 (10)	115 (28)	122 (21)	130 (14)	148
<b>DP 1-2</b>	12.2	40	570 (37)	530 (32)	540 (34)	550 (35)	358
		49	672 (30)	686 (31)	689 (32)	677 (31)	468
<b>DP4-1</b>	12.3	40	65 (51)	92 (66)	71 (55)	89 (64)	32
		49	90 (56)	119 (67)	93 (58)	101 (60)	40
<b>FP2-2</b>	13.5	40	23(35)	26 (19)	25 (24)	24 (29)	31
		49	46 (11)	66 (38)	75 (45)	52 (21)	41
<b>FP5-3</b>	13.7	40	14 (14)	18 (33)	19 (37)	19 (37)	12
		49	18 (0)	25 (28)	30 (40)	27 (33)	18
<b>GP2-2</b>	15.6	40	245 (22)	259 (27)	269 (30)	277 (32)	189
		49	297 (3)	316 (9)	339 (15)	341 (16)	288
<b>HP4-1</b>	15.2	40	30 (30)	32 (34)	41 (49)	28 (25)	21
		49	38 (13)	42 (21)	54 (21)	35 (1)	33
Avg. % diff		40	28	36	31	31	
		49	27	34	33	25	

\*Percentage average differences between theoretical and measured stresses in brackets

**Table 7.2** Computed and Field-Measured Stresses (April 2001).

Instrument	Temp (°C)	LOAD (kN)	EVERCALC (kPa)	PEDMOD (kPa)	ELMOD (kPa)	MICHBACK (kPa)	Field Response (kPa)
<b>AP2-1</b>	33	40	227 (9)*	190 (8)	219 (6)	238 (13)	206
		49	276 (16)	240 (5)	267 (14)	289 (20)	230
<b>AP5-3</b>	34.2	40	35 (25)	20 (30)	20 (30)	37 (29)	26
		49	43 (25)	26 (23)	26 (23)	45 (28)	32
<b>AP7-2</b>	33.8	40	18 (16)	16 (6)	16 (6)	19 (21)	15
		49	23 (13)	16 (25)	19 (6)	24 (17)	20
<b>BP 4-2</b>	34.9	40	151 (16)	129 (3)	152 (17)	159 (20)	126
		49	230 (26)	166 (3)	188 (9)	241 (29)	133
<b>DP 1-2</b>	40.4	40	576 (12)	559 (6)	563 (5)	607 (18)	492
		49	638 (1)	700 (8)	679 (5)	705 (9)	646
<b>DP4-1</b>	41.6	40	152 (36)	113 (14)	167 (41)	159 (38)	97
		49	183 (34)	157 (24)	210 (42)	192 (38)	120
<b>FP2-2</b>	42.5	40	145 (7)	157 (33)	156 (31)	187 (35)	134
		49	169 (7)	215 (15)	221 (18)	233 (22)	181
<b>FP5-3</b>	43	40	26 (30)	49 (30)	36 (5)	47 (27)	34
		49	21 (22)	69 (37)	44 (2)	55 (22)	43
<b>GP2-2</b>	45.5	40	138 (1)	178 (20)	162 (12)	186 (23)	142
		49	179 (10)	221 (11)	215 (9)	224 (13)	196
Avg. % diff		40	18	16	17	24	
		49	18	15	15	23	

\*Percentage average differences between theoretical and measured stresses in brackets

The percentage difference between the measured and computed stresses for most of the instruments in the wearing surface and BM-25.0 layers (AP2-1, DP1-2, FP2-2 and GP2-2) in April were low compared to the results in November. For example, instrument DP1-2 registered differences as low as 1 to 12% for both 40 and 49 kN load in April, whereas in November the differences ranged from 30 to 37% for the same loading. The results from DP4-1 (in the open graded drainage layer) in April were high for all the software used. The average percentage difference for each load category is averaged

for each software, EVERCALC, PEDMOD, ELMOD and MICHBACK, in Tables 7.1 and 7.2.

To further analyze results during cold and hot temperatures, two testing each at cold and hot months were chosen. Measured and computed stresses during November, 2001 and February, 2002 (average wearing surface temperature of 5 and 18 °C, respectively) and April and August 2001 (average wearing surface temperature of 33 and 45 °C, respectively) were plotted. Figures 7.13 and 7.14 show the plots of measured and computed pressure cell responses resulting from 40 kN FWD load collected in November 2000, February 2001, April 2001, and August 2001 for the four backcalculation software.

In summary at testing temperatures below 15 °C, the percentage differences between the measured and computed stresses (resulting from backcalculation software and the KENLAYER program) were much higher than those computed during testing at very warm temperatures. Generally, instruments in the deeper layers such as the subgrade and 21-B showed lower differences, compared to instruments in the upper layers, between measured and computed stress. The only exception to this were the pressure cells in the OGD layer (DP4-1 and HP4-1), which registered high differences (up to 66%) in the colder temperatures of November 2000 and February 2001.

During the warm temperatures of April and August, 2001, instruments in the BM-25.0 layer (AP2-1, FP2-2) at a depth of 188 mm produced very low percentage differences between measured and calculated stresses at that depth (10 to 30%) as compared to instrument measurements in the lower layers. Pressure cell FP2-2, in particular showed very high percentage differences between the measured and computed stresses at that instrument position during the cold temperatures (19 to 45%) in November 2000.

Tables 7.3 to 7.8 summarize the results from the four backcalculation software at the aforementioned selected instruments. The differences between the measured and computed are shown for each of the months of testing. Lower differences between measured and computed stress values are recorded in higher temperatures shown in brackets. Instrument DP4-1 shows high differences in both high and low temperatures. (April, August and November, February respectively).

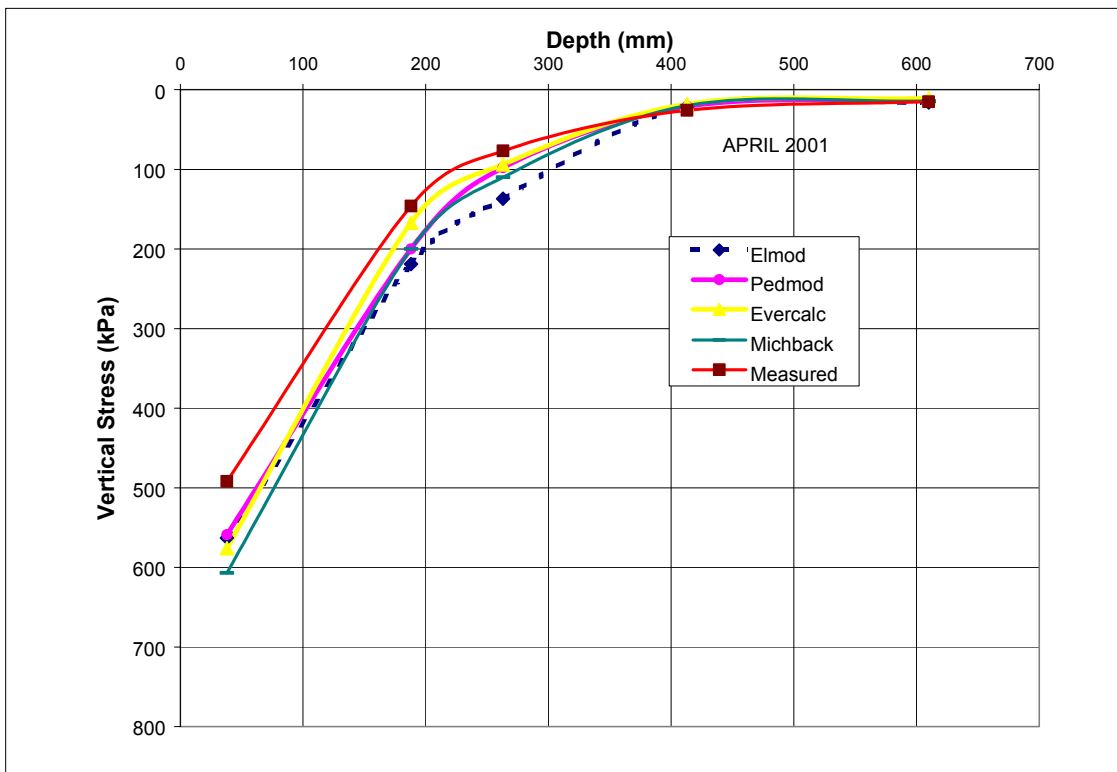
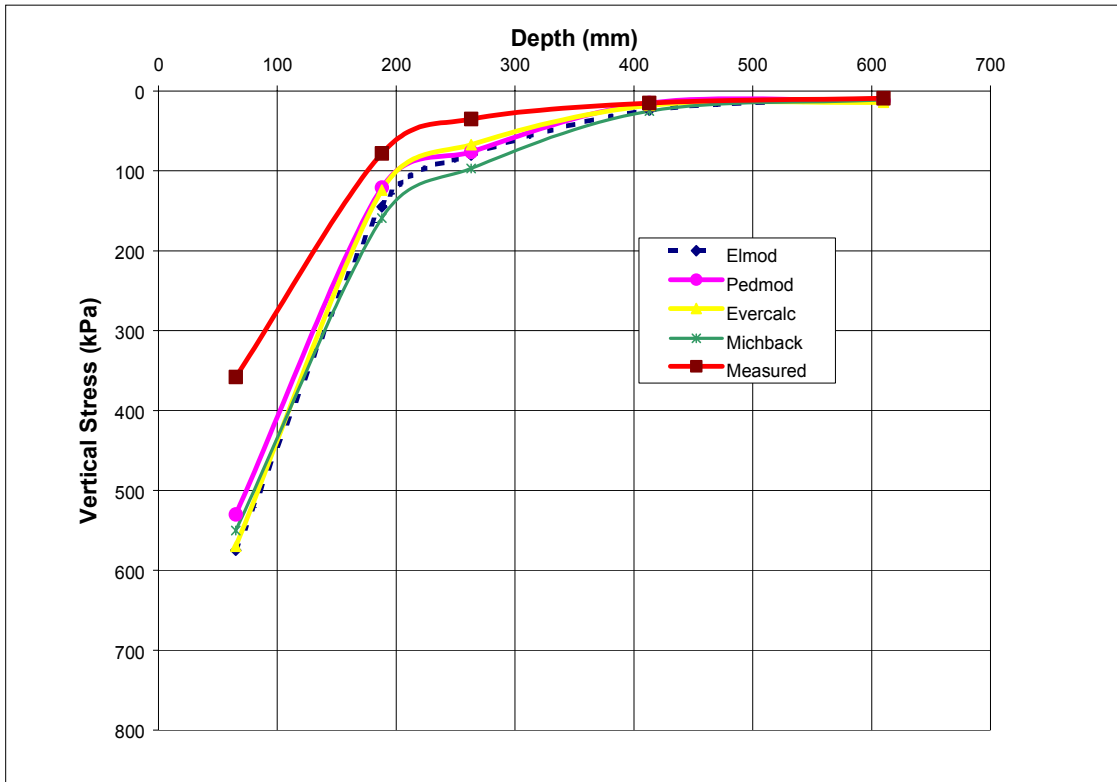


**Figure 7.13** Measured and Computed Stresses for 40 kN Loading in February 2001 and August 2001.

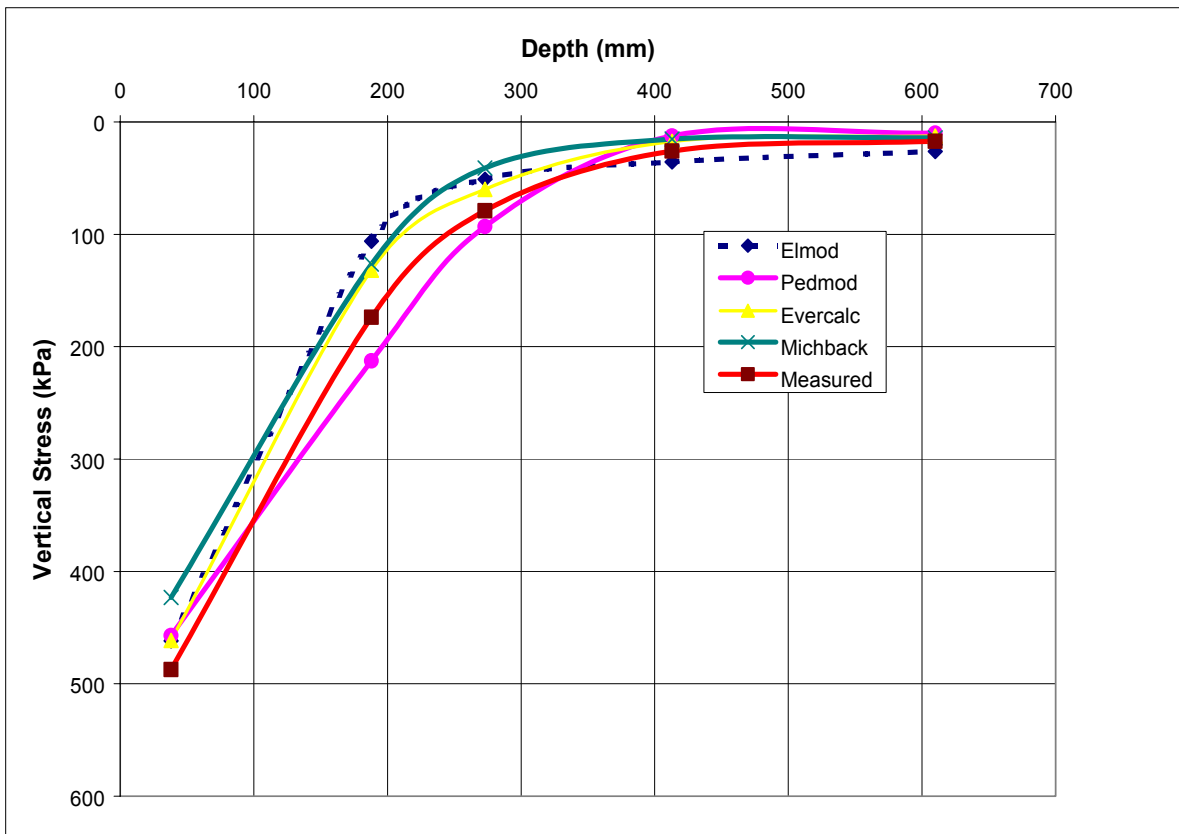
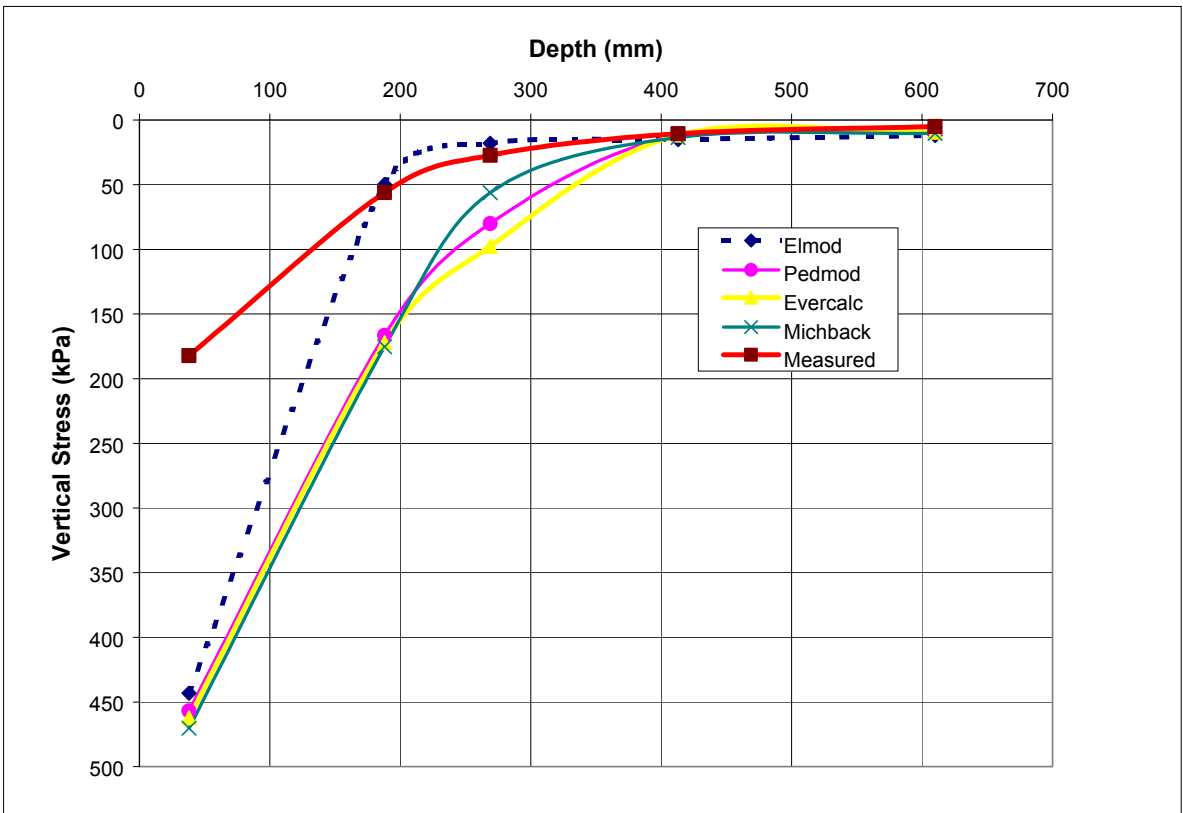


**Figure 7.14** Measured and Computed Stresses for 40 kN Loading in February 2001 and August 2001.

**Table 7.3** Percentage Differences for November and April for 40 kN Loading.

<b>Instrument</b>	<b>Depth (mm)</b>	<b>ELMOD</b>	<b>PEDMOD</b>	<b>EVERCALC</b>	<b>MICHBACK</b>
DP1-2	38	37 (5)	35 (6)	34 (12)	35 (18)
AP2-1	188	37 (6)	20 (8)	52 (9)	13 (13)
FP2-2	188	15 (31)	43 (33)	44(7)	36 (35)
AP5-3	413	38 (25)	54 (30)	48 (30)	40 (27)
AP7-2	610	37 (24)	19 (24)	17 (44)	40 (30)
DP4-1	263	55 (41)	66 (14)	51 (36)	64 (38)

**Table 7.4** Percentage Differences for November and April for 49 kN Loading.

<b>Instrument</b>	<b>Depth (mm)</b>	<b>ELMOD</b>	<b>PEDMOD</b>	<b>EVERCALC</b>	<b>MICHBACK</b>
DP1-2	38	37 (13)	32 (12)	37 (27)	35 (31)
AP2-1	188	27 (32)	33 (25)	52 (34)	25 (34)
FP2-2	188	56 (31)	100 (33)	28 (7)	52 (35)
AP5-3	413	40 (25)	19 (23)	27 (25)	18 (28)
AP7-2	610	15 (6)	38 (25)	34 (13)	35 (17)
DP4-1	263	58 (42)	67 (14)	56(34)	60 (38)

**Table 7.5** Percentage Differences for February and August for 40 kN Loading.

<b>Instrument</b>	<b>Depth (mm)</b>	<b>ELMOD</b>	<b>PEDMOD</b>	<b>EVERCALC</b>	<b>MICHBACK</b>
DP1-2	38	59 (6)	60 (7)	61(7)	61(15)
AP2-1	188	12 (64)	66 (18)	67 (56)	68 (37)
FP2-2	188	92 (29)	99 (35)	99 (38)	102 (41)
AP5-3	413	52 (14)	66 (4)	72 (2)	52 (60)
AP7-2	610	30 (27)	8 (109)	8 (49)	22 (69)
DP4-1	263	58 (35)	47 (72)	47(37)	51 (21)

**Table 7.6** Percentage Differences for February and August for 49 kN Loading.

<b>Instrument</b>	<b>Depth (mm)</b>	<b>ELMOD</b>	<b>PEDMOD</b>	<b>EVERCALC</b>	<b>MICHBACK</b>
DP1-2	38	39 (11)	47 (10)	44 (5)	45(8)
AP2-1	188	41 (6)	59 (16)	63 (62)	54 (28)
FP2-2	188	92 (23)	99 (30)	99 (25)	102 (33)
AP5-3	413	75 (25)	59 (23)	67 (29)	52 (19)
AP7-2	610	41 (28)	17(14)	16 (18)	26 (10)
DP4-1	263	30 (33)	10 (65)	11(40)	8 (6)

### 7.6.2 Strain Gage Analysis

Responses were obtained from the following strain gages, ASH1-2L, ASH1-4L, BSH4-1L, DSH1-2L, DSH6-2L, GSH2-3L, and BSH 2-6L. The loads of 31, 40, 49, and 58 kN were dropped on the position where the strain gages were located. Linear-elastic, nonlinear-elastic, and viscoelastic analyses were performed. For the viscoelastic analysis, creep compliance testing of mixes used at sections A, B, D, and G was conducted in the laboratory at 5, 25, and 40 °C. Figure 7.15 shows a typical master curve plot for section A. Shift factors ranging from 0.135 to 0.153 were determined from the creep compliance master curve. Creep data at 0.01, 0.03, 0.1, 1, 3, 10, 30, and 100 seconds were used as input in the KENLAYER software at the corresponding FWD testing temperatures.

Table 7.7 summarizes the analysis of the strain gages incorporating the creep behavior of the wearing surface. The results include linear elastic analysis, viscoelastic analysis and a combination of viscoelastic and nonlinear analysis. As would be expected, the viscoelastic analysis produced a closer match to the field-measured strains (10 to 25%) than the purely elastic analysis for most of the instruments installed in the wearing surface.

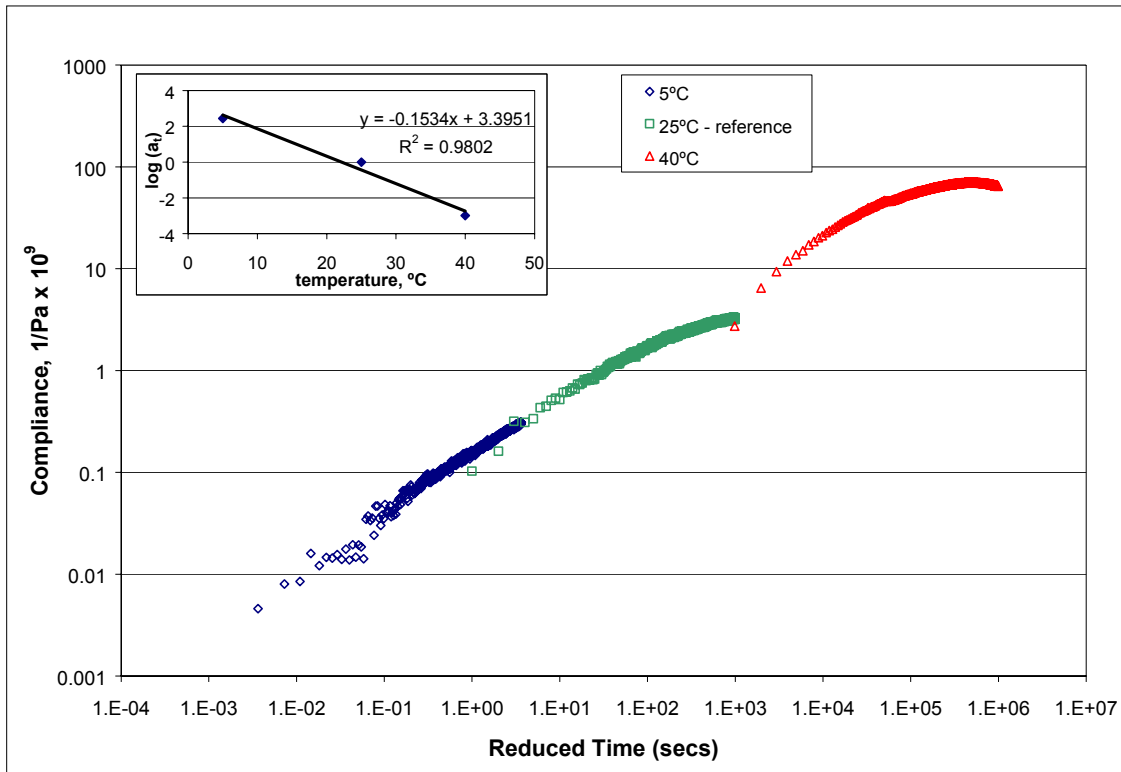


**Figure 7.15** Creep Master Curve for Section B.

The mix type for the wearing surface in Section A is SM-12.5D with a SuperPave binder PG70-22. For instrument ASH1-2L, the measured tensile strain at 32 °C for the 31 kN load was 46.6 microstrain. However, at 44 °C (12 °C higher), a tensile strain of 72.1 microstrain (an increase in 154%) was measured. At higher load of 40 kN, tensile strain of 54.4 microstrain was measured. At 44 °C, a tensile strain of 97.6 microstrain was measured (an increase of 179%). . At a higher load, of 49 kN the measured tensile strain at 33 °C was 71.2 microstrain, however, at higher temperature of 44 °C, the measured tensile strain was 111.7 microstrain (an increase of 156%).

Strain gage DSH1-2L in surface mix type SM-9.5A in Section D, the binder type is PG64-22 and the differences between measured and computed deflections ranged from 18 to 71% at a temperatures of 30 and 45 °C. The differences between the measured and computed strains, using the three types of analysis shown in the Table 7.9, are between 5 to 30% for this strain gage ASH1-2L at 32 °C. At the higher temperature of 44 °C, the difference ranged from 6 to 36%. The highest difference was found when using the linear elastic analysis while the lowest when the viscoelastic combined with the nonlinear analysis was used. For strain gage BSH2-6L, the mix type is the BM-25.0 with binder grade PG64-22, the difference between the measured and

computed strains are much higher ranging from 20 to 58%. For strain gage in GSH2-3L, the mix type is also BM-25.0 with binder grade PG64-22, the difference between the measured and computed strains range from 25 to 40% at 35 °C, while at a lower temperature of 25 °C the differences were 23 to 45%.

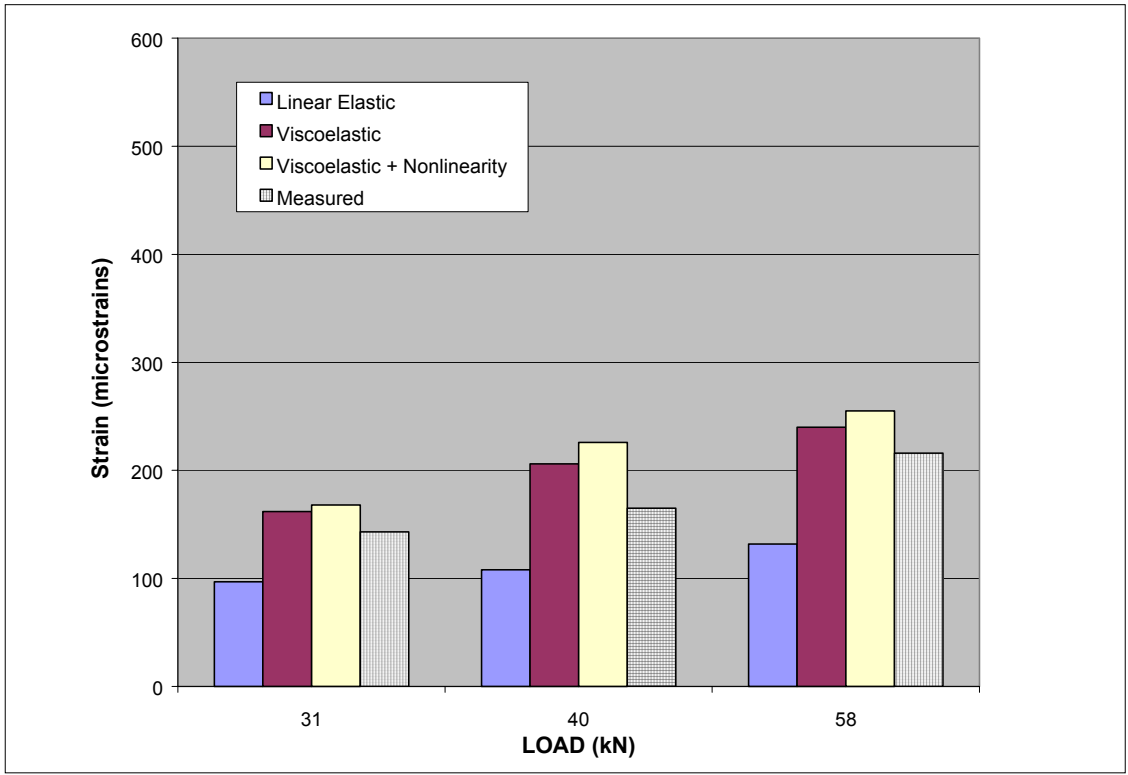
**Table 7.7** Calculated and Field Measured Strains.

Instrument	Temp (°C)	Load (kN)	Calculated Strain (Linear-elastic)	Calculated Strain (Viscoelasticity)	Calculated Strain (Viscoelasticity +Nonlinearity)	Measured Strain
ASH1-2L	32	31	31.6	37.7	39.86	46.56
ASH1-2L	32	40	42.9	51.2	54.42	54.43
ASH1-2L	33	49	49.8	58.3	61.83	71.2
BSH 2-6L	35	31	23.4	26.47	30.17	39.3
BSH2-6L	35	40	32.69	33.25	38.22	55.21
BSH2-6L	35	58	36.12	40.22	45.72	70.8
BSH2-6L	25	31	16.4	20.4	23.2	30.3
BSH2-6L	27	40	26.5	28.1	30.9	47.2
GSH2-3L	42	40	18.22	24.25	31.2	33.5
GSH2-3L	42	49	27.5	35.12	39.4	44.72
ASH1-2L	44	31	42.6	60.1	67.3	72.1
ASH1-2L	44	40	57.1	81.42	91.37	97.65
ASH1-2L	44	58	67.67	93.13	104.5	111.7
BSH 4-1L	45	31	22.9	12.76	17.96	44.7
BSH 4-1L	45	40	47.6	16.32	21.27	62.9
BSH 4-1L	45	58	51.2	18.56	31.46	85.1
DSH1-2L	30	31	97	162	168	143
DSH1-2L	30	40	108	206	226	165
DSH 1-2L	30	58	132	240	255	216
DSH1-2L	45	31	192.4	296	407.1	236.7
DSH1-2L	45	40	213.1	508	480	344.7
DSH 1-2L	45	58	233.6	517	534	462.9

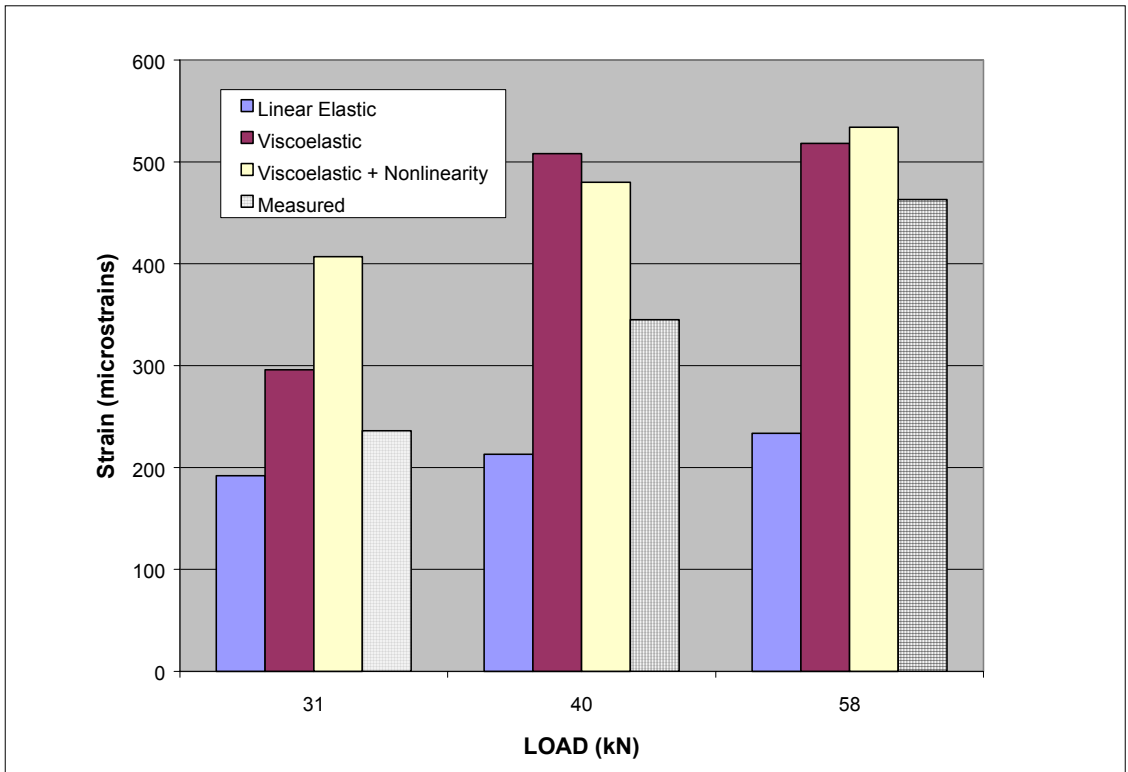
For the strain gage BSH4-1L, located at the bottom of the asphalt treated OGD layer, the tensile strains were under predicted by a greater amount for the viscoelastic analysis than the elastic analysis. The difference between measured and linear elastic calculated strains ranged from 24 to 39%, while the difference ranged from 59 to 78% when viscoelastic analysis was used. Figure 7.16 shows plots of the measured tensile strain response by instrument DSH1-4L under 31, 40, and 49 kN, respectively, and calculated strains. Table 7.8 shows the difference in percentage between the measured and calculated strains for mix types listed in Table 7.7. BM-25.0 and SM 9.5A mixes produced the highest differences between measured and calculated strains. Mix type and binder grade have an effect on measured and calculated strains.

**Table 7.8** Percentage Differences between Measured and Computed Strain Response.

Temp (°C)	Instrument	Mix Type	Linear elastic	Viscoelastic	Viscoelastic +Nonlinearity
32	ASH1-2L	SM-12.5D	32	19	14
32	ASH1-2L	SM-12.5D	21	6	0
33	ASH1-2L	SM-12.5D	30	18	13
35	BSH2-6L	BM-25.0	40	33	23
35	BSH2-6L	BM-25.0	40	39	30
35	BSH2-6L	BM-25.0	41	34	25
25	BSH2-6L	BM-25.0	45	33	23
27	BSH2-6L	BM-25.0	44	40	35
42	GSH2-3L	BM-25.0	46	28	7
42	GSH2-3L	BM-25.0	39	21	12
44	ASH1-2L	SM-12.5D	35	17	7
44	ASH1-2L	SM-12.5D	35	17	6
44	ASH1-2L	SM-12.5D	36	17	6
30	DSH1-2L	SM-9.5A	79	65	63
30	DSH1-2L	SM-9.5A	76	55	51
30	DSH1-2L	SM-9.5A	71	48	44
45	DSH1-2L	SM-9.5A	19	25	15
45	DSH1-2L	SM-9.5A	38	47	39
45	DSH1-2L	SM-9.5A	49	12	35



(a)



(b)

Figure 7.16 Measured (DSH1-2L) and Calculated Strains at Temperatures 30°C and 45°C.

In general, with the exception of the difference in measured and calculated strains for the strain gauge BSH4-1L, viscoelastic analysis has shown the least difference.

### 7.6.3 Mechanistic Empirical Modeling

Tensile strain results obtained from the strain gages installed in the wearing surface (SM-9.5A) were used to predict the number of loading cycles to fatigue cracking failure. It was assumed that debonding between the wearing surface and BM-25.0 layer existed due to friction between the two interfaces resulting in tensile strains. Fatigue cracking is known to be related to the tensile strain at the bottom of the HMA layer.

$$\text{Log}(N_f) = 15.95 - 3.29 \log(\epsilon_t) - 0.854E \quad (7.14)$$

where,

$N_f$  = allowable number of loading cycles to failure;

$\epsilon_t$  = tensile strain at the bottom of the wearing surface; and

$E$  = moduli of the HMA layer.

Using tensile strains recorded by ASH1-2L (at the bottom of SM 9.5A) due to 31 kN loading, the number of load repetitions to failure was calculated. Three types of analyses were used to calculate tensile strain: viscoelastic with nonlinearity, viscoelastic, and linear elastic. Using Equation 7.14, for strains calculated at the strain gage ASH1-2L location at 32 °C, the  $N_f$  was 3.09E+08 (viscoelastic with nonlinearity), 3.68E+08 (viscoelastic), and 6.18E+08 (linear elastic), respectively. The  $N_f$  based on the purely linear elastic analysis was 1.68 times the  $N_f$  based on the viscoelastic plus nonlinearity analysis, and 2 times that based on the purely viscoelastic analysis. If the tensile strains at the bottom of the BM-25.0 layer had been used the same trend in the three analysis would have resulted but with different values. At 44 °C, using strains measured at the same locations from the same load (31 kN) the  $N_f$  for the three types of analyses is 5.14E+07, 7.45E+07 and 2.31E+08. The  $N_f$  based on the purely linear elastic analysis was 4.5 times the  $N_f$  based on the viscoelastic plus nonlinearity analysis, and 3.1 times that based on the purely viscoelastic analysis. Figure 7.17 and Figure 7.18 presents the results from three analyses for the different loads 31 and 40 kN at different temperatures 32 and 44 °C. Using the criterion of tensile strain at the bottom of the HMA at higher temperatures for the same loading condition, higher tensile strains develops in the pavement and the number of loading cycles to cause fatigue failure decreases. As the

loading also increases for the same temperature the number of cycles to cause fatigue failure also increases. Also the linear elastic analysis results means more loading cycles are needed to cause fatigue failure than analysis incorporating nonlinear and viscoelastic properties of the pavement system. It also means linear elastic analysis results in over design.

Using the same fatigue equation shown in equation 7.14, the tensile strains resulting from the three types of analysis, linear elastic, viscoelastic and viscoelastic combined with nonlinearity at one strain location was plotted to determine the relationship between the elastic moduli and the number of cycles to failure to determine the effects between moduli changes on the number of cycles to failure. The resulting Figure 7.19 shows that at lower moduli a higher number of loading cycles to failure ( $N_d$ ) results. The viscoelastic analysis results in higher number of loading cycles to failure ( $N_d$ ) than the purely linear elastic analysis.

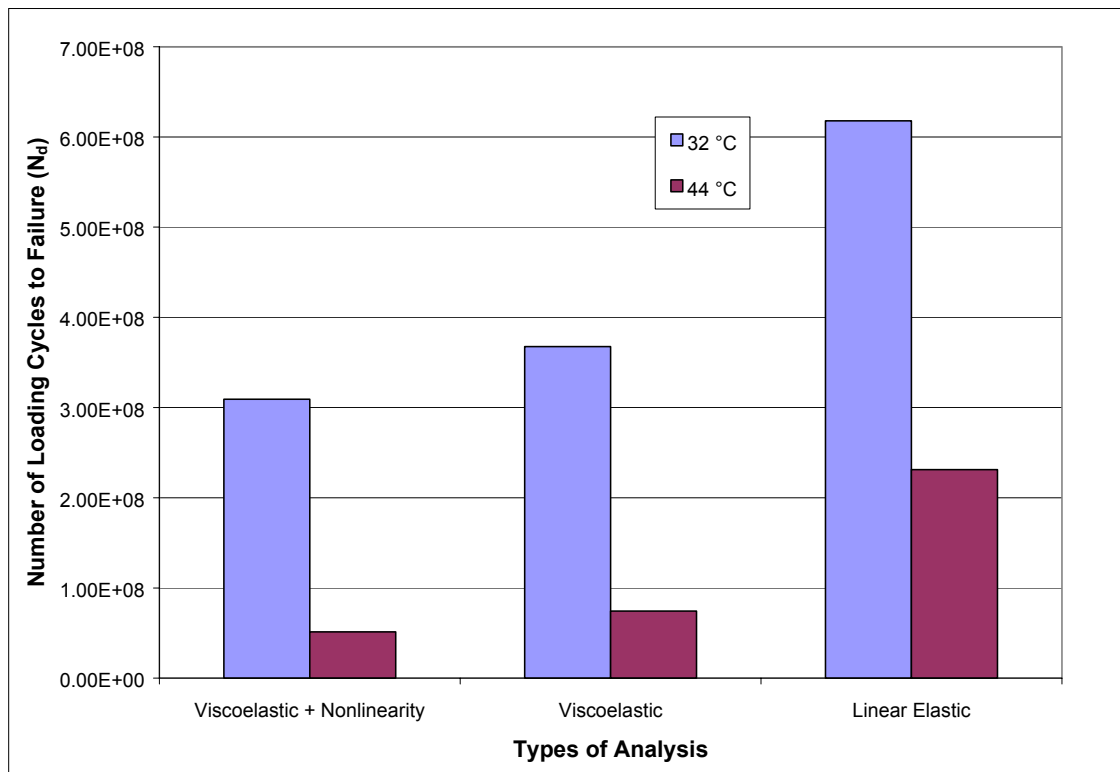


**Figure 7.17.** Number of Cycle to Failure for 31 kN Load at Different Temperatures.

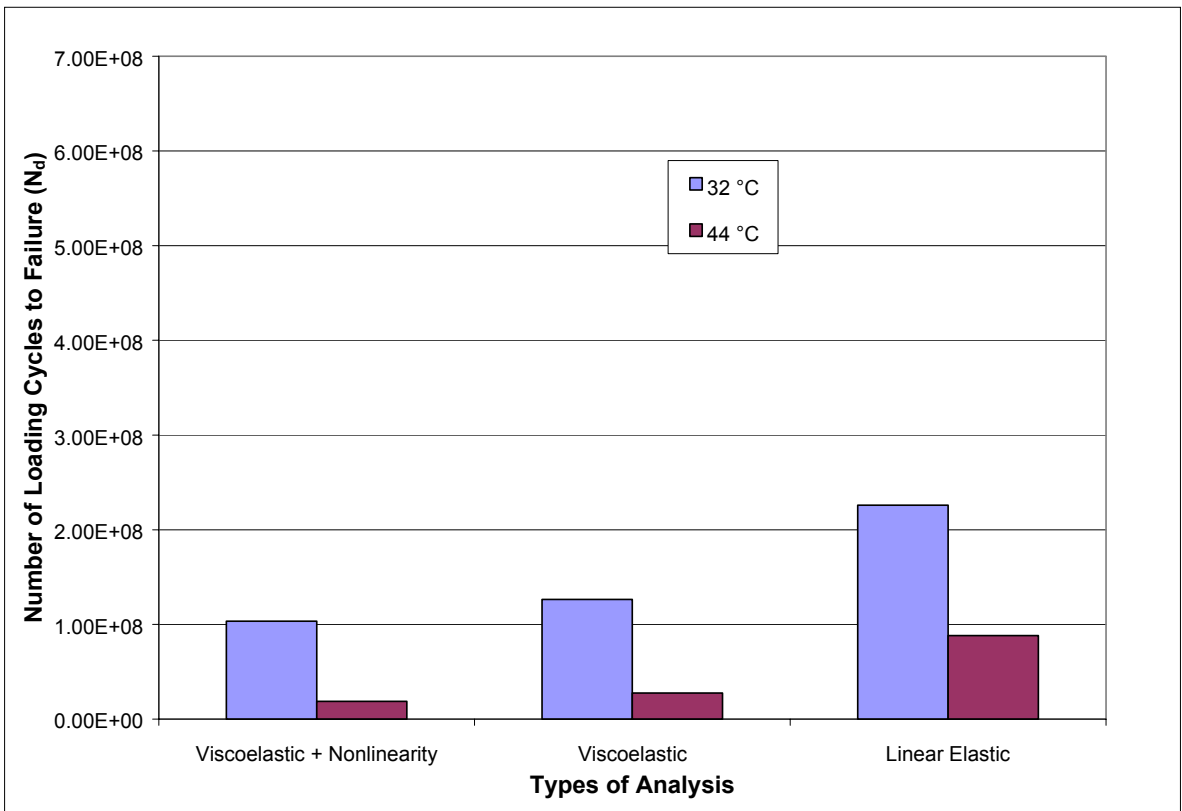


Figure 7.18. Number of Cycle to Failure for 40 kN Load at Different Temperatures.

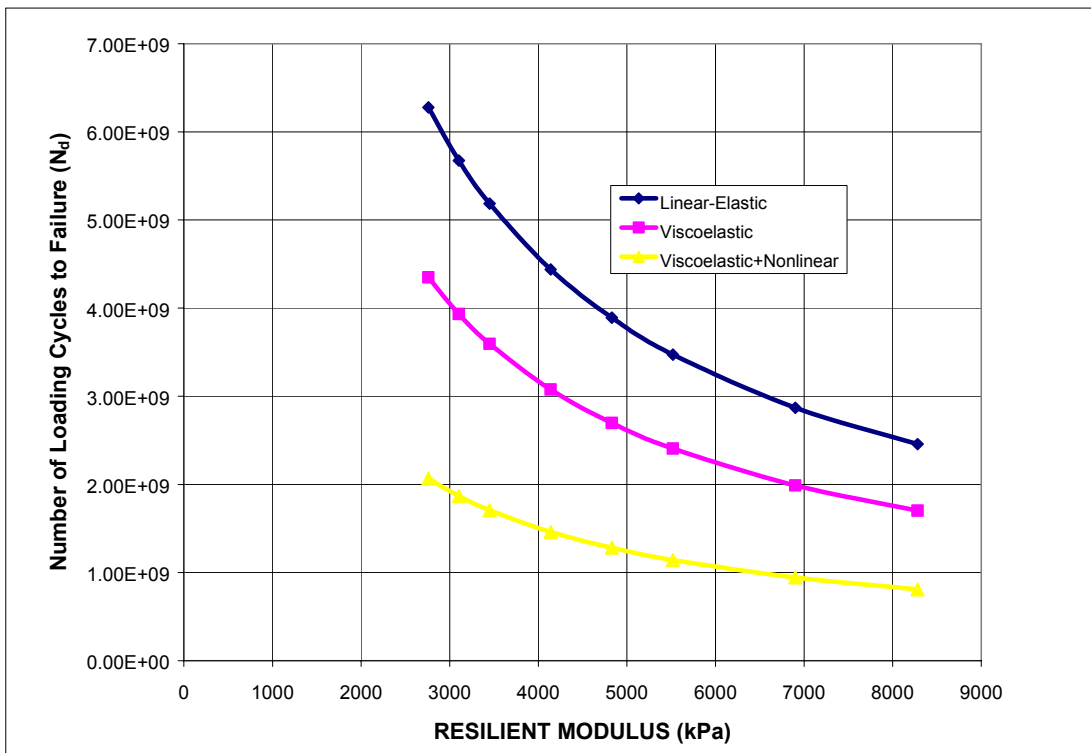


Figure 7.19 Number of Loading Cycles as a Function of Resilient Moduli for the Types of Analysis.

At 3000 MPa the viscoelastic analysis combined with nonlinearity, viscoelastic analysis and linear elastic analysis produces 2.00 E+09, 4.20 E+09 and 6.00 E+09 number of cycles to failure respectively. At an increased moduli at 8000 MPa the resulting number of cycles to failure are 2.50 E+09, 1.90E+09 and 0.9E+09 respectively. Sensitivity analyses shows that the ratios between the linear elastic values and the other analysis values reduces with increasing resilient moduli values, agreeing with earlier findings that the higher the temperature the higher the ratios, since higher temperatures results in lower moduli.

## **7.7 SUMMARY AND CONCLUSIONS**

Pavement instrumentation could provide an excellent tool for validating mechanistic models for pavements. In this Chapter, the resilient moduli resulting from several backcalculation software were used to compute stresses and strains at various depths in the different pavement layer systems at the Virginia Smart Road. Linear elastic, viscoelastic, and viscoelastic and nonlinear analytical models were utilized. At high temperatures of 33 °C and above, computed stresses showed a reasonable agreement with measured stresses at different depths than at low temperatures (below 15 °C). Results from the strain gage and pressure cell (BSH 4-1L, DP4-1) located at the bottom of the asphalt treated open graded drainage layer (OGDL) were different than the calculated values. This is possibly due to the fact of the low modulus of that layer, the aggregate gradation, and the difficulty of measurements. Incorporation of temperature correction of the HMA layer improved the stress prediction in that layer when compared to measured stresses.

It was found that the surface type and temperature influenced the difference between computed and measured strains. It appears that measured strains in SM-12.5D mix show better agreement with calculated values than those measured in SM-9.5A. The difference is reduced at high temperatures.

Strains from the three models (linear elastic, viscoelastic, and viscoelastic with nonlinearity incorporated) were used to calculate the pavement fatigue life. At 32 °C the number of cycles to failure based on the purely linear elastic were found to be twice the number of cycles based on the viscoelastic analysis and 1.68 times that based on viscoelastic combined with nonlinearity analysis. At higher temperature of 44 °C the ratios increased to 4.5 and 3.1 respectively.

The study concluded that elastic theory under predict the number of loading cycles to reach fatigue failure. This may explain the premature fatigue failure of many pavements. The study suggested that a viscoelastic model be used to design and analyze pavements exposed to intermediate and high temperatures.

## REFERENCES

Allen, J. J., and Thompson, M. R. (1974). "Resilient response of granular materials subjected to time dependent lateral stress." *Transportation Research Record 510*, TRB, National Research Council, Washington, D.C, pp. 1-13.

Chen, W. F., and Mizuno, E. (1990). "Non-linear Analysis in Soil Mechanics, Theory and Implementation." *Developments in Geotechnical Engineering.*" Vol. 53, 1990.

Desai, C. S., and Siriwardane, H. J. (1984). Constitutive Laws for Engineering Materials with Emphasis on Geologic Materials. Prentice Hall Inc., Englewood Cliffs, N J.

Flintsch, G. W., Appea, A. K., Al-Qadi I. L., and Loulizi, A. (2001). "Backcalculation Validation through Field Instrumentation Response at the Virginia Smart Road." 2nd International Symposium on Maintenance and Rehabilitation of Pavements and Technological Control, Waheed, U., Fortes, R.M., and Merighi, J.V., Eds., Auburn, AL.

Flintsch, G. W., Al-Qadi, I. L., Brandon, T. L., Park, Y., and Appea, A. K. (2003). "Relationship between Backcalculated and Laboratory-Measured Resilient Modulus of Subbase Materials at the Virginia Smart Road." To be Presented at the Transportation Research Board 82nd Annual Meeting Paper # 03-3434, Washington, D.C.

Hicks, R. G.(1970). "Factors Influencing Resilient Response of Granular Materials." PhD Dissertation, Civil Engineering Department, University of California, Berkeley, CA.

Hicks, R.G., and Monismith, C.L. (1971). "Factors Influencing The Resilient Properties of Granular Materials." *Highway Research Record 345*, TRB, National Research Council, Washington, D.C., 1968, pp. 15-31.

Huang, Y. J.(1993). Pavement Analysis and Design. Prentice Hall, Inc., Englewood Cliffs, NJ.

Huang, Y. H.(1994). “Stresses and Displacements in Nonlinear Soil Media.” *Journal of the Soil Mechanics and Foundation Division*, ASCE, Vol. 94, No. SM1, pp. 1-19.

Loulizi, A., Al-Qadi, I. L., Lahouar, S., and Freeman, T. E. (2001). “Data Collection and Management of the Instrumented Smart Road Flexible Pavement Sections.” Presented at the Transportation Research Board 81st Annual Meetings Paper # 01-2668, Washington, D.C., pp. 1-27.

Nasser, W., Al-Qadi, I. L., Flintsch, G.W., and Appea, A. K. (2000). “Evaluation of Pavement Layer Response at the Virginia Smart Road.” Proceedings of Geo-Denver 2000, Geotechnical Special Publication No. 98, Pavement Subgrade, Unbound Materials, and Nondestructive Testing, Mamlouk, M., Eds., ASCE, Denver, CO, pp.104-118.

Peutz, M. G. F., Van Kempen, H. P. M., and Jones, A. (1968). “Layered Systems under Normal Surface Loads.” *Highway Research Record* 228, TRB, National Research Council, Washington, D.C., pp. 35-45.

Scullion, T., Briggs, R. C. and Lytton, R. L. (1989). “Using the Multidepth Deflectometer to Verify Modulus Backcalculation Procedures.” Nondestructive Testing of Pavements and Backcalculation of Moduli, ASTM STP 1026, Bush, A. J., III and Baladi, G. Y., Eds., American Society for Testing and Materials, Philadelphia, PA, pp. 90-101.

Seeds, S., Alavi, S., Ott, W., Mikhail, M., and Mactutis, J. (1999). “Evaluation of Laboratory Determined and Nondestructive Test Based on Resilient Modulus Values from WesTrack Experiment.” Nondestructive Testing of Pavements and Backcalculation of Moduli (Vol III) ASTM STP 1375, Tayabji, S. D and Lukanen, E. O Eds., American Society for Testing and Materials, Seattle, WA, pp. 72-95.

Ullidtz, P. (1977). “Overlay and Stage by Stage Design.” Proceedings of 4th International Conference on the Structural Design of Asphalt Pavements, Vol. 1, Ann Arbor, MI, 1977, pp. 722-735.

Ullidtz, P., Askegaard, V., and Sjolín, F. O. (1996). "Normal Stresses in a Granular Material under Falling Weight Deflectometer Loading." *Transportation Research Record 1293*, TRB, National Research Council, Washington, D.C, pp. 24-29.

Uzan, J. (1985). "Characterization of Granular Materials." *Transportation Research Record 1022*, TRB, National Research Council, Washington, D.C, pp. 52-59.

Van Cauwlaert, F. J., Alexander, D. R. White, T. D. and Barker, W. R. (1989). "Multilayer Elastic Program for Backcalculating Layer Moduli in Pavement Evaluation." *Nondestructive Testing of Pavements and Backcalculation of Moduli*, ASTM STP 1026, Bush, III, A. J. and Baladi, G. Y. Eds., American Society for Testing and Materials, Philadelphia, PA, pp. 117-188.

Van Deusen, D. (1996). "Selection of Flexible Backcalculation Software for Minnesota Road Research Project." Report No. 96/29, Minnesota Department of Transportation, St Paul, Minnesota, MN.

Witczak, M. W., and Rada, G. (1981). "Comprehensive Evaluation of Laboratory Resilient Moduli Results for Granular Material." *Transportation Research Record 810*, TRB, National Research Council, Washington, D.C., pp. 23-33.

## CHAPTER EIGHT

### SUMMARY, FINDINGS, CONCLUSIONS, AND RECOMMENDATIONS

This research investigated the use of the FWD equipment to determine the structural capacity of the pavement layers at the Virginia Smart Road. It also analyzed the variability of deflections on the wearing surface by measuring deflections at the different sensor positions. Effect of FWD plate size when conducting testing at subgrade and granular base was also studied. Four backcalculation software (EVERCALC, ELMOD, PEDMOD, and MICHBACK) were utilized to determine the moduli of the pavement at different testing temperatures. The laboratory resilient moduli of the granular base layer was compared to the backcalculated moduli. While laboratory determined moduli of the BM-25.0 layer was compared to the backcalculated moduli at 5 °C, 25 °C and 40 °C. Responses of pressure cells and strain gages, installed at different positions in the pavement layers, to the FWD loading were compared to theoretically calculated stresses and strains.

#### 8.1 FINDINGS

Based on this research, the following findings were made:

- The subgrade could be modeled as linear elastic for most of the sections. The presence of stiff layer was detected in Sections E, F, G, J, K and L, however, since the first seven sections were built on a fill, the presence of large rocks was possible
- The backcalculated resilient moduli from FWD deflection data using the small plate loading are higher than the values obtained from the large plate for all sections. The bulk stress developed under the small plate is higher for the same load on the plate.
- There was good agreement between the estimated depth to bedrock and ELSYM5 software results using maximum deflection from the FWD large plate.
- Deflection results from the first sensor ( $D_0$ ) is enough for assessing the variability of deflections on the wearing surface. However, the results of statistical analysis of deflections from different sensor distances showed that the last sensor produced the highest coefficient of variation.
- The four backcalculation software evaluated in this study produced different results. At cold temperatures, it was difficult to get reasonable results for the

wearing surface moduli because RMSE values were more than 40% for some of the software. Because they produced repeatable and reasonable results, the EVERCALC and ELMOD software were selected for further analysis.

- Granular layers of 75mm or less may need to be combined with other layers during the backcalculation process, similarly for thin HMA wearing surface layers.
- Results of the statistical analysis of deflections between and within the test sections showed that the lowest COV's of 26% in deflections was obtained during low temperatures (up to 10°C) while the highest COV's, 42%, were produced at temperatures between 25 and 40°C.
- Backcalculated moduli of granular materials can be correlated to laboratory-measured moduli obtained using the k- $\theta$  model.
- Due to the viscoelastic nature of the HMA, the difference between backcalculated moduli (using the four software) and laboratory-measured ones increases with increasing temperature.
- A deflection-temperature correction model was developed and validated at the Virginia Smart Road for temperatures ranging from 5 to 35 °C.
- Three analytical methods (linear elastic, viscoelastic, viscoelastic combined with nonlinearity) were evaluated for predicting in situ stresses and strains. The viscoelastic combined with nonlinearity showed the best agreement with measured tensile strain.
- The mix type and binder grade of the HMA have an effect on measured and calculated strains.

## **8.2 CONCLUSIONS**

Based on objectives set out on this research, the following conclusions were drawn.

- Mathematical modeling of nonlinear behavior of granular materials and the incorporation of a temperature correction for HMA wearing surface improve the prediction of stresses and strains within the pavement system.
- The moduli of the unbound granular layers were estimated using the FWD small and large plate. Results of the large plate were used in subsequent backcalculation analysis because of high resultant stress when the small plate is used.

- Variation (spatial and temporal) exists in the measured deflections due to different material designs and effects of temperature between and within sections. A deflection temperature model was developed as a result of this to enable the comparison of different sections.
- Four software were compared and used in the determination of moduli of the pavement layers at different temperatures. The EVERCALC and ELMOD software were selected as the most suitable software for determining the reasonable moduli of the pavement layers for the Virginia Smart Road.
- A correlation existed between the backcalculated moduli and laboratory-measured moduli for pavement materials. For granular materials, laboratory and backcalculated results from the k- $\theta$  model were comparable if a representative state of stress was specified. For the hot-mix asphalt samples, the ratios of the backcalculated to laboratory determined moduli were temperature and loading frequency dependent. The difference in the loading period between laboratory testing and FWD load pulse, affects the materials calculated resilient modulus.

### **8.3 RECOMMENDATIONS**

Based on this study, the following recommendations are made:

- Further research should be conducted to optimize the number of FWD testing points per unit length. This is expected to be a project type dependent.
- Research investigation of laboratory-measured HMA resilient modulus need to be conducted. This may result in modifying the current procedures to reflect field loading conditions or developing accurate shift factors between laboratory-measured and field-backcalculated resilient moduli.
- Develop an appropriate universal temperature correction model that can be used for different HMA layers and mixes.
- Develop a resilient modulus backcalculation approach capable of calculating pavement stresses and strains utilizing the viscoelastic properties of HMA and the nonlinearity of granular materials.
- Further validation of FWD measurements using embedded instruments to calibrate analytical models.

**APPENDIX A**  
**SAS OUTPUT**

**data** FWD;  
Input section \$1 temp deflection;  
Title 'FWD Deflection-WITHIN SECTIONS';  
CARDS;  
A 1 42.9  
A 1 64.8  
A 1 51.6  
A 1 56.9  
A 1 45.7  
A 2 45.2  
A 2 66.5  
A 2 51.6  
A 2 55.4  
A 2 55.1  
A 3 43.6  
A 3 57.2  
A 3 59.7  
A 3 58.7  
A 3 58.4  
A 4 58.7  
A 4 112  
A 4 113  
A 4 116  
A 4 115  
A 5 107.7  
A 5 75.2  
A 5 85.6  
A 5 92.2  
A 5 92.5  
A 6 38.6  
A 6 42.2  
A 6 44.2  
A 6 68.3  
A 6 57.2  
A 7 73.0  
A 7 55.9  
A 7 56.4  
A 7 61.0  
A 7 57.4  
B 1 33.0  
B 1 41.7  
B 1 52.6  
B 1 35.6  
B 1 32.0  
B 2 34.8  
B 2 45.5  
B 2 56.1  
B 2 39.4  
B 2 38.4

B 3 35.2  
B 3 46.7  
B 3 56.4  
B 3 43.4  
B 3 37.9  
B 4 47.3  
B 4 111.0  
B 4 79.2  
B 4 88.4  
B 4 85.1  
B 5 85.2  
B 5 87.4  
B 5 70.4  
B 5 69.6  
B 5 70.4  
B 6 29.7  
B 6 33.8  
B 6 38.9  
B 6 34.5  
B 6 32.5  
B 7 62.7  
B 7 49.0  
B 7 67.3  
B 7 47.0  
B 7 44.5  
C 1 44.4  
C 1 41.9  
C 1 41.4  
C 1 47.5  
C 1 35.8  
C 2 46.6  
C 2 41.9  
C 2 42.9  
C 2 45.2  
C 2 42.4  
C 3 49.1  
C 3 44.45  
C 3 45.7  
C 3 45.2  
C 3 39.6  
C 4 64.4  
C 4 95.8  
C 4 94.2  
C 4 101.1  
C 4 98.8  
C 5 108.4  
C 5 75.2  
C 5 78.4  
C 5 73.4  
C 5 79.5  
C 6 44.0

C 6 42.4  
C 6 36.6  
C 6 31.0  
C 6 29.2  
C 7 81.0  
C 7 52.3  
C 7 51.1  
C 7 51.3  
C 7 50.3  
D 1 30.0  
D 1 35.6  
D 1 56.6  
D 1 37.8  
D 1 39.6  
D 2 32.3  
D 2 43.4  
D 2 56.9  
D 2 42.9  
D 2 40.9  
D 3 32.4  
D 3 46.9  
D 3 70.63  
D 3 43.2  
D 3 41.15  
D 4 49.5  
D 4 98.3  
D 4 124  
D 4 94.5  
D 4 89.9  
D 5 106.7  
D 5 94  
D 5 90.7  
D 5 84.6  
D 5 78.0  
D 6 30.5  
D 6 39.1  
D 6 37.6  
D 6 36.1  
D 6 33.3  
D 7 59.9  
D 7 60.5  
D 7 62.0  
D 7 52.6  
D 7 48.3  
E 1 37.3  
E 1 67.3  
E 1 41.9  
E 1 53.3  
E 1 41.9  
E 2 38.6  
E 2 48.5

E 2 40.4  
E 2 39.4  
E 2 40.1  
E 3 40.1  
E 3 55.8  
E 3 54.4  
E 3 53.1  
E 3 44.7  
E 4 53.8  
E 4 96  
E 4 106.2  
E 4 95.3  
E 4 83.8  
E 5 110.8  
E 5 82.6  
E 5 88.1  
E 5 106.9  
E 5 80.5  
E 6 36.1  
E 6 35.1  
E 6 48.3  
E 6 32.5  
E 6 32.5  
E 7 69.6  
E 7 53.6  
E 7 66.8  
E 7 51.8  
E 7 50.8  
F 1 39.7  
F 1 43.7  
F 1 50.5  
F 1 59.4  
F 1 42.4  
F 2 42.6  
F 2 49.3  
F 2 54.1  
F 2 58.2  
F 2 56.4  
F 3 43.0  
F 3 59.6  
F 3 58.7  
F 3 60.5  
F 3 67.8  
F 4 56.1  
F 4 114.3  
F 4 102.6  
F 4 108.2  
F 4 102.9  
F 5 110.3  
F 5 97.8  
F 5 81.5

F 5 92.7  
F 5 77.2  
F 6 38.7  
F 6 35.8  
F 6 55.1  
F 6 32.8  
F 6 46.0  
F 7 48.2  
F 7 53.6  
F 7 66.8  
F 7 51.8  
F 7 59.5  
G 1 57.5  
G 1 64.3  
G 1 67.8  
G 1 68.6  
G 1 88.1  
G 2 53.9  
G 2 70.1  
G 2 66.0  
G 2 77.7  
G 2 62.2  
G 3 53.0  
G 3 72.4  
G 3 71.1  
G 3 87.9  
G 3 62.9  
G 4 70.2  
G 4 112  
G 4 113  
G 4 135  
G 4 114  
G 5 118.7  
G 5 91.4  
G 5 81.8  
G 5 93.2  
G 5 84.1  
G 6 43.0  
G 6 53.6  
G 6 48  
G 6 65.3  
G 6 52.3  
G 7 83.7  
G 7 63.0  
G 7 68.6  
G 7 82.3  
G 7 71.6  
H 1 45.0  
H 1 51.6  
H 1 50  
H 1 37.8

H 1 52.1  
H 2 51.0  
H 2 69.6  
H 2 52.6  
H 2 52.6  
H 2 54.9  
H 3 48.8  
H 3 58.7  
H 3 58.2  
H 3 60.5  
H 3 51.5  
H 4 66.7  
H 4 120  
H 4 98  
H 4 87.6  
H 4 108.5  
H 5 108.5  
H 5 89.9  
H 5 79.8  
H 5 91.9  
H 5 78  
H 6 39.3  
H 6 36.6  
H 6 34.8  
H 6 43.9  
H 6 48.5  
H 7 82.5  
H 7 64.5  
H 7 54.4  
H 7 57.9  
H 7 59.9  
I 1 44.4  
I 1 43.9  
I 1 49.0  
I 1 43.9  
I 1 47.5  
I 2 49.6  
I 2 53.1  
I 2 48  
I 2 56.1  
I 2 46  
I 3 47.8  
I 3 56.4  
I 3 51.1  
I 3 60.4  
I 3 51.1  
I 4 66.4  
I 4 114.3  
I 4 107.7  
I 4 118.6  
I 4 104.4

I 5 126.3  
I 5 91.9  
I 5 103.4  
I 5 89.2  
I 5 82.0  
I 6 42.2  
I 6 41.4  
I 6 41.9  
I 6 34.3  
I 6 44.7  
I 7 42.2  
I 7 41.4  
I 7 41.9  
I 7 34.3  
I 7 62.2  
J 1 47.2  
J 1 67.3  
J 1 56.9  
J 1 56.6  
J 1 58.4  
J 2 53.1  
J 2 67.3  
J 2 70.9  
J 2 68.3  
J 2 71.4  
J 3 57.9  
J 3 69.1  
J 3 84.33  
J 3 76.4  
J 3 74.6  
J 4 81.0  
J 4 125.5  
J 4 180.6  
J 4 165.1  
J 4 175.5  
J 5 172.2  
J 5 109.7  
J 5 138.4  
J 5 173.7  
J 5 176.5  
J 6 44.9  
J 6 65  
J 6 53.8  
J 6 53.6  
J 6 56.9  
J 7 115.6  
J 7 61.2  
J 7 62.2  
J 7 53.3  
J 7 62.2  
K 1 60.3

K 1 56.1  
K 1 61.7  
K 1 65.3  
K 1 84.3  
K 2 67.3  
K 2 63.4  
K 2 62.5  
K 2 76.2  
K 2 82.3  
K 3 65.9  
K 3 59.4  
K 3 70.36  
K 3 70.36  
K 3 71.12  
K 4 85.0  
K 4 145.3  
K 4 128.5  
K 4 129.8  
K 4 155.2  
K 5 172  
K 5 128.5  
K 5 117.6  
K 5 123.7  
K 5 127  
K 6 57.4  
K 6 47.0  
K 6 57.2  
K 6 67.3  
K 6 59.7  
K 7 114.7  
K 7 80.8  
K 7 91.9  
K 7 105.7  
K 7 92.5  
L 1 68.5  
L 1 82  
L 1 101.6  
L 1 70.4  
L 1 73.2  
L 2 76.6  
L 2 96.8  
L 2 75.4  
L 2 71.6  
L 2 79.5  
L 3 73.8  
L 3 91.7  
L 3 94.91  
L 3 103.9  
L 3 82.81  
L 4 94.8  
L 4 188

L 4 197.9  
 L 4 150.9  
 L 4 159.8  
 L 5 155.1  
 L 5 178  
 L 5 150.4  
 L 5 118.9  
 L 5 133.9  
 L 6 59.5  
 L 6 75.9  
 L 6 88.9  
 L 6 63.2  
 L 6 59.2  
 L 7 126.7  
 L 7 96.3  
 L 7 102.6  
 L 7 118.4  
 L 7 95.3

```
proc glm;
class section temp;
model deflection=section temp/ss3;
means section/lsd;
quit;
```

**FWD Deflection 23:55 Thursday, September 13, 2001 1**

The GLM Procedure

Class Level Information

Class	Levels	Values
section	12	A B C D E F G H I J K L
date	7	1 2 3 4 5 6 7

Number of observations **420**

FWD Deflection **23:55 Thursday, September 13, 2001 2**

The GLM Procedure

Dependent Variable: deflection

Source	DF	Sum of Squares	Mean Square	F Value	Pr > F
Model	17	323644.0399	19037.8847	82.79	.0001
Error	402	92440.1364	229.9506		
Corrected Total	419	416084.1764			

R-Square	Coeff Var	Root MSE	deflection Mean
<b>0.777833</b>	<b>21.61427</b>	<b>15.16412</b>	<b>70.15790</b>

Source	DF	Type III SS	Mean Square	F Value	Pr > F
section	11	97721.2119	8883.7465	38.63	<.0001
temp	6	225922.8280	37653.8047	163.75	<.0001

FWD Deflection **23:55** Thursday, September **13, 2001** **3**

The GLM Procedure

t Tests (LSD) for deflection

NOTE: This test controls the Type I comparisonwise error rate, not the experimentwise error rate.

Alpha **0.05**  
 Error Degrees of Freedom **402**  
 Error Mean Square **229.9506**  
 Critical Value of t **1.96588**  
 Least Significant Difference **7.1262**

Means with the same letter are not significantly different.

t Grouping	Mean	N	section
A	<b>104.469</b>	<b>35</b>	L
B	<b>88.761</b>	<b>35</b>	J
B	<b>88.667</b>	<b>35</b>	K
C	<b>76.237</b>	<b>35</b>	G
D	<b>66.726</b>	<b>35</b>	A
D	<b>64.174</b>	<b>35</b>	H
E D	<b>63.366</b>	<b>35</b>	F
E D F	<b>62.257</b>	<b>35</b>	I
E F	<b>59.369</b>	<b>35</b>	E
E G F	<b>57.725</b>	<b>35</b>	D
G F	<b>56.927</b>	<b>35</b>	C

G  
G 53.217 35 B

data FWD;  
Input section temp deflection;  
Title 'FWD Center Deflection';  
CARDS;

1 1 42.9  
1 2 45.2  
1 3 43.6  
1 4 58.7  
1 5 76.6  
1 6 107.7  
1 7 38.6  
1 8 73.8  
1 9 73.0  
2 1 33.0  
2 2 34.8  
2 3 35.2  
2 4 47.3  
2 5 63.0  
2 6 85.2  
2 7 29.7  
2 8 58.8  
2 9 62.7  
3 1 44.4  
3 2 46.6  
3 3 49.1  
3 4 64.4  
3 5 78.6  
3 6 108.4  
3 7 44.0  
3 8 68.8  
3 9 81.0  
4 1 30.0  
4 2 32.3  
4 3 32.4  
4 4 49.5  
4 5 66.7  
4 6 106.7  
4 7 30.5  
4 8 62.2  
4 9 59.9  
5 1 37.3  
5 2 38.6  
5 3 40.1  
5 4 53.8  
5 5 69.0  
5 6 110.8  
5 7 36.1  
5 8 66.4  
5 9 69.6

6 1 39.7  
6 2 42.6  
6 3 43.0  
6 4 56.1  
6 5 73.4  
6 6 110.3  
6 7 38.7  
6 8 61.5  
6 9 48.2  
7 1 57.5  
7 2 53.9  
7 3 53.0  
7 4 70.2  
7 5 89.6  
7 6 118.7  
7 7 43.0  
7 8 77.3  
7 9 83.7  
8 1 45.0  
8 2 51.0  
8 3 48.8  
8 4 66.7  
8 5 84.7  
8 6 108.5  
8 7 39.3  
8 8 78.1  
8 9 82.5  
9 1 44.5  
9 2 49.6  
9 3 47.8  
9 4 66.4  
9 5 88.4  
9 6 126.3  
9 7 42.2  
9 8 88.2  
9 9 85.6  
10 1 47.2  
10 2 53.1  
10 3 57.9  
10 4 81.0  
10 5 105.5  
10 6 172.2  
10 7 44.9  
10 8 108.6  
10 9 115.6  
11 1 60.3  
11 2 67.3  
11 3 65.9  
11 4 85.0  
11 5 115.3  
11 6 172.0

```

11 7 57.4
11 8 123.5
11 9 114.7
12 1 68.5
12 2 76.6
12 3 73.8
12 4 94.8
12 5 115.7
12 6 155.1
12 7 59.5
12 8 89.9
12 9 126.7

```

```

proc glm;
class section date;
model deflection=section temp/ss3;
means section/lsd;
Contrast '1 vs 2'section 1 -1 0 0 0 0 0 0 0 0 0 0 0;
Contrast '1 vs 3'section 1 0 -1 0 0 0 0 0 0 0 0 0;
Contrast '2 vs 3'section 0 -1 1 0 0 0 0 0 0 0 0 0;
Contrast '3 vs 4'section 0 0 -1 1 0 0 0 0 0 0 0 0;
Contrast '2 vs 4'section 0 -1 0 1 0 0 0 0 0 0 0 0;
run;
quit;

```

FWD Deflection 14:49 Thursday, August 30, 2001 1

The GLM Procedure

Class Level Information

Class	Levels	Values
section	12	1 2 3 4 5 6 7 8 9 10 11 12
date	9	1 2 3 4 5 6 7 8 9

Number of observations 108

FWD Deflection 14:49 Thursday, August 30, 2001 2

The GLM Procedure

Dependent Variable: deflection

Source	DF	Sum of Squares	Mean Square	F Value	Pr > F
Model	19	92137.86093	4849.36110	67.41	<.0001
Error	88	6330.90537	71.94211		

Corrected Total **107 98468.76630**

R-Square **0.935706**    Coeff Var **12.21552**    Root MSE **8.481869**    deflection Mean **69.43519**

Source	DF	Type III SS	Mean Square	F Value	Pr > F
section	<b>11</b>	<b>24665.48630</b>	<b>2242.31694</b>	<b>31.17</b>	<b>&lt;.0001</b>
temp	<b>8</b>	<b>67472.37463</b>	<b>8434.04683</b>	<b>117.23</b>	<b>&lt;.0001</b>

FWD Deflection **14:49** Thursday, August **30, 2001 3**

The GLM Procedure

t Tests (LSD) for deflection

NOTE: This test controls the Type I comparisonwise error rate, not the experimentwise error rate.

Alpha **0.05**  
 Error Degrees of Freedom **88**  
 Error Mean Square **71.94211**  
 Critical Value of t **1.98729**  
 Least Significant Difference **7.946**

Means with the same letter are not significantly different.

t Grouping	Mean	N	section
A	<b>95.711</b>	<b>9</b>	<b>11</b>
A			
A	<b>95.622</b>	<b>9</b>	<b>12</b>
B	<b>87.333</b>	<b>9</b>	<b>10</b>
C	<b>71.878</b>	<b>9</b>	<b>7</b>
C			
C	<b>71.000</b>	<b>9</b>	<b>9</b>
C			
D	<b>67.178</b>	<b>9</b>	<b>8</b>
D			
D	<b>65.033</b>	<b>9</b>	<b>3</b>
D			
			E
			E

D	F	E	<b>62.233</b>	<b>9</b>	<b>1</b>
	F	E			
G	F	E	<b>57.967</b>	<b>9</b>	<b>5</b>
G	F				
G	F	H	<b>57.056</b>	<b>9</b>	<b>6</b>
G		H			
G		H	<b>52.244</b>	<b>9</b>	<b>4</b>
		H			
		H	<b>49.967</b>	<b>9</b>	<b>2</b>

FWD Deflection **14:49** Thursday, August **30, 2001** **4**  
The GLM Procedure

Dependent Variable: deflection

Contrast	DF	Contrast SS	Mean Square	F Value	Pr > F
<b>1 vs 2</b>	<b>1</b>	<b>677.120000</b>	<b>677.120000</b>	<b>9.41</b>	<b>0.0029</b>
<b>1 vs 3</b>	<b>1</b>	<b>35.280000</b>	<b>35.280000</b>	<b>0.49</b>	<b>0.4856</b>
<b>2 vs 3</b>	<b>1</b>	<b>1021.520000</b>	<b>1021.520000</b>	<b>14.20</b>	<b>0.0003</b>
<b>3 vs 4</b>	<b>1</b>	<b>736.000556</b>	<b>736.000556</b>	<b>10.23</b>	<b>0.0019</b>

FWD Deflection **14:49** Thursday, August **30, 2001** **5**

The GLM Procedure

Class Level Information

Class	Levels	Values
section	<b>12</b>	<b>1 2 3 4 5 6 7 8 9 10 11 12</b>
date	<b>9</b>	<b>1 2 3 4 5 6 7 8 9</b>

Number of observations **108**

FWD Deflection **14:49** Thursday, August **30, 2001** **6**

The GLM Procedure

Dependent Variable: deflection

Source	DF	Sum of Squares	Mean Square	F Value	Pr > F
Model	<b>19</b>	<b>92137.86093</b>	<b>4849.36110</b>	<b>67.41</b>	<b>&lt;.0001</b>
Error	<b>88</b>	<b>6330.90537</b>	<b>71.94211</b>		



G	F	E	57.967	9	5
G	F				
G	F	H	57.056	9	6
G		H			
G		H	52.244	9	4
		H			
		H	49.967	9	2

FWD Deflection 14:49 Thursday, August 30, 2001 8

The GLM Procedure

Dependent Variable: deflection

Contrast	DF	Contrast SS	Mean Square	F Value	Pr > F
1 vs 2	1	677.120000	677.120000	9.41	0.0029
1 vs 3	1	35.280000	35.280000	0.49	0.4856
2 vs 3	1	1021.520000	1021.520000	14.20	0.0003
3 vs 4	1	736.000556	736.000556	10.23	0.0019
2 vs 4	1	23.347222	23.347222	0.32	0.5704

**data** FWD;  
Input section temp deflection;  
Title 'FWD Deflection-Fifth Sensor';  
CARDS;  
1 1 22.9  
1 2 25.9  
1 3 25.7  
1 4 27.5  
1 5 29.4  
1 6 27.9  
1 7 24.7  
1 8 25.2  
1 9 30.1  
2 1 18.1  
2 2 18.8  
2 3 18.9  
2 4 19.3  
2 5 19.5  
2 6 20.3  
2 7 17.2  
2 8 17.3  
2 9 23.1  
3 1 24.3  
3 2 24.1  
3 3 25.0  
3 4 24.6  
3 5 25.0  
3 6 23.6  
3 7 25.2  
3 8 20.6  
3 9 23.1  
4 1 18.3  
4 2 18.8  
4 3 19.0  
4 4 21.9  
4 5 22.4  
4 6 21.9  
4 7 18.6  
4 8 20.6  
4 9 27.9  
5 1 21.6  
5 2 22.4  
5 3 22.9  
5 4 23.6  
5 5 24.3  
5 6 24.2  
5 7 22.0  
5 8 21.5  
5 9 24.2

6 1 21.7  
6 2 22.2  
6 3 22.9  
6 4 24.4  
6 5 25.7  
6 6 26.0  
6 7 21.2  
6 8 21.9  
6 9 27.3  
7 1 27.0  
7 2 26.8  
7 3 25.7  
7 4 28.5  
7 5 31.5  
7 6 31.6  
7 7 24.9  
7 8 29.2  
7 9 32.0  
8 1 25.3  
8 2 27.7  
8 3 26.8  
8 4 28.5  
8 5 30.7  
8 6 31.2  
8 7 24.1  
8 8 28.1  
8 9 30.8  
9 1 27.2  
9 2 29.3  
9 3 30.0  
9 4 29.5  
9 5 30.7  
9 6 32.1  
9 7 25.7  
9 8 28.4  
9 9 32.6  
10 1 26.4  
10 2 30.2  
10 3 32.2  
10 4 34.4  
10 5 35.3  
10 6 33.8  
10 7 27.8  
10 8 31.3  
10 9 38.8  
11 1 37.5  
11 2 37.6  
11 3 35.1  
11 4 33.2  
11 5 34.0  
11 6 34.5

11 7 33.8  
 11 8 34.8  
 11 9 34.1  
 12 1 34.7  
 12 2 31.0  
 12 3 34.6  
 12 4 36.4  
 12 5 37.2  
 12 6 35.3  
 12 7 31.7  
 12 8 30.1  
 12 9 39.5

```
proc glm;
class section temp;
model deflection=section temp/ss3;
means section/lcd;
run;
quit;
```

**FWD Deflection** 18:17 Sunday, September 9, 2001 1

The GLM Procedure

Class Level Information

Class	Levels	Values
section	12	1 2 3 4 5 6 7 8 9 10 11 12
temp	9	1 2 3 4 5 6 7 8 9

Number of observations 108

FWD Deflection 18:17 Sunday, September 9, 2001 2

The GLM Procedure

Dependent Variable: deflection

Source	DF	Sum of Squares	Mean Square	F Value	Pr > F
Model	19	2807.592222	147.768012	64.14	<.0001
Error	88	202.734444	2.303801		
Corrected Total	107	3010.326667			



E 23.7000 9 6  
 E  
 E 22.9667 9 5  
 F 21.0444 9 4  
 G 19.1667 9 2

FWD Deflection 18:17 Sunday, September 9, 2001 4

The GLM Procedure

Class Level Information

Class	Levels	Values
section	12	1 2 3 4 5 6 7 8 9 10 11 12
temp	9	1 2 3 4 5 6 7 8 9

Number of observations 108

FWD Deflection 18:17 Sunday, September 9, 2001 5

The GLM Procedure

Dependent Variable: deflection

Source	DF	Sum of Squares	Mean Square	F Value	Pr > F
Model	19	2784.712222	146.563801	57.17	<.0001
Error	88	225.614444	2.563801		
Corrected Total	107	3010.326667			

R-Square	Coeff Var	Root MSE	deflection Mean
0.925053	5.932764	1.601187	26.98889

Source	DF	Type III SS	Mean Square	F Value	Pr > F
section	11	2425.675556	220.515960	86.01	<.0001
temp	8	359.036667	44.879583	17.51	<.0001

FWD Deflection 18:17 Sunday, September 9, 2001 6

The GLM Procedure

t Tests (LSD) for deflection

NOTE: This test controls the Type I comparisonwise error rate, not the experimentwise error rate.

Alpha **0.05**  
 Error Degrees of Freedom **88**  
 Error Mean Square **2.563801**  
 Critical Value of t **1.98729**  
 Least Significant Difference **1.5**

Means with the same letter are not significantly different.

t Grouping	Mean	N	section
A	<b>34.5000</b>	<b>9</b>	<b>12</b>
A			
B A	<b>33.5000</b>	<b>9</b>	<b>11</b>
B			
B	<b>32.2444</b>	<b>9</b>	<b>10</b>
C	<b>29.5000</b>	<b>9</b>	<b>9</b>
C			
C	<b>28.5778</b>	<b>9</b>	<b>7</b>
C			
C	<b>28.1333</b>	<b>9</b>	<b>8</b>
D	<b>26.5889</b>	<b>9</b>	<b>1</b>
E	<b>23.9444</b>	<b>9</b>	<b>3</b>
E			
E	<b>23.7000</b>	<b>9</b>	<b>6</b>
E			
E	<b>22.9667</b>	<b>9</b>	<b>5</b>
F	<b>21.0444</b>	<b>9</b>	<b>4</b>
G	<b>19.1667</b>	<b>9</b>	<b>2</b>

FWD Deflection 18:17 Sunday, September 9, 2001 7

The GLM Procedure

Class Level Information

Class	Levels	Values
section	12	1 2 3 4 5 6 7 8 9 10 11 12
temp	9	1 2 3 4 5 6 7 8 9

Number of observations 108

FWD Deflection 18:17 Sunday, September 9, 2001 8

The GLM Procedure

Dependent Variable: deflection

Source	DF	Sum of Squares	Mean Square	F Value	Pr > F
Model	19	2834.796759	149.199829	58.33	<.0001
Error	88	225.075370	2.557675		
Corrected Total	107	3059.872130			

R-Square	Coeff Var	Root MSE	deflection Mean
0.926443	5.917349	1.599273	27.02685

Source	DF	Type III SS	Mean Square	F Value	Pr > F
section	11	2480.778796	225.525345	88.18	<.0001
date	8	354.017963	44.252245	17.30	<.0001

FWD Deflection 18:17 Sunday, September 9, 2001 9

The GLM Procedure

t Tests (LSD) for deflection

NOTE: This test controls the Type I comparisonwise error rate, not the experimentwise error rate.

Alpha **0.05**  
 Error Degrees of Freedom **88**  
 Error Mean Square **2.557675**  
 Critical Value of t **1.98729**  
 Least Significant Difference **1.4982**

Means with the same letter are not significantly different.

t Grouping	Mean	N	section
A	<b>34.5000</b>	<b>9</b>	<b>12</b>
A			
A	<b>33.9556</b>	<b>9</b>	<b>11</b>
B	<b>32.2444</b>	<b>9</b>	<b>10</b>
C	<b>29.5000</b>	<b>9</b>	<b>9</b>
C			
C	<b>28.5778</b>	<b>9</b>	<b>7</b>
C			
C	<b>28.1333</b>	<b>9</b>	<b>8</b>
D	<b>26.5889</b>	<b>9</b>	<b>1</b>
E	<b>23.9444</b>	<b>9</b>	<b>3</b>
E			
E	<b>23.7000</b>	<b>9</b>	<b>6</b>
E			
E	<b>22.9667</b>	<b>9</b>	<b>5</b>
F	<b>21.0444</b>	<b>9</b>	<b>4</b>
G	<b>19.1667</b>	<b>9</b>	<b>2</b>

FWD Deflection **18:17** Sunday, September **9, 2001 10**

The GLM Procedure

Class Level Information

Class	Levels	Values
section	<b>12</b>	<b>1 2 3 4 5 6 7 8 9 10 11 12</b>
temp	<b>9</b>	<b>1 2 3 4 5 6 7 8 9</b>

Number of observations **108**

FWD Deflection 18:17 Sunday, September 9, 2001 11

The GLM Procedure

Dependent Variable: deflection

Source	DF	Sum of Squares	Mean Square	F Value	Pr > F
Model	19	2914.017870	153.369362	54.96	<.0001
Error	88	245.589815	2.790793		
Corrected Total	107	3159.607685			

R-Square	Coeff Var	Root MSE	deflection Mean
0.922272	6.165506	1.670567	27.09537

Source	DF	Type III SS	Mean Square	F Value	Pr > F
section	11	2588.901019	235.354638	84.33	<.0001
temp	8	325.116852	40.639606	14.56	<.0001

FWD Deflection 18:17 Sunday, September 9, 2001 12

The GLM Procedure

t Tests (LSD) for deflection

NOTE: This test controls the Type I comparisonwise error rate, not the experimentwise error rate.

Alpha	0.05
Error Degrees of Freedom	88
Error Mean Square	2.790793
Critical Value of t	1.98729
Least Significant Difference	1.565

Means with the same letter are not significantly different.

t Grouping	Mean	N	section
A	34.7778	9	11
A			

A	34.5000	9	12
B	32.2444	9	10
C	29.5000	9	9
C			
C	28.5778	9	7
C			
D C	28.1333	9	8
D			
D	26.5889	9	1
E	23.9444	9	3
E			
E	23.7000	9	6
E			
E	22.9667	9	5
F	21.0444	9	4
G	19.1667	9	2

FWD Deflection 18:17 Sunday, September 9, 2001 13

The GLM Procedure

Class Level Information

Class	Levels	Values
section	12	1 2 3 4 5 6 7 8 9 10 11 12
temp	9	1 2 3 4 5 6 7 8 9

Number of observations 108  
 FWD Deflection 18:17 Sunday, September 9, 2001 14

The GLM Procedure

Dependent Variable: deflection

Source	DF	Sum of Squares	Mean Square	F Value	Pr > F
Model	19	2934.320093	154.437900	54.94	<.0001
Error	88	247.358704	2.810894		
Corrected Total	107	3181.678796			

R-Square	Coeff Var	Root MSE	deflection Mean
<b>0.922255</b>	<b>6.184289</b>	<b>1.676572</b>	<b>27.11019</b>

Source	DF	Type III SS	Mean Square	F Value	Pr > F
section	<b>11</b>	<b>2613.745463</b>	<b>237.613224</b>	<b>84.53</b>	<b>&lt;.0001</b>
temp	<b>8</b>	<b>320.574630</b>	<b>40.071829</b>	<b>14.26</b>	<b>&lt;.0001</b>

FWD Deflection **18:17** Sunday, September **9, 2001 15**

The GLM Procedure

t Tests (LSD) for deflection

NOTE: This test controls the Type I comparisonwise error rate, not the experimentwise error rate.

Alpha	<b>0.05</b>
Error Degrees of Freedom	<b>88</b>
Error Mean Square	<b>2.810894</b>
Critical Value of t	<b>1.98729</b>
Least Significant Difference	<b>1.5706</b>

Means with the same letter are not significantly different.

t Grouping	Mean	N	section
A	<b>34.9556</b>	<b>9</b>	<b>11</b>
A			
A	<b>34.5000</b>	<b>9</b>	<b>12</b>
B	<b>32.2444</b>	<b>9</b>	<b>10</b>
C	<b>29.5000</b>	<b>9</b>	<b>9</b>
C			
C	<b>28.5778</b>	<b>9</b>	<b>7</b>
C			
D C	<b>28.1333</b>	<b>9</b>	<b>8</b>
D			
D	<b>26.5889</b>	<b>9</b>	<b>1</b>
E	<b>23.9444</b>	<b>9</b>	<b>3</b>
E			
E	<b>23.7000</b>	<b>9</b>	<b>6</b>
E			
E	<b>22.9667</b>	<b>9</b>	<b>5</b>
F	<b>21.0444</b>	<b>9</b>	<b>4</b>

G 19.1667 9 2

data FWD;

Input section temp deflection;

Title 'FWD Deflection-Last Sensor';

CARDS;

1 1 7.6  
1 2 10.1  
1 3 10.0  
1 4 9.4  
1 5 8.9  
1 6 7.9  
1 7 10.9  
1 8 8.0  
1 9 9.3  
2 1 6.9  
2 2 6.8  
2 3 6.8  
2 4 6.7  
2 5 6.2  
2 6 5.2  
2 7 6.7  
2 8 5.1  
2 9 6.3  
3 1 7.9  
3 2 8.0  
3 3 8.1  
3 4 7.7  
3 5 7.9  
3 6 7.9  
3 7 8.4  
3 8 7.0  
3 9 8.6  
4 1 8.2  
4 2 8.3  
4 3 8.8  
4 4 8.4  
4 5 8.1  
4 6 7.9  
4 7 8.4  
4 8 7.0  
4 9 8.6  
5 1 8.9  
5 2 9.4  
5 3 9.4  
5 4 8.7  
5 5 8.1  
5 6 7.9  
5 7 9.2  
5 8 7.7  
5 9 8.1

6 1 7.0  
6 2 6.8  
6 3 6.9  
6 4 6.5  
6 5 6.2  
6 6 5.1  
6 7 7.6  
6 8 5.1  
6 9 6.4  
7 1 6.4  
7 2 6.8  
7 3 6.6  
7 4 6.1  
7 5 6.1  
7 6 5.1  
7 7 6.8  
7 8 5.4  
7 9 6.1  
8 1 12.0  
8 2 13.0  
8 3 13.2  
8 4 12.5  
8 5 13.0  
8 6 12.7  
8 7 11.5  
8 8 12.3  
8 9 12.2  
9 1 11.0  
9 2 11.3  
9 3 11.4  
9 4 11.2  
9 5 11.5  
9 6 12.7  
9 7 10.9  
9 8 11.1  
9 9 11.9  
10 1 8.6  
10 2 8.2  
10 3 8.5  
10 4 7.7  
10 5 7.7  
10 6 6.7  
10 7 8.5  
10 8 6.3  
10 9 7.3  
11 1 5.1  
11 2 4.6  
11 3 4.5  
11 4 5.0  
11 5 4.3  
11 6 4.0

11 7 7.8  
 11 8 4.1  
 11 9 4.4  
 12 1 10.0  
 12 2 9.7  
 12 3 10.0  
 12 4 8.6  
 12 5 9.4  
 12 6 8.1  
 12 7 9.5  
 12 8 8.0  
 12 9 9.0

```
proc glm;
class section temp;
model deflection=section temp/ss3;
means section/lsd;
run;
quit;
```

**FWD Deflection** 18:49 Sunday, September 9, 2001 1

The GLM Procedure

Class Level Information

Class	Levels	Values
section	12	1 2 3 4 5 6 7 8 9 10 11 12
temp	9	1 2 3 4 5 6 7 8 9

Number of observations 108

**FWD Deflection** 18:49 Sunday, September 9, 2001 2

The GLM Procedure

Dependent Variable: deflection

Source	DF	Sum of Squares	Mean Square	F Value	Pr > F
Model	19	504.1264815	26.5329727	76.12	<.0001
Error	88	30.6731481	0.3485585		
Corrected Total	107	534.7996296			

R-Square    Coeff Var    Root MSE    deflection Mean  
**0.942646    7.201485    0.590388    8.198148**

Source	DF	Type III SS	Mean Square	F Value	Pr > F
section	<b>11</b>	<b>479.3218519</b>	<b>43.5747138</b>	<b>125.01</b>	<b>&lt;.0001</b>
temp	<b>8</b>	<b>24.8046296</b>	<b>3.1005787</b>	<b>8.90</b>	<b>&lt;.0001</b>

FWD Deflection    **18:49** Sunday, September **9, 2001**    **3**

The GLM Procedure

t Tests (LSD) for deflection

NOTE: This test controls the Type I comparisonwise error rate, not the experimentwise error rate.

Alpha                            **0.05**  
Error Degrees of Freedom        **88**  
Error Mean Square                **0.348559**  
Critical Value of t                **1.98729**  
Least Significant Difference    **0.5531**

Means with the same letter are not significantly different.

t Grouping	Mean	N	section
A	<b>12.4889</b>	<b>9</b>	<b>8</b>
B	<b>11.4444</b>	<b>9</b>	<b>9</b>
C	<b>9.1444</b>	<b>9</b>	<b>12</b>
C			
C	<b>9.1222</b>	<b>9</b>	<b>1</b>
C			
D C	<b>8.6000</b>	<b>9</b>	<b>5</b>
D			
D E	<b>8.1889</b>	<b>9</b>	<b>4</b>
E			
E	<b>7.9444</b>	<b>9</b>	<b>3</b>
E			
E	<b>7.7222</b>	<b>9</b>	<b>10</b>
F	<b>6.4000</b>	<b>9</b>	<b>6</b>
F			
F	<b>6.3000</b>	<b>9</b>	<b>2</b>
F			
F	<b>6.1556</b>	<b>9</b>	<b>7</b>

G 4.8667 9 11

**APPENDIX B**  
**RESULTS OF MODULI BACKCALCULATION**

**Table B-1.** Backcalculated Moduli for selected Sections Using Different Software Packages for August 2000.

Sect.	Date	Software	Modulus (MPa)					Bedrock. Depth (m)
			WS+BM	OGDL	21-A	21-B	Subgrade.	
A	Aug-00	PEDMOD	9,528	1,283	4,551	364	351	15
		EVERCALC	6,347	932	10,350	380	552	15
		MICHBACK	26,910	1,380	12,655	414	380	21
		ELMOD4	3,767	1,014	6,928	255	863	--
B	Aug-00	PEDMOD	9,908	1,653	5,940	358	370	15
		EVERCALC	6,672	1,380	10,350	345	552	19
		MICHBACK	14,642	1,297	8,970	480	552	28
		ELMOD4	4,175	1,553	7,790	524	1,256	--
C	Aug-00	PEDMOD	7,921	1,380	4,030	244	280	15
		EVERCALC	6,486	1,380	10,350	311	380	--
		MICHBACK	18,092	759	10,350	476	587	--
		ELMOD4	3,222	1,559	6,155	1,484	987	--
D	Aug-00	PEDMOD	12,599	1,901	6,885	380	296	15
		EVERCALC	5,658	1,380	10,350	345	414	--
		MICHBACK	11,737	1,380	11,218	518	552	
		ELMOD4	3,250	1,249	13,469	380	904	--
E	Aug-00	PEDMOD	4,313	--	4,944	276	276	--
		EVERCALC	5,941	--	10,350	331	359	--
		MICHBACK	4,140	--	10,350	431	552	
		ELMOD4	3,064	--	5,078	1,173	952	--
F	Aug-00	PEDMOD	7,790	--	4,733	307	292	15
		EVERCALC	6,590	--	10,350	552	505	--
		MICHBACK	8,218	--	10,350	311	552	
		ELMOD4	3,802	--	6,672	1,415	704	--
G	Aug-00	PEDMOD	13,800	--	5,373	282	355	
		EVERCALC	6,286	--	4,830	552	290	
		MICHBACK	3,395	--	9,315	276	552	
		ELMOD4	3,402	--	7,217	484	368	
H	Aug-00	PEDMOD	4,933	1,380	5,373	282	392	6
		EVERCALC	5,575	1,380	10,350	380	552	--
		MICHBACK	10,764	1,311	4,830	276	332	
		ELMOD4	3,940	1,394	9,025	335	362	--

**Table B-2.** Backcalculated Moduli for selected Sections Using Different Software Packages for November 2000.

Sect.	Date	Software	Modulus (MPa)					Bedrock. Depth (m)
			WS+BM	OGDL	21-A	21-B	Subgrade.	
A	Nov-00	PEDMOD	13,800	1,242	10,550	310	379	15
		EVERCALC	6,453	1,028	5,237	329	552	15
		MICHBACK	15,525	1,380	13,800	483	345	21
		ELMOD4	21,673	1,773	17,195	297	400	--
B	Nov-00	PEDMOD	13,800	1311	8970	358	370	15
		EVERCALC	12,420	1,704	6,072	338	450	19
		MICHBACK	26,910	1,525	8,501	497	380	28
		ELMOD4	20,265	1,484	19,713	524	540	--
C	Nov-00	PEDMOD	13110	1173	9,315	355	380	15
		EVERCALC	8,280	966	6,900	290	414	--
		MICHBACK	20,776	1380	13,814	455	345	
		ELMOD4	17,212	3,959	14,223	503	441	--
D	Nov-00	PEDMOD	12,420	1242	6,990	353	400	15
		EVERCALC	10,350	1,725	6,976	246	552	--
		MICHBACK	26,910	1,380	15,180	483	345	
		ELMOD4	10,115	1,242	9,025	290	331	--
E	Nov-00	PEDMOD	13,800	--	5,278	450	420	--
		EVERCALC	7,280	--	5,175	248	414	--
		MICHBACK	26,910	--	4,830	483	345	
		ELMOD4	26,287	--	3,526	197	407	--
F	Nov-00	PEDMOD	13,800	--	4,733	351	378	15
		EVERCALC	8,632	--	4,761	331	311	--
		MICHBACK	19,016	--	4,830	483	345	
		ELMOD4	20,067	--	22,318	284	535	--
G	Nov-00	PEDMOD	12,424	--	6,111	282	355	
		EVERCALC	10,709	--	5,175	269	414	
		MICHBACK	6,845	--	8,218	207	345	
		ELMOD4	15,698	--	11,958	627	597	
H	Nov-00	PEDMOD	13,110	1,380	9,660	482	350	6
		EVERCALC	15,180	1,304	5,451	290	352	--
		MICHBACK	26,910	1,380	13,800	483	332	
		ELMOD4	8,197	787	7,735	368	362	--

**Table B-3.** Backcalculated Moduli for selected Sections Using Different Software Packages for January 2001.

Sect.	Date	Software	Modulus (MPa)					Bedrock. Depth (m)
			WS+BM	OGDL	21-A	21-B	Subgr.	
A	Jan-01	PEDMOD	13,800	1,242	10,550	310	379	15
		EVERCALC	10,522	1,104	5,382	329	552	15
		MICHBACK	26,910	1,380	10,640	483	345	21
		ELMOD4	16,554	1,415	16,225	265	350	--
B	Jan-01	PEDMOD	13,800	1311	8970	358	370	15
		EVERCALC	10,769	1,042	4,830	380	518	19
		MICHBACK	26,910	1,394	11,903	524	359	28
		ELMOD4	16,575	1,115	15,332	395	476	--
C	Jan-01	PEDMOD	13110	1173	9,315	355	380	15
		EVERCALC	9,735	1,380	10,350	414	552	--
		MICHBACK	26,910	1,380	13,814	455	345	
		ELMOD4	16,331	1,211	9,244	331	289	--
D	Jan-01	PEDMOD	12,420	1242	6,990	353	400	15
		EVERCALC	10,800	1,380	10,350	414	552	--
		MICHBACK	26,910	1,380	15,180	483	345	
		ELMOD4	14,167	2,629	12,703	329	331	--
E	Jan-01	PEDMOD	13,800	--	5,278	450	420	--
		EVERCALC	9,280	--	5,175	248	414	--
		MICHBACK	16,910	--	13,800	483	345	
		ELMOD4	11,121	--	20,071	573	507	--
F	Jan-01	PEDMOD	6,755	--	21,733	351	378	15
		EVERCALC	9,632	--	4,761	331	311	--
		MICHBACK	13,800	--	4,733	307	292	
		ELMOD4	7,756	--	20,318	384	435	--
G	Jan-01	PEDMOD	12,424	--	6,111	282	355	
		EVERCALC	10,709	--	5,175	269	414	
		MICHBACK	17,396	--	8,011	435	345	
		ELMOD4	11,298	--	11,958	527	597	
H	Jan-01	PEDMOD	13,110	1,380	9,660	482	350	6
		EVERCALC	12,180	1,304	5,451	290	352	--
		MICHBACK	26,910	1,380	4,830	483	332	
		ELMOD4	7,197	687	9,735	368	362	--

\*

**Table B-4.** Backcalculated Moduli for selected Sections Using Different Software for February 2001.

Sect.	Date	Software	Modulus (MPa)					Bedrock Depth (m)
			WS+BM	OGDL	21-A	21-B	Subgrade.	
A	Feb-01	PEDMOD	13,800	1,242	10,550	310	379	15
		EVERCALC	9,391	1,328	10,350	552	450	15
		MICHBACK	26,910	1,380	10,640	483	345	21
		ELMOD4	18,885	1,546	14,959	255	352	--
B	Feb-01	PEDMOD	13,800	1311	8970	358	370	15
		EVERCALC	10,861	1,380	10,350	400	552	19
		MICHBACK	26,910	1,394	11,903	524	359	28
		ELMOD4	17,630	1,290	17,153	455	476	--
C	Feb-01	PEDMOD	13110	1173	9,315	355	380	15
		EVERCALC	8,743	1,097	10,350	414	552	--
		MICHBACK	26,910	1,380	13,814	455	345	
		ELMOD4	10,981	1,488	16,141	348	487	--
D	Feb-01	PEDMOD	12,420	1242	6,990	353	400	15
		EVERCALC	12,289	1,380	10,350	359	552	--
		MICHBACK	26,910	1,380	15,180	483	345	
		ELMOD4	16,167	3,629	13,703	256	331	--
E	Feb-01	PEDMOD	13,800	--	5,278	450	420	--
		EVERCALC	7,459	--	10,350	345	552	--
		MICHBACK	26,910	--	13,800	483	345	
		ELMOD4	17,871	--	13,071	173	497	--
F	Feb-01	PEDMOD	13,800	--	4,733	351	378	15
		EVERCALC	10,288	--	13,800	483	505	--
		MICHBACK	13,800	--	4,733	307	292	
		ELMOD4	8,756	--	16,318	284	535	--
G	Feb-01	PEDMOD	12,424	--	6,111	282	355	
		EVERCALC	8,908	--	10,350	428	551	
		MICHBACK	19,396	--	8,011	435	345	
		ELMOD4	13,655	--	10,398	427	497	
H	Feb-01	PEDMOD	13,110	1,380	9,660	482	350	6
		EVERCALC	10,391	1,380	10,350	442	518	--
		MICHBACK	26,910	1,380	4,830	483	332	
		ELMOD4	7,128	683	11,735	319	442	--

**Table B-5.** Backcalculated Moduli for selected Sections Using Different Software for April 2001.

Sect.	Date	Software	Modulus (MPa)					Bedrock Depth (m)
			WS+BM	OGDL	21-A	21-B	Subgrade	
A	Apr-01	PEDMOD	10812	1,283	4,554	366	414	15
		EVERCALC	4,248	1,159	5,520	339	552	15
		MICHBACK	13,455	1,083	12,655	414	483	21
		ELMOD4	8,197	1,235	9,928	276	311	--
B	Apr-01	PEDMOD	9,757	1,656	5,941	359	380	15
		EVERCALC	5,755	1,339	17,250	345	515	19
		MICHBACK	9,757	1,380	12,655	455	380	28
		ELMOD4	8,867	2,125	9,210	242	380	--
C	Apr-01	PEDMOD	8,991	1,380	4,030	269	311	15
		EVERCALC	5,113	828	9,398	483	552	--
		MICHBACK	11,730	1,297	12,655	414	380	
		ELMOD4	9,412	2,108	8,855	348	487	--
D	Apr-01	PEDMOD	7,452	1,904	6,886	331	380	15
		EVERCALC	5,630	1,373	16,477	476	552	--
		MICHBACK	14,842	745	12,427	483	385	
		ELMOD4	10,115	1,242	9,025	290	331	--
E	Apr-01	PEDMOD	8,287	--	5,941	359	380	--
		EVERCALC	5,520	--	13,800	552	544	--
		MICHBACK	4,140	--	6,107	311	380	
		ELMOD4	8,872	--	7,313	1001	890	--
F	Apr-01	PEDMOD	10,626	--	4,030	269	311	15
		EVERCALC	5,521	--	12,420	524	550	--
		MICHBACK	3,774	--	10,150	276	552	
		ELMOD4	6,665	--	6,210	262	451	--
G	Apr-01	PEDMOD	13,800	--	4,733	311	290	
		EVERCALC	5,396	--	12,420	566	582	
		MICHBACK	16,719	--	6,210	414	345	
		ELMOD4	8,411	--	7,217	283	395	
H	Apr-01	PEDMOD	7,700	1,297	5,223	311	350	6
		EVERCALC	5,575	1,380	12,420	552	519	--
		MICHBACK	9,833	1,097	8,970	388	392	
		ELMOD4	10,219	1,242	9,025	345	332	--

**Table B-6.** Backcalculated Moduli for selected Sections Using Different Software for May 29th 2001.

Sect.	Date	Software	Modulus (MPa)					Bedrock. Depth (m)
			WS+BM	OGDL	21-A	21-B	Subgrade	
A	May-01	PEDMOD	4,242	1,380	32,837	290	290	15
		EVERCALC	4,202	1,346	12,420	452	522	15
		MICHBACK	15,801	1,076	13,800	483	345	21
		ELMOD4	3,229	1,001	14,697	745	464	--
B	May-01	PEDMOD	4,844	1,380	41,941	359	380	15
		EVERCALC	6,100	1,380	12,420	480	552	19
		MICHBACK	15,525	1,332	13,800	483	359	28
		ELMOD4	3,195	1,760	10,861	1,007	1,070	--
C	May-01	PEDMOD	3,222	690	35,928	455	455	15
		EVERCALC	6,289	1,056	12,420	422	512	--
		MICHBACK	15,891	1,076	13,807	483	345	
		ELMOD4	3,133	1,242	9,970	380	388	--
D	May-01	PEDMOD	7,217	1,380	41,393	345	345	15
		EVERCALC	5,354	1,380	12,420	405	520	--
		MICHBACK	21,218	835	13,800	490	345	
		ELMOD4	8,239	1,242	10,970	380	449	--
E	May-01	PEDMOD	3,671	--	34,493	355	355	--
		EVERCALC	6,803	--	5,520	482	552	--
		MICHBACK	7,086	--	10,226	552	483	
		ELMOD4	7,500	--	9,003	462	380	--
F	May-01	PEDMOD	4,740	--	17,250	373	373	15
		EVERCALC	6,803	--	5,520	452	450	--
		MICHBACK	4,830	--	13,800	483	552	
		ELMOD4	7,211	--	8,846	352	828	--
G	May-01	PEDMOD	4,292	--	7,362	311	311	
		EVERCALC	6,617	--	10,592	414	552	
		MICHBACK	4,140	--	13,800	483	345	
		ELMOD4	5,078	--	6,217	338	386	
H	May-01	PEDMOD	2,974	1,380	34,493	248	248	6
		EVERCALC	4,382	690	12,420	518	552	--
		MICHBACK	21,833	1,380	6,458	276	392	
		ELMOD4	5,575	1,242	9,833	1,063	573	--

**Table B-7.** Backcalculated Moduli for selected Sections Using Different Software Packages for July 7th 2001.

Sect.	Date	Software	Modulus (MPa)					Bedrock Depth (m)
			WS+BM	OGDL	21-A	21-B	Subgrade	
A	July-01	PEDMOD	2,160	1,463	17,250	317	317	15
		EVERCALC	3,002	840	10,350	552	380	15
		MICHBACK	14,624	690	13,621	348	414	21
		ELMOD4	2,746	1,242	12,420	311	835	--
B	July-01	PEDMOD	2,726	1,304	17,250	469	469	15
		EVERCALC	3809	1,242	10,350	552	380	19
		MICHBACK	14,028	800	15,156	304	483	28
		ELMOD4	1,884	1,573	12,903	718	745	--
C	July-01	PEDMOD	1,746	1,380	17,250	386	367	15
		EVERCALC	3,008	887	10,350	552	380	--
		MICHBACK	20,141	1,511	9,504	331	428	23
		ELMOD4	2,801	885	11,903	357	542	--
D	July-01	PEDMOD	2,795	690	17,250	424	424	15
		EVERCALC	2,070	1,377	10,350	552	380	--
		MICHBACK	7,790	904	22,000	345	414	22
		ELMOD4	3,209	932	21,038	311	647	--
E	July-01	PEDMOD	1,732		17,250	380	380	15
		EVERCALC	3,416		10,350	345	552	--
		MICHBACK	7,052		15,560	276	424	
		ELMOD4	2,015		20,735	932	477	--
F	July-01	PEDMOD	1,711		17,250	398	400	15
		EVERCALC	3,522		10,350	345	552	--
		MICHBACK	5,927		7,245	276	414	
		ELMOD4	1,628		17,416	449	582	--
G	July-01	PEDMOD	2,305		5,775	324	328	
		EVERCALC	2,070		4,323	345	552	
		MICHBACK	4,140		10,350	345	414	
		ELMOD4	2,070		11,275	400	384	
H	July-01	PEDMOD	2,477	1,449	17,250	262	260	15
		EVERCALC	2,228	1,241	12,551	276	450	--
		MICHBACK	4,692	1,594	12,875	345	424	
		ELMOD4	2,049	911	12,123	328	313	--

**Table B-8.** Backcalculated Moduli for selected Sections Using Different Software Packages for October 9th 2001.

Sect.	Date	Software	Modulus (MPa)					Bedrock Depth (m)
			WS+BM	OGDL	21-A	21-B	Subgrade	
A	Apr-01	PEDMOD	13,800	1,463	17,250	317	317	15
		EVERCALC	9,674	1,380	7,293	414	579	
		MICHBACK	13,800	1,380	17,250	443	433	21
		ELMOD4	10,536	725	25,772	311	449	--
B	Apr-01	PEDMOD	13,800	1,304	17,250	469	469	15
		EVERCALC	9,674	1,380	6,210	325	690	19
		MICHBACK	13,800	1,380	17,250	379	379	28
		ELMOD4	11,778	1,504	23,329	311	600	--
C	Apr-01	PEDMOD	13,800	1,380	17,250	386	367	15
		EVERCALC	10,792	690	13,110	325	690	--
		MICHBACK	13,800	1,380	17,250	493	493	23
		ELMOD4	10,992	828	18,540	497	580	--
D	Apr-01	PEDMOD	13,800	690	17,250	424	424	15
		EVERCALC	20,403	1,045	22,305	414	690	--
		MICHBACK	7,790	904	22,000	345	414	22
		ELMOD4	10,316	738	14,331	335	433	--
E	Apr-01	PEDMOD	13,800		17,250	380	380	--
		EVERCALC	9,287		13,586	406	690	--
		MICHBACK	13,800		17,250	395	395	18
		ELMOD4	9,529		31,085	384	444	--
F	Apr-01	PEDMOD	13,800		17,250	398	400	15
		EVERCALC	10,115		22,128	414	690	--
		MICHBACK	13,800		17,250	497	497	18
		ELMOD4	7,128		8,142	414	543	--
G	Apr-01	PEDMOD	11,040		5,775	324	328	
		EVERCALC	9,109		8,033	367	690	
		MICHBACK	8,335		13,800	352	483	
		ELMOD4	7,362		25,658	293	442	
H	Apr-01	PEDMOD	10,384	1,449	17,250	262	260	6
		EVERCALC	11,682	1,380	462	528	440	--
		MICHBACK	5,250	1,380	13,800	414	345	
		ELMOD4	7,335	842	13,800	381	414	--

## **APPENDIX C**

### **RESULTS OF BACKCALCULATION SOFTWARE FOR PRESSURE CELLS**

**Table C1.** Measured and Computed Stress ( EVERCALC, ELMOD) in August 2000 (kPa).

<b>Instrument</b>	<b>Evercalc(LE)</b>	<b>Evercalc*</b>	<b>Elmod(LE)</b>	<b>Elmod*</b>	<b>Measured</b>
AP2-1	83.84	141.73	142.28	185.27	149.60
	105.71	178.43	180.71	234.26	184.40
	131.93	225.22	226.60	293.32	256.31
AP5-3	16.70	16.70	14.12	27.46	19.19
	21.07	21.07	18.28	34.76	25.74
	25.99	25.99	24.45	37.67	32.22
AP7-2	12.48	12.25	34.47	23.91	11.48
	15.73	16.00	43.41	30.22	15.35
	19.64	19.95	54.15	36.34	19.00
BP4-2	69.55	91.63	207.35	135.72	15.92
	86.46	117.30	261.65	171.60	22.35
	108.74	141.59	327.06	214.94	29.61
BP5-3	17.36	14.31	38.99	31.88	9.19
	21.47	18.75	49.22	37.83	12.40
	27.42	23.60	61.54	50.44	17.02
DP1-2	426.42	436.98	436.43	441.88	278.49
	528.68	551.52	551.72	558.62	378.67
	667.30	690.69	690.69	699.66	505.31
DP4-1	54.87	78.05	117.37	126.20	65.74
	68.03	104.89	148.70	159.46	88.21
	85.84	136.84	186.71	199.69	120.46
FP 2-2	118.68	151.80	146.63	141.80	132.62
	151.80	175.26	161.46	157.32	166.29
	171.12	186.30	199.41	187.68	180.78

\* Nonlinear Analysis with temperature correction

LE- Linear Elastic Analysis

**Table C2.** Measured and Computed Stress (PEDMOD, MICBACK) in August 2000 (kPa).

<b>Pedmod(LE)</b>	<b>Pedmod*</b>	<b>Michback(LE)</b>	<b>Michback*</b>	<b>Measured</b>
100.95	141.73	203.79	224.17	149.60
129.24	178.43	257.68	283.45	184.40
158.70	225.22	322.65	354.92	256.31
13.03	15.86	30.21	33.23	19.19
16.89	15.75	38.24	42.06	25.74
21.15	21.15	41.43	45.58	32.22
10.49	12.25	26.30	28.93	11.48
13.48	16.00	33.24	36.57	15.35
16.79	19.95	39.97	43.97	19.00
62.85	62.85	149.30	164.22	15.92
80.45	80.45	188.76	207.64	22.35
99.22	99.22	236.43	260.07	29.61
12.19	91.63	35.07	38.58	9.19
15.47	117.30	41.61	45.77	12.40
19.42	141.59	55.48	61.03	17.02
436.49	436.98	486.06	534.67	278.49
555.11	551.52	614.49	675.94	378.67
690.69	690.69	769.63	846.59	505.31
96.67	75.42	138.82	152.70	65.74
131.17	96.12	175.40	192.95	88.21
164.36	120.75	219.65	241.62	120.46
138.97	201.48	155.97	171.57	132.62
173.88	214.59	173.05	190.36	166.29
193.89	245.64	206.45	227.09	180.78

\* Nonlinear Analysis with temperature correction  
LE- Linear Elastic Analysis

**Table C3.** Measured and Computed Stress (EVERCALC, ELMOD) in February 2001 (kPa).

<b>Instrument</b>	<b>Evercalc(W T)</b>	<b>Evercalc*</b>	<b>Elmod(W T)</b>	<b>Elmod*</b>	<b>Measured</b>
AP2-1	154.63	166.43	40.74	49.84	56.03
	200.86	216.94	50.87	62.24	88.18
	226.60	244.74	61.13	74.80	104.67
AP5-3	15.03	11.45	14.99	17.11	10.52
	13.16	15.18	19.27	21.46	12.68
	15.03	17.33	22.65	25.88	21.06
AP7-2	9.77	9.36	13.39	11.87	4.97
	12.96	12.29	17.63	15.75	11.07
	14.77	14.01	19.21	17.88	12.62
BP4-2	8.85	13.67	20.27	22.89	4.19
	11.54	17.26	25.60	28.93	6.79
	13.05	20.94	31.06	35.15	8.62
BP5-3	16.44	16.30	15.46	16.97	6.69
	21.29	21.98	19.38	22.70	10.99
	27.53	25.27	23.37	25.88	13.40
DP1-2	449.67	462.16	444.22	443.26	182.09
	590.71	590.71	547.58	546.20	328.79
	665.78	665.78	650.26	648.61	553.73
DP4-1	36.25	37.64	23.54	17.93	17.53
	54.19	57.04	29.77	24.21	27.26
	62.06	63.45	36.17	32.55	42.44
FP 2-2	242.27	220.32	248.06	236.74	118.77
	298.63	301.60	305.81	291.80	126.29
	354.73	358.25	363.15	345.14	150.03
FP5-3	13.22	11.03	15.04	15.39	11.60
	17.38	14.70	18.96	19.32	19.55
	20.22	16.79	22.95	23.22	23.74
GP 2-2	306.29	323.40	279.86	292.15	126.55
	391.40	420.14	345.07	360.25	177.19
	441.63	473.48	409.93	427.87	242.74
GP7-2	10.99	9.92	11.64	12.42	9.34
	14.26	12.79	14.48	15.46	12.17
	16.08	14.78	17.33	18.50	14.84

WT- Without temperature Correction

\*Temperature correction with nonlinear analysis

**Table C4.** Measured and Computed Stress (PEDMOD, MICBACK) in February 2001 (kPa).

<b>Instrument</b>	<b>Pedmod(WT)</b>	<b>Pedmod*</b>	<b>Michback(WT)</b>	<b>Michback*</b>	<b>Measured</b>
AP2-1	166.43	133.72	199.71	167.15	56.03
	216.94	169.95	260.32	212.43	88.18
	244.74	193.68	293.69	242.10	104.67
AP5-3	11.45	15.03	13.74	18.79	10.52
	15.18	13.16	18.22	16.45	12.68
	17.33	15.03	20.79	18.79	21.06
AP7-2	9.36	8.23	11.23	10.29	4.97
	12.29	10.80	14.75	13.50	11.07
	14.01	12.29	16.81	15.36	12.62
BP4-2	117.99	93.91	141.59	117.39	4.19
	153.11	120.41	183.73	150.51	6.79
	172.85	137.93	207.41	172.41	8.62
BP5-3	12.97	11.30	15.57	14.13	6.69
	17.39	15.12	20.87	18.91	10.99
	19.93	17.32	23.92	21.65	13.40
DP1-2	456.85	457.06	548.22	571.32	182.09
	616.86	580.22	740.23	725.28	328.79
	668.68	663.64	802.41	829.55	553.73
DP4-1	117.99	93.91	141.59	117.39	17.53
	153.11	122.20	183.73	152.75	27.26
	172.85	137.93	207.41	172.41	42.44
FP 2-2	220.32	196.86	264.38	246.07	18.77
	288.28	251.99	345.94	314.99	26.29
	325.20	288.49	390.24	360.61	50.03
FP5-3	11.03	13.22	13.23	16.53	11.60
	14.70	17.38	17.64	21.73	19.55
	16.79	20.22	20.15	25.27	23.74
GP 2-2	323.40	306.29	388.08	382.86	126.55
	420.14	391.40	504.17	489.25	177.19
	473.48	441.63	568.17	552.03	242.74
GP7-2	9.92	8.36	11.90	10.45	9.34
	12.79	10.45	15.35	13.06	12.17
	14.78	12.55	17.74	15.69	14.84

WT- Without temperature Correction

\*Temperature correction with nonlinear analysis

**Table C5.** Measured and Computed Stress (EVERCALC) in July 2001 (kPa).

<b>Instrument</b>	<b>Evercalc(LE)</b>	<b>Evercalc*</b>	<b>Evercalc(WT)</b>	<b>Measured</b>
AP2-1	153.90	181.06	160.22	173.81
	189.67	223.15	206.22	221.35
	225.45	265.24	232.12	282.76
AP5-3	14.81	17.42	19.15	26.01
	18.74	22.05	24.23	32.27
	22.80	26.82	29.53	41.19
AP7-2	10.67	12.55	15.06	17.26
	13.39	15.75	18.90	22.07
	16.16	19.01	22.81	27.54
BP4-2	106.86	125.72	150.86	59.06
	136.30	160.36	192.43	76.38
	172.43	202.86	243.43	96.26
BP5-3	17.92	15.26	18.32	10.74
	27.18	24.92	29.91	14.41
	30.19	28.46	34.16	18.53
DP1-2	246.92	290.49	348.59	487.35
	336.30	395.65	474.78	569.11
	406.15	477.83	573.39	682.89
DP4-1	105.00	123.52	148.23	125.17
	129.68	152.57	183.08	165.63
	154.29	181.52	217.82	205.41
FP 2-2	130.81	153.90	186.22	183.33
	161.22	189.67	229.51	237.91
	191.63	225.45	272.80	323.40
FP5-3	9.86	11.60	9.59	32.02
	12.90	15.18	12.55	39.81
	16.55	19.47	16.09	48.89
GP 2-2	170.97	201.14	223.49	255.65
	301.40	354.58	393.98	289.87
	398.50	468.82	520.92	531.92

WT- Without temperature Correction

\*Temperature correction with nonlinear analysis

LE –Linear Elastic analysis

**Table C6.** Measured and Computed Stress (ELMOD) in July 2001 (kPa).

<b>Instrument</b>	<b>Elmod(L E)</b>	<b>Elmod*</b>	<b>Elmod(WT)</b>	<b>Measured</b>
AP2-1	175.19	161.18	119.92	173.81
	138.69	127.59	156.56	221.35
	156.91	144.35	177.10	282.76
AP5-3	35.55	32.70	39.66	26.01
	44.86	41.27	53.03	32.27
	25.88	23.81	60.62	41.19
AP7-2	26.33	24.22	25.25	17.26
	32.91	30.28	33.46	22.07
	39.61	36.44	38.09	27.54
BP4-2	149.94	137.94	175.12	59.06
	185.20	170.38	188.92	76.38
	220.32	202.69	222.73	96.26
BP5-3	16.97	15.61	18.12	10.74
	22.70	20.88	24.48	14.41
	25.88	23.81	28.16	18.53
DP1-2	461.82	461.40	463.27	487.35
	568.97	598.71	570.98	569.11
	674.20	675.03	677.86	682.89
DP4-1	159.47	158.15	152.74	125.17
	196.91	194.86	198.58	165.63
	233.98	231.36	224.18	205.41
FP 2-2	236.74	217.80	253.30	183.33
	291.80	268.46	312.43	237.91
	345.14	317.53	371.29	323.40
FP5-3	24.50	22.54	33.01	32.02
	30.93	28.45	41.63	39.81
	38.12	35.07	50.40	48.89
GP 2-2	150.42	148.99	191.04	255.65
	250.06	262.66	290.48	289.87
	342.80	347.28	383.02	531.92

WT- Without temperature Correction

\*Temperature correction with nonlinear analysis

LE –Linear Elastic analysis

**Table C7.** Measured and Computed Stress (PEDMOD) in July 2001 (kPa).

<b>Instrument</b>	<b>Pedmod(L E)</b>	<b>Pedmod*</b>	<b>Pedmod(WT)</b>	<b>Measured</b>
AP2-1	236.54	205.69	279.12	173.81
	261.70	227.56	308.80	221.35
	318.30	276.78	375.59	282.76
AP5-3	50.17	43.63	59.20	26.01
	67.08	58.33	79.15	32.27
	76.69	66.69	90.49	41.19
AP7-2	31.94	27.77	37.69	17.26
	42.32	36.80	49.94	22.07
	48.18	41.90	56.85	27.54
BP4-2	221.53	192.63	261.40	59.06
	238.99	207.81	282.00	76.38
	281.76	245.01	332.47	96.26
BP5-3	22.92	19.93	27.05	10.74
	30.97	26.93	36.54	14.41
	35.62	30.97	42.03	18.53
DP1-2	456.99	509.59	539.24	487.35
	563.39	628.07	664.79	569.11
	669.16	745.64	789.61	682.89
DP4-1	130.82	168.01	154.37	125.17
	161.39	218.44	190.44	165.63
	192.03	246.60	226.59	205.41
FP 2-2	229.15	278.63	270.40	183.33
	270.62	343.68	319.33	237.91
	290.84	408.42	343.19	323.40
FP5-3	44.16	36.31	52.11	32.02
	48.99	45.80	57.81	39.81
	58.65	55.44	69.21	48.89
GP 2-2	223.91	194.86	264.21	255.65
	304.43	296.29	359.23	289.87
	415.73	390.68	490.56	531.92

WT- Without temperature Correction

\*Temperature correction with nonlinear analysis

LE –Linear Elastic analysis

**Table C8.** Measured and Computed Stress (MICHBACK) in July 2001 (kPa).

<b>Instrument</b>	<b>Michback(LE)</b>	<b>Michback*</b>	<b>Michback(WT)</b>	<b>Measured</b>
AP2-1	226.13	260.05	208.04	173.81
	179.02	205.87	164.69	221.35
	202.53	232.91	186.33	282.76
AP5-3	45.88	52.77	42.21	26.01
	57.91	66.59	53.28	32.27
	33.41	38.42	30.73	41.19
AP7-2	33.99	39.08	31.27	17.26
	42.48	48.86	39.08	22.07
	51.12	58.79	47.03	27.54
BP4-2	193.53	222.56	178.05	59.06
	239.04	274.90	219.92	76.38
	284.38	327.03	261.63	96.26
BP5-3	21.90	25.19	20.15	10.74
	29.30	33.70	26.96	14.41
	33.41	38.42	30.73	18.53
DP1-2	647.35	744.45	595.56	487.35
	839.99	965.99	772.79	569.11
	947.06	1089.12	871.30	682.89
DP4-1	221.88	255.16	204.13	125.17
	273.38	314.39	251.51	165.63
	324.59	373.28	298.63	205.41
FP 2-2	305.57	351.41	281.13	183.33
	376.65	433.14	346.51	237.91
	445.49	512.31	409.85	323.40
FP5-3	31.62	36.36	29.09	32.02
	39.92	45.91	36.72	39.81
	49.20	56.58	45.26	48.89
GP 2-2	209.04	240.39	192.31	255.65
	368.51	423.78	339.03	289.87
	487.23	560.31	448.25	531.92

WT- Without temperature Correction

\*Temperature correction with nonlinear analysis

LE –Linear Elastic analysis

**Table C9.** Measured and Computed Stress (EVERCALC) in November 2000 (kPa).

<b>Instrument</b>	<b>Evercalc(LE)</b>	<b>Evercalc*</b>	<b>Evercalc(WT)</b>	<b>Measured</b>
AP2-1	74.66	107.30	69.14	93.43
	93.56	134.62	87.42	138.35
	117.99	170.36	110.95	177.54
AP5-3	16.86	13.76	10.63	11.76
	21.29	17.57	15.19	15.18
	26.40	22.75	17.37	18.70
AP7-2	17.62	11.04	10.70	11.48
	22.41	14.06	14.32	8.69
	25.79	18.02	17.09	11.25
BP4-2	56.28	83.97	50.48	56.68
	74.24	105.71	65.72	103.91
	86.60	133.52	78.11	147.59
BP5-3	15.08	6.31	18.03	16.08
	19.80	8.10	24.03	25.94
	23.83	10.29	30.26	30.77
DP1-2	429.80	432.98	433.80	242.09
	564.28	530.13	569.60	358.32
	679.10	685.52	672.27	468.10
DP4-1	57.53	74.87	51.23	19.78
	71.07	91.84	64.78	31.53
	89.56	119.09	79.97	39.68
FP 2-2	137.66	118.06	124.34	20.15
	170.71	144.83	157.18	31.26
	219.63	187.68	197.41	41.75
FP5-3	21.45	13.97	12.45	12.32
	28.19	18.24	16.15	17.85
	34.21	22.91	20.75	19.26
GP 2-2	240.47	245.16	235.01	188.92
	305.05	297.60	296.29	288.14
	383.64	385.16	375.43	408.04
GP7-2	12.90	10.02	10.47	7.27
	16.90	12.66	13.94	9.28
	20.65	16.34	17.30	12.09

WT- Without temperature Correction

\*Temperature correction with nonlinear analysis

LE –Linear Elastic analysis

**Table C10.** Measured and Computed Stress (ELMOD) in November 2000 (kPa).

<b>Instrument</b>	<b>Elmod(L E)</b>	<b>Elmod*</b>	<b>Elmod(WT)</b>	<b>Measured</b>
AP2-1	121.30	163.39	142.49	93.43
	150.42	203.41	174.57	138.35
	191.34	258.75	225.15	177.54
AP5-3	24.03	27.53	19.53	11.76
	29.82	34.72	24.37	15.18
	37.93	44.24	31.31	18.70
AP7-2	11.52	10.36	8.18	11.48
	14.45	13.15	10.34	8.69
	18.20	16.77	13.19	11.25
BP4-2	116.75	102.05	77.21	56.68
	144.76	126.68	95.84	103.91
	184.85	161.67	122.34	147.59
BP5-3	30.61	11.46	11.46	16.08
	37.94	14.53	14.53	25.94
	48.32	19.05	19.05	30.77
DP1-2	436.36	437.18	435.46	242.09
	505.36	540.62	539.79	358.32
	690.00	696.21	689.38	468.10
DP4-1	111.30	114.06	93.29	19.78
	137.93	142.49	115.78	31.53
	176.02	181.88	147.73	39.68
FP 2-2	155.39	127.79	138.83	20.15
	189.89	146.63	169.40	31.26
	242.33	196.31	228.53	41.75
FP5-3	39.42	10.58	10.83	12.32
	48.87	13.39	13.59	17.85
	62.29	17.56	17.97	19.26
GP 2-2	316.43	269.93	311.67	188.92
	392.27	331.06	381.92	288.14
	500.04	421.25	492.80	408.04
GP7-2	17.53	10.66	14.54	7.27
	13.61	18.35	16.75	9.28
	17.50	23.92	21.32	12.09

WT- Without temperature Correction

\*Temperature correction with nonlinear analysis

LE –Linear Elastic analysis

**Table C11.** Measured and Computed Stress (PEDMOD) in November 2000 (kPa).

<b>Instrument</b>	<b>Pedmod(L E)</b>	<b>Pedmod*</b>	<b>Pedmod(WT)</b>	<b>Measured</b>
AP2-1	134.62	107.30	96.53	93.43
	161.12	134.62	121.30	138.35
	212.87	170.36	153.32	177.54
AP5-3	23.80	13.76	11.76	11.76
	29.79	17.57	15.00	15.18
	37.67	22.75	19.38	18.70
AP7-2	14.68	11.04	9.63	11.48
	18.38	14.06	12.25	8.69
	18.38	18.02	15.69	11.25
BP4-2	79.14	83.97	72.59	56.68
	97.15	105.71	89.08	103.91
	125.30	133.52	115.30	147.59
BP5-3	20.36	12.41	11.56	16.08
	25.77	15.74	14.64	25.94
	32.43	20.43	18.97	30.77
DP1-2	433.25	432.98	430.97	242.09
	542.41	530.13	527.71	358.32
	685.93	685.52	682.34	468.10
DP4-1	90.25	74.87	83.35	19.78
	110.54	91.84	104.88	31.53
	142.90	119.09	132.62	39.68
FP 2-2	144.97	118.06	131.17	20.15
	181.54	144.83	160.91	31.26
	229.56	187.68	208.52	41.75
FP5-3	39.42	10.58	10.83	12.32
	48.87	13.39	13.59	17.85
	62.29	17.56	17.97	19.26
GP 2-2	269.93	269.93	311.67	188.92
	331.06	331.06	381.92	288.14
	421.25	421.25	492.80	408.04
GP7-2	13.66	10.02	9.09	7.27
	12.66	11.54	20.10	9.28
	16.34	14.79	25.59	12.09

WT- Without temperature Correction

\*Temperature correction with nonlinear analysis

LE –Linear Elastic analysis

**Table C12.** Measured and Computed Stress (MICHBACK) in November 2000 (kPa).

<b>Instrument</b>	<b>Michback(LE)</b>	<b>Michback*</b>	<b>Michback(WT)</b>	<b>Measured</b>
AP2-1	161.54	139.48	135.14	93.43
	193.34	175.00	169.82	138.35
	255.44	221.47	214.65	177.54
AP5-3	28.56	17.89	16.47	11.76
	35.75	22.85	21.00	15.18
	45.21	29.57	27.13	18.70
AP7-2	17.62	14.35	13.49	11.48
	22.06	18.27	17.16	8.69
	22.06	23.43	21.97	11.25
BP4-2	94.97	109.16	101.62	56.68
	116.58	137.42	124.71	103.91
	150.36	173.57	161.42	147.59
BP5-3	24.43	16.14	16.18	16.08
	30.93	20.46	20.50	25.94
	38.92	26.56	26.56	30.77
DP1-2	519.90	562.87	603.36	242.09
	650.89	689.17	738.80	358.32
	823.11	891.17	955.28	468.10
DP4-1	108.30	97.32	116.69	19.78
	132.65	119.39	146.83	31.53
	171.48	154.82	185.67	39.68
FP 2-2	173.96	153.48	183.64	20.15
	217.85	188.28	225.27	31.26
	275.48	243.98	291.93	41.75
FP5-3	47.30	13.75	15.17	12.32
	58.64	17.40	19.03	17.85
	74.74	22.83	25.15	19.26
GP 2-2	323.91	350.91	436.34	188.92
	397.27	430.38	534.68	288.14
	505.49	547.62	689.92	408.04
GP7-2	16.39	13.02	12.73	7.27
	16.46	16.16	9.28	9.28
	21.24	17.74	12.09	12.09

WT- Without temperature Correction

\*Temperature correction with nonlinear analysis

LE –Linear Elastic analysis

**Table C13.** Measured and Computed Stress (EVERCALC, ELMOD) in April 2001 (kPa).

<b>Instrument</b>	<b>Evercalc*</b>	<b>Evercalc(W T)</b>	<b>Elmod(L.E)</b>	<b>Elmod*</b>	<b>Elmod(W T)</b>	<b>Measured</b>
AP2-1	176.53	211.66	144.69	169.33	141.31	146.02
	227.88	273.76	186.78	219.01	191.54	138.55
	276.78	333.10	226.87	266.48	221.90	180.50
AP5-3	27.21	19.60	22.31	15.68	13.94	20.67
	35.20	26.13	28.85	20.90	18.55	26.47
	42.75	32.58	35.04	26.06	23.10	32.33
AP7-2	13.81	14.85	11.32	11.88	11.32	11.54
	18.23	19.61	14.95	15.69	14.95	15.28
	22.56	24.27	18.49	19.42	18.49	19.94
BP4-2	117.52	146.45	96.32	117.16	94.19	97.83
	151.69	190.01	124.34	152.01	122.27	126.03
	230.48	236.15	188.92	188.92	149.18	171.11
BP5-3	22.15	23.12	18.15	18.50	15.97	11.87
	28.59	31.17	23.43	24.94	21.46	18.50
	34.72	33.72	28.46	26.98	26.98	20.78
DP1-2	530.00	551.74	434.42	441.39	434.01	384.12
	676.64	704.32	554.62	563.45	554.14	491.69
	815.20	848.36	668.20	678.68	670.68	646.12
DP4-1	119.20	161.03	97.70	128.82	90.11	72.11
	152.20	208.73	124.75	166.98	116.75	97.50
	183.34	262.63	150.28	210.11	139.93	120.27
FP 2-2	133.52	149.54	146.42	177.17	160.08	85.70
	145.25	162.67	162.50	196.62	176.64	134.78
	169.40	189.72	182.85	221.25	208.38	181.04
FP5-3	12.32	14.50	22.29	28.17	30.62	25.74
	16.13	18.98	29.12	35.56	38.66	34.98
	20.69	24.34	42.85	43.83	47.64	43.47

WT- Without temperature Correction

\*Temperature correction with nonlinear analysis

LE –Linear Elastic analysis

**Table C14.** Measured and Computed Stress (PEDMOD) in April 2001 (kPa).

<b>Instrument</b>	<b>Pedmod(L.E)</b>	<b>Pedmod*</b>	<b>Pedmod(W T)</b>	<b>Measured</b>
AP2-1	157.80	150.83	144.42	146.02
	197.75	190.37	182.16	166.55
	246.54	240.26	226.53	190.50
AP5-3	22.87	15.93	15.47	20.67
	20.78	20.61	20.01	26.47
	27.68	25.94	25.18	32.33
AP7-2	13.27	10.36	10.07	11.54
	13.88	13.25	12.92	15.28
	17.60	16.75	16.30	19.94
BP4-2	107.73	102.60	92.53	97.83
	136.13	129.65	117.58	126.03
	174.82	166.50	151.11	171.11
BP5-3	23.60	23.13	20.82	11.87
	30.46	29.85	26.87	18.50
	37.00	36.26	32.64	20.78
DP1-2	564.75	438.98	438.43	384.12
	721.01	559.18	557.93	491.69
	868.65	707.60	685.79	646.12
DP4-1	127.02	89.56	109.99	72.11
	162.18	113.09	113.09	97.50
	195.37	140.35	140.35	120.27
FP 2-2	190.34	167.05	155.39	85.70
	211.24	201.83	196.79	134.78
	237.71	215.42	222.32	181.04
FP5-3	41.26	38.78	36.02	25.74
	52.04	49.13	51.89	34.98
	63.00	69.83	77.63	43.47

WT- Without temperature Correction

\*Temperature correction with nonlinear analysis

LE –Linear Elastic analysis

**Table C15.** Measured and Computed Stress (MICHBACK) in April 2001 (kPa).

<b>Instrument</b>	<b>Michback*</b>	<b>Michback(W T)</b>	<b>Measured</b>
AP2-1	217.04	253.99	146.02
	280.17	328.51	166.55
	340.31	399.72	190.50
AP5-3	33.46	23.53	20.67
	43.27	31.35	26.47
	52.56	39.09	32.33
AP7-2	16.98	17.82	11.54
	22.42	23.54	15.28
	27.74	29.12	19.94
BP4-2	144.49	175.74	97.83
	186.51	228.01	126.03
	283.38	283.38	171.11
BP5-3	27.23	27.75	11.87
	35.15	37.40	18.50
	42.69	40.47	20.78
DP1-2	651.64	662.09	384.12
	831.93	845.18	491.69
	1002.29	1018.03	646.12
DP4-1	146.56	193.23	72.11
	187.13	250.47	97.50
	225.42	315.16	120.27
FP 2-2	219.63	201.83	85.70
	243.74	208.52	134.78
	274.28	238.19	181.94
FP5-3	35.33	42.92	25.74
	43.68	49.75	34.98
	64.27	70.45	43.47

WT- Without temperature Correction

\*Temperature correction with nonlinear analysis

## VITAE

Alexander Kwasi Appea was born on October 9<sup>th</sup> 1966 in Tamale, in the Republic of Ghana. He graduated from St Peter's Secondary School in June 1985. In October 1990, he received his Bachelor degree in Civil Engineering from the Kwame Nkrumah University of Science and Technology in Kumasi, the seat of the Ashanti Kingdom in West Africa. He worked for two years as a transportation engineer with the Ghana Highway Authority in the Planning division. He proceeded to the United States to study for a Master of Science program in civil engineering at the Materials Division of Virginia Tech. He worked for a year with the Hemispherical Center for Environmental Technology at the Florida International University in Miami as a research engineer. In 1999 he decided to come back to Virginia Tech to work on a PhD program under the supervision of Dr Imad L Al-Qadi in the Transportation Systems and Infrastructure Division. In January of 2003 he was hired to work with the State Materials Office in Gainesville at the Florida Department of Transportation on a sponsored project with the University of North Florida as a consultant on a three year contract.